5-2015

# Redox-Controlled Biogeochemical Processes Affecting Arsenic Solubility in Sediments from a Basin-Fill Aquifer in Northern Utah

Xianyu Meng
*Utah State University*

# REDOX-CONTROLLED BIOGEOCHEMICAL PROCESSES AFFECTING ARSENIC SOLUBILITY IN SEDIMENTS FROM A BASIN-FILL AQUIFER IN NORTHERN UTAH

by

Xianyu Meng

A dissertation submitted in partial fulfillment
of the requirements for the degree

of

DOCTOR OF PHILOSOPHY

in

Civil and Environmental Engineering

Approved:

| | |
|---|---|
| Professor Joan E. McLean<br>Major Professor | Dr. R. Ryan Dupont<br>Committee Member |
| Dr. Darwin L. Sorensen<br>Committee Member | Dr. Jagath J. Kaluarachchi<br>Committee Member |
| Dr. Astrid R. Jacobson<br>Committee Member | Dr. Mark R. McLellan<br>Vice President for Research and<br>Dean of the School of Graduate Studies |

UTAH STATE UNIVERSITY
Logan, Utah

2015

# ABSTRACT

Redox Controlled Biogeochemical Processes Affecting Arsenic Solubility in Sediments from a Basin-fill Aquifer in Northern Utah

by

Xianyu Meng, Doctor of Philosophy

Utah State University, 2014

Major Professor: Prof. Joan E. McLean
Department: Civil and Environmental Engineering

The basin-fill aquifers of the American Southwest host elevated concentrations of arsenic in groundwater due to the local geology. Limited information is available on arsenic dynamics in semi-arid and arid regions of the world. This study describes arsenic biogeochemistry and mechanisms of arsenic solubilization for a soil profile collected from the surface to the depth of groundwater in the Cache Valley Basin, Northern Utah.

The first objective was to delineate mechanisms of arsenic solubilization from sediments collected at the study site. Microcosms containing site groundwater and site-oxidized and site-reduced sediments, were monitored over time to observe changes in the solubilization and oxidation state of arsenic and changes in mineral phases of arsenic and iron. The observed solubilization of arsenic was decoupled from iron reduction in the site-oxidized sediments in the presence of native organic carbon, which disagreed with the widely accepted hypothesis that arsenic solubilization is derived from microbial

driven reductive dissolution of iron oxides. Carbonate minerals were defined as the mineral phase associated with arsenic that contributed to the arsenic measured in solution.

The second objective was to determine how altering redox and water conditions down a profile affects arsenic geochemistry and hence solubility. Redox stratification was delineated in two sediment cores based on chemical analyses and visual observation of redox-sensitive parameters. The vadose zone released a considerable amount of arsenic, while the next zone, the carbonate enrichment zone, released the highest concentration of arsenic. Soluble arsenic was exclusively As(V) in the redox transition zone, where As was primarily associated with iron oxides. Solubilization of arsenic was limited in the deeply reduced depletion zone due to the formation of sulfide minerals.

Lateral resolution of oxidation state and elemental association of arsenic at the micron scale were delineated using synchrotron-based X-ray absorption spectroscopy under Objective 3. The presence of unaltered arsenic sulfides was revealed in the vadose zone, suggesting that arsenic was inputted continuously to the ground surface. From the water table to the deeply reduced depletion zone sediments, arsenic mineral association was dominated by manganese-bearing carbonate minerals and amorphous iron oxides, which are vulnerable to groundwater fluctuation and redox-cycling.

(191 pages)

# PUBLIC ABSTRACT

Redox Controlled Biogeochemical Processes Affecting Arsenic Solubility in Sediments from a Basin-fill Aquifer in Northern Utah

by

Xianyu Meng, Doctor of Philosophy

Utah State University, 2014

Major Professor: Prof. Joan E. McLean
Department: Civil and Environmental Engineering

Elevated arsenic concentrations in groundwater have caused worldwide health concerns to humans. A groundwater monitoring program performed in a shallow aquifer in the semi-arid Cache Valley Basin, Utah, indicated that the highest arsenic concentration was 100 μg/L, which is ten times the maximum contaminant level of arsenic (10 μg/L) set by the USEPA. Determining the source of arsenic and the processes that control the solubilization of arsenic in this semi-arid environment are necessary to ensure water management that minimizes human exposure to contaminated groundwater in this basin and other basin-fill aquifers throughout the Southwestern U.S.

Evaluation of aquifer solids collected from the soil surface to below the depth of the groundwater using macro- to molecular-scale techniques showed that the arsenic was associated with carbonate minerals and iron oxides throughout the profile. These minerals provided sinks, keeping the arsenic out of the water phase; however, with water saturation, and particularly within the fluctuating water table, carbonates and iron oxides

dissolve, releasing arsenic to the groundwater. The continued source of arsenic was determined to be the input of arsenic-bearing minerals leaching from the mountains surrounding the Cache Valley Basin. The minerals are not stable when exposed to the atmosphere, and they provide arsenic to the subsurface with infiltrating water. These mechanisms were further supported with laboratory microcosm studies where carbonate minerals formed the main pool of arsenic that was solubilized under the conditions of the study.

Most studies in the literature that report on arsenic solubility in aquifer systems have been from systems that are not rich in carbonates. The presence of carbonate minerals is a characteristic of the Cache Valley Basin and the other basin-fill aquifer systems in the Southwestern U.S. This study has illustrated that the conditions characteristic of semi-arid, arid parts of the world do influence arsenic concentrations in groundwater.

(191 pages)

# DEDICATION

This dissertation is dedicated to my grandmother and my parents. You educated me in a variety of ways and taught me to be a good man. Thank you for understanding when I came to a place that is thousands of miles away from you to pursue my career. This dissertation is also dedicated to my wife. Your patience and encouragement motivated me when I felt depressed.

# ACKNOWLEDGMENTS

It is difficult to “measure” how grateful I am to my major advisor, Professor Joan E. McLean, for her consistent support. In the past six years, she helped me to overcome difficulties in my study and build my attitude of research. This study could not have been completed without her knowledge and support. I offer my gratitude to all my committee members, including Dr. R. Ryan Dupont, Dr. Darwin L. Sorensen, Dr. Astrid R. Jacobson, and Dr. Jagath J. Kaluarachchi, for your help in improving the quality of my research.

I also give my gratitude to the Utah Water Research Laboratory for providing me financial support and a perfect atmosphere for research.

I am thankful to Dr. Erich U. Petersen and Quintin Sahratian at the University of Utah, Sue Wirick at Brookhaven National Laboratory, and Robert A. Gordon at Argonne National Laboratory for their assistance with the imaging analyses involved in my study.

In 2009, my wife, Ting, flew to the United States to be with me. You were a girl who just wanted to stay with parents. Thank you for your sacrifice. It has been fantastic becoming interdependent in a place away from our hometown. Your patience and encouragement provide huge spiritual support to me.

I am greatly indebted to my beloved parents, Mr. Zhaoshuang Meng and Ms. Shuying Li, and my grandmother. Being away from parents is not normal for a child from Tianjin. I have dreamt about you and Tianjin so many times.

I also thank my dear friends in China and the United States. You all ease my life and make it colorful.

Xianyu Meng

CONTENTS

Page

# LIST OF TABLES

# LIST OF FIGURES

# CHAPTER 1

# INTRODUCTION

Groundwater is the main drinking water source in many parts of the world either because surface water is limited or because it has been contaminated. In order to develop new water sources for people in Bangladesh and West Bengal, the World Health Organization (WHO) installed tube-wells in these areas in the 1970s. The wells provided water without pathogens, but the underlying aquifer material released arsenic (As) into the well water, exposing 57 million people to toxic levels of As. Arsenic is considered one of the primary environmental causes of cancer mortality. The WHO and USEPA have decreased their standards for As in drinking water to 10 μg/L from the previous value of 50 μg/L (US-EPA, 2001; WHO, 2004).

Contamination of groundwater from As is frequently proven to be derived from geochemical sources rather than the presence of a well-defined As source generated by human activities (deLemos et al., 2006). Arsenic is the 20th most common element in the earth's crust, with an average crustal abundance of 24 μmol/kg (1,800 μg/kg) (Frankenberger, 2002). Although As-bearing minerals are relatively stable, changes in environmental factors may result in dissolution of minerals, followed by As mobilization.

A number of studies have been performed with deltaic sediments in Southern and Southeastern Asia to delineate mechanisms behind solubilization of geologic As in these subsurface systems. Despite continued debates over the details of these mechanisms, there is a general consensus that microbial driven reductive dissolution of host iron (Fe) oxide minerals results in the release of adsorbed and co-precipitated As (McArthur et al.,

2001; Nickson et al., 2000; Ravenscroft et al., 2001; Swartz et al., 2004) when sufficient bioavailable organic carbon is present (Islam et al., 2004; Liao et al., 2011; McLean et al., 2006). The enzymatic reduction of As(V) to As(III) has also been demonstrated to mobilize As from synthesized minerals and environmental samples (Ahmann et al., 1997; Tufano et al., 2008).

In some regions where primary As minerals are present due to natural weathering or mining activity, oxidative dissolution of As-bearing sulfides in surficial sediments has also been proposed as a contributing mechanism to As contamination of groundwater (Chowdhury et al., 1999). As the Himalayan debris weathers, primary As sulfides deposited at the near-surface liberate As from mineral phases, providing a continuous source of As to the river deltas of Southern and Southeastern Asia (Polizzotto et al., 2006). These findings suggest that sources and sinks of As from the soil surface to groundwater depths should be considered in determining processes that control As solubilization.

The mechanisms of As solubilization have been studied for several decades, but research attention tends to focus on the influence of reducing conditions under groundwater saturation. This approach is justified in humid Southern and Southeastern Asia where the monsoonal climate causes a distinct wet season annually. Elevated As concentrations in groundwater, however, are not limited to these regions; there are increasing reports of As in groundwater throughout the arid and semi-arid regions of world, including parts of Mexico, Argentina, Chile, China, and the U.S. Compared to humid regions, these arid and semi-arid regions are characterized by low annual rainfall, high evapotranspiration rates, and low soil organic matter. Thus, mechanisms other than

reductive dissolution of Fe and As minerals have been proposed in these regions, including release of surface bound arsenic due to high pH and counterion effects (Bhattacharya et al., 2006; Scanlon et al., 2009; Smedley et al., 2005). Bicarbonate ions, prevalent in the aquifers in semi-arid and arid regions, facilitate As solubilization by competing for adsorption sites and forming As-carbonate complexes (Anawar et al., 2004; Kim et al., 2000). Evaporative concentration of chloride also facilitates desorption of As (Welch and Lico, 1998).

Modeling efforts by the USGS have predicted that 43% percent of the groundwater in basin-fill aquifers underlying the Southwestern U.S. has As concentrations that exceed 10 µg/L (Anning et al., 2012; Fig. 1-1). The water table in basin-fill aquifers is recharged by precipitation in the surrounding mountains and ranges, irrigation, and snow-melt and is consistently discharged by evapotranspiration; the water table rises and recedes frequently rather than experiencing a distinct wet season. The high carbonate content in the aquifer systems of semi-arid and arid regions also differs from humid regions. The role of carbonate minerals has not received attention in previous studies due to its low retention efficiency compared to oxides, and the low carbonate content in humid regions. In semi-arid and arid regions, the formation of carbonate mineral occurs near the water table due to capillary rise and evapotranspiration of calcareous groundwater.

In Cache County, Utah, the groundwater in 23 of 157 wells sampled by the Utah Geological Survey had As concentrations exceeding 10 µg/L (Lowe et al., 2003). These wells were located throughout the Cache Valley, from the mountain fronts to the basin,

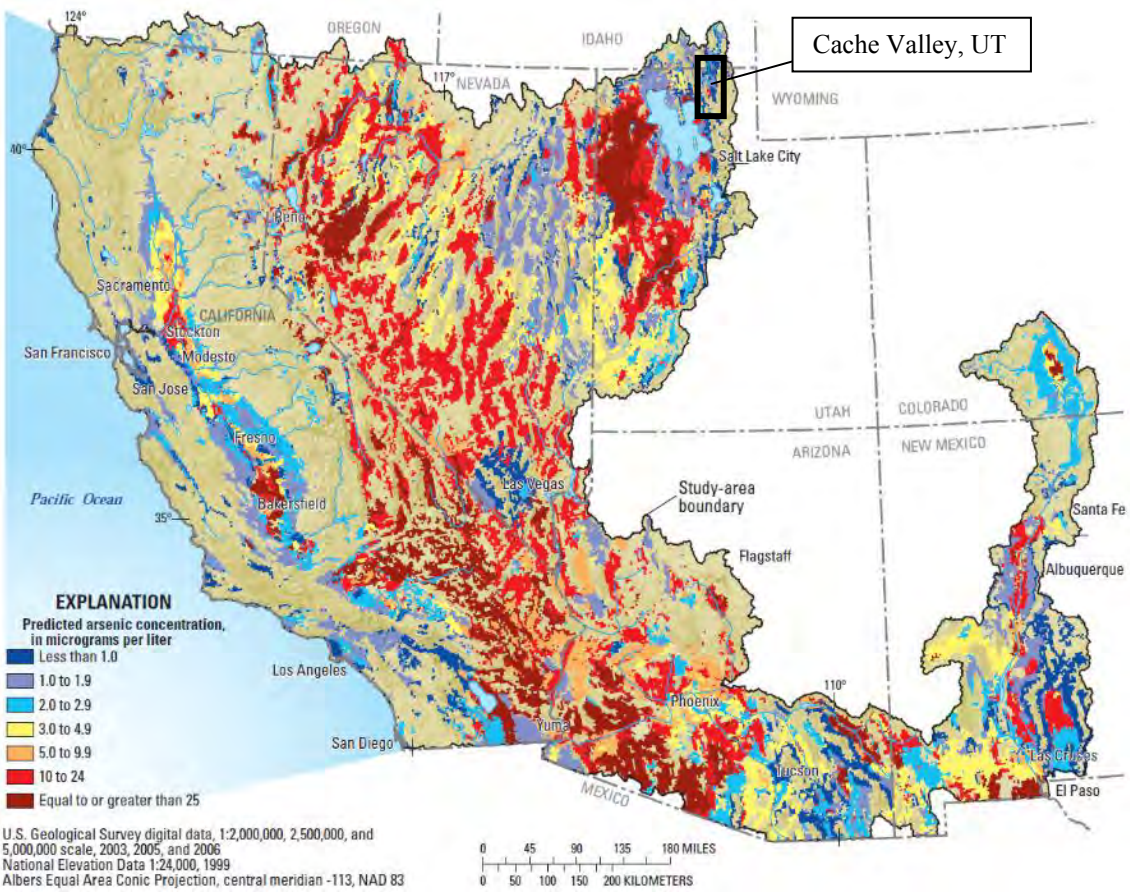


**Fig. 1-1.** Predicted As concentrations in the basin-fill aquifers underlying the Southwestern U.S. (adapted from Anning et al., 2012). The location of Cache Valley, UT is indicated by the black frame.

with no obvious pattern within the distribution of spatial location (Fig. 1-2). Well water is used by individual households for domestic purposes and for irrigation. Most previous research efforts have dealt with subsurface material collected from depths greater than 50 m in humid regions. In semi-arid regions such as Cache Valley, processes occurring in shallow aquifers (< 5 m) must be considered, including formation and transport of evaporites and seasonal oxidation-reduction cycling caused by changes in water table elevation due to precipitation and irrigation practices.

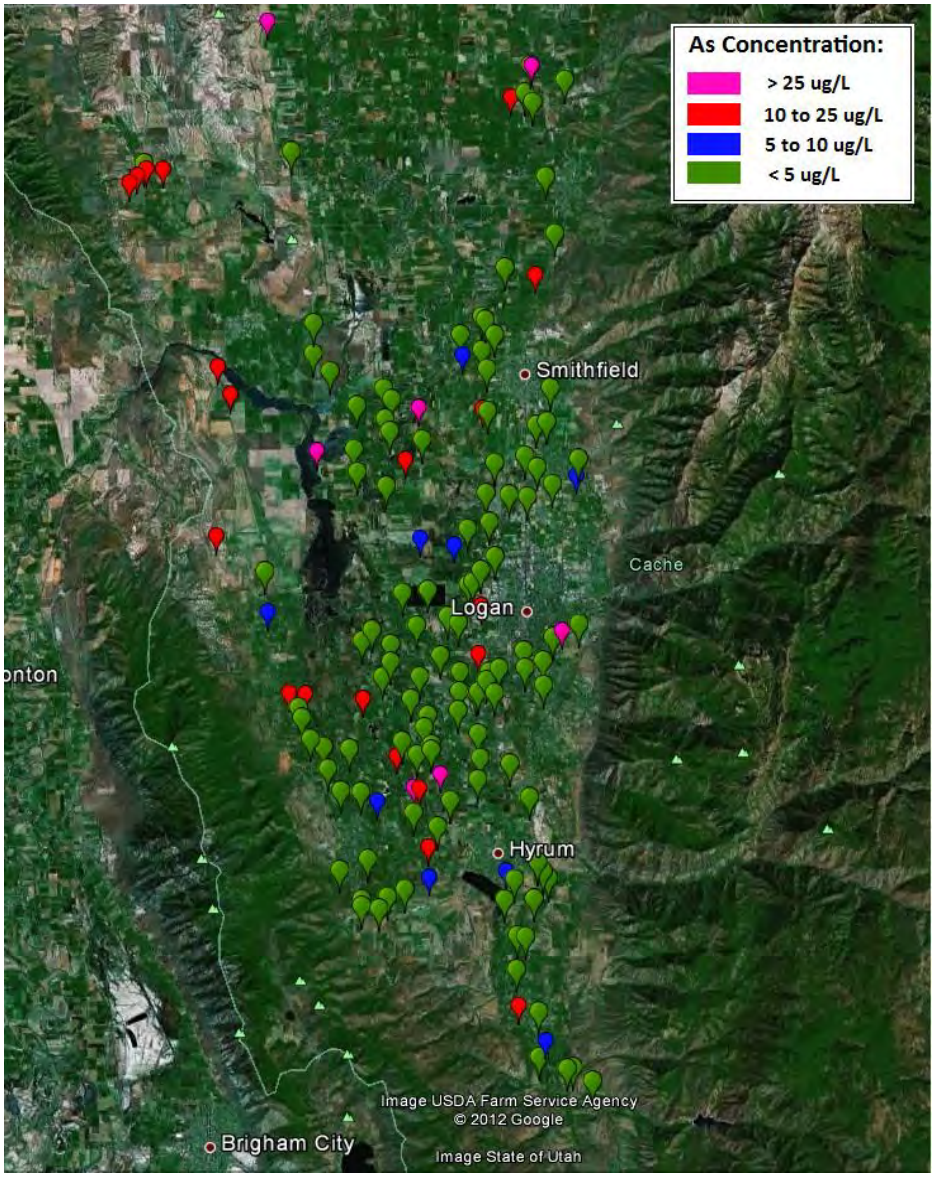


**Fig. 1-2.** Distribution of ground water wells that have been sampled and analyzed for arsenic concentrations in Cache Valley, UT. Pinhead denotes: green for As content less than 5 µg/L, blue for As content from 5 µg/L to 10 µg/L, red for As content from 10 to 25 µg/L, and pink for As content of 25 and above (Data from the Lowe et al., 2003).

The study area of this project is located near the City of Logan's municipal landfill. This area was selected because there is a network of monitoring wells around the landfill that has been sampled for As concentration for over 10 years. Additional piezometers were installed (Fig. 1-3) by personnel from the Utah Water Research

Laboratory in July 2008. Water samples were analyzed for major cations and anions, trace elements, including As and metals, organic carbon characterizations, and other water quality parameters from all available wells in July 2008 and May 2009. Elevated As concentrations (> 10 µg/L) were found in 68% of those locations and ranged from 16 µg/L to 94 µg/L. Preliminary results from field studies with core material collected during well installation showed that As was associated with geologic material, and elevated concentrations of As, relative to average crustal levels, occurs from the soil surface to a sampling depth of 4.9 m.

Arsenic sulfide minerals are a potential source of As in the Cache Valley Basin. The Cache Valley consists of Lake Bonneville deposits that filled the valley approximately 14,000 years ago. These lacustrine and alluvial deposits overlay the Salt Lake Formation which consists of tertiary sedimentary and volcanic rocks. The Salt Lake Formation was deposited with the migration of lava from Northern Nevada to its present location in the Yellowstone area over 2 million years ago (Hintze, 2005). The Salt Lake Formation is exposed in the mountains surrounding the Cache Valley Basin. This formation was eroded by rising and lowering levels of Lake Bonneville and, after this lake receded, continued water and wind erosion has resulted in deposition of As sulfides in the basin. With oxidation of As sulfide minerals, the As may also be associated with Fe and Mn oxides and with carbonate minerals. Because carbonates sequester less As compared to Fe oxides on a weight basis (Smedley and Kinniburgh, 2002), the role of carbonate minerals in As solubilization has not been well studied. Subsurface materials in semi-arid regions,

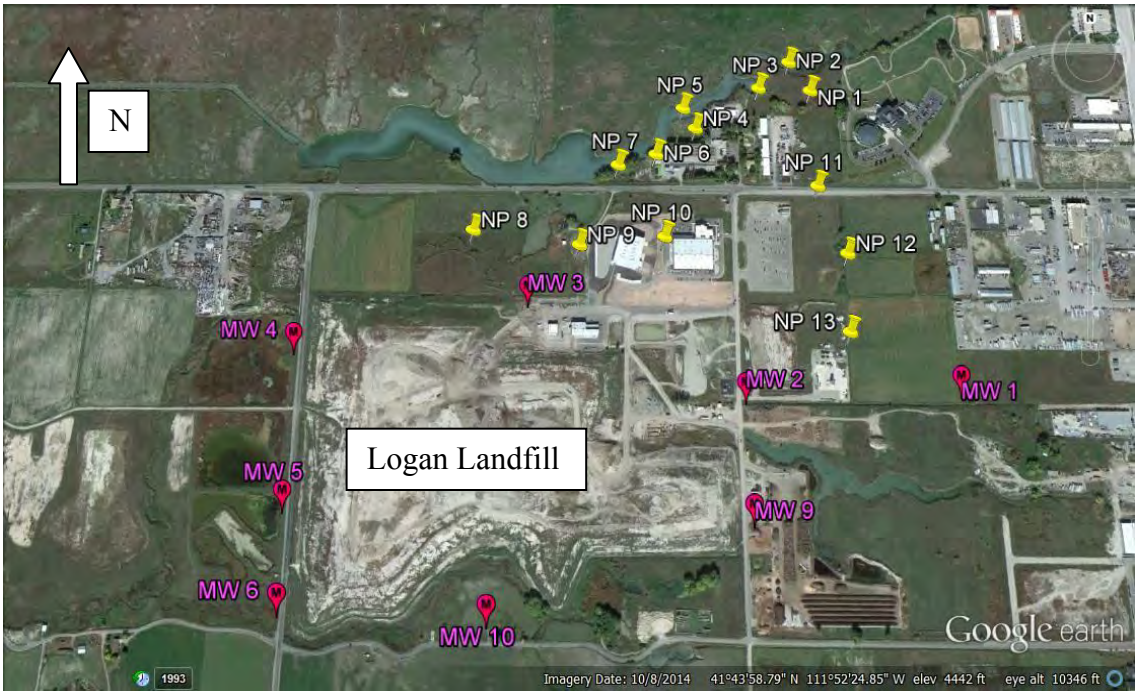


**Fig. 1-3.** Location maps of study site. (Color denotes: yellow for piezometers installed by Utah Water Research Laboratory in 2008; red for monitoring wells by the city of Logan.

however, are rich in carbonate due to the high evapotranspiration rate. Our study site in the semi-arid Cache Valley Basin provides an opportunity to investigate the role of carbonate minerals in affecting As solubility. Studies are needed to understand how geochemical processes, including dissolution of carbonate minerals and re-adsorption and precipitation of Fe(III)/Fe(II) and As(V)/As(III) with altering redox conditions down the profile, affect As solubilization. Understanding As geochemistry and mechanisms of solubilization is crucial for reducing the risk of human exposure to this toxin. The knowledge gained is also applicable to other areas in Utah, and the other semi-arid areas of the Western U.S. with similar underlying basin-fill aquifer systems.

## Research Objectives

The overall research goal was to determine the processes that control the solubilization of geologic As occurring in a shallow aquifer in the Cache Valley Basin, Utah. Findings from this study will help reduce the risk of unintended As solubilization due to irrigation practice, poor groundwater management, and remediation processes. The task specific objectives were:

1) Identify geochemical processes, occurring in two site-oxidized and one site-reduced sediments collected from the Cache Valley Basin, that influence As solubilization and redistribution among solid phases under anoxic conditions using laboratory microcosm studies. The relationship between As solubilization/reduction and Fe reduction were contrasted under conditions with native organic carbon and with the addition of an external carbon and energy source: glucose. Since these sediments are rich in carbonate minerals, the relationship between As solubilization and As mineral distribution with carbonate and Fe oxides were evaluated at the end of the study using sequential chemical extractions;
2) Identify As oxidation states and mineral associations from the soil surface to the depletion zone by evaluating solution chemistry and sediment properties including the use of sequential chemical extractions to define mineral phases. This information was used to elucidate sources and processes affecting As distribution down the profile;
3) Determine the oxidation states and elemental associations of As in the sediments using synchrotron-based spectroscopic imaging methods. This molecular scale

information is needed to confirm macroscale observations under Objectives 1 and 2.

## References

Ahmann, D., Krumholz, L.R., Hemond, H.F., Lovley, D.R., Morel, F.M.M., 1997. Microbial mobilization of arsenic from sediments of the Aberjona Watershed. Environ. Sci. Technol. 31, 2923-2930.

Anawar, H.M., Akai, J., Sakugawa, H., 2004. Mobilization of arsenic from subsurface sediments by effect of bicarbonate ions in groundwater. Chemosphere 54, 753-762.

Anning, D.W., Paul, A.P., McKinney, T.S., Huntington, J.M., Bexfield, L.M., Thiros, S.A., 2012. Predicted nitrate and arsenic concentrations in basin-fill aquifers of the Southwestern United States, Scientific Investigations Report 2012-5065 U.S. Geological Survey, Reston, VA.

Bhattacharya, P., Claesson, M., Bundschuh, J., Sracek, O., Fagerberg, J., Jacks, G., Martin, R.A., Storniolo, A.D., Thir, J.M., 2006. Distribution and mobility of arsenic in the Rio Dulce alluvial aquifers in Santiago del Estero Province, Argentina. Sci. Total Environ. 358, 97-120.

Chowdhury, T.R., Basu, G.K., Mandal, B.K., Biswas, B.K., Samanta, G., Chowdhury, U.K., Chanda, C.R., Lodh, D., Lal Roy, S., Saha, K.C., Roy, S., Kabir, S., Quamruzzaman, Q., Chakraborti, D., 1999. Arsenic poisoning in the Ganges delta. Nature 401, 545-546.

deLemos, J.L., Bostick, B.C., Renshaw, C.E., Sturup, S., Feng, X.H., 2006. Landfill-stimulated iron reduction and arsenic release at the Coakley Superfund Site (NH). Environ. Sci. Technol. 40, 67-73.

Frankenberger, W.T., 2002. Environmental chemistry of arsenic. Marcel Dekker, New York.

Hintze, L.F., 2005. Utah's spectacular geology: how it came to be. Department of Geology, Brigham Young University.

Islam, F.S., Gault, A.G., Boothman, C., Polya, D.A., Charnock, J.M., Chatterjee, D., Lloyd, J.R., 2004. Role of metal-reducing bacteria in arsenic release from Bengal delta sediments. Nature 430, 68-71.

Kim, M.J., Nriagu, J., Haack, S., 2000. Carbonate ions and arsenic dissolution by groundwater. Environ. Sci. Technol. 34, 3094-3100.

Liao, V.H.C., Chu, Y.J., Su, Y.C., Lin, P.C., Hwang, Y.H., Liu, C.W., Liao, C.M., Chang, F.J., Yu, C.W., 2011. Assessing the mechanisms controlling the mobilization of arsenic in the arsenic contaminated shallow alluvial aquifer in the blackfoot disease endemic area. J. Hazard. Mater. 197, 397-403.

Lowe, M., Wallace, J., Bishop, C., Hurlow, H., 2003. Ground-water quality classification and recommended septic tank soil-absorption-system density maps, Utah Geological Survey Special Study 101. Utah Geology Survey, Salt Lake City, UT, p. 31.

McArthur, J.M., Ravenscroft, P., Safiulla, S., Thirlwall, M.F., 2001. Arsenic in groundwater: Testing pollution mechanisms for sedimentary aquifers in Bangladesh. Water Resources Research 37, 109-117.

McLean, J.E., Dupont, R.R., Sorensen, D.L., 2006. Iron and arsenic release from aquifer solids in response to biostimulation. J Environ Qual 35, 1193-1203.

Nickson, R.T., McArthur, J.M., Ravenscroft, P., Burgess, W.G., Ahmed, K.M., 2000. Mechanism of arsenic release to groundwater, Bangladesh and West Bengal. Appl. Geochem. 15, 403-413.

Polizzotto, M.L., Harvey, C.F., Li, G.C., Badruzzman, B., Ali, A., Newville, M., Sutton, S., Fendorf, S., 2006. Solid-phases and desorption processes of arsenic within Bangladesh sediments. Chem. Geol. 228, 97-111.

Ravenscroft, P., McArthur, J.M., Hoque, B.A., 2001. Geochemical and palaeohydrological controls on pollution of groundwater by arsenic. In: W.R. Chappell, C.O. Abernathy, R.L. Calderon (Eds.), 4th Internat. Conf. on Arsenic Exposure and Health Effects, Elsevier Oxford.

Scanlon, B.R., Nicot, J.P., Reedy, R.C., Kurtzman, D., Mukherjee, A., Nordstrom, D.K., 2009. Elevated naturally occurring arsenic in a semiarid oxidizing system, Southern High Plains aquifer, Texas, USA. Appl. Geochem. 24, 2061-2071.

Smedley, P.L., Kinniburgh, D.G., 2002. A review of the source, behaviour and distribution of arsenic in natural waters. Appl. Geochem. 17, 517-568..

Swartz, C.H., Blute, N.K., Badruzzman, B., Ali, A., Brabander, D., Jay, J., Besancon, J., Islam, S., Hemond, H.F., Harvey, C.F., 2004. Mobility of arsenic in a Bangladesh aquifer: Inferences from geochemical profiles, leaching data, and mineralogical characterization. Geochim. Cosmochim. Acta 68, 4539-4557.

Tufano, K.J., Reyes, C., Saltikov, C.W., Fendorf, S., 2008. Reductive processes controlling arsenic retention: revealing the relative importance of iron and arsenic reduction. Environ. Sci. Technol. 42, 8283-8289.

US-EPA, 2001. Fact sheet: Drinking water standard for arsenic, Environmental Protection Agency, Washington, DC. EPA 815-F-00-015.

WHO, 2004. Guidelines for Drinking-Water Quality. Vol I: Recommendations. World Health Organization, Geneva, 515.

# CHAPTER 2

# ARSENIC SOLUBILIZATION AND REDISTRIBUTION UNDER ANOXIC CONDITIONS IN THREE AQUIFER SEDIMENTS FROM A BASIN-FILL AQUIFER IN NORTHERN UTAH


## Abstract

The basin-fill aquifers of the Western U.S. are characterized by arsenic-rich geology. Microcosms were constructed using two site-oxidized sediments and, by contrast, a site-reduced sediment collected from a shallow basin-fill aquifer in the Cache Valley Basin, Northern Utah to evaluate the fate of geologic arsenic under anoxic conditions. Sequential extractions indicated the primary arsenic host mineral was amorphous iron oxides, but 13% to 17% of total arsenic was associated with carbonate minerals. Arsenic was solubilized from the sediments when incubated with groundwater in the presence of native organic carbon. Arsenic solubilization occurred prior to iron reduction rather than the commonly observed co-reactivity. As(V) associated with carbonate minerals was the main source of arsenic released to solution and redistributed onto less soluble minerals. Arsenic reduction occurred only in the site-oxidized sediments. The addition of a carbon and energy source, glucose, resulted in enhanced arsenic solubilization, which was coupled with iron reduction from the site-oxidized sediments. Adding glucose promoted iron reduction that masked the mechanism of arsenic solubilization observed with incubation with groundwater only.

## 1. Introduction

Modeling efforts by the USGS estimated that 43% of the groundwater in basin-fill aquifers of the Southwestern U.S. have As concentrations that exceed the USEPA maximum contaminant level (MCL) for drinking water (10 μg/L).[1] A survey of domestic wells in the Cache Valley Basin located in Northern Utah on the eastern edge of the Basin and Range Province, showed that 23 of the 157 wells tested (15%) had As in excess of the MCL.[2] Concentrations of As above the MCL ranged from 11 to 100 μg/L, with a mean concentration (±SD) of 24.2 ± 18 μg/L. Arsenic released to groundwater has been attributed to the microbial reductive dissolution of host iron (Fe) oxide minerals in the deltaic sediments in Bangladesh and West Bengal.[3-6] Arsenic can also be solubilized through direct microbial reduction of As(V) to the more mobile As(III).[7,8] These redox processes are not limited to deltaic sediments of Southeastern Asia but are also attributed to As solubilization in the Pannonian Basin underlying Hungary, Romania, Croatia, and Serbia, and in the Hetao Basin, Inner Mongolia.[9,10] The diversity of dissimilatory arsenate respiring bacteria (DARB) has been described in ecosystems from Mono and Searles Lakes, CA, aquifers in Cambodia and West Bengal, estuarine sediments from Chesapeake Bay, stream sediments from the Inner Coastal Plains, NJ, and in the Cache Valley basin-fill aquifer, UT.[11-17]

Elevated As in groundwater has been studied in several locations in the arid and semi-arid Western U.S., where processes other than reductive dissolution of Fe oxides and reduction of sorbed As(V) were reported to result in the elevated As concentrations. Evaporative concentration was concluded to cause the high As concentration in groundwater in the Carson Desert, NV and Tulare Basin, CA.[18,19] Busbee et al. [20]

excluded reductive dissolution of Fe oxides but concluded that the As in surficial sediments was leached to the groundwater by infiltrating irrigation waters in the Western Snake River Plain, ID. These previous studies suggest that As solubilization in the West is not controlled exclusively by redox processes.

Basin-fill aquifers, underlying the American West, consistently contain As-bearing sulfides derived from volcanic rock. Contact of As-bearing pyritic materials with the atmosphere and surface water or groundwater results in the oxidative dissolution of As-bearing sulfides resulting in repartitioning of As with Fe oxides, as proposed by Polizzotto et al.[21,22] Variation in redox conditions, due to groundwater fluctuation, inevitably releases this fraction of As, through reductive dissolution of Fe oxides and reduction of sorbed As(V). Carbonate minerals, such as calcite and siderite, also sequester As through adsorption, co-precipitation, and substitution.[23-27] Although carbonate minerals sequester much less As than oxides on a weight basis,[28] they are substantial soil components and are widely distributed in semi-arid subsurface systems, including in the Cache Valley Basin. Our study site provided a unique opportunity to explore the role of carbonate minerals in controlling As solubilization.

The aim of this study was to identify geochemical processes that influence As solubilization and redistribution among aquifer solids under anoxic conditions, simulating a rise in the water table. Irrigation and recharge from the surrounding mountain ranges causes groundwater fluctuations. Groundwater fluctuation causes not only the cycling of redox conditions but also the formation and dissolution of carbonate minerals. Microcosms were set up under anoxic conditions using three sediments, two site-oxidized and one site-reduced sediment, with site groundwater from an As-bearing aquifer in the

Cache Valley Basin. The microbial reduction of Fe and/or As requires organic carbon (OC) to be bioavailable rather than simply being high in concentration.[29] An external carbon source is commonly used in microcosm studies to amplify and expedite microbial processes while exploring As solubilization mechanisms.[30,31] This study emphasized As solubilization in the presence of native OC (NOC), whereas the influence of the external carbon source on the mechanisms of solubilization was evaluated for comparison. Since the As entering groundwater is a health concern, the As in solution in relation to Fe and carbonate chemistry was first explored. Arsenic speciation was then investigated in the solid phase because what is re-adsorbed and precipitated could provide mechanistic information about As biogeochemistry. We revealed decoupled As solubilization and Fe reduction when only NOC was present. The external carbon source stimulated As solubilization from the site-oxidized sediments but overwhelmed the naturally dominant mechanism. The shift in As mineralogy determined from sequential extractions further revealed mechanisms of As solubilization and in particular the role of carbonate minerals in determining the long-term fate of As in these sediments.

## 2. Materials and Methods

**2.1. Study Site.** Detailed geology of the study site has been described by Evans and Oaks.[32] The Cache Valley Basin consists of Lake Bonneville deposits that filled the valley approximately 14,500 years ago. These lacustrine and alluvial deposits overlay the Salt Lake Formation consisting of tertiary sedimentary and volcanic rocks. This formation is exposed in the surrounding Wellsville and Bear River Ranges.[33] Typical of basin-fill systems, the aquifer is recharged by precipitation in the surrounding mountain ranges rather than by the limited rainfall and snow melt in the valley. The study area is on

city-owned property near the Logan City Municipal Landfill (41°44'03N and 111°52'22W) in the center of Cache Valley, where a network of monitoring wells has been sampled for As concentration for over 10 years.

**2.2. Sample Collection.** Thirteen aquifer cores were collected using a Geoprobe driller by direct push technology. Cores were collected from 0.9 m above the water table to 0.6 m below the water table. Water depths at the time of sampling ranged from 0.2 to 2.2 m below ground surface. The plastic sleeves were immediately capped and taped, stored on ice and returned to the Utah Water Research Laboratory, Utah State University, within 2 hours of collection. Each core was divided into three or four sections based on the observed changes in texture and visible redoximorphic features generating a total of 43 sediments samples. All processing was performed in a glove bag filled with 95%$N_2$/5%$H_2$. Sediments were stored under field-moisture conditions in the glove bag in a 15±1˚C constant temperature room during preliminary sediment analyses.

**2.3. Sediment Analyses.** An HCl extraction procedure, described in Appendix A, was performed in the glove bag using 0.5 M HCl to recover Fe from $FeCO_3$, FeS, and a very small fraction of Fe oxides,[34] and As associated with these minerals and other minerals that have similar solubility. The HCl-extractable $Fe_T$ (Fe(II)+Fe(III)) and $As_T$ (As(III)+As(V)) were analyzed using Inductively Coupled Plasma Mass Spectrometry (ICP-MS) with a helium collision cell to minimize polyatomic interferences from ArCl (ICP-MS, Agilent 7500C). The As(III) concentration was determined by Hydride Generation Atomic Absorption Spectrometry (HG-AAS) (Perkin Elmer FIAS mercury/hydride flow injection system with a Perkin Elmer Analyst 800 AAS). The Fe(II) concentration was determined using a Genesys 10Vis spectrophotometer (Thermo

Scientific) at a wavelength of 562 nm after complexing with ferrozine.[35] Analysis for Fe(II) was performed in the glove bag within minutes of sample preparation. As(III) was analyzed within 6 hours of sample preparation.

A series of extractants developed by Amacher[36] was used to recover ionically bound As and As associated with carbonates, Mn oxides, amorphous Fe oxides, crystalline Fe oxides, and the residual phase (Table 2-1). For all sequential extraction methods, there are limitations due to non-selectivity of reagents for a specific solid phase, potential re-adsorption of elements onto other solids phases, and other considerations as discussed by Bacon and Davison.[37] Some extraction procedures for As include a step for removal of ligand-exchangeable As using a phosphate solution. We emphasized here mineral-associated As and Fe; As and Fe associated with procedure-defined mineral phases may be surface-bound. The Fe and As in the extracts were determined using ICP-MS. Fe(II) and As(III) were analyzed for the first two extraction steps only, since reducing reagents were used thereafter. The first two extraction steps were performed in the glove bag to avoid changes in Fe and As oxidation state.

**Table 2-1. Sequential Extraction Procedure for Determination of As Fractionation in the Sediments**

| Fraction | Extractant | Volume | Extraction conditions | Target phase |
|---|---|---|---|---|
| F1 | 0.05 M $CaCl_2$ | 20mL | 24 hr, shaking, room temperature | Ionically bound |
| F2 | pH 5, 1M $NH_4OAc$ | 25mL | 24 hr, shaking, room temperature | Carbonates |
| F3 | pH 2, 0.01M $NH_2OH.HCl$ | 25mL | 30 min, shaking, room temperature | Mn oxides |
| F4 | 0.25 M $NH_2OH$ + 0.25M HCl | 25mL | 2 hr, shaking, 50°C | Amorphous Fe oxides |
| F5 | 0.2 M Ammonium oxalate + 0.2 M Oxalic acid + 0.1 M Ascorbic acid (fresh) | 35mL | 15min in boiling bath followed by 15 min in ice bath, 1 repetition | Crystalline Fe oxides |
| F6 | $HNO_3$ and $H_2O_2$ | USEPA 3050B | | Insoluble As mainly associated with silicates and sulfides |

The Walkley-Black method was performed to determine the sediment NOC content, and acid addition with $CO_2$ evolution was used to determine carbonate content.[38] pH of the sediments was determined on a 1:1 ratio of solid to deionized water slurry. Particle size distribution was determined by the hydrometer method.[39]

**2.4. Microcosm Study Configuration.** Cluster analysis, using JMP statistical software (JMP 5.01 Statistical Software; SAS Institute, Cary, NC) was used to separate the 43 sediments into three groups based on similar physicochemical properties (Table 2-2). Discriminating variables were HCl extractable As(III), arsenic associated with carbonates and amorphous Fe oxides, and soil properties including NOC and sand content. Since carbonates and amorphous Fe oxides are pools of primary interest, the aquifer solids with carbonates and amorphous Fe oxides associated As, within the 95% confidence interval of each cluster were selected as representative of the cluster for the microcosm study.

Microcosms were constructed using groundwater collected from the site that contains 0.96 μg/L As (100% as As(III)), 193 μg/L Fe (100% as Fe(II)), total alkalinity of 290 mg/L as $CaCO_3$, 8.6 mg/L $SO_4^{2-}$, 188 μg/L $PO_4$-P, and 6.9 mg/L dissolved organic carbon(DOC), a pH of 7.4, and an EC of 483 μS/cm. To construct a microcosm unit, 10-g (equivalent dry weight) of the sediment was mixed with 40 mL of autoclaved and oxygen-free groundwater in a 50 mL sterile polypropylene centrifuge tube (Fisherbrand®).

**Table 2-2. Major Physicochemical Characteristics of Selected Aquifer Solids**

| Cluster No. | Fe associated with carbonates (mg/kg) | HCl extractable As(III) (μg/kg) | As associated with carbonates (μg/kg) | NOC (w/w%) | Sand (w/w%) | As associated with am. Fe oxides (μg/kg) |
|---|---|---|---|---|---|---|
| 1 (n=28) | 99.3 (±17.1) | 225 (±33.0) | 908 ± (150) | 0.18 ± (0.02) | 17.6 ± (5.1) | 2789 ± (561) |
| 2 (n=11) | 91.2 ± (31.3) | 78.2 ± (16.3) | 468 ± (82) | 0.14 ± (0.06) | 32.6 ± (5.6) | 825 ± (215) |
| 3 (n=4) | 1124 ± (698) | 38.2 ± (9.0) | 1106 ± (335) | 0.42 ± (0.07) | 5.83 ± (5.0) | 1070 ± (302) |

The experimental treatments were groundwater and groundwater with glucose, in triplicate. Filter-sterilized glucose was added to the microcosms at a final concentration of 2,000 mg C/L (167 mM C). The selection of glucose as a carbon source was based on the results of previous study in which we used a number of different carbon sources and the highest As reduction was detected in response to glucose addition.[40] Abiotic controls were generated by autoclaving individual centrifuge tubes with 10 g of field moist sediment at 121˚C at 1.1 atm for 1 h, with this procedure repeated after 48 h.[41] Groundwater and glucose were added to these microcosms. The microcosms were capped and placed horizontally in the glove bag at 15˚C in the dark. They were sacrificed at discrete time points over 54 days by separating the aqueous and solid phases by centrifugation at 7,000 x g for 20 min. The supernatant was decanted and filtered through a 0.2 µm nylon filter (Life Science Products, Inc.) for aqueous phase analyses including As and Fe species, as described above. Concentrations of aqueous phase As and Fe were expressed as µg/kg or mg/kg, dry weight basis of the sediment instead of on a volume basis, to normalize the data. The aqueous phase was also analyzed for sulfate by ion chromatography, pH, and EC.

Arsenic and Fe speciation in the incubated solids was determined after 0.5 M HCl extraction at each sampling interval, while the sequential extraction procedure was performed at Day 0 and Day 54 to evaluate changes in As mineralogy over the course of the experiment. As(III) and Fe(II) were determined in the independent HCl extraction and the first two sequential extraction steps. Huang and Kretzschmar have discussed the necessity of preserving the oxidation state of As through the extraction procedure by adding chemicals including mercury chloride.[42] In this study, all processing was

performed in the glove bag except centrifugation. Fe(II) was analyzed using ferrozine immediately in the glove bag. Extracts for As(III) analysis were stored in the glove bag until analyzed by HGAA within 6 h.

A one-way ANOVA was used to determine the significance of the difference between the mean concentration of Fe(II), aqueous phase plus HCl extraction, and of mean As solubilized and reduced over time using JMP (JMP 5.01 Statistical Software; SAS Institute, Cary, NC). Post-hoc testing was performed using Tukey's Honestly Significant Difference (HSD) ($\alpha$=0.05). Since the data analysis involves a multiple comparison, a common, family error rate as described by the HSD is more appropriate than using a standard deviation for determining differences. The common Tukey error rate is a scaled average of the individual values. For the sequential extractions, As and Fe recovered within each step at Day 0 and Day 54 were compared using an independent t-test ($\alpha$=0.05).

## 3. Results and Discussion

**3.1. Sediment Properties.** The three representative sediment samples, NP1, NP3, and NP8 were calcareous (30–55% $CaCO_3$), with pH values from 7.2 to 7.7 (Table 2-3). NP1 and NP3 were site-oxidized sediments, indicated by the orange-brown to dark brown Fe oxides patches and the presence of HCl-extractable Fe(III) (78.9 mg/kg and 400 mg/kg) (Table 2-3). These sediments were low in NOC (0.09% and 0.12%) and high in sand content (33% and 42%). The greenish coloration in NP8 indicated that NP8 was site-reduced. The NOC content of NP8 (0.31%) was approximately three times higher than of NP1 and NP3. Total As content in NP3 (9,470 µg/kg) was approximately twice that in NP1 (4,110 µg/kg) and approximately three times that in NP8 (3,750 µg/kg).

Across the study site total $As_T$ ranged from 1,680 to 16,900 µg/kg, with a mean concentration of 6,530 µg/kg.

The majority of total As in both NP1 and NP3 was associated with Fe oxides (amorphous and crystalline), while the residual phase was the dominant As pool in NP8 (Table 2-4). Although carbonate minerals host less As than Fe oxides**,** the amounts of total As associated with carbonate minerals were high compared with sediments collected from other semi-arid regions.[20,43] Arsenic sequestered by natural calcite occurs primarily as As(V),[25] in agreement with the dominance of As(V) in the carbonate fraction of these sediments (Table 2-4). As(V) was always the dominant oxidation state in HCl-soluble minerals, even for the site-reduced NP8. Crystalline Fe oxides and the residual phase constituted over 86% of the Fe in the three sediments; the remaining Fe was primarily distributed in amorphous Fe oxides (Table A-1 in Appendix A).

**3.2. As Solubilization and Fe Reduction during Incubation with Groundwater.** Addition of groundwater (Day 0) to the sediments resulted in immediate release of $As_T$ to solution (Figure 2-1 A-C) equivalent in concentration to the ionically bound $As_T$, as defined by chemical extraction (Table 2-1). With incubation, the concentration of $As_T$ and As(III) in solution increased by Day 6 compared to the concentration on Day 0 (Figure 2-1 A-C). This increase, however, was not accompanied by discernible Fe reduction, since there was no detectable increase of Fe(II) associated with the solids or in solution, indicating the release of $As_T$ and As(III) was not due to the reductive dissolution of Fe minerals. Others reporting the decoupling of As and Fe reactivity have ignored the amount of Fe(II) produced that is re-sorbed to surface,[40,44]

## Table 2-3. Major Chemical Characteristics of Selected Sediments

| Sample | Depth | pH | NOC | Carbonate | Clay | Sand | Total | | HCl Extraction | | | |
|---|---|---|---|---|---|---|---|---|---|---|---|---|
| | m | | (w/w%) | (w/w%) | (w/w%) | (w/w%) | Fe (mg/kg) | As (µg/kg) | Fe(III) (mg/kg) | Fe(II) (mg/kg) | As(V) (µg/kg) | As(III) (µg/kg) |
| NP3 (Cluster 1) | 3.1-3.6 | 7.4 | 0.12 | 39.3 | 19 | 41.8 | 12,000 | 9,470 | 400 | 14.2 | 2550 | 294 |
| NP1 (Cluster 2) | 2.7-3.4 | 7.2 | 0.09 | 28.8 | 21.7 | 33.2 | 13,100 | 4,110 | 78.9 | 129 | 811 | 57.2 |
| NP8 (Cluster 3) | 4.7-4.9 | 7.7 | 0.31 | 55.1 | 30 | 15.6 | 14,700 | 3,750 | ND[b] | 2420 | 499 | 38 |

[b]ND, non-detectable

## Table 2-4. The Distribution of Arsenic among Solid Phases in Selected Sediments

| Sample | Ionically bound | | | Carbonates | | | Mn oxides | | Amorphous Fe oxides | | Crystalline Fe oxides | | Residual | |
|---|---|---|---|---|---|---|---|---|---|---|---|---|---|---|
| | % of total As | As(V) µg/kg | As(III) µg/kg | % of total As | As(V) µg/kg | As(III) µg/kg | % of total As | µg/kg | % of total As | µg/kg | % of total As | µg/kg | % of total As | µg/kg |
| NP3 | 0.30% | 10.7 | 1.56 | 13% | 499 | 33.9 | 5.40% | 222 | 28% | 1,160 | 34% | 1,390 | 19% | 791 |
| NP1 | 0.68% | 63.3 | 1.1 | 14% | 1,300 | 39.7 | 6.30% | 597 | 34% | 3,280 | 36% | 3,420 | 8.20% | 775 |
| NP8 | 1.60% | 32.7 | 27.8 | 17% | 529 | 131 | 2.60% | 99 | 26% | 1,010 | 15% | 581 | 38% | 1,470 |

underestimating the rate and extent of Fe reduction.[45] However, in this present study, there was no discernible Fe reduction in the solution or on the solid phase until Day 12 (NP1), Day 25 (NP3), and Day 54 (NP8), but $As_T$ was released to solution by Day 6. The decoupled As solubilization and Fe reduction indicated that As solubilization was not exclusively limited by Fe reduction in these studied sediments. The initial release of $As_T$ was probably due to desorption of As or dissolution of As-containing non Fe minerals. The desorption of As can be attributed to bicarbonate formed during incubation. Bicarbonate ion is reported to result in As solubilization through competitive sorption.[46,47] Over the 54-day incubation period, the pH decreased from 8.7±0.02 to 7.7±0.03 in the microcosms of the three sediments (Figure A-1). Geochemical modeling (MINEQL+ 4.6, Environmental Research Software) with solution phase ion constituents indicated carbonates and Fe oxides remained as solid phases in this pH range; the As released to solution was not exclusively due to dissolution of minerals with decreasing pH.

The increase in As(III) in solution by Day 6 was not due exclusively to the desorption of surface-bound As(III) or release of As(III) associated with carbonate minerals, since the concentration of As(III) in solution exceeded the concentration of As(III) associated with these two pools in the original NP1 and NP3 sediments (Table 2-4). NP3, for example, initially had 39.7±6.9 μg/kg As(III) associated with the first two extraction steps; by Day 6 the concentration of As(III) in solution was equivalent to 131±13.0 μg/kg. From Day 0 to Day 6, the percentage of As(III) in solution increased from 32% for NP1 and 18% for NP3 to 100% (Figure 2-1 A & B), indicating that the As(V) was reduced to As(III) more likely on the solid phase; soluble As(V) should be

observed at Day 6 if As(V) was released to solution prior to reduction. Microbial activity has been shown to be necessary for As(V) reduction even when the Eh is sufficiently low for As(III) dominance.[48] We attempted to establish abiotic controls but the autoclaving process was not successful in eliminating all spore-forming bacteria. Other microcosm studies have shown that As reduction is minimal in sterilized control samples,[14,49] although there have been reports of limited abiotic reduction of As(V) under specific conditions.[50,51] However, even without abiotic controls, the microbial reduction of As(V), independent of Fe reduction, was evident.[11] Dissimilatory arsenate respiring bacteria (DARB) were present in these microcosms.[11] DARB carrying the arsenate respiring reductase coding gene (arrA) are capable of reducing the As in both solution and solid phases.[52,53]

After the initial lag phase for Fe reduction, NP1 and NP3 showed co-occurrence of Fe reduction and As solubilization (primarily As(V) since As(III) leveled off as shown in Figure 2-1 A&B), supporting the mechanism of As release with the reductive dissolution of Fe oxides.[3,28] Microcosm studies using sediments from West Bengal and Taiwan have shown increased Fe reduction with increased solution phase As(III).[17,30,31] In this study, solution phase As(V) increased, but the As(III) reached steady-state conditions; As(III) was either precipitated or sequestered by the solid phase, or production of As(III) stopped. Further exploration of solid phase As will distinguish these processes, as discussed below.

In NP8, the concentration of As(III) in solution equaled the ionically bound As(III) and approximately half of the carbonate-bound As(III), suggesting that the occurrence of As(III) in the solution may be due to As(III) released from these pools. Although

laboratory-imposed reducing conditions produced Fe(II) after Day 25 in this site-reduced sediment, there was no evidence of further As reduction with incubation. There were bacteria with the arrA gene in NP8 after incubation, as in NP1 and NP3;[11] the potential for As reduction existed but was not observed.

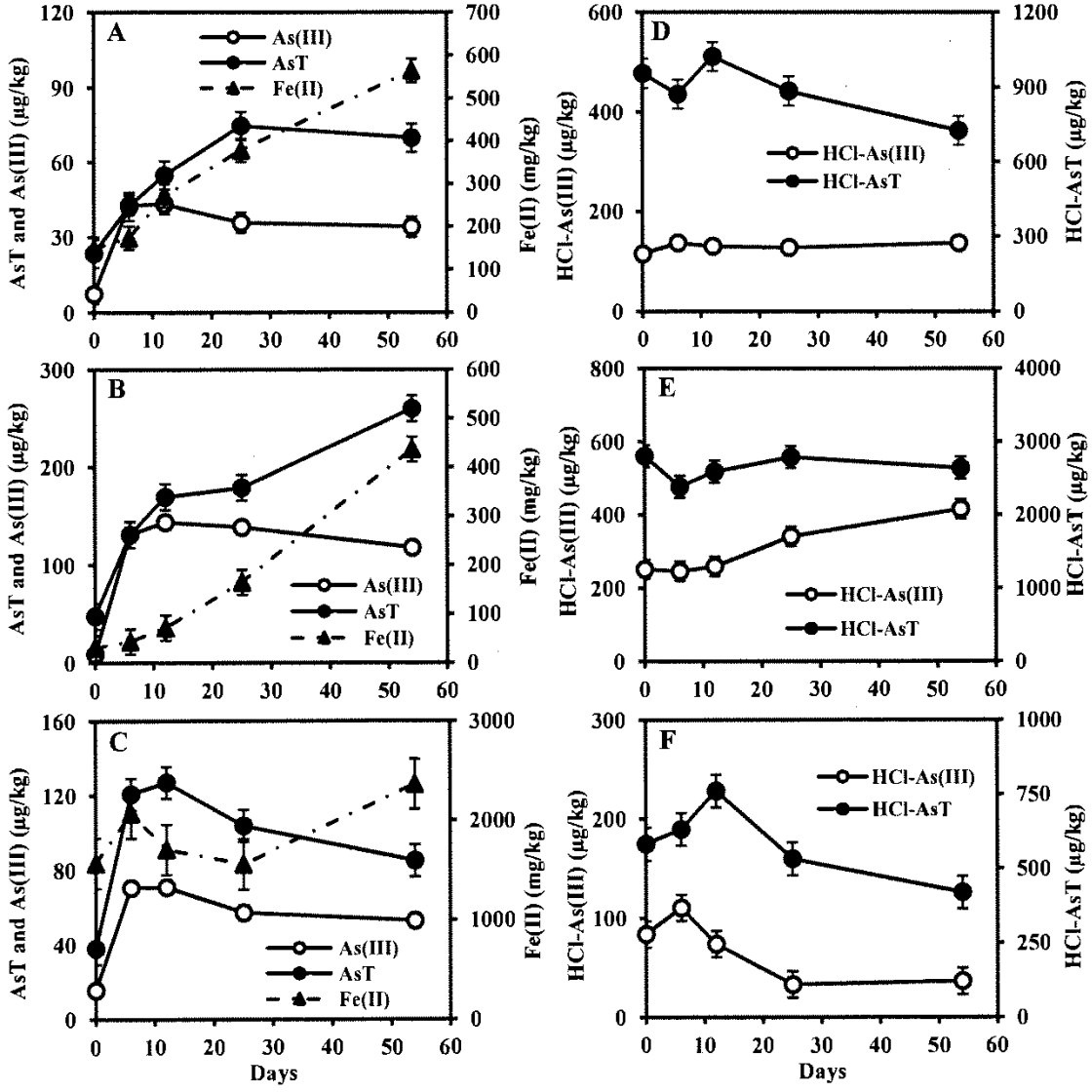


**Figure 2-1.** Arsenic solubilization and Fe reduction (Fe(II) in solution + extractable with HCl) in microcosms containing the three sediments A) NP1, B) NP3, and C) NP8 incubated with groundwater. Arsenic speciation in the 0.5 M HCl extractable solid phase in the three sediments D) NP1, E) NP3, and F) NP8. Error bars represent Tukey HSD ($\alpha$=0.05).

The As solubilization, and reduction in NP1 and NP3, without adding a carbon source observed in this study has also been observed in the field and in other laboratory microcosm studies.[9,30,31,54] The NOC content in these sediments was low (≤0.3%), but the bioavailability was sufficient to drive the microcosms to sulfate reducing conditions (Figure A-2). In NP3 the decrease in sulfate was not as rapid as in NP1 and NP8 because NP3 was relatively rich in HCl extractable Fe(III), presumably bioavailable, which suppresses sulfate reduction in sediments.[55] The NOC at the study site was, at least partially, labile, driving Fe, As, and sulfate reduction reactions and As solubilization.

**3.3. Changes in Solid Phase As with Groundwater Treatment.** Solution phase As(V) and As(III) may be re-adsorbed by the solid phase or may form precipitates. Solid phase As must be investigated over time to understand the fate of As in groundwater systems, although such studies have seldom been reported in previous microcosm studies.[15,40,45] Aqueous phase As(III) in NP3 reached steady-state conditions (Figure 2-1 B) and may lead one to conclude that reduction of As(V) only occurred within the first sampling interval. HCl extractable As(III), however, continued to increase with time (Figure 2-1 E); As(III) was produced but was accumulated in the solid phase. Because this accumulation co-occurred with the production of Fe(II), after Day 12, the As(III) sink may be newly formed Fe(II) minerals. Ahmann et al.[7] suggested that the solid sink of aqueous As(III) may be siderite, $FeCO_3$. The accumulation of As(III) in the solid phase may also be due to the direct enzymatic reduction of As(V) on the solid phase by DARB.[56] The reduction of As(V) at the mineral surfaces facilitates As solubilization,[7,8,56] but the As(III) produced in NP3 remained on the solid phase. In contrast, no discernible change occurred in the HCl-extractable As(III) in NP1, the other site-oxidized sediment

(Figure 2-1 D), indicating As reduction was limited to the aqueous phase for this sediment. The As(V) associated with minerals in NP1 appeared to not be as bioavailable to its native microbe community as that in NP3, as indicated by the lack of As(III) production in the solid phase of NP1 (Figure 2-1 D).

The HCl-extractable $As_T$ and As(III) followed a similar pattern with time in NP8 (Figure 2-1 F). In this site-reduced sediment, $As_T$ had precipitated as non-HCl-soluble minerals, such as crystalline Fe oxides and/or pyrite ($FeS_2$), supported by sequential extraction (Table 2-4). The depleted sulfate concentration (Figure A-2) indicated more complete bacterial sulfate reduction in NP8. Sulfide may occur in the NP8 microcosm, thereby forming more $FeS_2$ which was reported to sequester As.[57]

**3.4. The Redistribution of As and Fe in the Mineral Phase.** The redistribution of As(III) and As(V) was examined by comparing significant changes, as determined using a t-test, in aqueous and mineral phases defined by sequential extraction and 0.5 M HCl extraction between Day 0 and Day 54 (Figure 2-2 A-C). Distinguishing the oxidation state of As was possible in extracts for ionically bound, acetate-, and HCl-soluble defined fractions. The other extractants used reducing reagents for dissolving Mn and Fe oxides. The acetate extraction may also dissolve Ca and Mg arsenate,[58] but the procedure is relatively specific to the dissolution of carbonate minerals,[59] with an exception of siderite ($FeCO_3$). Heron et al.[34] reported that 1 M sodium acetate at pH 5 only extracted 1.1% of total Fe(II) in siderite. Thus the 0.5M HCl solution extracts As associated with the first two extraction steps and parts of As associated with FeS, $FeCO_3$, and HCl-soluble Fe oxides, i.e., the portion of Fe oxides that are solubilized without addition of a reducing reagent such as hydroxylamine hydrochloride. Arsenic associated with FeS, $FeCO_3$, and

HCl-soluble Fe oxides was therefore operationally defined as the difference between As(III) or As(V) in the HCl extract and in the sum of the ionically bound and carbonate-associated extracts. The less soluble Fe oxide fraction was defined as the As remaining in

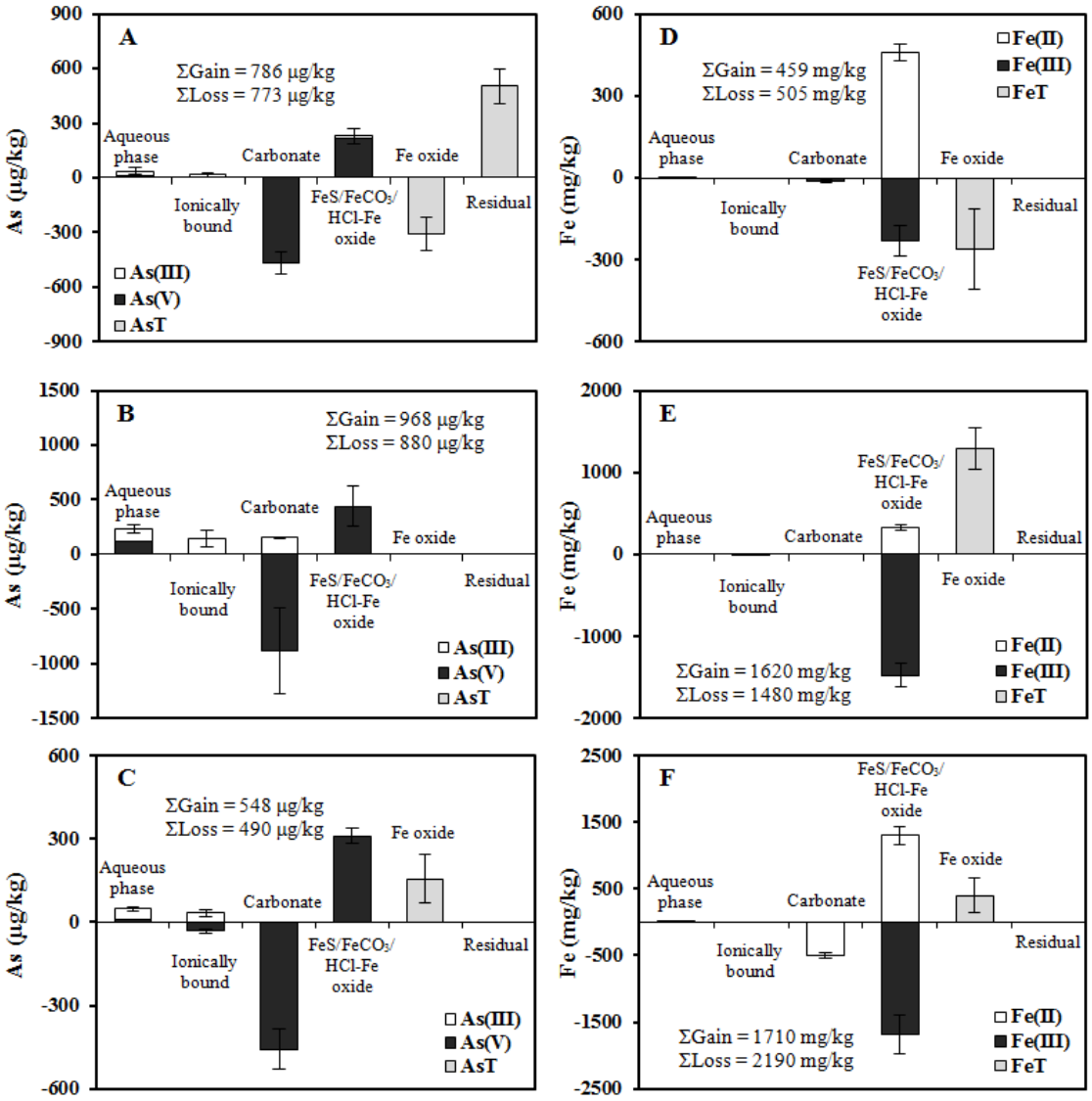


**Figure 2-2.** Redistribution of As and Fe in microcosms made from three sediments and groundwater after 54 days of incubation. The change of As or Fe in each pool is shown after 54-day of incubation; a bar above the x-axis indicates a gain and a bar below the x-axis indicates a loss that is statistically significant indicated by a T-test (α=0.05). As: A) NP1, B) NP3, and C) NP8, and Fe: D) NP1, E) NP3, and F) NP8. Error bars represent one standard deviation of triplicate microcosms.

the hydroxylamine hydrochloride-HCl extract minus the As in the HCl extract plus the As in the crystalline Fe oxides extract. The mass balance of As and Fe, as loss and gain from the different mineral phases, was within 10%, except for Fe in NP8 (Figure 2-2 A-F).

The As, all as As(V), was removed from mineral phases soluble in 1 M acetate buffer (pH 5) (Figure 2-2 A-C). The dissolution of carbonate minerals with the acetate buffer would remove As both associated with the surface and incorporated into the structure of carbonate minerals.[60] Acetate is not an effective ligand for removal of As from ligand exchange sites; As(V) surface bound to non-acetate soluble minerals, such as Fe oxides, would not be removed by this extractant. These observations defined the major portion of As that is subject to solubilization in these sediments as carbonate-associated As, not amorphous Fe oxides. As(V) was reduced and the produced As(III) was associated with the aqueous phase, ionically bound to solid surfaces, and also associated with carbonate minerals (NP3) and FeS/$FeCO_3$/HCl-Fe oxide pool (NP1, NP3, and NP8). As(V) from the carbonates was also redistributed into the more insoluble minerals in NP1 and NP8, but the oxidation state of this As could not be distinguished.

Fe(II) increased in the FeS/$FeCO_3$/HCl-Fe oxide pool in all three sediments (Figure 2-2 D-F), indicating Fe(II)-bearing FeS and/or $FeCO_3$ formed with incubation. FeS and/or $FeCO_3$ accumulated As in the solid phase as illustrated by the simultaneous gain of $As_T$ (Figure 2-2). By assuming that half of the decreased sulfate, which is the difference between Day 0 and Day 54, was converted to sulfide, FeS was supersaturated in all three microcosms (Table 2-5). The saturation condition of $FeCO_3$ was unknown since bicarbonate was not determined. The formation of $FeCO_3$ was a reasonable

**Table 2-5. Calculation for Ion Activity Product of $Fe^{2+}$ and $S^{2-}$ in the Three Microcosms**

| Sample | [Fe2+] M | Estimated [$S^{2-}$] M | [$Fe^{2+}$]*[$S^{2-}$] | $K_s$ of FeS |
|---|---|---|---|---|
| NP1 | $0.95x10^{-4}$ | $1.67x10^{-4}$ | $1.59x10^{-8}$ | |
| NP3 | $1.01x10^{-4}$ | $0.95x10^{-4}$ | $0.95x10^{-8}$ | $8x10^{-19}$ |
| NP8 | $1.19x10^{-4}$ | $1.63x10^{-4}$ | $1.94x10^{-8}$ | |

assumption given that the sediments were alkaline and $CO_2$ was produced during incubation due to microbial activity. The major solid phase loss of Fe(III) was from the HCl-Fe oxide (FeS and $FeCO_3$ were excluded since they contain only Fe(II)) for all three sediments. This process, however, was not accompanied by a loss of As from this pool. The microbial dissolution of Fe oxides, with the metabolism of NOC, did not contribute to the solubilization of As from the sediments.

**3.5. Influence of Glucose Addition on As Solubilization.** The addition of glucose stimulated As solubilization from NP1 (Figure 2-3 A); the solution phase As reached 138±32.0 μg/kg at Day 6, compared to the maximal solution $As_T$ concentration of 74.6±3.9 μg/kg without glucose addition (Figure 2-1 A). The stimulated $As_T$ solubilization was concomitant with enhanced Fe reduction. Similarly in NP3, the $As_T$ solubilization and Fe(III) reduction were both stimulated by glucose (Figure 2-3 B), with three times the soluble $As_T$ concentration and four times the Fe reduction observed as compared to the microcosms without glucose addition. The solubilized $As_T$ was dominated by As(III) at all sampling intervals after Day 0 in both NP1 and NP3 (Figure 2-3 A & B). Glucose has been observed to successfully stimulate As solubilization,[61,62] as do other carbon sources, including acetate, lactate, and whey.[15,31,40,54] The lag between $As_T$ solubilization and Fe reduction observed without glucose was overwhelmed by

glucose addition, which significantly promoted Fe reduction. The glucose addition produced coupled $As_T$ solubilization and Fe reduction which would fit the most-described mechanism of As solubilization in the literature,[3-6] but it concealed As solubilization independent of Fe as observed in this study in the absence of glucose. The addition of glucose in microcosm studies may result in overestimating the importance of Fe oxides in As solubilization and over-predicting As solubilization, because high rates of microbial dissolution of Fe oxides would be rare under typical subsurface environments where labile carbon sources are limited. Glucose stimulated a population of fermenting bacteria in this microcosm study.[11] Fermenting bacteria have been shown to reduce Fe(III) via electron shuttling compounds,[63-65] increasing the bioavailability of Fe(III) within sediments.

As observed by others,[17,31,54] glucose addition enhanced the proportion of As(III) in solution, whereas As(V) was the dominant species in the groundwater only treatment (Figure 2-1 A & B). Enhanced production of solid phase As(III) (Figure 2-3 D & E) in NP1 and NP3 may contribute to As solubilization. Microbial reduction of As(V) to As(III) faciliated As solubilziation since As(III) has a lower affinity for solid surfaces.[7,8,56] Another explanation is that the solubilized As(V) was reduced to As(III) in solution and then proportionally and consistently partitioned between the solid and solution phases. The enhanced reducing conditions following glucose addition support the microbially mediated reduction of As, which is further supported by the increasing population of DARB after 54 days of incubation.[11]

Glucose addition caused an unanticipated attenuation of As solubilization from the NP8 sediment. Soluble As decreased after incubation started, reaching a

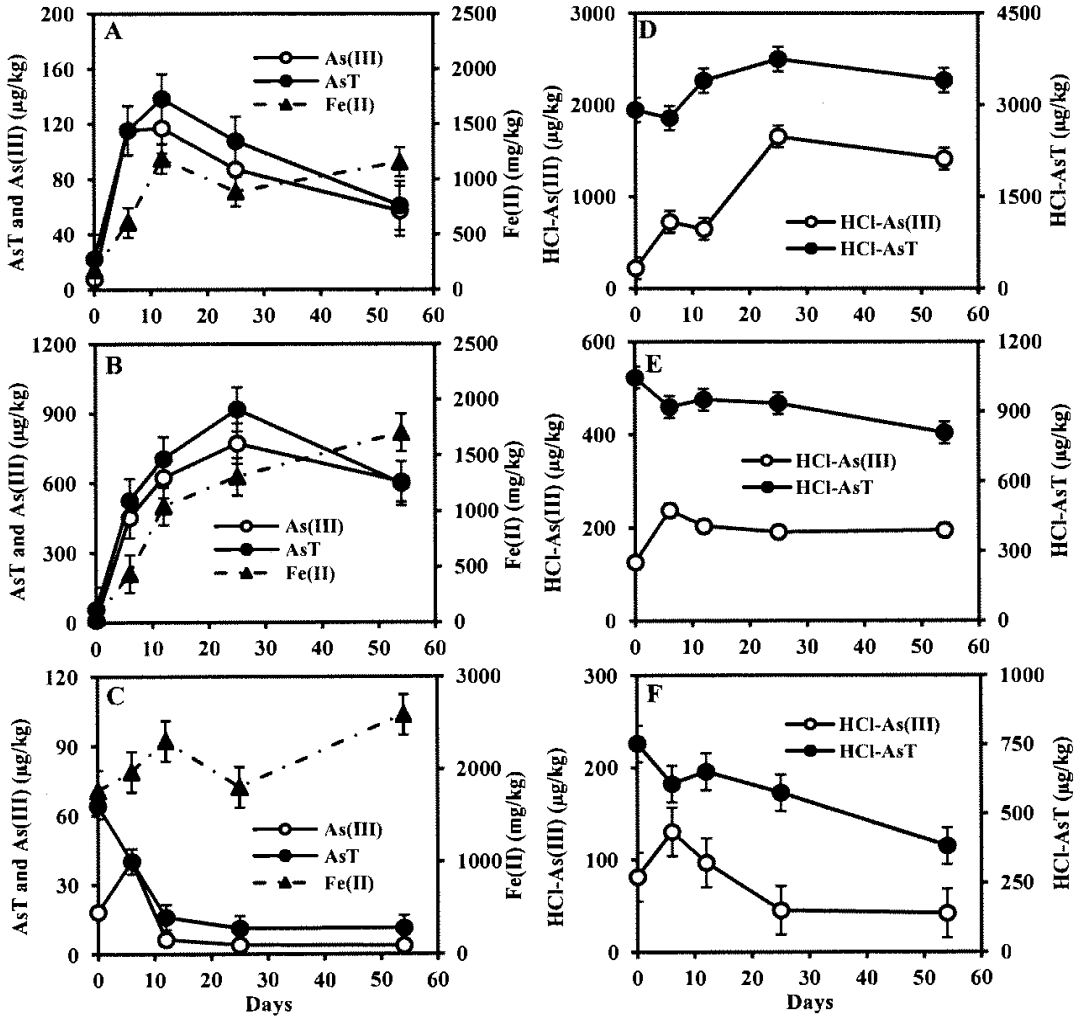


**Figure 2-3.** Arsenic solubilization and Fe reduction in microcosms containing the three sediments A) NP1, B) NP3, and C) NP8 incubated with groundwater plus glucose amendment. Arsenic speciation in the 0.5 M HCl extractable solid phase in the three sediments D) NP1, E) NP3, and F) NP8. Error bars represent Tukey HSD (α=0.05).

concentration as low as 11.2±3.8 µg/kg at Day 25 (Figure 2-3 C). The amount of ionically bound As (Table 2-1) was equal to the maximal amount of As in the aqueous phase. The simplest assumption would be that only the ionically bound As was released and glucose addition inhibited further solubilization (Figure 2-3 F). The HCl extractability of $As_T$ and As(III) in NP8 decreased to the level observed in the groundwater alone treatment (Figure 2-1 F); the cessation of As solubilization was not

due to the association of As with HCl-soluble minerals but with the more insoluble minerals.

The loss of As from carbonate minerals in the three sediments was not enhanced by the addition of glucose (Figure 2-4 A-C) compared to groundwater (Figure 2-2 A-C); solubilization of As(V) from the carbonates was not associated with the stimulation of the microbial population. The enhanced As solubilization in NP1 and NP3 therefore involved the loss of As from other mineral phases. In NP3, the major loss of As was from Fe oxides, which was also the main mineral phase for loss of Fe (Figure 2-4 E). The microbially produced As(III) was redistributed onto minerals surfaces and associations with carbonates and the $FeS/FeCO_3$/HCl-Fe oxide pool. Due to excessive error with the extractions steps in NP1 (mass balance was 72%) other contributing solid phases were not discernible (Figure 2-4 D).

Although enhanced microbial activity caused a two-fold decrease in the pH of the microcosms after 54 days of incubation (Figure A-1), this circumneutral pH should not significantly contribute to the dissolution of Fe oxides. Furthermore, pH-related processes do not explain the dramatic increases in aqueous and solid phase Fe(II) and As(III). The utilization of glucose by fermenting microbes produced electron shuttles and chelating agents that enable the microbes to utilize Fe in more crystalline Fe oxides or even in the residual phase.[40] An indicator of redox conditions was sulfate reduction (Figure A-2). With groundwater only, the microcosms moved beyond Fe reduction to sulfate reducing conditions by Day 25; the Fe was not bioavailable in these carbon limited systems. With glucose addition, sulfate reduction was delayed, as microbes accessed Fe(III) minerals through utilization of electron shuttles. The utilization of Fe(III) within Fe oxides in the

site-oxidized sediments caused loss of Fe in this pool (Figure 2-4 D-F). Incubation of NP8 with glucose caused dissolution of insoluble Fe-bearing minerals, i.e., in the residual phase, which was accompanied by a major loss of As (Figure 2-4 C & F). The As was sequestered by crystalline Fe oxide type minerals limiting solubilization of As.

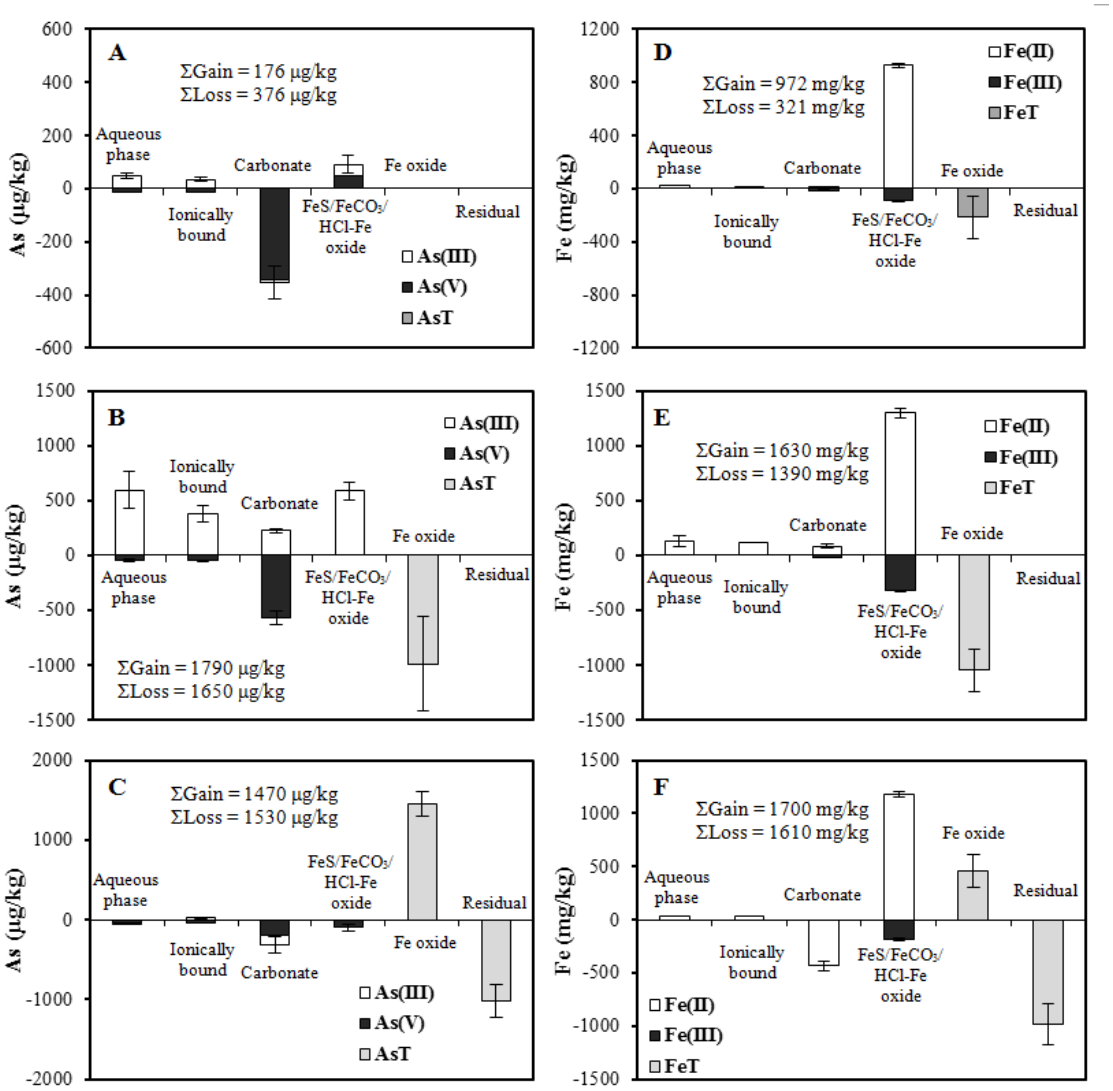


**Figure 2-4.** Redistribution of As and Fe in microcosms made from three sediments and groundwater plus glucose after 54 days of incubation. The column shows the change of As or Fe in each pool after 54-day of incubation; a bar above x-axis indicates a gain and a bar below x-axis indicates a loss that is statistically significant indicated by T-test (α=0.05). As: A) NP1, B) NP3, and C) NP8, and Fe: D) NP1, E) NP3, and F) NP8. Error bars represent standard deviation.

## 4. Environmental Relevance

Carbon addition dramatically changed the dominant As speciation in the aqueous phase to the more toxic As(III). Soil-based waste treatment, biostimulation of aquifer remediation, domestic development, and irrigation can increase carbon loading in the subsurface, resulting in inadvertent As solubilization. The vulnerability of an aquifer to As reduction and mobilization needs to be investigated before any carbon-importing practice is performed.

Carbonate associated As contributed significantly to As solubilization in solids from this basin-fill aquifer. Aquifers that contain As-bearing deposits in semi-arid environments are at risk of producing groundwater that contain As at concentrations exceeding the MCL without the input of an exogenous carbon source, even in systems that have low organic carbon. Adding a carbon and energy source stimulates microbial activity and promotes extensive Fe reduction, masking the mechanisms of As solubilization and reduction that would occur under natural conditions of seasonal groundwater fluctuations.

## References

(1) Anning, D. W.; Paul, A. P.; McKinney, T. S.; Huntington, J. M.; Bexfield, L. M.; Thiros, S. A. *Predicted nitrate and arsenic concentrations in basin-fill aquifers of the Southwestern United States*; Scientific Investigations Report 2012-5065 U.S. Geological Survey: Reston, VA, 2012. http://pubs.usgs.gov/sir/2012/5065/pdf/sir20125065.pdf.

(2) Lowe, M.; Wallace, J.; Bishop, C.; Hurlow, H. *Ground-water quality classification and recommended septic tank soil-absorption-system density maps*; Utah Geological Survey Special Study 101; Utah Geology Survey: Salt Lake City, UT, 2003. http://geology.utah.gov/online/ss/ss-101/ss-101text.pdf.

(3) Nickson, R. T.; McArthur, J. M.; Ravenscroft, P.; Burgess, W. G.; Ahmed, K. M. Mechanism of arsenic release to groundwater, Bangladesh and West Bengal. *Appl. Geochem.* **2000,** *15* (4), 403-413.

(4) Ravenscroft, P.; McArthur, J.; Hoque, B. Geochemical and palaeohydrological controls on pollution of groundwater by arsenic. In *Arsenic Exposure and Health Effects IV*; Chappell, W. R., Abernathy, C. O., Calderon, R. L., Eds.; Elsevier Science Ltd.: Oxford, 2001; pp 53-77.

(5) Swartz, C. H.; Blute, N. K.; Badruzzman, B.; Ali, A.; Brabander, D.; Jay, J.; Besancon, J.; Islam, S.; Hemond, H. F.; Harvey, C. F. Mobility of arsenic in a Bangladesh aquifer: Inferences from geochemical profiles, leaching data, and mineralogical characterization. *Geochim. Cosmochim. Acta* **2004,** *68* (22), 4539-4557.

(6) McArthur, J. M.; Banerjee, D. M.; Hudson-Edwards, K. A.; Mishra, R.; Purohit, R.; Ravenscroft, P.; Cronin, A.; Howarth, R. J.; Chatterjee, A.; Talukder, T.; Lowry, D.; Houghton, S.; Chadha, D. K. Natural organic matter in sedimentary basins and its relation to arsenic in anoxic ground water: the example of West Bengal and its worldwide implications. *Appl. Geochem.* **2004,** *19* (8), 1255-1293.

(7) Ahmann, D.; Krumholz, L. R.; Hemond, H. F.; Lovley, D. R.; Morel, F. M. M. Microbial mobilization of arsenic from sediments of the Aberjona Watershed. *Environ. Sci. Technol.* **1997,** *31* (10), 2923-2930.

(8) Tufano, K. J.; Reyes, C.; Saltikov, C. W.; Fendorf, S. Reductive processes controlling arsenic retention: revealing the relative importance of iron and arsenic reduction. *Environ. Sci. Technol.* **2008,** *42* (22), 8283-8289.

(9) Rowland, H. A. L.; Omoregie, E. O.; Millot, R.; Jimenez, C.; Mertens, J.; Baciu, C.; Hug, S. J.; Berg, M. Geochemistry and arsenic behaviour in groundwater resources of the Pannonian Basin (Hungary and Romania). *Appl. Geochem.* **2011,** *26* (1), 1-17.

(10) Guo, H. M.; Yang, S. Z.; Tang, X. H.; Li, Y.; Shen, Z. L. Groundwater geochemistry and its implications for arsenic mobilization in shallow aquifers of the Hetao Basin, Inner Mongolia. *Sci. Total Environ.* **2008,** *393* (1), 131-144.

(11) Mirza, B. S.; Muruganadam, S.; Meng, X.; Sorensen, D. L.; Dupont, R. R.; McLean, J. E. Arsenic(V) reduction in relation to iron(III) transformation and molecular characterization of the structural and functional microbial community in sediments of a Northern Utah, basin-fill aquifer. *Appl. Environ. Microbiol.* **2014**, AEM. 00240-14.

(12) Song, B.; Chyun, E.; Jaffe, P. R.; Ward, B. B. Molecular methods to detect and monitor dissimilatory arsenate-respiring bacteria (DARB) in sediments. *FEMS Microbiol. Ecol.* **2009,** *68* (1), 108-117.

(13) Barringer, J. L.; Mumford, A.; Young, L. Y.; Reilly, P. A.; Bonin, J. L.; Rosman, R. Pathways for arsenic from sediments to groundwater to streams: Biogeochemical processes in the Inner Coastal Plain, New Jersey, USA. *Water Res.* **2010,** *44* (19), 5532-5544.

(14) Lear, G.; Song, B.; Gault, A.; Polya, D.; Lloyd, J. Molecular analysis of arsenate-reducing bacteria within Cambodian sediments following amendment with acetate. *Appl. Environ. Microbiol.* **2007,** *73* (4), 1041.

(15) Pederick, R. L.; Gault, A. G.; Charnock, J. M.; Polya, D. A.; Lloyd, J. R. Probing the biogeochemistry of arsenic: Response of two contrasting aquifer sediments from Cambodia to stimulation by arsenate and ferric iron. *J. Environ. Sci. Health Part A* **2007,** *42* (12), 1763-1774.

(16) Kulp, T.; Hoeft, S.; Miller, L.; Saltikov, C.; Murphy, J.; Han, S.; Lanoil, B.; Oremland, R. Dissimilatory arsenate and sulfate reduction in sediments of two hypersaline, arsenic-rich soda lakes: Mono and Searles Lakes, California. *Appl. Environ. Microbiol.* **2006,** *72* (10), 6514-6526.

(17) Hery, M.; van Dongen, B. E.; Gill, F.; Mondal, D.; Vaughan, D. J.; Pancost, R. D.; Polya, D. A.; Lloyd, J. R. Arsenic release and attenuation in low organic carbon aquifer sediments from West Bengal. *Geobiol.* **2010,** *8* (2), 155-168.

(18) Welch, A. H.; Lico, M. S. Factors controlling As and U in shallow ground water, southern Carson Desert, Nevada. *Appl. Geochem.* **1998,** *13* (4), 521-539.

(19) Fujii, R.; Swain, W. C. *Areal distribution of selected trace elements, salinity, and major ions in shallow ground water, Tulare Basin, Southern San Joaquin Valley, California*; Water-Resources Investigations Report 95-4048; U.S. Geological Survey: Sacramento, CA, 1995. http://wwwrcamnl.wr.usgs.gov/Selenium/Library_articles/FujiiSwain_text.pdf.

(20) Busbee, M. W.; Kocar, B. D.; Benner, S. G. Irrigation produces elevated arsenic in the underlying groundwater of a semi-arid basin in Southwestern Idaho. *Appl. Geochem.* **2009,** *24* (5), 843-859.

(21) Polizzotto, M. L.; Harvey, C. F.; Sutton, S. R.; Fendorf, S. Processes conducive to the release and transport of arsenic into aquifers of Bangladesh. *Proc. Natl. Acad. Sci.USA* **2005,** *102* (52), 18819-18823.

(22) Polizzotto, M. L.; Harvey, C. F.; Li, G. C.; Badruzzman, B.; Ali, A.; Newville, M.; Sutton, S.; Fendorf, S. Solid-phases and desorption processes of arsenic within Bangladesh sediments. *Chem. Geol.* **2006,** *228* (1-3), 97-111.

(23) So, H. U.; Postma, D.; Jakobsen, R.; Larsen, F. Sorption and desorption of arsenate and arsenite on calcite. *Geochim. Cosmochim. Acta* **2008,** *72* (24), 5871-5884.

(24) Costagliola, P.; Bardelli, F.; Benvenuti, M.; Di Benedetto, F.; Lattanzi, P.; Romanelli, M.; Paolieri, M.; Rimondi, V.; Vaggelli, G. Arsenic-bearing calcite in natural travertines: Evidence from sequential extraction, μXAS, and μXRF. *Environ. Sci. Technol.* **2013**.

(25) Bardelli, F.; Benvenuti, M.; Costagliola, P.; Di Benedetto, F.; Lattanzi, P.; Meneghini, C.; Romanelli, M.; Valenzano, L. Arsenic uptake by natural calcite: An XAS study. *Geochim. Cosmochim. Acta* **2011,** *75* (11), 3011-3023.

(26) Roman-Ross, G.; Cuello, G. J.; Turrillas, X.; Fernandez-Martinez, A.; Charlet, L. Arsenite sorption and co-precipitation with calcite. *Chem. Geol.* **2006,** *233* (3-4), 328-336.

(27) Jonsson, J.; Sherman, D. M. Sorption of As(III) and As(V) to siderite, green rust (fougerite) and magnetite: Implications for arsenic release in anoxic groundwaters. *Chem. Geol.* **2008,** *255* (1-2), 173-181.

(28) Smedley, P. L.; Kinniburgh, D. G. A review of the source, behaviour and distribution of arsenic in natural waters. *Appl. Geochem.* **2002,** *17* (5), 517-568.

(29) Fendorf, S.; Michael, H. A.; van Geen, A. Spatial and temporal variations of groundwater arsenic in South and Southeast Asia. *Science* **2010,** *328* (5982), 1123-1127.

(30) Liao, V. H. C.; Chu, Y. J.; Su, Y. C.; Lin, P. C.; Hwang, Y. H.; Liu, C. W.; Liao, C. M.; Chang, F. J.; Yu, C. W. Assessing the mechanisms controlling the mobilization of arsenic in the arsenic contaminated shallow alluvial aquifer in the blackfoot disease endemic area. *J. Hazard. Mater.* **2011,** *197*, 397-403.

(31) Islam, F. S.; Gault, A. G.; Boothman, C.; Polya, D. A.; Charnock, J. M.; Chatterjee, D.; Lloyd, J. R. Role of metal-reducing bacteria in arsenic release from Bengal delta sediments. *Nature* **2004,** *430* (6995), 68-71.

(32) Oaks Jr, R. Q.; Smith, K. A.; Janecke, S. U.; Perkins, M. E.; Nash, W. P. Stratigraphy and tectonics of Tertiary strata of southern Cache Valley. *Utah Geol. Assoc. Pub.* **1999,** *27*, 71-110.

(33) Dover, J. H., Geologic Map of the Logan 30’ x 60’ Quadrangle, Cache and Rich Counties, Utah and Lincoln and Uinta Counties, Wyoming, Map I-2210. In *Miscellaneous Investigations Series*, Utah Geological Survey, 2005.

(34) Heron, G.; Crouzet, C.; Bourg, A. C. M.; Christensen, T. H. Speciation of Fe(II) and Fe(III) in contaminated aquifer sediments using chemical-extraction techniques. *Environ. Sci. Technol.* **1994,** *28* (9), 1698-1705.

(35) Lovley, D. R.; Phillips, E. J. P. Availability of ferric iron for microbial reduction in bottom sediments of the fresh-water tidal Potomac River. *Appl. Environ. Microbiol.* **1986,** *52* (4), 751-757.

(36) Amacher, M. C., Nickel, cadmium, and lead. In *Methods of Soil Analysis. Part 3-Chemical Methods.*, Sparks, D.; Page, A.; Helmke, P.; Loeppert, R.; Soltanpour, P.; Tabatabai, M.; Johnston, C.; Sumner, M., Eds. 1996; pp 739-768.

(37) Bacon, J. R.; Davidson, C. M. Is there a future for sequential chemical extraction? *Analyst* **2008,** *133* (1), 25-46.

(38) Sparks, D. L.; Page, A.; Helmke, P.; Loeppert, R.; Soltanpour, P.; Tabatabai, M.; Johnston, C.; Sumner, M., *Methods of Soil Analysis. Part 3-Chemical Methods*. Soil Science Society of America Inc.: Madison, WI, 1996.

(39) Klute, A., *Methods of Soil Analysis. Part 1. Physical and Mineralogical Methods*. American Society of Agronomy, Inc.: Madison, WI, 1986.

(40) McLean, J. E.; Dupont, R. R.; Sorensen, D. L. Iron and arsenic release from aquifer solids in response to biostimulation. *J. Environ. Qual.* **2006,** *35* (4), 1193-1203.

(41) Trevors, J. T. Sterilization and inhibition of microbial activity in soil. *J. Microbiol. Methods* **1996,** *26* (1-2), 53-59.

(42) Huang, J. H.; Kretzschmar, R. Sequential extraction method for speciation of arsenate and arsenite in mineral soils. *Anal. Chem.* **2010,** *82* (13), 5534-5540.

(43) Bhattacharya, P.; Claesson, M.; Bundschuh, J.; Sracek, O.; Fagerberg, J.; Jacks, G.; Martin, R. A.; Storniolo, A. D.; Thir, J. M. Distribution and mobility of arsenic in the Rio Dulce alluvial aquifers in Santiago del Estero Province, Argentina. *Sci. Total Environ.* **2006,** *358* (1-3), 97-120.

(44) Van Geen, A.; Rose, J.; Thoral, S.; Garnier, J. M.; Zheng, Y.; Bottero, J. Y. Decoupling of As and Fe release to Bangladesh groundwater under reducing conditions. Part II: Evidence from sediment incubations. *Geochim. Cosmochim. Acta* **2004,** *68* (17), 3475-3486.

(45) Weber, F. A.; Hofacker, A. F.; Voegelin, A.; Kretzschmar, R. Temperature dependence and coupling of iron and arsenic reduction and release during flooding of a contaminated soil. *Environ. Sci. Technol.* **2010,** *44* (1), 116-122.

(46) Appelo, C. A. J.; Van der Weiden, M. J. J.; Tournassat, C.; Charlet, L. Surface complexation of ferrous iron and carbonate on ferrihydrite and the mobilization of arsenic. *Environ. Sci. Technol.* **2002,** *36* (14), 3096-3103.

(47) Holm, T. R. Effects of $CO_3^{2-}$/bicarbonate, Si, and $PO_4^{3-}$ on arsenic sorption to HFO. *J. Am. Water Works Assoc.* **2002,** *94* (4), 174-181.

(48) Yamaguchi, N.; Nakamura, T.; Dong, D.; Takahashi, Y.; Amachi, S.; Makino, T. Arsenic release from flooded paddy soils is influenced by speciation, Eh, pH, and iron dissolution. *Chemosphere* **2011,** *83* (7), 925-932.

(49) Pearcy, C. A.; Chevis, D. A.; Haug, T. J.; Jeffries, H. A.; Yang, N. F.; Tang, J. W.; Grimm, D. A.; Johannesson, K. H. Evidence of microbially mediated arsenic

mobilization from sediments of the Aquia aquifer, Maryland, USA. *Appl. Geochem.* **2011,** *26* (4), 575-586.

(50) Zobrist, J.; Dowdle, P. R.; Davis, J. A.; Oremland, R. S. Mobilization of arsenite by dissimilatory reduction of adsorbed arsenate. *Environ. Sci. Technol.* **2000,** *34* (22), 4747-4753.

(51) Kocar, B. D.; Herbel, M. J.; Tufano, K. J.; Fendorf, S. Contrasting effects of dissimilatory iron(III) and arsenic(V) reduction on arsenic retention and transport. *Environ. Sci. Technol.* **2006,** *40* (21), 6715-6721.

(52) Oremland, R.; Stolz, J. Arsenic, microbes and contaminated aquifers. *Trends Microbiol.* **2005,** *13* (2), 45-49.

(53) Malasarn, D.; Saltikov, W.; Campbell, K. M.; Santini, J. M.; Hering, J. G.; Newman, D. K. arrA is a reliable marker for As(V) respiration. *Science* **2004,** *306* (5695), 455-455.

(54) Rowland, H. A. L.; Pederick, R. L.; Polya, D. A.; Pancost, R. D.; Van Dongen, B. E.; Gault, A. G.; Vaughan, D. J.; Bryant, C.; Anderson, B.; Lloyd, J. R. The control of organic matter on microbially mediated iron reduction and arsenic release in shallow alluvial aquifers, Cambodia. *Geobiology.***2007,** *5* (3), 281-292.

(55) Lovley, D. R.; Phillips, E. J. P. Competitive mechanisms for inhibition of sulfate reduction and methane production in the zone of ferric iron reduction in sediments. *Appl. Environ. Microbiol.* **1987,** *53* (11), 2636-2641.

(56) Ohtsuka, T.; Yamaguchi, N.; Makino, T.; Sakurai, K.; Kimura, K.; Kudo, K.; Homma, E.; Dong, D. T.; Amachi, S. Arsenic dissolution from Japanese paddy soil by a dissimilatory arsenate-reducing bacterium *Geobacter* sp. OR-1. *Environ. Sci. Technol.* **2013,** *47* (12), 6263-71.

(57) Bostick, B. C.; Fendorf, S. Arsenite sorption on troilite (FeS) and pyrite (FeS2). *Geochim. Cosmochim. Acta* **2003,** *67* (5), 909-921.

(58) Ryu, J. H.; Gao, S. D.; Tanji, K. K. Speciation and behavior of arsenic in evaporation basins, California, USA. *Environ. Earth Sci.* **2010,** *61* (8), 1599-1612.

(59) Tessier, A.; Campbell, P. G. C.; Bisson, M. Sequential extraction procedure for the speciation of particulate trace-metals. *Anal. Chem.* **1979,** *51* (7), 844-851.

(60) La Force, M. J.; Hansel, C. M.; Fendorf, S. Arsenic speciation, seasonal transformations, and co-distribution with iron in a mine waste-influenced palustrine emergent wetland. *Environ. Sci. Technol.* **2000,** *34* (18), 3937-3943.

(61) Corsini, A.; Cavalca, L.; Crippa, L.; Zaccheo, P.; Andreoni, V. Impact of glucose on microbial community of a soil containing pyrite cinders: Role of bacteria in arsenic mobilization under submerged condition. *Soil Biol. Biochem.* **2010,** *42* (5), 699-707.

(62) Duan, M. Y.; Xie, Z. M.; Wang, Y. X.; Xie, X. J. Microcosm studies on iron and arsenic mobilization from aquifer sediments under different conditions of microbial activity and carbon source. *Environ. Geol.* **2009,** *57* (5), 997-1003.

(63) Akob, D. M.; Mills, H. J.; Gihring, T. M.; Kerkhof, L.; Stucki, J. W.; Anastacio, A. S.; Chin, K. J.; Kusel, K.; Palumbo, A. V.; Watson, D. B.; Kostka, J. E. Functional diversity and electron donor dependence of microbial populations capable of U(VI) reduction in radionuclide-contaminated subsurface sediments. *Appl. Environ. Microbiol.* **2008,** *74* (10), 3159-3170.

(64) Gerlach, R.; Field, E. K.; Viamajala, S.; Peyton, B. M.; Apel, W. A.; Cunningham, A. B. Influence of carbon sources and electron shuttles on ferric iron reduction by Cellulomonas sp strain ES6. *Biodegradation* **2011,** *22* (5), 983-995.

(65) Kappler, A.; Benz, M.; Schink, B.; Brune, A. Electron shuttling via humic acids in microbial iron(III) reduction in a freshwater sediment. *FEMS Microbiol. Ecol.* **2004,** *47* (1), 85-92.

# CHAPTER 3

# MINERALOGY AND GEOCHEMISTRY AFFECTING ARSENIC SOLUBILITY IN SEDIMENT PROFILES FROM THE SHALLOW BASIN-FILL AQUIFER OF CACHE VALLEY BASIN, UTAH


## Abstract

Elevated arsenic concentrations have been reported in groundwater samples collected from the semi-arid Western U.S., including the Cache Valley Basin, Utah. The volcanic rock in the basin-fill aquifers underlying portions of the West is considered the primary source of arsenic, but there is debate about the mechanisms that control arsenic solubilization. Sediment cores were collected from a shallow basin fill aquifer in the Cache Valley Basin to systematically determine arsenic mineralogy and solubilization mechanisms in relation to non-redox and redox induced soil processes. Soluble arsenic was present throughout the two studied profiles in varying abundance and oxidation state, with the highest concentration of soluble As(V) and As(III) at the depth of the water table. Sequential chemical extractions of As, with oxidation preservation strategies, revealed mineral sources and sinks of As vulnerable to altering redox conditions down the profile. Weathering of primary arsenic-bearing minerals resulted in soluble arsenic in the vadose zone. Once soluble arsenic was leached to the deeper profile, arsenic solubility was controlled by carbonate minerals that concentrate at the water table. In the zone with alternating oxidizing and reducing conditions, Fe oxides became the controlling mineral phase. The association between As and sulfides limited As solubility at depths under permanent saturation conditions. Arsenic solubility was revealed to be controlled by a sequence of processes that prevail under different redox regimes down the profile.

## 1. Introduction

The occurrence of elevated arsenic (As) concentrations in groundwater threatens human health. Chronic ingestion of As bearing groundwater causes arsenicosis, which results in skin, bladder and kidney cancers, and blood vessel diseases (Ng et al., 2003). Affected aquifers have been found worldwide, most notoriously in Southern Asia where over a 100 million people have been exposed to As contaminated groundwater. As reviewed by Smedley and Kinniburgh (2002), As entering groundwater is mostly naturally occurring rather than anthropogenic. Natural As sources include primary and secondary As minerals, and secondarily formed As-containing Fe oxyhydroxides and other oxides. Microbial reductive dissolution of the host Fe oxide minerals is the major mechanism of As solubilization in groundwater systems in Southern Asia (McArthur et al., 2001; Nickson et al., 2000; Ravenscroft et al., 2001; Swartz et al., 2004). Direct microbial reduction of arsenate by dissimilatory arsenate respiring bacteria has also been reported (Ahmann et al., 1997; Weber et al., 2010). These microbial driven mechanisms require reducing conditions and the presence of labile organic carbon (OC) as carbon and energy sources for the dissimilatory reduction of Fe and/or As. The published studies delineating these mechanisms have been conducted in the field and laboratory using aquifer solids under fluctuating redox conditions and are characterized by accumulation of Fe and Mn oxides. Sources and mechanisms of As solubilization in sediments above the redox fluctuation zone are less studied.

Elevated As concentrations derived from near surface materials have been reported at some locations. Polizzotto et al. (2006) and Fendorf et al. (2010) stated that the weathering of primary As containing minerals in the Himalayas results in deposition

of these materials in the river basins of Southern and Southeastern Asia. These As-S minerals are oxidized at the soil surface, with sorption of the As(V) to Fe oxides. This provides the continued source of As in deeper sediments where the Fe oxides undergo microbial reductive dissolution and release As to the groundwater. Thus, under oxidizing conditions Fe oxides are a sink for soluble As, but with redox cycling, under reducing conditions they become the source of groundwater contamination.

Primary As-bearing sulfides are often related to high temperature geological activities (Drahota and Filippi, 2009). Volcanic related minerals were reported to be the primary source of As, including volcanic ash in the Southern High Plains aquifer of West Texas (Scanlon et al., 2009) and volcanic glass in the Rio Dulce alluvial aquifers of Argentina (Bhattacharya et al., 2006). The basin-fill aquifers of the American West, covering parts of New Mexico, Arizona, Southern California, Nevada, Oregon, Idaho, and Utah, contain volcanic rocks. Groundwater As concentrations that exceed the EPA maximum contaminant level (MCL) for As (10μg/L) were reported in the Safford and San Pedro basins of Arizona (Robertson, 1989), the Socorro Valley of New Mexico (Brandvold, 2001), the Tulare Basin of the San Joaquin Valley of California (Fujii and Swain, 1995), the Willemette Basin of Oregon (Hinkle and Polette, 1999), the Western Snake River Plain Basin of Idaho (Busbee et al., 2009), and the Cache Valley Basin of Utah (Lowe et al., 2003). The role of primary As-bearing sulfides in the basin-fill aquifers in the West needs to be investigated.

Fluctuation of the water table not only alters redox conditions within the aquifers, it also causes the formation and dissolution of carbonate minerals. Although carbonate minerals sequester much less As than oxides on a weight basis (Smedley and Kinniburgh,

2002), they are substantial soil components and are widely distributed in semi-arid subsurface systems. Calcite has been reported to sequester As through inner-sphere chemisorption, substitution, and surface complexation (Alexandratos et al., 2007; Bardelli et al., 2011; So et al., 2008). In addition to elevated concentrations of As in groundwater in the Cache Valley Basin, the groundwater and geology is highly carbonaceous. A microcosm study, using sediments collected from the depth of the water table in the shallow aquifer in this basin, showed that the solubilization of As from carbonate minerals, not Fe oxides, caused the elevated As concentration in the aqueous phase (Chapter 2).

The solubilization of As cannot be attributed to a single process or mechanism from the soil surface to depth of groundwater; different processes will dominate as redox regimes alter with depth. The overall aim of this study was to determine the redox-induced variation in mechanisms of As solubilization in sediment profiles collected from a shallow aquifer in the Cache Valley Basin in Northern Utah. Elevated As concentrations, that exceed MCL, were observed in 23 out of 157 wells sampled throughout Cache County, Utah (Lowe et al., 2003). The selected study area (41°44’03N and 111°52’22W) is located at the center of southern Cache Valley. This site provided a unique opportunity to explore the role of carbonate minerals in controlling As solubilization. Two continuous sediment cores were collected from the ground surface into the permanently water saturated, reducing layers. Understanding the behavior of geologic arsenic in this location is important because these processes also affect other regions in the Western U.S. due to similarity in the basin-fill geology and climate.

## 1.1. Geological settings

Cache Valley Basin is located in northeastern Utah and extends into southeastern Idaho with an area of about 1710 $km^2$ (Fig. 3-1). The elevation of the valley floor ranges from 1,340 to 1,650 m. The eastern portion of the valley is located on top of an ancient alluvial fan, caused by the withdrawal of Lake Bonneville, with steep slopes that reach into the rest of the basin and to the Logan River bottom (Hintze, 2005; USGS, 1962). The southern half of the basin is bounded by the western slopes of the Bear River Range and the eastern slopes of the northernmost branch of the Wasatch Range, the Wellsville Mountains. The Salt Lake Formation, which consists of Tertiary sedimentary and volcanic rocks, is exposed to the atmosphere along the foothills surrounding Cache Valley (Evans and Oaks, 1996), especially at the southern tip (Dover, 2005). Hintze (2005) attributed the volcanic rocks within the Salt Lake Formation to the migration of the Yellowstone "hotspot" from Northern Nevada, beginning 17 million years ago, to its current location. The valley floor is underlain by more than 300 m of unconsolidated basin-fill deposits consisting of Late Tertiary and Quaternary lacustrine sediments, due to ancient Lake Bonneville, and fluvial deposits (Brummer, 1991). Below that, lies up to 2,100 m of the Salt Lake Formation.

## 1.2. Climate and Hydrology

Climatic information (1981–2010) for this study was obtained from the weather station (Station ID: 425182) nearest to the study site, belonging to the Global Historical Climatology Network. Temperature varied from a minimum of -34.4 ˚C to a maximum 39.4 ˚C. During the same time period, annual precipitation ranged from 217 to 833 mm,

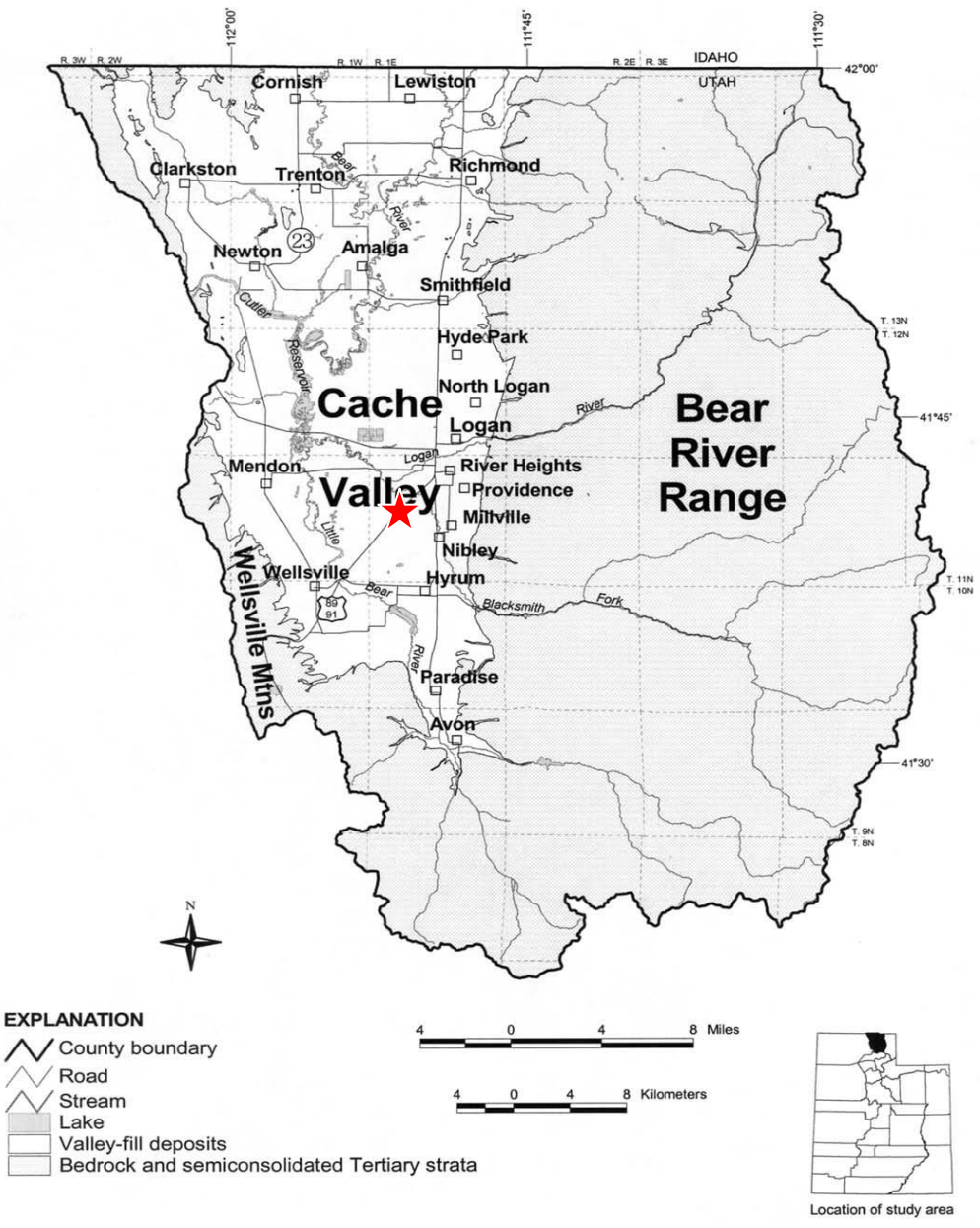


**Fig. 3-1.** Cache Valley, Utah, location map (adapted from Lowe et al., 2003). The red star indicates the location of the study site.

while annual evapotranspiration ranged from 987 to 1,190 mm. Cache Valley is therefore classified as a steppeland in the Koppen-Geiger Climate Classification System, characterized by a cold semiarid climate (Kottek et al., 2006). Cache Valley basin is the

easternmost extension of the Great Basin. The underlain aquifer consists mainly of unconsolidated basin-fill deposits of quaternary age from Lake Bonneville and older lakes, and the rest is younger alluvium at the margins of the valley (Kariya et al., 1994; USGS, 1962). The basin-fill aquifer is recharged by infiltration of precipitation, streams, irrigation water, and runoff from the surrounding mountains. In the center of the valley, groundwater is confined below depths typically of about 15 m because the interceded clays act as confining layers that impede the upward flow of water. The horizontal hydraulic gradients decrease toward the center of the valley. In the shallow zone the water table is expected to be an approximate replica of the valley topography. The water table in the unconfined shallow aquifer ranged from less than 1 m to about 6 m (Kariya et al., 1994). Utah Water Research Laboratory (UWRL) personnel installed a total of 13 sampling wells at the center of the valley into the shallow aquifer. Groundwater depth was monitored from January 2009 to January 2010 by the UWRL. The highest water table was at the ground surface, while the lowest water table was 260 cm below ground surface (bgs); the highest and lowest water tables occurred in April and July, respectively. The groundwater can fluctuate up to 300 cm at a nearby U.S. Geological Survey groundwater monitoring site 414721111590001 (http://nwis.waterdata.usgs.gov/nwis/gwlevels/?site_no=414721111590001).

## 2. Materials and Methods

### 2.1. Soil Collection and Processing

Continuous cores were collected in October 2012 from the areas to the east, NP9, and north, NP13, of the Logan Landfill (41°44’03N and 111°52’22W) (Fig. 2-1). NP9 is located 540 m away in the down-gradient direction from NP13. The land surface

elevation of NP9 is 1,354 m, while that of NP13 is 1,356 m. At each location, two cores (5 cm diameter) were collected using a direct push technique in 1.5-m increments. The core material was held in a stainless steel sampling tube that contained a plastic sleeve. One sleeve from each duplicate set of cores was opened laterally in the field to observe sediment morphology. Significant changes in texture and color along the profile, especially the occurrence of redoximorphic features (RMFs), were recorded and used as a guide in sectioning the second core in the laboratory. Drilling was terminated when at least 1.5 m of low chroma and bluish/greenish sediment was obtained. Total depths at NP9 and NP13 were 6.0 m and 4.6 m bgs, respectively. For the duplicate core, each sleeve was capped and taped to minimize exposure to air. Sleeves were stored on ice and returned to the lab within an hour of collection. All sleeves were stored and processed, within 12 hours of collection, in a glove bag under $N_2$ atmosphere (Coy Laboratory Products, Grass Lake, MI) in a 15°C±1°C constant temperature room to minimize redox reactions. The sleeves were cut open laterally. The sediment within the sleeve was divided into layers based on field observations and further distinction of RMFs in the lab. Sediment from each section was transferred into a Ziploc bag. To facilitate mixing of the sediments, autoclaved deionized (DI) water was added. The DI water was allowed to equilibrate in the $N_2$ glove box for a week before adding to the sediments. Water content was determined before and after water addition to calculate the amount of water that was added.

### 2.2. General Sediment Properties

Air-dried sediment samples were sent to Utah State University Analytical Laboratories for analyses of particle size distribution using the hydrometer method (Klute,

1986). Acid addition with $CO_2$ evolution was used to determine calcium carbonate equivalent (Sparks et al., 1996). The electrical conductivity (EC) and pH were determined using probes on a saturation paste extract (Sparks et al., 1996). Total carbon (TC) and inorganic carbon (IC) content were determined using a Skalar Primacs-SLC TOC Analyzer (Skalar, Netherlands) after the sediments were oven-dried at 105°C for 24 h and ground to pass through a 246 micron sieve. The total organic carbon (TOC) is the difference between TC and IC values.

### 2.3. Water Extraction

The fine-textured sediments at NP9 and NP13 would not yield enough pore water for analysis using the traditional saturation paste method. To estimate the chemistry of the pore water, a water extraction was performed on the solids. A 30-g sample was transferred into a plastic beaker and stirred with 10 mL of degassed DI water to make slurry. After 30 min, the slurry was split between two 50 mL centrifuge tubes with removable 0.22 μm filters (UltraClean® Maxi Plasmid Prep Spin Filter, Mo Bio Laboratories). The tubes were centrifuged for 20 min at 10,000 x g to obtain the water extracts, and the two filtrates from the same sample were combined into a sample storage vial. Except for centrifugation, the process was performed in a glove bag under $N_2$ atmosphere at 15°C. The Fe(II) concentration of the filtrate was determined using a Genesys 10Vis spectrophotometer (Thermo Scientific) at a wavelength of 562 nm after complexing with ferrozine (Lovley and Phillips, 1986). Fe(II) was analyzed immediately after separation and As speciation was performed within 24 h. Subsamples to be analyzed for As speciation were loaded in 300 μL IC vials (Fisher Scientific Inc.) and preserved with 5% v/v 0.25 M ethylenediaminetetraacetic acid (EDTA) solution (McCleskey et al.,

2004). As(III) and As(V) were separated with liquid chromatography (Agilent 1200 Series) on a C-18 column with an isocratic elution using 5 mM tetrabutylammonium hydroxide and 3mM malonic acid in 5% methanol at pH 5.8 and detection with inductively coupled plasma mass spectrometry (ICP-MS, Agilent 7500C) using He collision to minimize interferences from ArCl. Trace elements were determined in the water extracts, after preservation with $HNO_3$, using ICP-MS. Ion chromatography (IC; Dionex 3000) was used to determine nitrate-N, sulfate, and chloride (Dionex, Application Note 123) using a KOH gradient elution; major cations were determined by IC using 30 mM $H_2SO_4$. Bicarbonate concentration was calculated by subtracting the summed milliequivalent of dominant anions, Cl, $SO_4$, and $NO_3$, from the summed milliequivalent of major cations, Na, K, Ca, and Mg.

### 2.4. Selective Sequential Extraction of the Sediments

A seven-step chemical extraction procedure (Table 3-1) was performed on the core material to investigate the changes in As mineral association down the profile. Five steps, adapted from Huang and Kretzschmar (2010), were designed to remove As associated with the following operationally defined minerals: (1) ligand-exchangeable, (2) acid volatile sulfides and very poorly crystalline Fe oxides, (3) poorly crystalline Fe oxides (which is equivalent to “amorphous Fe oxides” in Chapter 2), (4) sulfides, and (5) crystalline Fe oxides. The 1 M HCl used to dissolve acid volatile sulfides and very poorly crystalline Fe oxides also dissolves Mn oxides (Keon et al., 2001). A step for the dissolution of carbonate minerals (Amacher, 1996) was inserted after the ligand exchangeable step. Microwave assisted acid digestion (US EPA 3052: 1996) was performed as the final step to recover As in the residual phase. For the sequential

extraction, 1 g samples were placed into 50 mL centrifuge tubes with a volume of each extractant and under conditions specified in the procedure (Table 3-1). The first four steps were performed in the glove bag, whereas the last three steps were carried out in the lab because water baths, hot plates, and/or a fume hood were needed. At the end of the shaking time required by each step, the tubes were centrifuged at 10,000 x g for 20 min. The supernatant was filtered through 0.2 μm nylon filters (Life Science) into sample storage vials. A wash procedure with 5 mL of degassed DI water was performed after each step.

The five steps from Huang and Kretzschmar (2010) included preservation strategies for the oxidation state of As. In the inserted carbonate step, the Fe(III)-acetate complex prevents As(III) from being oxidized during the carbonate extraction. The extracts from the first six steps were analyzed for As(III) and As(V) using LC-ICP-MS. The preservation strategies were validated by Huang and Kretzschmar (2010) for As but not for Fe. Therefore Fe speciation was not distinguished in the last four steps where Fe

**Table 3-1**
Selective sequential extraction procedure for determination of As associated with chemically defined surface and mineral phases[a].

| # | Extractant | Target | Conditions | Reference |
|---|---|---|---|---|
| F1 | 5 mM $NaH_2PO_4$, pH 7 + 0.2% NaDDC[a] (w/v) | ligand exchangeable As | 8 h, 15 °C, glove bag, shaking | Huang and Kretzschmar, 2010 |
| F2 | 1 M $NH_4OAc$, pH 5 | carbonate minerals | 2 h, 15°C, glove bag, shaking | Amacher, 1996 |
| F3 | 1 M HCl + 10% HOAc (v/v) + 50 mM $HgCl_2$ | acid volatile sulfides, Mn oxides, and very poorly crystalline Fe oxide | 1 h, 15 °C, glove bag, shaking, 1 repetition | Huang and Kretzschmar, 2010; Keon et al., 2001 |
| F4 | 0.2 M $NH_4^+$-oxalate buffer (pH 3.25) + 1 mM $HgCl_2$ | As associated with poorly crystalline Fe oxide | 2 h, RT, shaking, 1 repetition | Huang and Kretzschmar, 2010 |
| F5 | 4 M $HNO_3$ + 0.5% APDC[b] (w/v) | sulfides | 1 h, 65 °C, shaking, 1 repetition | Huang and Kretzschmar, 2010 |
| F6 | 4 M HCl +10% HOAc (v/v) | crystalline Fe oxide | 1 h, 95 °C, shaking | Huang and Kretzschmar, 2010 |
| F7 | Nitric acid (USEPA 3052) | residual phase | microwave nitric acid digestion | |

[a] Abbreviation legend: NaDDC: sodium diethyldithiocarbomate trihydrate; APDC: pyrrolidinedithiocarbmate ammonium sslt; RT: room temperature.

speciation was potentially modified. The addition of sodium diethyldithiocarbomate (NaDDC), added to preserve As speciation, interfered with Fe(II) analysis using ferrozine in the first step. Therefore Fe speciation was only distinguished in the second and third steps. Total Fe was determined using ICP-MS, while Fe(II) was determined in F2 and F3 using the ferrozine method. Because the mechanism of the first extraction step is ligand exchange of As with phosphate, only water soluble Fe would be removed. Results for Fe(II) and Fe from the initial water extraction was used for F1 to define Fe speciation. Ca, Mg, and Mn in F2 and F3 were also analyzed using ICP-MS.

### 2.5. HCl Extraction

A separate HCl extraction procedure was performed in the glove bag using 0.5 M HCl to recover Fe from $FeCO_3$, FeS, and very poorly crystalline Fe oxides (Heron et al., 1994) and As associated with these Fe minerals and other minerals that have similar solubility. To perform the HCl extraction, 20 mL of 0.5 M trace metal grade HCl (Fisher Scientific) and 1 g (dry weight) of solids were mixed in a 50 mL polypropylene centrifuge tube. The samples were shaken for 2 hr in the $N_2$ glove bag and then centrifuged at 10,000 x g for 20 min. The supernatants were filtered through 0.2 μm nylon filters for analyses of Fe (Fe(II)+Fe(III)) and As (As(III)+As(V)) by the methods described above.

### 2.6. Acid Volatile Sulfide Extraction

Acid volatile sulfide (AVS) was determined following the procedure of van Griethuysen et al. (2002). A 25-mL glass vial was secured onto the upper inside wall of a 125 mL glass jar that contained a stir bar. Inside the anaerobic glove bag, 2 g of each

sample were transferred into the large glass jar. Teflon-lined jar lids were secured immediately after the addition of 10 mL of SAOB (sulfide anti-oxidizing buffer) solution into the small glass vial. A total of 20 mL of degassed 1 M HCl was injected through the septum. The jars were placed on stir plates for 3–4 h. The $H_2S$ produced from the reaction between HCl and AVS was trapped by the SAOB solution inside the glass vial. The SAOB solution was then analyzed for sulfide with an ion selective electrode.

### 2.7. Mineral Composition

Based on field and laboratory observed properties, the layers from the NP9 and NP13 cores were grouped into four defined zones: vadose zone (unsaturated), carbonate enrichment zone (sediments adjacent to the current water table with the highest carbonate content), redox transition zone (saturated sediments with accumulation of Fe and Mn oxides, indicating alternating redox concentration) and depletion zone (the permanently saturated zone).

One layer from each zone from the two cores was used for analysis of mineral composition by QEMSCAN® 4300 (Quantitative Evaluation of Minerals by SCANning electron microscopy) at the College of Mines and Earth Sciences, University of Utah. Sample selection within each zone was based on the abundance of total As; sediments rich in As were selected. The samples were ground and made in to epoxy plugs 3 cm in diameter, using EpoxiCure® (Buehler, ITW Inc.). The images were collected for an area of 4 $cm^2$ at a resolution of 100 μm X 100 μm to qualitatively identify mineral composition. The instrument was a Carl Zeiss Evo 50 scanning electron microscope (SEM) equipped with four Intellection X275HR Silicon Drift X-ray detectors. The system features fully automated electron beam and stage control, combined with

automated spectrum acquisition and classification. It relies on the collection of spatially resolved X-ray spectra within a specified region on the sample surface. Measurements were performed in field scan mode, which provided a complete characterization of particle surfaces above a predefined electron backscatter threshold. Spectra were collected with 1000 total X-ray counts and were compared to a Species Identification Protocol (SIP; Barick 710) that discriminates minerals on the basis of their characteristic X-ray and electron backscatter intensities.

### 2.8. Statistical Analyses

Multiple core collection and analysis to establish sampling/analytical variance was not economically or practically feasible in this study nor in similar studies reported in the literature. The solids of each layer were homogenized before subsampling for all analyses. Triplicate subsamples were processed and analyzed for pore water and solids for two randomly selected layers of each core. The standard deviations calculated from these layers were used to define the precision of laboratory processing, extraction and analysis for each reported parameter.

Cluster analysis was used to group sediment layers with similar chemistries. Discriminant analysis was used to define the variables that most strongly influenced the clustering. Regression analysis was performed to determine: (1) if the concentration of soluble As species was correlated with the other measured variables in the water extraction and As in the different solid phase pools defined by sequential extractions, and (2) if the abundance of As species in each extraction pool was correlated with other measured variables. Significant correlations were required to have a p-value less than 0.05. The dependent variables must be normally distributed for regression analysis.

Soluble and solid phase As(V), As(III), and $As_T$ were not normally distributed, so they were log transformed prior to regression analysis. Statistical analyses were performed using JMP 8.0.2 (Statistical Software; SAS Institute, Cary, NC).

## 3. Results

### 3.1. Total As in the Sediment Profiles

Arsenic occurred throughout the NP9 and NP13 profiles. Solid phase As in NP9 ranged from 4.6 to 26.1 mg/kg, with a maximum value of 51.6 mg/kg (Fig. 3-2 $a_1$). An accumulation of As was observed at a depth of 208–345 cm. The As content in NP13 fluctuated in the range of 3.8 to 15.9 mg/kg (Fig. 3-2 $a_2$). The As concentration range in these two cores equaled or even exceeded that reported for sediments collected in Bangladesh, Cambodia, and Vietnam (Polizzotto et al., 2006; Rowland et al., 2008; Seddique et al., 2011). The concentration range of solid phase As in unconsolidated sediments worldwide is 3 to10 mg/kg (Smedley and Kinniburgh, 2002). A limited number of studies report As concentrations in sediment cores down to ~600 cm bgs in the United States. The range revealed in this study was similar to that in the Snake River Plain, Idaho, which was 4.2 to 45 mg/kg (Busbee et al., 2009).

### 3.2. Sediment Redox Stratification

The vadose zone, the unsaturated surface soil (Fig. 3-2 $b_1$ & $b_2$), belongs to the Carson soil series (fine, montmorillonitic, mesic Chromic Pelloxerets). These sediments were oxidized due to contact with atmospheric oxygen and active plant growth that provided labile OC. The high percentage of HCl extractable Fe(II) (Fig. 3-2 $c_1$ & $c_2$) distinguished the carbonate enrichment zone from the vadose zone. Fe(II) was 100% of

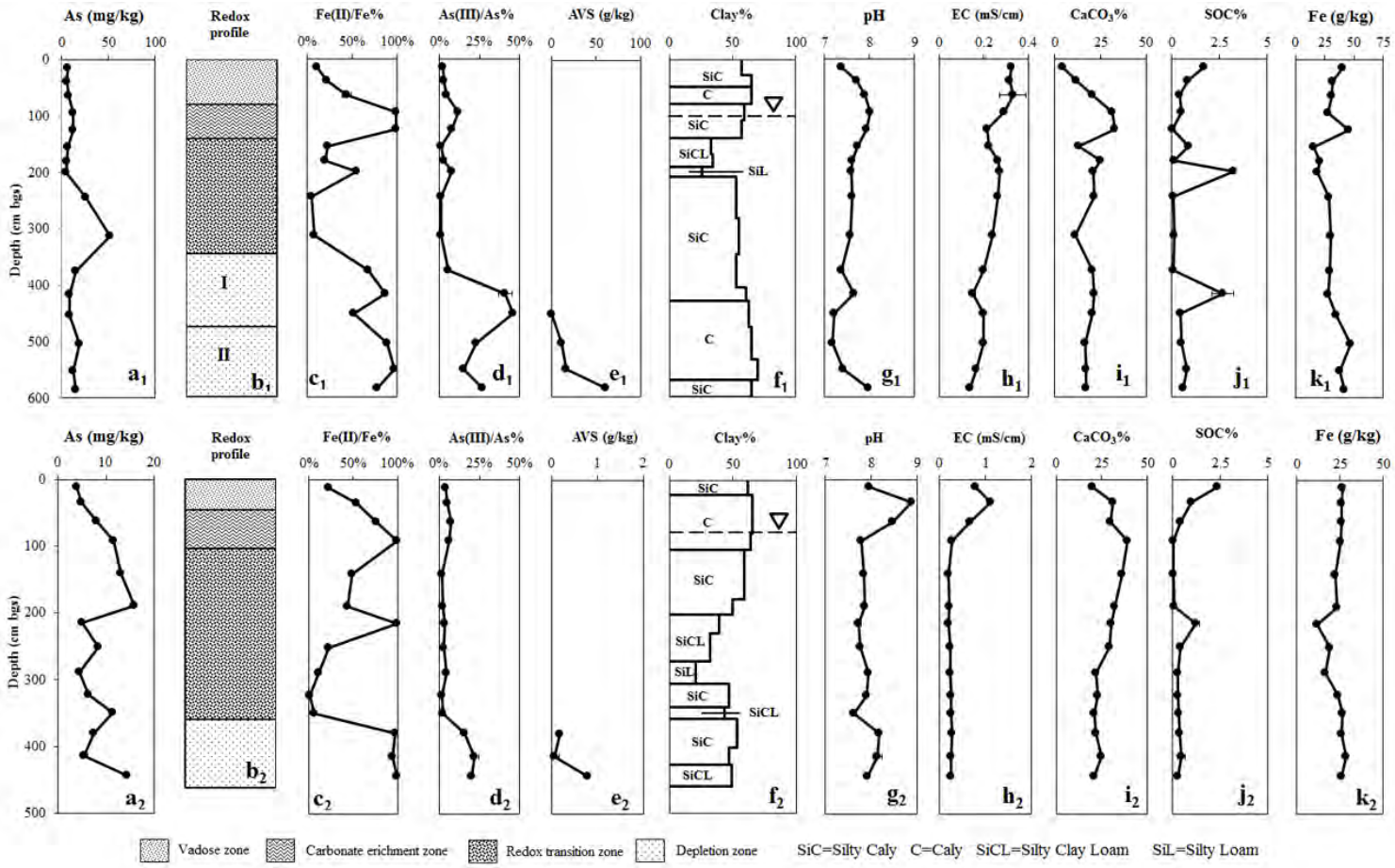


**Fig. 3-2.** Depth profile of sediment core with vertical distribution of sediment properties at the NP9 and NP13 location: ($a_1$ and $a_2$) total As content; ($b_1$ and $b_2$) defined redox profile; ($c_1$ and $c_2$) percentage of Fe(II) in Fe in HCl extraction; ($d_1$ and $d_2$) percentage of As(III) in As in HCl extraction; ($e_1$ and $e_2$) acid volatile sulfides content; ($f_1$ and $f_2$) clay content (w/w%); ($g_1$ and $g_2$) pH; ($h_1$ and $h_2$) EC; ($i_1$ and $i_2$) calcium carbonate equivalent (w/w%); ($j_1$ and $j_2$) SOC (w/w%); and ($k_1$ and $k_2$) total Fe content. Error bars represent standard deviations.

the Fe extracted with 0.5 M HCl in both cores at the depth of the water table. Although the HCl-extractable As was still dominated by As(V), the percentage of As(III)/As were higher in the sediments in the carbonate enrichment zone compared to those in the vadose zone (Fig. 3-2 $d_1$ & $d_2$).

The color of the sediments below the carbonate enrichment zone was reddish brown with black patches and embedded nodules, indicating accumulation of Fe oxides and Mn oxides due to fluctuating redox conditions. These sediments, at depths of 140–345 cm in NP9 and 104–340 cm in NP13, were affected by varying redox conditions, thus defining the redox transition zone. The percentage of Fe(II)/Fe was below 50% in this zone, with exceptions of 100% at 191–208 cm in NP9 and 201–229 cm in NP13.

More permanent reducing conditions developed below 345 cm in NP9. An immediate increase in the percentage of Fe(II)/Fe in the HCl extraction was observed from 345–404 cm. The reddish brown patches were interspersed with greenish and bluish colorations at 404–475 cm in NP9. The greenish and bluish colors, which are characteristic of the depletion zone, indicated that the sediments were under reducing conditions due to prolonged saturation. The co-occurring oxide patches and depletion features indicated heterogeneity in redox conditions. Detection of AVS at 429–475 cm in NP9 (Fig. 3-2 $e_1$) indicated that sulfate-reducing conditions had developed. Thus the sediments at 345–475 cm were classified as depletion zone I, which was at an early stage of depletion conditions. The predominant depletion features and high AVS (Fig. 3-2 $e_1$) in the sediments below 475 cm in NP9 defined depletion zone II. The boundary between the redox transition and depletion zone was distinct in the NP13 profile: below 340 cm

bgs the sediments immediately showed predominant depletion features and measureable AVS in these depletion zone sediments (Fig. 3-2 $e_2$).

### 3.3. Sediment Properties

The water table was at a depth of 104 cm bgs at NP9 and 80 cm at NP13 at the time of sample collection (Fig. 3-2 $f_1$ & $f_2$). The water depth at NP9 was typical of observations of water depths in September and October of pervious years, whereas the water depth at NP13 was shallower than the depth of 168 cm observed in October during the yearly monitoring program. The water depth was probably influenced by irrigation activity up-gradient of NP13; NP9 was less affected. Both sediment cores primarily consisted of fine-textured particles with textures from silty clay loam to clay (Fig. 3-2 $f_1$&$f_2$). The particle size distribution within the sediments at this study site was much finer than in the sandy sediments in other reported studies (Liao et al., 2011; Rowland et al., 2008; Scanlon et al., 2009). A section of sediments that contained relatively lower clay content compared to the rest of the core was intercalated at 108 to 208 cm depth at NP9 and 201 to 305 cm depth at NP13. These layers had higher permeability due to the coarser texture.

The sediments in the core from NP9 were neutral to moderately alkaline, with pH ranging from 7.2 to 8.0 (Fig. 3-2 $g_1$). EC decreased from 0.33 mS/cm to 0.14 mS/cm with depth (Fig. 3-2 $h_1$). The pH and EC values of NP13 sediments were similar to NP9, except that higher pH (8.5 and 8.9) and EC (0.66 to 1.0 mS/cm) occurred above the water table (Fig. 3-2 $g_2$ & $h_2$) in NP13. The higher salinity at the shallower depths was indicative of evaporative accumulation towards the ground surface. Groundwater was

wicked to the ground surface by capillary action when the water table was high, followed by strong evaporation in this semi-arid region.

As is typical for a semi-arid region, the sediments were calcareous. At NP9, sediments from the surface to adjacent to the water table contained increasing carbonate content, from 4 to 33 wt% $CaCO_3$ equivalent, while the carbonate content in the rest of the core fluctuated around 25 wt% (Fig. 3-2 $i_1$). The carbonate content in the sediment core from NP13 varied from 20 to 39 wt% (Fig. 3-2 $i_2$). Generally, sediment organic carbon (SOC) contents were higher at the surface (~2 wt%) and decreased with depth in both profiles (Fig. 3-2 $j_1$ & $j_2$). Several layers of high SOC were observed at the depths corresponding to the coarser textured material.

Solid phase Fe content ranges were 15.9–47.0 g/kg and 11.9–28.6 g/kg for the sediments from NP9 and NP13, respectively (Fig. 3-2 $k_1$ & $k_2$). Total As throughout the profiles did not correspond with sediment properties including percentages of sand, silt or clay, pH, EC, and $CaCO_3$ in either core, but As was negatively correlated with SOC content ($r^2$=0.26 and p=0.0450 for NP9 and $r^2$=0.45 and p=0.0084 for NP13). A correlation between As and Fe was not observed either, although the lowest As and lowest Fe concentrations indeed co-occurred.

### 3.4. Major Mineral Component

The major mineral composition, determined using QEMSCAN, was similar for the two cores, although the relative abundance of each mineral was distinctly different from zone to zone. The most abundant mineral was plagioclase in all measured sediment samples. The second most abundant mineral varied between feldspar (excluding plagioclase), amphibole, or micas. The two most abundant minerals accounted for 70.8%

to 86.0% of the scanned area (Table 3-2). The next most abundant minerals included quartz, chlorite, calcite, and dolomite.

Arsenic-bearing phases were not identified, either as primary minerals or as adsorbed phases. At the speed of the QEMSCAN analyses (1-2 milliseconds), the presence of As would be documented if a particular analyzed location contained in excess of 50,000 mg/kg As by weight (i.e. 0.5 wt%) (personal communication with Dr. Erich Petersen at University of Utah). The weight percentage of As in primary As minerals is much higher than this threshold value. Therefore, failure to detect As minerals indicated that either the As was adsorbed to mineral surfaces at a concentration that is below the detection limit, or the grain size of As-bearing minerals was too small to be observed. Crystalline Fe oxides, such as goethite and hematite, were very rarely documented (< 0.01%), even in the redox transition zone where the red coloration of Fe oxide was evident. Fe oxides were therefore primarily amorphous (poorly crystalline). Pyrite ($FeS_2$) in the depletion zones of NP9 and NP13 accounted for 0.18% and 0.82% to the total minerals, respectively, while pyrite in the other zones was <0.01%. Geochemical

**Table 3-2**
Mineral components in selected sediments (percent area>0.1% is shown).

| | Vadose Zone | | Carbonate Enrichment Zone | | Redox Transition Zone | | Depletion Zone | |
|---|---|---|---|---|---|---|---|---|
| | NP9-2 | NP13-1 | NP9-4 | NP13-4 | NP9-10 | NP13-5 | NP9-16 | NP13-12 |
| Plagioclase | 55.5 | 52.7 | 64.8 | 69.9 | 55.7 | 57.5 | 45.1 | 54.8 |
| Amphibole | <0.1 | 6.88 | 14.8 | 16.2 | 7.68 | 20.8 | 3.97 | 7.89 |
| Micas | 15.9 | 15.4 | 4.58 | 3.12 | 15.1 | 6.49 | 27.3 | 17.0 |
| Feldspar | 13.9 | 13.9 | 2.01 | 1.17 | 6.18 | 2.1 | 8.28 | 6.29 |
| Quartz | 10.7 | 6.99 | 7.72 | 5.5 | 9.92 | 7.43 | 6.23 | 9.26 |
| Calcite | 0.31 | 0.96 | 2.43 | 1.55 | 1.6 | 1.66 | 0.57 | 1.40 |
| Dolomite | 0.40 | 0.75 | 2.58 | 1.76 | 1.78 | 2.52 | 0.60 | 1.38 |
| Chlorite | 2.80 | 1.84 | 0.51 | 0.24 | 1.52 | 0.88 | 6.59 | 1.39 |
| Pyrite | <0.1 | <0.1 | <0.1 | <0.1 | <0.1 | <0.1 | 0.82 | 0.18 |
| Others | 0.50 | 0.58 | 0.57 | 0.62 | 0.52 | 0.62 | 1.31 | 0.59 |

modeling, using MINTEQ+ 4.6 (Environmental Research Software) and water extractable parameters, indicated the presence of ferrihydrite, goethite, hematite, lepidocrocite, magnetite, and rhodochrosite (Mn carbonate).

### 3.5. As Solubility and Water Extract Chemistry

Table 3-3 shows the concentrations of various parameters, including major cations and anions, trace elements, and DOC, measured for individual water extract for all sediment samples throughout the two cores. Selected parameters are plotted in Figures 3-3 and 3-4. Scatter plots, for regression consideration, are shown in Figures B-1 and B-2 in Appendix B.

#### 3.5.1. NP9 Core

Water extractable $As_T$ (As(III) + As(V)) reached maximal concentrations in the carbonate enrichment zone sediments, with ~30% of $As_T$ as As(III) (Fig. 3-3 a). Arsenic decreased in the coarser texture section and then reached the second peak (~104 μg/L) within the redox transition zone at 208–345 cm. Differing from the carbonate enrichment zone, the soluble As in the redox transition zone contained only negligible amounts of As(III). The $As_T$ immediately decreased at the depletion zone, which became As(III)-dominant.

The water extracts shifted from Na-Cl-$SO_4$-dominant to Na-$HCO_3$-dominant system between the vadose zone and the redox transition zone (Table 3-3). Sodium, which ranged from 41.1 to 135 mg/L, was higher above the water table (Fig. 3-3 b). Bicarbonate concentrations varied from 126 to 234 mg/L (Fig. 3-3 c). The concentrations of Cl and $SO_4$ continuously decreased through the profile except the lowest values, which

**Table 3-3**
Geochemical parameters of water extracts.

| Sample | Fe(II) mg/L | Fe mg/L | As(III) µg/L | As(V) µg/L | DOC mg/L | Al µg/L | Mn µg/L | Cu µg/L | Zn µg/L | Ba µg/L | Na mg/L | K mg/L | Mg mg/L | Ca mg/L | Cl mg/L | $NO_2^-$ mg/L | $NO_3^-$ mg/L | $SO_4^{2-}$ mg/L | $PO_4^{3-}$ mg/L | $HCO^{3-}$ mg/L |
|---|---|---|---|---|---|---|---|---|---|---|---|---|---|---|---|---|---|---|---|---|
| NP9-1 | <0.012 | 0.01 | 7.06 | 7.52 | 19.4 | 3.62 | 9.8 | 7.36 | 15.3 | 318 | 104 | 9.28 | 14.6 | 32 | 136 | 0.12 | 0.62 | 80.1 | 0.43 | 127 |
| NP9-2 | <0.012 | 0.01 | 4.71 | 5.73 | 13.7 | 12.5 | 2.77 | 4.69 | 18.1 | 325 | 124 | 4.26 | 10.9 | 17 | 108 | 0.01 | 1.92 | 92.2 | 0.25 | 140 |
| NP9-3 | <0.012 | 0.04 | 5.6 | 17.6 | 17.3 | 16 | 1.87 | 5.09 | 18.7 | 196 | 135 | 5.56 | 7 | 7.7 | 96 | 0.03 | 0.08 | 74.1 | 0.22 | 167 |
| NP9-4 | <0.012 | 0.03 | 45.4 | 113 | 6.41 | 6.47 | 2.1 | 7.6 | 25.9 | 145 | 134 | 6.9 | 4.81 | 5.04 | 57.5 | 0.01 | 0.14 | 72.4 | 0.14 | 216 |
| NP9-5 | <0.012 | 0.01 | 36.1 | 92.4 | 12.3 | 6.5 | 5.15 | 2.9 | 15.1 | 300 | 89.1 | 4.56 | 2.54 | 1.73 | 11.7 | 3.02 | 2.52 | 10.3 | 2.61 | 228 |
| NP9-6 | 0.05 | 0.05 | 0.39 | 50.2 | 7.13 | 43 | 8.6 | 3.6 | 18.8 | 248 | 104 | 4.55 | 4.77 | 2.03 | 27.3 | 0.03 | 1.91 | 58 | 0.19 | 193 |
| NP9-7 | 0.04 | 0.04 | 0.54 | 65.6 | 8.06 | 10.8 | 13.7 | 4.26 | 24.1 | 393 | 103 | 3.93 | 4.23 | 2.37 | 26 | 0.02 | 0.66 | 41.1 | 0.21 | 211 |
| NP9-8 | <0.012 | 0.01 | 1.59 | 45.4 | 10.8 | 13 | 4.79 | 5.97 | 16.6 | 413 | 108 | 4.81 | 3.25 | 2.61 | 31.2 | 0.01 | 0.56 | 45.1 | 0.08 | 207 |
| NP9-9 | 0.03 | 0.11 | 0.08 | 96.7 | 12 | 54.2 | 7.36 | 6.27 | 22.1 | 594 | 107 | 8.38 | 3.58 | 4.26 | 21.2 | <0.01 | 0.5 | 45.1 | 0.21 | 234 |
| NP9-10 | <0.012 | 0.07 | 0.18 | 104 | 12.3 | 30.7 | 3.76 | 6.5 | 21.5 | 621 | 105 | 5.58 | 3.86 | 4.6 | 25.8 | <0.01 | 0.36 | 42.9 | 0.22 | 221 |
| NP9-11 | <0.012 | 0 | 0.18 | 5.34 | 16.5 | 20.4 | 9.61 | 5.34 | 39.9 | 563 | 85.1 | 4.64 | 5.58 | 5.58 | 16.3 | <0.01 | 0.36 | 41.2 | 0.27 | 198 |
| NP9-12 | <0.012 | 0.01 | 2.84 | 4.06 | 10.8 | 56.8 | 15.5 | 4.05 | 26.1 | 935 | 63.5 | 3.93 | 6.63 | 7.24 | 13.4 | 0.35 | 0.37 | 31.8 | 0.58 | 167 |
| NP9-13 | <0.012 | 0.04 | 7.07 | 1.98 | 5 | 54.4 | 17.3 | 3.14 | 24.3 | 584 | 51.6 | 3.49 | 7.29 | 8.03 | 10.8 | <0.01 | 0.26 | 27 | 0.67 | 151 |
| NP9-14 | 0.04 | 0.1 | 0.98 | 0.58 | 14.5 | 81.2 | 30.2 | 5.56 | 31.2 | 516 | 44.4 | 3.95 | 7.1 | 7.77 | 9.8 | <0.01 | 0.53 | 30.6 | 0.67 | 128 |
| NP9-15 | 0.11 | 0.15 | 1.77 | 1.17 | 29.2 | 112 | 35.8 | 6.24 | 25.4 | 493 | 43.7 | 3.18 | 6.73 | 7.83 | 8.3 | <0.01 | 0.21 | 30.4 | 0.66 | 126 |
| NP9-16 | 0.13 | 0.16 | 12.9 | 4.46 | 34.2 | 156 | 71.1 | 2.2 | 23.6 | 555 | 41.1 | 5.02 | 6.44 | 9.16 | 8.5 | <0.01 | 0.17 | 29 | 0.57 | 126 |
| NP13-1 | 0.05 | 0.58 | 1.21 | 15.8 | 15.8 | 815 | 32.9 | 38.5 | 116 | 85 | 323 | 4.11 | 4.1 | 10.1 | 146 | 0.06 | 0.51 | 249 | 0.62 | 348 |
| NP13-2 | <0.012 | 0.08 | 6.93 | 53.4 | 2.32 | 246 | 2.84 | 29 | 172 | 242 | 438 | 7.6 | 7.67 | 6.6 | 214 | 0.08 | 0.61 | 315 | 0.31 | 463 |
| NP13-3 | <0.012 | 0.07 | 31.9 | 86.6 | 11.4 | 232 | 1.64 | 25.2 | 63.6 | 268 | 214 | 11.3 | 18.3 | 5.35 | 170 | 0.17 | 0.18 | 106 | 0.24 | 268 |
| NP13-4 | <0.012 | 0.1 | 30.9 | 77.3 | 6.65 | 172 | 7.88 | 22.9 | 79.2 | 737 | 55.5 | 7.44 | 19.6 | 8.08 | 26.7 | <0.01 | 0.33 | 42.7 | 0.17 | 183 |
| NP13-5 | <0.012 | 0 | 2.48 | 46.1 | 5.62 | 53.6 | 3.56 | 5.6 | 25.7 | 781 | 38.8 | 8.59 | 19.1 | 7.27 | 18.4 | <0.01 | 0.35 | 28.3 | 0.18 | 168 |
| NP13-6 | <0.012 | 0.02 | 0.07 | 39.4 | 6.1 | 56.1 | 4.4 | 3.5 | 16.6 | 884 | 42.6 | 9.16 | 22.8 | 8.81 | 28.6 | <0.01 | 0.39 | 32.1 | 0.22 | 180 |
| NP13-7 | <0.012 | 0.01 | 0.31 | 27.9 | 5.28 | 33.3 | 5.46 | 2.22 | 19.5 | 1050 | 40.2 | 10.7 | 23.6 | 7.81 | 27.1 | <0.01 | 0.21 | 26.7 | 0.2 | 186 |
| NP13-8 | <0.012 | 0.03 | 0.04 | 29.7 | 10.5 | 73.9 | 6.51 | 1.89 | 11.1 | 904 | 51.2 | 11.1 | 20.4 | 7.97 | 23.7 | <0.01 | 0.45 | 29.9 | 0.29 | 202 |
| NP13-9 | <0.012 | 0.01 | 0.05 | 27.8 | 6.76 | 77.3 | 0.65 | 4.2 | 21.9 | 945 | 53 | 14.1 | 21.5 | 7.12 | 23.9 | <0.01 | 0.39 | 27.9 | 0.31 | 217 |
| NP13-10 | <0.012 | 0.03 | 0.04 | 23.6 | 7.6 | 113 | 1.13 | 5.9 | 19 | 513 | 69.8 | 9.84 | 12.7 | 6.3 | 19.2 | <0.01 | 0.57 | 33.3 | 0.57 | 209 |
| NP13-11 | <0.012 | 0.05 | 0.22 | 30 | 12 | 140 | 12.4 | 8.1 | 36.7 | 609 | 73.1 | 8.15 | 9.6 | 6.24 | 18.6 | <0.01 | 0.28 | 33.4 | 0.83 | 200 |
| NP13-12 | 0.05 | 0.49 | 9.3 | 10.6 | 18.8 | 486 | 34.7 | 30.8 | 34.5 | 592 | 89.8 | 8.15 | 8.13 | 7.18 | 24.3 | <0.01 | 0.34 | 42.6 | 0.82 | 218 |
| NP13-13 | 0.1 | 0.7 | 7.45 | 6.07 | 36.2 | 449 | 35.8 | 70.3 | 43.2 | 452 | 84.8 | 5.88 | 5.6 | 5.3 | 23.3 | <0.01 | 0.3 | 31 | 1.45 | 199 |
| NP13-14 | 0.21 | 1.33 | 8.38 | 3.81 | 46 | 629 | 81.4 | 88.4 | 39.6 | 261 | 72.5 | 8.12 | 5.85 | 4.47 | 26.8 | <0.01 | 0.19 | 19.1 | 1.38 | 178 |

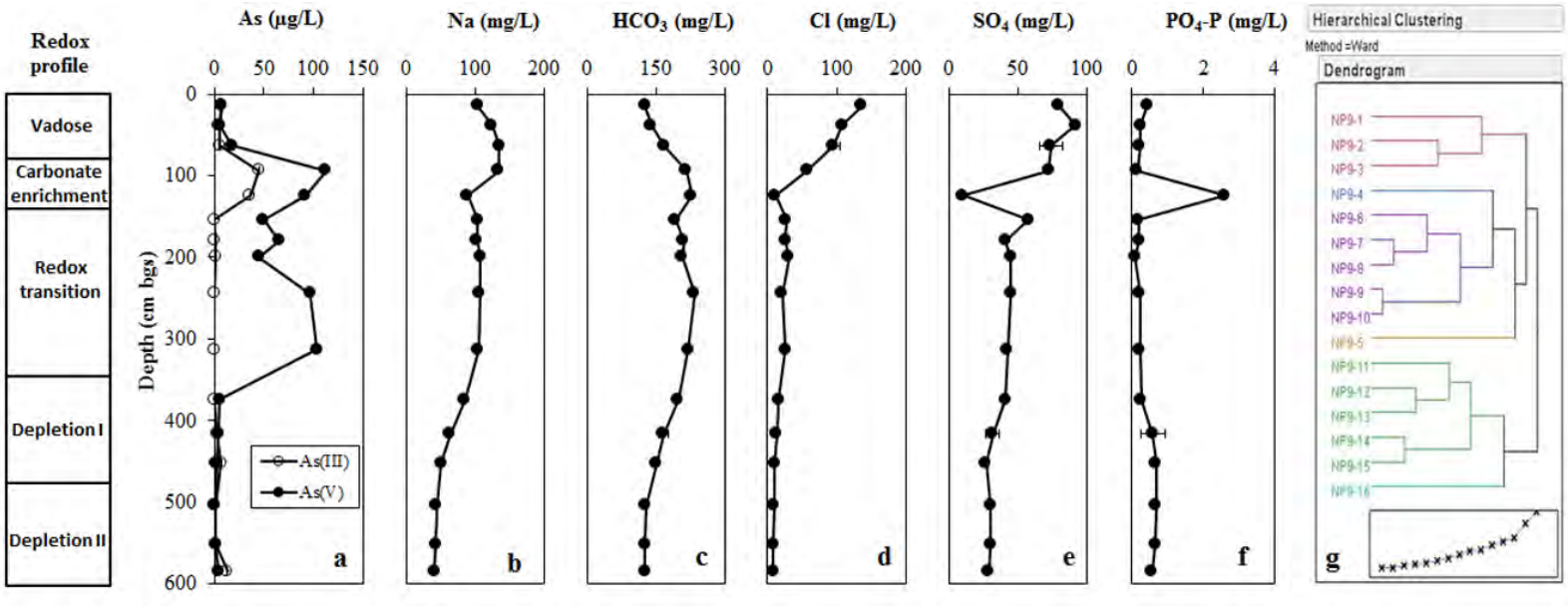


**Fig. 3-3.** Depth profile of the concentration of selected solutes in water extracts at NP9 with the redox profile on the left: (a) As speciation, (b) Na, (c) HCO3, (d) Cl, (e) SO4, (f) PO4-P. (g) is the hierarchical cluster. Error bars represent standard deviations.

occurred at 108–140 cm (Fig. 3-3 d & e). The water extracts from the NP9 profile contained low $PO_4$-P (0.08–0.67 mg/L with an outlier of 2.61 mg/L; Fig. 3-3 f) and $NO_3$-N (0.08–2.52 mg/L), and $NO_2$-N (below detection limit to 3.02 mg/L).The water extracts clustered into six groups, based on all measured parameters and sediment pH and EC (Fig. 3-3 g). The clustering was similar to the redox stratification defined by visual inspection and redox chemistry, except that each of the two carbonate enrichment zone sediments were self-clustered and the deepest layer stood out from the rest of the depletion zone (Fig. 3-3 g). The most discriminating factors were, in order of decreasing power: As(III), $PO_4$-P, Na, and Cl. Extraordinarily high $PO_4$-P differentiated NP9-5 from NP9-4 (Fig. 3-3 f); otherwise NP9-4 and NP9-5 would be grouped in the same cluster.

As(V) correlated with $HCO_3$, Na, pH, Mg, Mn, and Al (Table 3-4). The positive correlation between As(V) and $HCO_3$ may suggest desorption of As due to competitive sorption of bicarbonate. This positive correlation may also suggest production of bicarbonate with the oxidation of DOC coupled with microbial driven reductive dissolution of Fe oxides contributing to As(V) solubilization (Nickson et al., 2000). Correlation of As(V) with Fe(II) was not calculated because Fe(II) was below the detection limit (0.012 mg/L) in about half of the profile. Poor correlation between As and Fe(II) was observed by other researchers and was attributed to the formation of secondary Fe(II) minerals removing Fe(II) from solution (Horneman et al., 2004; Nickson et al., 2000). The positive correlation with Na indicated that evaporative concentration contributed to the enrichment of As(V). As(V) was also correlated with $Na/Ca^{0.5}$ indicating that a counterion effect contributed to As(V) desorption, as concluded by Scanlon et al. (2009) for an oxidizing system in the South High Plain aquifer of Texas.

**Table 3-4**
Coefficients of determination between various parameters and As(III) and As(V) in water extracts of NP9. Significant correlations ($p<0.05$) are shown in bold.

| Parameter | As(V) | | As(III) | |
|---|---|---|---|---|
| | $r^2$ | p | $r^2$ | p |
| pH | **(+)0.35** | **0.0151** | (+)0.20 | 0.0844 |
| EC | (+)0.20 | 0.0822 | (+)0.01 | 0.7923 |
| $Fe_T$ | (-)0.09 | 0.2471 | (-)0.03 | 0.5236 |
| DOC | (-)0.20 | 0.0803 | (+)0.02 | 0.6417 |
| Al | **(-)0.31** | **0.0264** | (+)0.00 | 0.9231 |
| Mn | **(-)0.30** | **0.0277** | (+)0.02 | 0.5888 |
| Cu | (+)0.03 | 0.5491 | (-)0.04 | 0.4533 |
| Zn | (-)0.18 | 0.0967 | (-)0.12 | 0.1956 |
| Ba | (-)0.14 | 0.1525 | (-)0.15 | 0.1390 |
| Na | **(+)0.53** | **0.0015** | (+)0.00 | 0.9898 |
| K | (+)0.18 | 0.1033 | (-)0.00 | 0.9533 |
| Mg | **(-)0.30** | **0.0284** | (+)0.07 | 0.3174 |
| Ca | (-)0.15 | 0.1455 | (+)0.07 | 0.3132 |
| Cl | (+)0.01 | 0.7664 | (+)0.08 | 0.2837 |
| $NO_3$-N | (+)0.07 | 0.3065 | (+)0.02 | 0.6267 |
| $SO_4$ | (+)0.03 | 0.5424 | (+)0.01 | 0.7673 |
| $PO_4$-P | (-)0.00 | 0.9579 | (+)0.21 | 0.0761 |
| $HCO_3$ | **(+)0.77** | **<0.0001** | (-)0.09 | 0.2602 |

The positive correlation with pH agreed with the observed behavior of As(V) when it is sorbed to Fe and Mn oxides (Dixit and Hering, 2003; Grossl and Sparks, 1995; Pierce and Moore, 1982) and to soils (Manning and Goldberg, 1997); As(V) sorption decreases with increasing pH. High pH under arid, oxidizing conditions is considered as a trigger for As desorption (Smedley and Kinniburgh, 2002). The As(V) was negatively correlated with $PO_4$-P ($r^2$=0.76 and $p<0.0001$), when the layer with extraordinarily high $PO_4$-P was excluded (Fig. B-1). As(III) was not correlated with any of the other solutes.

### 3.5.2. NP13 Core

Water extractable As(V) and As(III) both peaked in the carbonate enrichment zone (~110 µg/L and ~80 µg/L) of NP13 (Fig. 3-4 a). A discernible portion of As(III) was observed in the vadose zone, while As(III) was below the detection limit in the redox transition zone. The fraction of As(III) reached approximately 50% in the depletion zone.

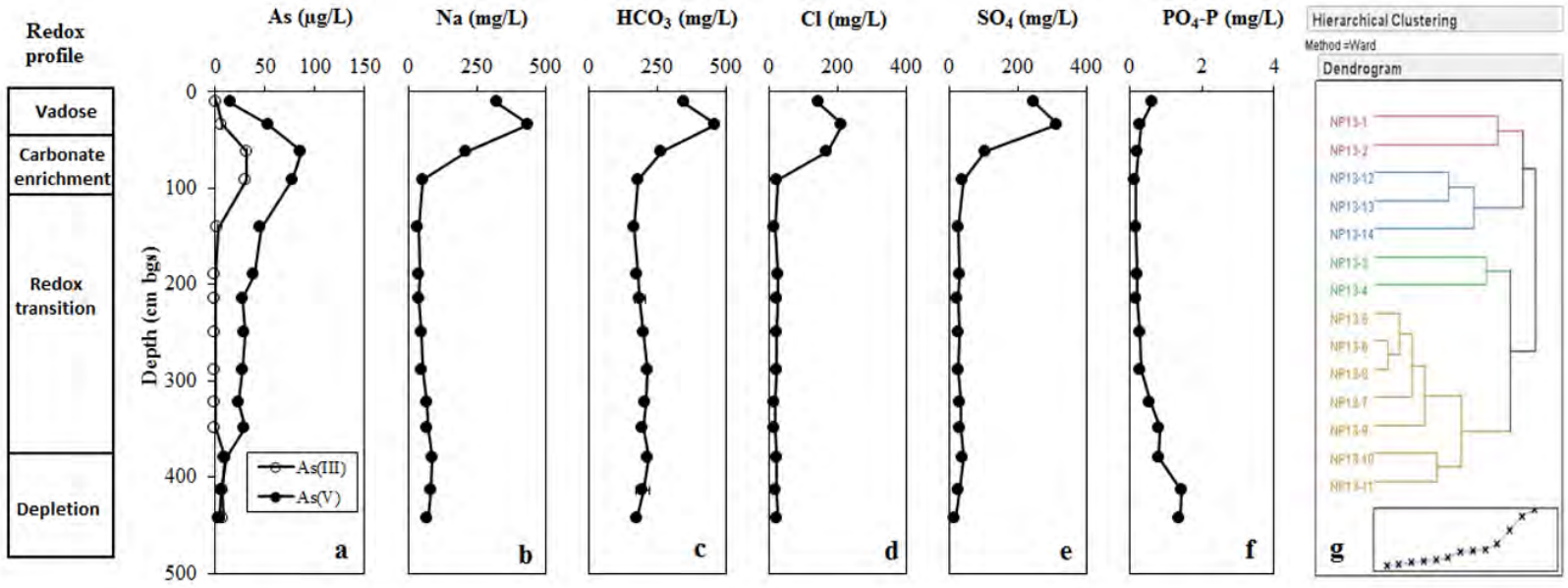


**Fig. 3-4.** Depth profile of the concentration of selected solutes in water extracts at NP13 with the redox profile on the left: (a) As speciation, (b) Na, (c) $HCO_3$, (d) Cl, (e) $SO_4$, (f) $PO_4$-P. (g) is the hierarchical cluster. Error bars represent standard deviations.

The water extracts were consistently Na-$HCO_3$-dominant throughout the core of NP13 (Table 3-3). As shown by the EC profile (Fig. 3-2 $c_2$), Na, $HCO_3$, Cl, and $SO_4$, accumulated toward the ground surface (Fig. 3-4 b-e). The $NO_2$-N, $NO_3$-N, and $PO_4$-P were consistently low and fell in the same range as in the NP9 profile (Fig. 3-4 f-h).

The water extracts of NP13 were grouped into four clusters using cluster analysis (Fig. 3-4 g) and were identical to the redox stratification as previously defined by visual inspection of the sediments and the distribution of redox species. Sulfate and As(III) were the discriminating factors that differentiate the water extracts from NP13. The $SO_4$ concentrations in the two vadose zone samples were 249 and 325 mg/L, then rapidly decreased in the carbonate enrichment zone and remained low at the greater depths (Fig. 3-4 d). As(V) was correlated with $Fe_T$, Mn, DOC, and $PO_4$-P (Table 3-5). The negative correlations between As(V) and Fe, Mn, and DOC indicated that reductive dissolution of Fe or Mn oxides, driven by microbial activity, might not be the mechanism of As

**Table 3-5**
Coefficients of determination between various parameters and As(III) and As(V) in water extracts of NP13. Significant correlations ($p<0.05$) are shown in bold.

| Parameter | As(V) | | As(III) | |
|---|---|---|---|---|
| | $r^2$ | p | $r^2$ | p |
| pH | (+)0.02 | 0.6453 | (+)0.25 | 0.0698 |
| EC | (+)0.07 | 0.3736 | (+)0.13 | 0.1969 |
| $Fe_T$ | **(-)0.73** | **0.0001** | (+)0.18 | 0.1285 |
| DOC | **(-)0.75** | **0.0001** | (+)0.13 | 0.2080 |
| Al | **(-)0.42** | **0.0120** | (+)0.22 | 0.0886 |
| Mn | **(-)0.74** | **0.0001** | (+)0.14 | 0.1811 |
| Cu | **(-)0.52** | **0.0035** | **(+)0.37** | **0.0201** |
| Zn | (+)0.04 | 0.4743 | (+)0.26 | 0.0622 |
| Ba | (+)0.07 | 0.3567 | **(-)0.29** | **0.0456** |
| Na | (+)0.03 | 0.5665 | (+)0.12 | 0.2162 |
| K | (+)0.11 | 0.2380 | (-)0.21 | 0.0983 |
| Mg | **(+)0.40** | **0.0159** | (-)0.15 | 0.1783 |
| Ca | (+)0.10 | 0.2680 | (-)0.11 | 0.2475 |
| Cl | (+)0.11 | 0.2373 | (+)0.16 | 0.1589 |
| $NO_3$-N | (+)0.03 | 0.5626 | (-)0.13 | 0.1997 |
| $SO_4$ | (+)0.04 | 0.4668 | (+)0.08 | 0.3401 |
| $PO_4$-P | **(-)0.79** | **<0.0001** | (+)0.06 | 0.4153 |
| $HCO_3$ | (+)0.04 | 0.4905 | (+)0.05 | 0.4287 |

solubilization. The negative correlation between As(V) and $PO_4$-P indicated that ligand exchange may contribute to the As(V) solubilization. The As(III) was positively correlated with Cu (Table 3-5), indicating that As(III) could be released by the dissolution of As-bearing Cu minerals. Mining activities for enargite ($Cu_3AsS_4$; http://www.mindat.org/loc-36951.html) and tennantite ($Cu_{12}As_4S_{13}$; http://www.mindat.org/loc-36957.html) were documented in the surrounding mountains. The transport of these minerals into the valley via erosion is possible.

## 3.6. Sequential Extraction

### 3.6.1. Arsenic Association with Mineral Surfaces and Soluble Minerals

The As associated with mineral surfaces, defined by ligand exchange reactions with phosphate and As associated with minerals, such as carbonates and poorly crystalline Fe oxides, can be the sources of As with altering water and redox conditions.

#### 3.6.1.1. Ligand-exchangeable and Carbonate-associated As (F1 & F2)

Phosphate has been shown to be a strong competitor for As(V) and As(III) adsorbed onto oxides (Jain and Loeppert, 2000; Manning and Goldberg, 1996). A phosphate solution, therefore, is often used to extract ligand-exchangeable As ($As_{LE}$) in soil without dissolving minerals. The addition of NaDDC to the phosphate extractant used here has been reported to successfully prevent oxidation of As(III) to As(V) within the time span chosen in this study (Georgiadis et al., 2006). An acetate buffer is widely used to access As associated with carbonate minerals ($As_{Carb}$) (Akai et al., 2004; Anawar et al., 2003; Seddique et al., 2011; Wenzel et al., 2001), but Heron et al. (1994) revealed that only 1.1% of Fe(II) in siderite could be recovered by this extraction step. While

dissolving most carbonate minerals, the acetate buffer was reported to also extract 28% of Fe(II) in FeS (Heron et al., 1994). This acetate extraction may also dissolve Ca and Mg arsenate (Ryu et al., 2010), although the extractant is considered to be relatively specific to carbonate minerals (Tessier et al., 1979)

The vertical distribution of $As_{LE}$ and $As_{Carb}$ were similar (Fig. 3-5 $a_1$ & $a_2$ vs. Fig. 3-5 $b_1$ & $b_2$), with the highest concentration of As extracted from the two solutions at

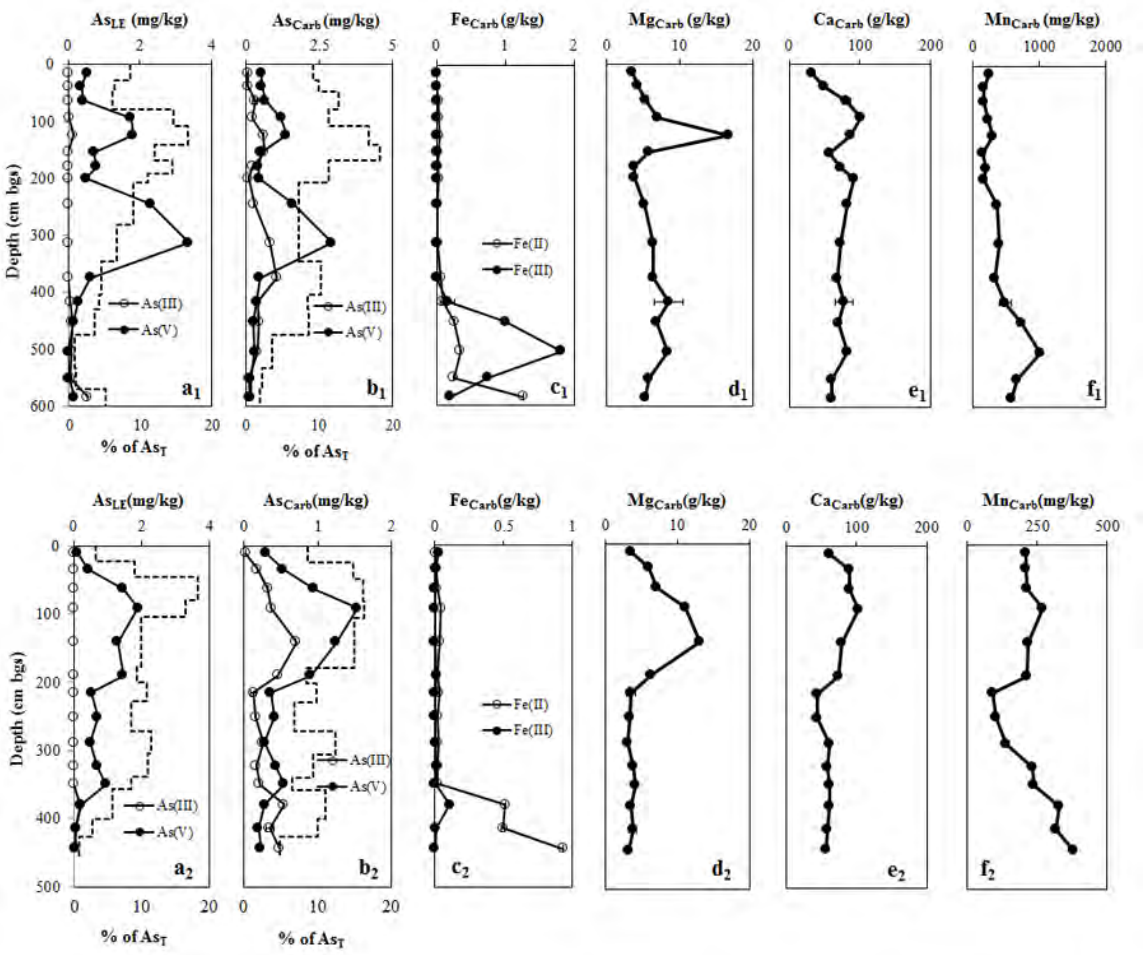


**Fig. 3-5.** Sequential extraction results for phospahte exchangeable As in ($a_1$) NP9 and ($a_2$) NP13 and carbonate fraction in NP9 ($b_1$–$f_1$) and NP13 ($b_2$–$f_2$): ($b_1$ and $b_2$) As speciation, ($c_1$ and $c_2$) Fe speciation, ($d_1$ and $d_2$) Mg, ($e_1$ and $e_2$) Ca, and ($f_1$ and $f_2$) Mn. Dashed line indicates percenrtage of total solid phase As recovered in each fraction. Error bars represent standard deviations.

approximately the same depth as the highest concentration of total As (Fig. 3-1). These two extractions together accounted for 3% to 33% of the total As in the profiles, with ligand-exchangeable and carbonate minerals being major labile pools of As, particularly in the carbonate enrichment and redox transition zone sediments.

The relatively high $As_{LE}$ in the carbonate enrichment zone and redox transition zone sediments indicated that the mineral phases in these sediments provided more surficial adsorption sites. The dominance of $As(V)_{LE}$ in $As_{LE}$ was observed from the vadose zone through the redox transition zone, while $As(III)_{LE}$ was approximately equal to or higher than $As(V)_{LE}$ in the depletion zone (Fig. III-5 $a_1$ & $a_2$).

Unlike the ligand exchange phase, $As_{Carb}$ contained a discernible percentage of As(III) in all sediments. Calcite has been reported to sequester both As(III) and As(V) by complexation and adsorption. Arsenate is associated with calcite through inner-sphere complexation (Alexandratos et al., 2007) and would have been removed in the first extraction step. Recent findings suggest that the association between arsenite and calcite is stable since As(III) is effectively trapped in the crystal lattice (Bardelli et al., 2011; Costagliola et al., 2007). Therefore As(III) was not observed in the ligand exchangeable step but was associated with the dissolution of carbonate minerals.

Fe(II) extracted with the acetate buffer ($Fe(II)_{Carb}$) increased in the depletion zones of the two cores (Fig. 3-5 $b_1$ & $b_2$). The increase in $Fe(II)_{Carb}$ could be derived from unwanted dissolution of FeS, formed under the reducing conditions in the depletion zone. In the depletion zone of NP9, Fe(II)-Fe(III) carbonate mineral, presumably fougerite, was dissolved, which was indicated by co-existing $Fe(II)_{Carb}$ and $Fe(III)_{carb}$. The increase in $Fe_{Carb}$ in the depletion zone sediments was not accompanied by an increase in $As_{Carb}$,

indicating that the role of Fe-bearing mineral extracted in this step was limited. $As(V)_{Carb}$ was not correlated with acetate extractable Ca or Mg ($Ca_{Carb}$ or $Mg_{Carb}$), which are the major forms of carbonate minerals, in the NP9 profile. A correlation between $As(V)_{carb}$ and acetate extractable Mn ($Mn_{Carb}$) ($r^2$=0.82 and p=0.0003), however, was observed when the depletion zone sediments were excluded (Fig. B-3) suggesting that Mn-bearing carbonates had a higher affinity for As(V) compared to the other carbonates. $As(III)_{Carb}$ was correlated with $Mg_{Carb}$ in NP9 ($r^2$=0.26 and p=0.0447). $As(V)_{Carb}$ in NP13 corresponded with both $Ca_{Carb}$ ($r^2$=0.56 and p<0.0021) and $Mg_{Carb}$ ($r^2$=0.75 and p<0.0001), but not with $Mn_{Carb}$ as in NP9. The $As(III)_{carb}$ was also correlated with $Mg_{Carb}$ in the vadose zone through the redox transition zone ($r^2$=0.45 and p=0.0230) suggesting the importance of Mg-bearing carbonates in retaining As in the NP13 profile (Fig. B-6).

$As(V)_{LE}$ and $As(III)_{LE}$ were both correlated with water extractable As(V) and As(III) in the two cores (Table 3-6 and Fig. B-2) indicating the importance of adsorption/desorption in controlling As(V) and As(III) solubilization in the profile. Water extractable As(V) was also correlated with $As(V)_{Carb}$ in both cores, but the correlation was weaker than with the ligand-exchangeable pool (Table 3-6). $As(III)_{Carb}$ was not correlated with water extractable As(III), since $As(IIII)_{Carb}$ was associated with the mineral structure and was not water soluble. Anoxic incubation of sediments from the redox transition zone (Chapter 2), from cores from this research site, demonstrated that the majority of the As(V) solubilized over a 54-day period was from the carbonate fraction.

**Table 3-6**

Coefficients of determination between water extractable As and As in each sequential extraction fraction. Significant correlations ($p<0.05$) are shown in bold. (+) and (-) indicated positive and negative correlation coefficient.

| Sequential extraction fraction | | Water extractable | | | | | | | | | | | |
|---|---|---|---|---|---|---|---|---|---|---|---|---|---|
| | | NP9 | | | | | | NP13 | | | | | |
| | | As(V) | | As(III) | | As | | As(V) | | As(III) | | As | |
| | | p | $r^2$ | p | $r^2$ | p | $r^2$ | p | $r^2$ | p | $r^2$ | p | $r^2$ |
| $As(V)_{LE}$ | | **<0.0001** | **(+)0.76** | | | | | **<0.0001** | **(+)0.84** | | | | |
| $As(III)_{LE}$ | F1 | | | **0.0045** | **(+)0.45** | | | | | **0.017** | **(+)0.39** | | |
| $As_{LE}$ | | | | | | **<0.0001** | **(+)0.80** | | | | | **4E-04** | **(+)0.66** |
| $As(V)_{Carb}$ | | **0.0003** | **(+)0.63** | | | | | **0.0002** | **(+)0.71** | | | | |
| $As(III)_{Carb}$ | F2 | | | 0.1812 | (-)0.12 | | | | | 0.294 | (+)0.09 | | |
| $As_{Carb}$ | | | | | | **0.0177** | **(+)0.34** | | | | | **0.006** | **(+)0.49** |
| $As(V)_{VPC}$ | | **0.0256** | **(+)0.31** | | | | | **0.001** | **(+)0.61** | | | | |
| $As(III)_{VPC}$ | F3 | | | 0.7755 | (-)0.01 | | | | | **0.032** | **(+)0.33** | | |
| $As_{VPC}$ | | | | | | 0.36 | (+)0.06 | | | | | 0.128 | (+)0.18 |
| $As_{PC}$ | F4 | | | | | 0.6215 | (+)0.02 | | | | | 0.67 | (+)0.02 |

### 3.6.1.2. Poorly Crystalline Fe Oxides (F3&F4)

Huang and Kretzshmar (2010) indicated that a 1 M HCl solution, which was used in F3, recovered As associated with very poorly crystalline Fe oxides and AVS, primarily as FeS. Siderite ($FeCO_3$) and Mn oxides were also extracted by the 1 M HCl solution (Heron et al., 1994; Keon et al., 2001). Arsenic extracted in this fraction is designated as $As_{VPC}$. To distinguish the relative solubility of poorly crystalline Fe oxides, Huang and Kretzshmar (2010) also used an extraction step (F4) with acid ammonium oxalate solution. This extractant has traditionally been used for evaluating As associated with poorly crystalline Fe oxides (Pederick et al., 2007; Rowland et al., 2007; Wenzel et al., 2001) and is designated as $As_{PC}$. Arsenic bonded to these mineral fractions (F3 and F4) is susceptible to release due to redox cycling.

$As_{VPC}$ ranged from 1.1–10.0 mg/kg in NP9 and 0.7–4.5 mg/kg in NP13, which accounted for approximately 25% of $As_T$ (Fig. 3-7 $a_1$ & $a_2$). $As(III)_{VPC}$ was less than 5% of $As_{VPC}$ from the vadose zone though the redox transition zone. In the depletion zone, the percentage of As(III) increased from 1% to 56 % in NP9 and was consistently above 60% in NP13. The increase in $As(III)_{VPC}$ in both depletion zones (Fig. 3-2$e_1$ vs 2$e_2$) was accompanied by an increase in $Fe(II)_{VPC}$ (Fig. 3-7 $b_1$ & $b_2$). The $Fe(II)_{VPC}$ was derived from FeS and/or sidertite in these depletion zone sediments.

The mineral phases dissolved by 1 M HCl were very poorly crystalline Fe oxides and/or Mn oxides in the sediments above the depletion zone, since there was no evidence of detectable quantities of directly, independently measured AVS. Because $Mn_{VPC}$ was many (10–20) orders of magnitude lower than $Fe_{VPC}$ (Fig. 3-7 $c_1$ & $c_2$), very poorly crystalline Fe oxide was the major mineral phase for association with As. $As(V)_{VPC}$ and

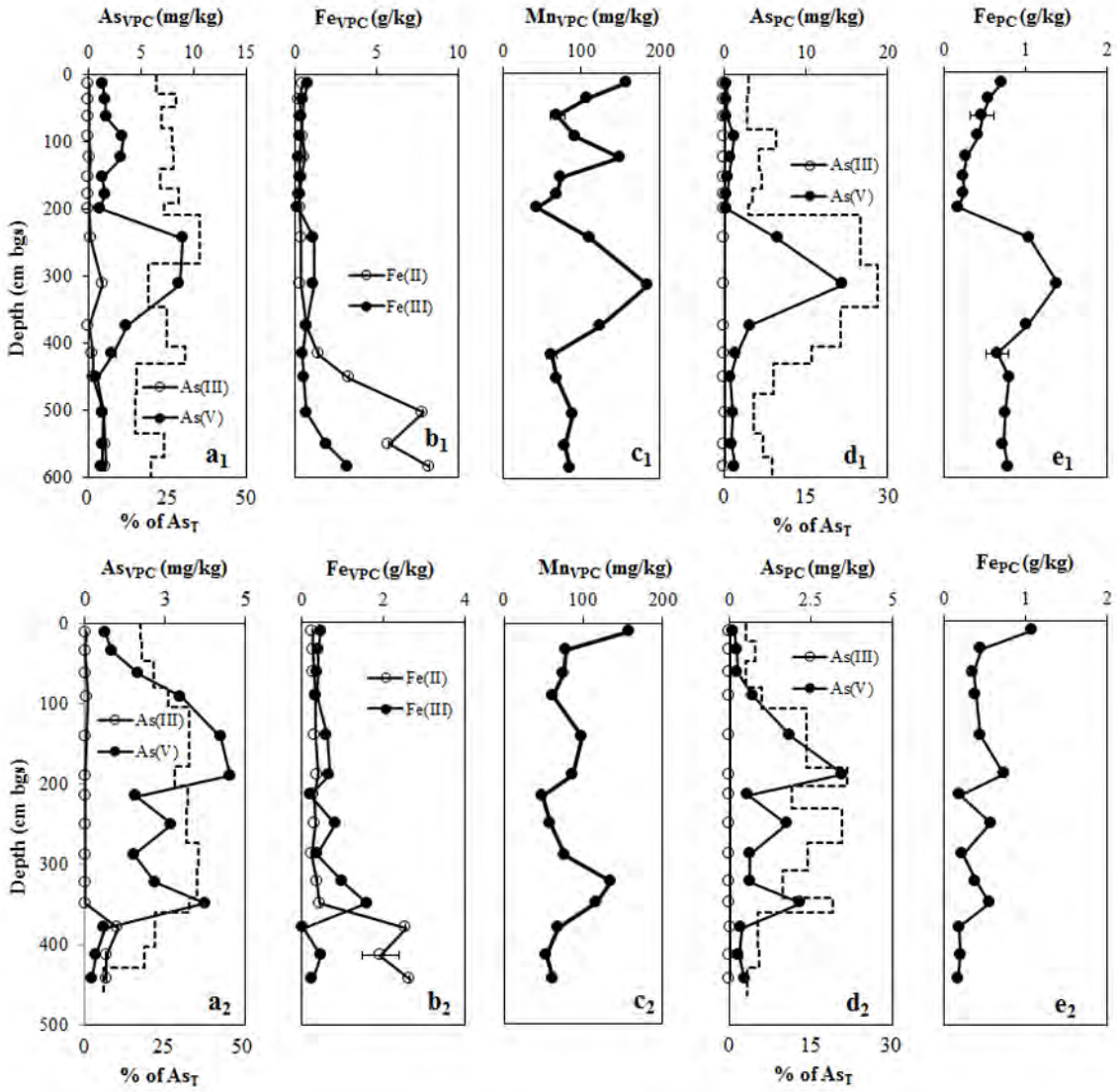


**Fig. 3-6.** Sequential extraction results for AVS, Mn oxides, and very poorly crystalline Fe oxides in NP9 ($a_1$–$c_1$) and NP13 ($a_2$–$c_2$): ($a_1$ and $a_2$) As speciation, ($b_1$ and $b_2$) Fe speciation, ($c_1$ and $c_2$) Mn; Sequential extraction results for poorly crystalline Fe oxides in NP9 ($d_1$–$e_1$) and NP13 ($d_2$–$e_2$): ($d_1$ and $d_2$) As speciation and ($e_1$ and $e_2$) Fe. Dashed line indicates percenrtage of total solid phase As recovered in each fraction. Error bars represent standard deviations.

As(III)$_{VPC}$ were both positively correlated with Fe$_{VPC}$ ($r^2$=0.62 and p=0.0071; $r^2$=0.59 and p=0.0093, respectively) in the sediments above the depletion zone of NP9 (Fig. 3-7); these correlations coefficients were higher if the vadose zone was excluded ($r^2$=0.94 and p=0.0004; $r^2$=0.79 and p=0.0072, respectively). In NP13, however, neither As(V)$_{VPC}$ nor

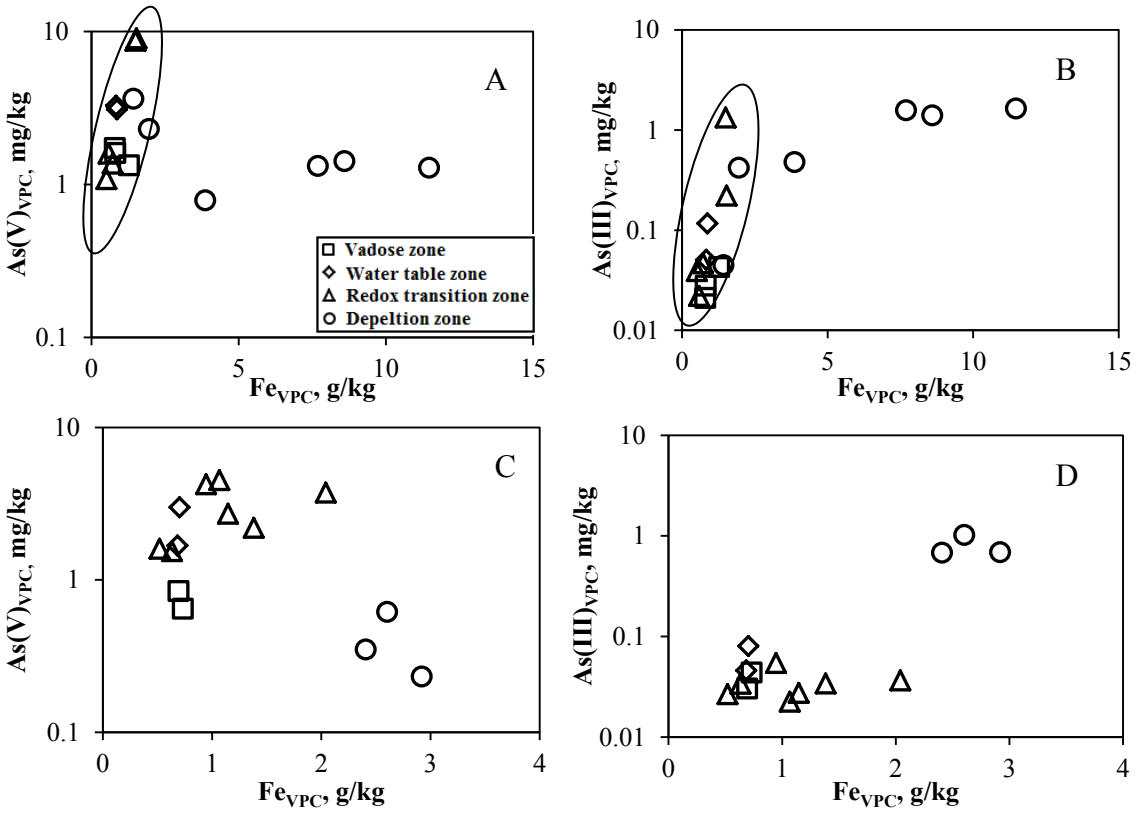


**Fig. 3-7.** Scatter plots of As(III) and As(V) against Fe in the extraction step of very poorly crystalline Fe oxides in NP9 (A & B) and NP13(C & D).

$As(III)_{VPC}$ correlated with $Fe_{VPC}$ above the depletion zone or in the redox transition zone. There was no correlation observed between $As_{VPC}$ and water-extractable As (Table 3-6). $As(V)_{VPC}$, however, was correlated with water-extractable As(V) in both cores, but the correlations were weaker compared to the first two steps. $As(III)_{VPC}$ was only correlated with water-extractable As(III) in NP13 (Table 3-6).

The concentrations of As associated with poorly crystalline Fe oxides, $As_{PC}$, ranged from 0.21 to 1.4 mg/kg and 0.12 to 3.48 mg/kg in NP9 and NP13, respectively (Fig. 3-6 $d_1$&$d_2$). $As(III)_{PC}$ was lower than 0.02 mg/kg in NP9 and below the detection limit in most of the layers in NP13. $As_{PC}$, primarily As(V), were usually lower than $As_{VPC}$ except in 208 to 404 cm of NP9. The oxidation state of $As_{VPC}$ was not distinguished for

correlation consideration since $As(III)_{VPC}$ was low. The higher $As_{PC}$ concentrations were accompanied by higher $Fe_{PC}$ concentrations (Fig. 3-6 $e_1$ & $e_2$); $As_{PC}$ correlated with $Fe_{PC}$ in NP9 ($r^2$=0.68 and p=0.0241) but not in NP13 (scatter plots are shown in Fig. B-8). Correlation between $As_{PC}$ and water-extractable As was not observed in either of the two cores.

### 3.6.2. Crystalline and Residual Phases (F5-F7)

The last three extraction steps are designed to extract As associated with crystalline sulfides ($As_{Sul}$), crystalline Fe oxides ($As_{Cry}$), and the residual phase ($As_{Res}$). Although these mineral phases are less soluble, they are weathered by soil forming processes, slowly releasing As. Correlation was not observed between As in any of these three pools and the water-extractable As.

$As_{Sul}$ was predominantly As(V) in both cores (Fig. 3-8 $a_1$ & $a_2$). The dominance of As(V) in $As_{Sul}$ has to be interpreted with caution. As(V) bound to sulfides is more likely to be surficially bound, since As(V) should not be in the lattice structure of any sulfide. Sulfide-bound As(V) should have been extracted in the previous steps, thus $As_{Sul}$ should be dominated by reduced As species. A portion of $As(V)_{Sul}$ could be derived from either the oxidation of As(III) or from other As(V)-bearing mineral(s) that has similar solubilities to crystalline sulfides. Insufficient removal of poorly crystalline Fe oxides, during the previous steps, could cause inevitable oxidation of As(III) (Huang and Kretzschmar, 2010). A discernible amount of $As(III)_{Sul}$ was detected in depletion zone II of NP9 and the depletion zone of NP13, although the concentrations of $As(III)_{Sul}$ were low compared to $As(V)_{Sul}$. The presence of pyrite was supported by QEMSCAN analyses

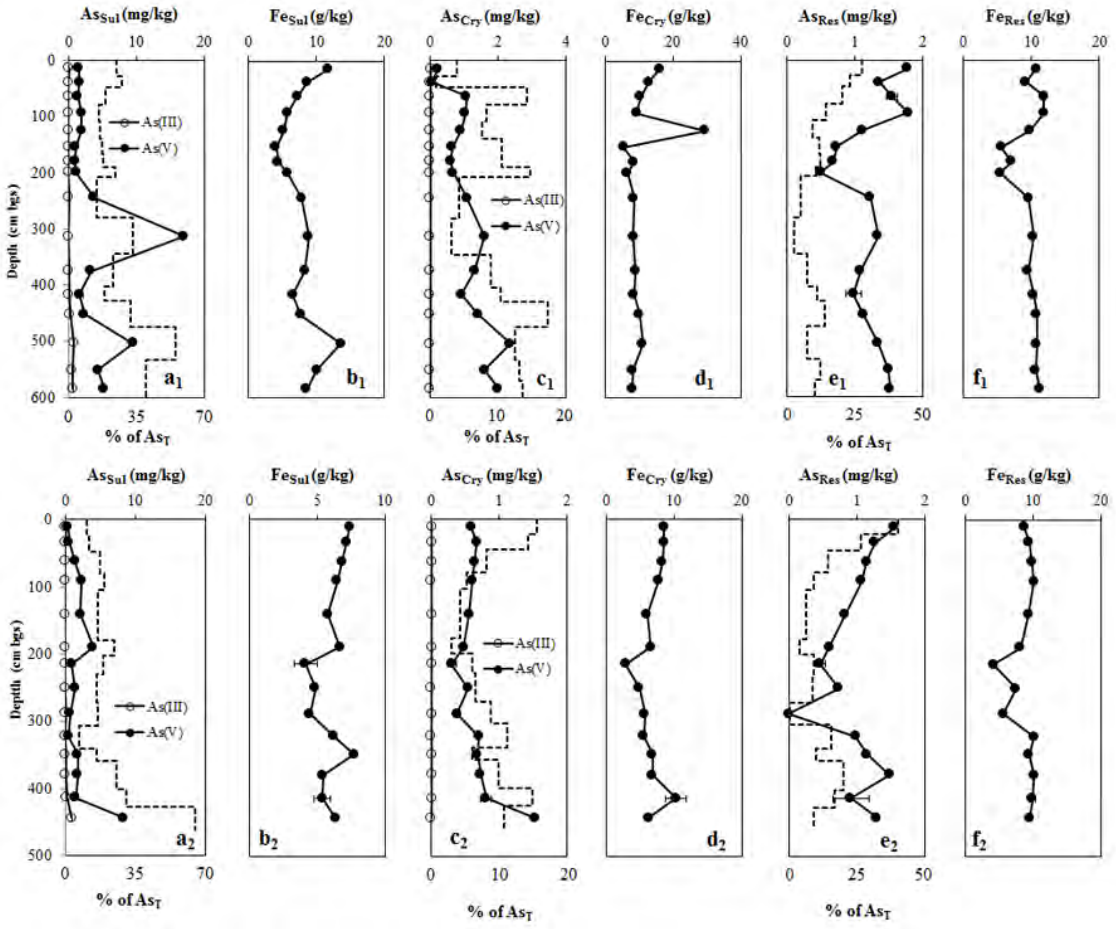


**Fig. 3-8.** As and Fe associated with sulfides ($a_1$ and $b_1$), crystalline Fe oxides ($c_1$ and $d_1$), and residual phase ($e_1$ and $f_1$) in NP9; As and Fe associated with sulfides ($a_2$ and $b_2$), crystalline Fe oxides ($c_2$ and $d_2$), and residual phase ($e_2$ and $f_2$) in NP13. Dashed line indicates percentage of total solid phase As recovered in each fraction. Error bars represent standard deviations.

(Table 3-2). These sediments also contained detectable FeS, which is needed for formation of $FeS_2$ (Berner, 1984). These $As(III)_{Sul}$ could be pyrite-associated. The $As(III)_{Sul}$, however, can also be derived from As sulfides such as orpiment ($As_2S_3$) and realgar (AsS). Geochemical modeling indicated formation of orpiment in most layers of the profile. In the sediments above the depletion zone, the highest $As(III)_{Sul}$ occurred in the vadose zone sediments.

$Fe_{Cry}$ ranged from 5.4–29.5 g/kg in NP9 and 2.9–10.3 g/kg in NP13 (Fig. 3-8 $d_1$ & $d_2$), accounting for ~30% of the total solid phase Fe. Although $Fe_{Cry}$ was much greater than $Fe_{VPC}$ and $Fe_{PC}$, $As_{Cry}$ was only <2.4 mg/kg in NP9 and <2.0 mg/kg in NP13 (Fig. 3-8 $c_1$ & $c_2$). This agreed with the widely reported observation that the adsorption efficiency of As(III) and As(V) on crystalline Fe oxides is much less than on poorly crystalline Fe oxides (Grafe et al., 2001; Grafe et al., 2002). $As(III)_{Cry}$ was consistently less than 5 μg/kg even in the depletion zone. The range of $As_{Res}$, <2.5 g/kg, was similar to $As_{Cry}$ (Fig. 3-8 $f_1$ & $f_2$). Neither $As_{Cry}$ nor $As_{Res}$ correlated with Fe in the corresponding extraction step.

## 4. Discussion

### 4.1. Vadose Zone

In the vadose zone, As-bearing minerals with low solubilities, targeted by extraction fractions F5–F7, played an indispensable role in As cycling deeper in the profile. The portion of As associated with crystalline Fe oxides, crystalline sulfides, and the residual phase exceeded 50% of total solid phase As in both cores (Fig. 3-9).

The low solubility As-bearing minerals, occurring in the vadose zone are potentially derived from the Salt Lake Formation. The Salt Lake Formation, which contains volcanic rocks, is found in the surrounding mountains (Dover, 2005; Evans and Oaks, 1996). The exposed Salt Lake Formation was eroded by ancient lake movements and deposited as lacustrine materials. The basin floor is covered by offshore lacustrine silt and clay deposits (Oviatt et al., 1992). Eolian process also eroded and delivered the Salt Lake Formation sediments into the basin. Anaerobic microsites within the vadose zone serve to preserve these reduced forms of As. These arsenic-bearing materials may

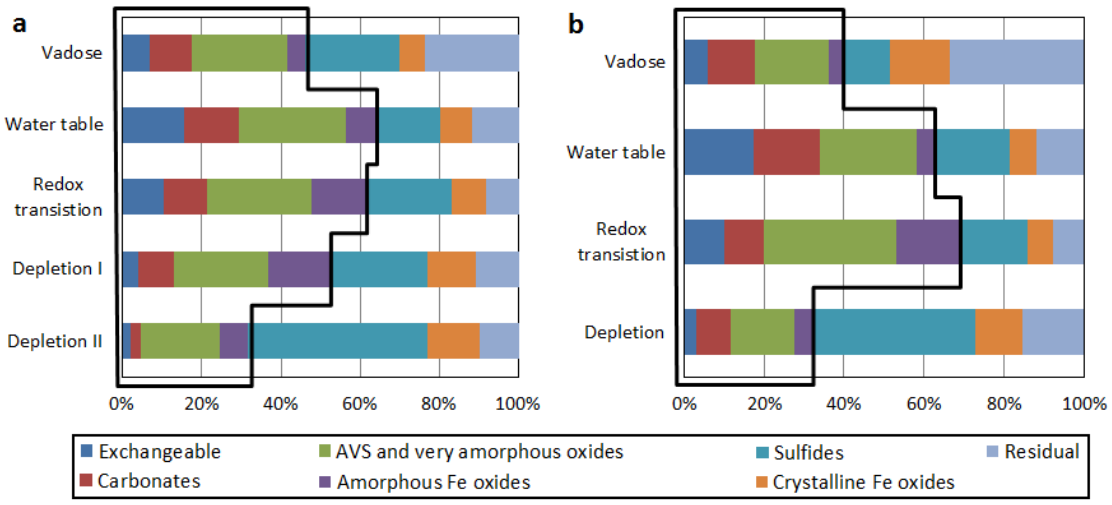


**Fig. 3-9.** Averaged percentage of As in each pool of the total As in NP9 (a) and NP13 (b). The squared box indicates the labile pools.

be continuously deposited on the soil surface. These low solubility As-bearing minerals undergo slow weathering processes under surficial conditions, particular in this semi-arid climate. The As that was originally associated with these less soluble As pools would be re-partitioned to more labile pools and would produce soluble As over time.

The presence of low solubility As-bearing mineral in the vadose zone is supported by the observation that the water-soluble and carbonate-associated As in the vadose zone of NP9 and NP13 contained not only As(V) but also As(III). The presence of As(III) under oxidizing conditions indicated that a source of As(III) was present. As emphasized by Polizzotto et al. (2006), there must be a replenishing source of As for the continuous cycling of As down the profile. Arsenopyrite as well as realgar and orpiment, oxidizes to produce soluble As(III) and As(V) when supplied with air and water (Basu and Schreiber, 2013; Islam et al., 2013; Lengke et al., 2009). The As(III) present in the vadose zone therefore was probably due to the oxidative dissolution of sulfides and/or micro reduced environments.

Along with the weathering of As-bearing materials in the vadose zone, soluble As is leached to greater depths with infiltration from precipitation, snow-melt, and irrigation. This vertical transport of As, fueled by near-surface processes, has been proposed by others (Busbee et al., 2009; Polizzotto et al., 2005). Polizzotto et al. (2006), and similarly Fendorf et al. (2010), hypothesized the As-bearing pyritic deposits from eroded Himalayan sediments are oxidized to form As-associated Fe oxides. Under reducing conditions imposed during monsoonal and flooding events in Bangladesh, As is released due to reductive dissolution of the host Fe oxide. Likewise, Busbee et al. (2009) stated that As(V) is leached from surficial sediments by irrigation in the Snake Plain, ID, although they did not delineate the source of As. The weathering of crystalline As-bearing minerals deposited in the surface soil, provides soluble As(III) and As(V) from the vadose zone through the carbonate enrichment zone, directly impacting groundwater quality. The mineral species are still unknown due to limitations in the chemical extraction methods. The exact species of the As-bearing mineral(s) were determined using synchrotron-based X-ray absorption spectroscopy as described in Chapter 4.

## 4.2. Carbonate Enrichment Zone

The maximum concentration of soluble As was consistently observed in the carbonate enrichment zone sediments in both profiles. Therefore, a considerable amount of As would be expected to enter the groundwater when the carbonate enrichment zone is affected by downward infiltration and groundwater fluctuation.

In term of percentages, the carbonate enrichment zone sediments contained more As within the labile pools, which was extracted in the first four fractions of sequential extraction. The association of As with the labile pools increased from the vadose zone to

the carbonate enrichment zone, 46% to 64% in NP9 and 40% to 63% in NP13, which was mainly due to the increases in ligand exchangeable As and carbonate-associated As (Fig. 3-9). This shift in As mineral association indicated that weathering-induced re-partitioning of As occurs from the surface soil to the carbonate enrichment zone.

Without a separate carbonate extraction step the carbonate fraction would be included with Mn oxides and very poorly crystalline Fe oxides with the use of 1 M HCl as an extractant (Kocar et al., 2008; Swartz et al., 2004). The sediments in this study are, however, rich in carbonate minerals (Fig. 3-2 $j_1$ & $j_2$), so an additional acetate buffer extraction step was added to define this important mineral phase in semi-arid and arid environments. Due to high evapotranspiration rates, soluble salts were accumulated in the vadose zone (Fig. 3-2 $c_1$ & $c_2$), while the carbonate minerals, which have low solubilities, precipitated out in the carbonate enrichment zone. The correlation between As and carbonate minerals in both NP9 and NP13 suggested that Mn-bearing carbonate and Ca/Mg-bearing carbonate, potentially dolomite, hosted a significant amount of As. The adsorption of As onto Mn carbonate has not been studied, but the mechanism and efficiency should be similar to the sorption of As on to Ca carbonate due to their similar structure. Dolomite was reported to sorb As(V) (Thornburg and Sahai, 2004).

The carbonate enrichment zone sediments sequestered As leached from the vadose zone. The retention of As(III) was attributable to the carbonate minerals formed in the carbonate enrichment zone, while As(V) was associated with ligand-exchangeable surfaces, carbonates, Mn oxides, and poorly crystalline Fe oxides. Although carbonate minerals were thought to be effective As traps due to their low solubility, As(V) associated with the carbonate phase was the source of solubilized As in microcosm

studies using sediments from this study area. A high water table event may trigger the desorption process, due to the change in water content and solute composition.

### 4.3. Redox Transition Zone

Although an enrichment of As was observed in the carbonate enrichment zone, the highest total sediment As content in both profiles occurred within the redox transition zone, where Mn oxides and poorly crystalline Fe oxides (dissolved by 1 M HCl and oxalate solutions) comprised the most important pool of As. Since the surface-bound As was removed by phosphate via ligand exchange in the first step of the sequential extraction, this As was associated with the mineral structure of Fe and Mn oxides.

Fe and Mn oxides accumulate in the zone with fluctuating redox conditions. Although the formation and dissolution of these oxides is not necessarily synchronized with groundwater fluctuation, it is reasonable to assume that a low water table facilitates the formation of Fe and Mn oxides. As the water table recedes, oxygen diffusion to pore space is enhanced, and previously soluble Fe(II) and Mn(II) oxidize to insoluble forms. The As leached with irrigation water or rainfall from the vadose zone and carbonate enrichment zone is then adsorbed or co-precipitated with the newly formed and deposited Fe and Mn oxides. This may explain the accumulation of As at 208–345 cm in NP9 (Fig. 3-2 $a_1$) and 104–201 in NP13 (Fig. 3-2 $a_2$).

During the wet season, when the water table is high and the redox transition zone is saturated, the sediments become less and less oxidized. When oxygen and nitrate are depleted, Fe and Mn in oxides are reduced by microbial activity as native organic carbon (NOC) is oxidized, releasing As into the pore water. This mechanism of As solubilization has been hypothesized by many researchers (Nickson et al., 2000; Smedley and

Kinniburgh, 2002; Swartz et al., 2004). The SOC ranged from 0.05 to 3.24 (w/w%) in the redox transition zone (Fig. 3-2e & 3e), but the organic carbon that fuels As solubilization does not have to be abundant, just bioavailable (Fendorf et al., 2010). In a microcosm study in which sediments from redox transition zones were incubated with groundwater from this site, decoupled As(V) solubilization and Fe reduction were observed (Chapter 2). Arsenic solubilization fueled by NOC has been observed in the field and in other laboratory microcosm studies (Rowland et al., 2011; Rowland et al., 2007). The NOC content, in these reported studies was less than or equal to 0.1% w/w. Arsenic solubilization can be enhanced by the direct microbial reduction of As(V) when the system is switched to reducing conditions (Ahmann et al., 1997; Ohtsuka et al., 2013; Tufano et al., 2008). Dissimilatory arsenic reducing bacteria (DARB) that contribute to As reduction have been identified in sediments collected from the same site as in this study (Mirza et al., 2014).

### 4.4. Depletion Zone

The shift in oxidation state was captured in the NP9 profile. Depletion zone I of NP9 showed visible Fe oxides and depletion features. The percentage of Fe(II) in the HCl-extractable Fe increased, and AVS began to form in this changing zone (Fig. 3-2 $b_1$ & $b_2$ and 3-2 $e_1$ & $e_2$). The shift in the oxidation state in the NP13 profile is not as distinct. The total sediment As content decreased compared to the overlaying redox transition zone sediments, indicating that permanent saturation resulted in a decrease in the As retention capability of the solid phase. Sequential extraction results revealed that the decrease was due to changes in poorly crystalline Fe oxides fractions, including the microbial dissolution of Fe oxides, as described above, and crystallization of poorly

crystalline Fe oxides. The presence of Fe(II) catalyzes crystallization of Fe oxides under anoxic conditions (Pedersen et al., 2005; Yang et al., 2010; Yee et al., 2006), which causes a loss of adsorption sites and a dramatic decrease in adsorption efficiency.

Although permanent saturation triggers the loss of poorly crystalline Fe oxides, new As scavenging minerals would form as soon as microbial sulfidogenesis initiates. Both FeS and $FeS_2$ were formed in the depletion zone of the two studied sediment cores, as indicated by AVS extraction and F5 in the sequential extractions. The crystalline sulfides fraction, presumably $FeS_2$, was the dominant As pool (45% in NP9 and 40% in NP13) in the depletion zone sediments. The crystalline sulfide in the depletion zone should be authigenic since the conditions facilitated the formation of crystalline sulfides. The formation of FeS indicated sulfate reducing conditions, which are required for $FeS_2$ (Berner, 1984). FeS and $FeS_2$ were reported to adsorb As(III) by forming FeAsS-like precipitation (Bostick and Fendorf, 2003). The As can also be fixed in solid phases due to the formation of $As_2S_3$ and AsS. The As sulfides are stable under reducing conditions. This attenuation process by sulfides could be limited by deficient sulfate concentrations (Fendorf et al., 2010; O'Day et al., 2004). This study site, however, had sufficient soluble sulfate for reduction in the depletion zone sediments (Fig. 3-3 d & 3-4 d).

## 5. Conclusions

The present study investigates As mineralogy and how this mineralogy affects As solubilization in two sediment profiles from the ground surface to the depth of permanent water saturation (depletion zone). The result reveals that As mineral association varies along the profile according to water conditions and redox conditions (Figure 3-10 a & b). The less soluble As-bearing minerals, probably sulfides, were deposited at the soil

surface. The continued presence of As sulfide minerals would indicate a continuous source of these minerals from wind and water erosion of the exposed Salt Lake Formation at the margins of the valley and the surrounding mountains. Weathering of these As-bearing minerals in the vadose zone, results in soluble As and As associated with labile pools. Below the vadose zone As is associated with carbonate minerals in the carbonate enrichment zone and with Fe/Mn oxides in the redox transition zone. These two zones are influenced by the rising and lowering water table throughout the year. Figure 3-10 a shows conditions down the profile with a lowered water table, conditions at the time of sampling. Under these conditions, carbonates are formed as the water in the profile evaporates and oxygen penetrates deeper into the profile with formation of Fe(III) and Mn (III/IV) oxides. These mineral surfaces sorb solubilized and transported As(V) and As(III) from the vadose zone. With a rising water table (Figure 3-10 b), carbonate minerals dissolve and reducing conditions facilitate reductive dissolution of Fe and Mn oxides releasing As. Under both water regimes, As precipitates with sulfide minerals in the depletion zone.

As a consequence of varying As mineral association, the solubilization of naturally occurring As in the basin-fill aquifer in Cache Valley, Utah, involves a series of redox and non-redox processes occurring at different depths. Processes occurring within the vadose zone, the redox transition zone and the depletion zone have been proposed in other studied locations, but this present study demonstrates that these processes can co-exist within a shallow aquifer, 5~6 m deep. The role of carbonate minerals in As solubilization has received less research attention, and therefore has not previously been

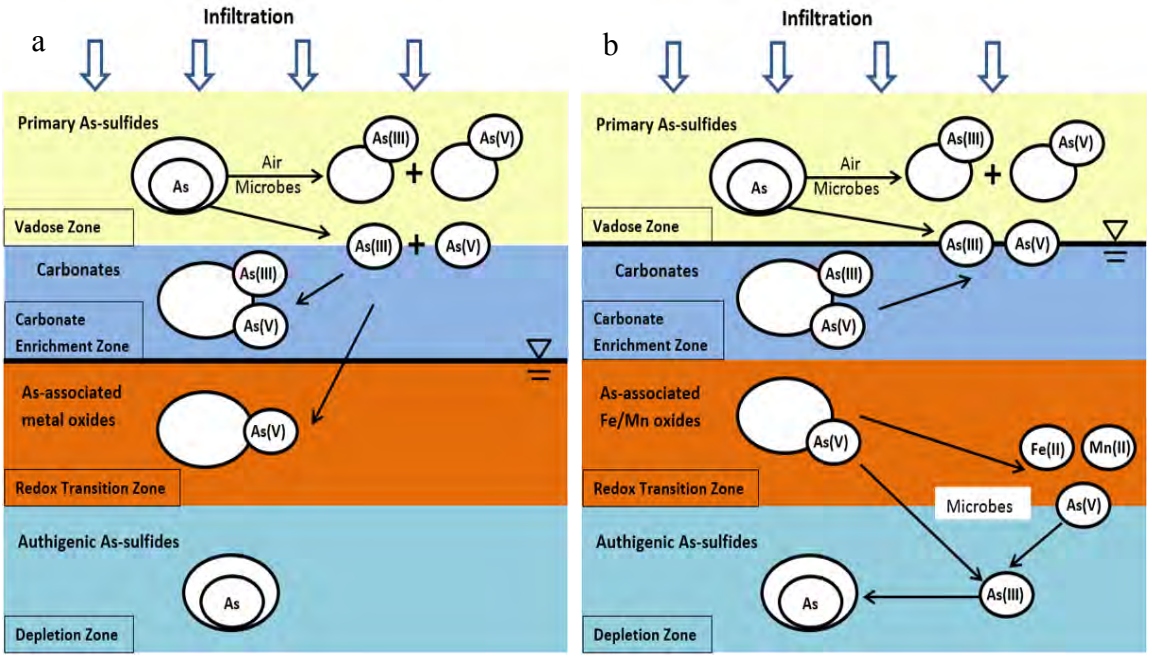


**Fig. 3-10.** Sketches of varying As mineralogy in the sediment profile (a) and As solubilization triggered by rising water table (b).

reported. Carbonate minerals are common in semi-arid and arid regions, but they are not a significant pool for As association in the humid regions of the world where As solubilization has been most studied.

The specific information of As speciation, including oxidation state and mineral association in each zone, especially the vadose zone and carbonate enrichment zone, will be investigated in the next chapter. This information is needed to clarify the species of As sources occurring at the ground surface and the role of carbonate minerals in affecting As distribution to the groundwater. Since the basin-fill aquifer groundwater is the primary source of domestic and irrigation water supply in the semi-arid southwestern U.S., understanding As mineralogy and processes that affect As solubility is urgent.

## References

Ahmann, D., Krumholz, L.R., Hemond, H.F., Lovley, D.R., Morel, F.M.M., 1997. Microbial mobilization of arsenic from sediments of the Aberjona Watershed. Environ. Sci. Technol. 31, 2923-2930.

Akai, J., Izumi, K., Fukuhara, H., Masuda, H., Nakano, S., Yoshimura, T., Ohfuji, H., Anawar, H.M., Akai, K., 2004. Mineralogical and geomicrobiological investigations on groundwater arsenic enrichment in Bangladesh. Appl. Geochem. 19, 215-230.

Alexandratos, V.G., Elzinga, E.J., Reeder, R.J., 2007. Arsenate uptake by calcite: Macroscopic and spectroscopic characterization of adsorption and incorporation mechanisms. Geochim. Cosmochim. Acta 71, 4172-4187.

Amacher, M.C., 1996. Nickel, cadmium, and lead, In: Sparks, D., Page, A., Helmke, P., Loeppert, R., Soltanpour, P., Tabatabai, M., Johnston, C., Sumner, M. (Eds.), Methods of Soil Analysis. Part 3-Chemical Methods, Soil Science Society of America, Madison, WI, pp. 739-768.

Anawar, H.M., Akai, J., Komaki, K., Terao, H., Yoshioka, T., Ishizuka, T., Safiullah, S., Kato, K., 2003. Geochemical occurrence of arsenic in groundwater of Bangladesh: sources and mobilization processes. J. Geochem. Explor. 77, 109-131.

Bardelli, F., Benvenuti, M., Costagliola, P., Di Benedetto, F., Lattanzi, P., Meneghini, C., Romanelli, M., Valenzano, L., 2011. Arsenic uptake by natural calcite: an XAS study. Geochim. Cosmochim. Acta 75, 3011-3023.

Basu, A., Schreiber, M.E., 2013. Arsenic release from arsenopyrite weathering: insights from sequential extraction and microscopic studies. J. Hazard. Mater. 262, 896-904.

Berner, R.A., 1984. Sedimentary pyrite formation - an update. Geochim. Cosmochim. Acta 48, 605-615.

Bhattacharya, P., Claesson, M., Bundschuh, J., Sracek, O., Fagerberg, J., Jacks, G., Martin, R.A., Storniolo, A.D., Thir, J.M., 2006. Distribution and mobility of arsenic in the Rio Dulce alluvial aquifers in Santiago del Estero Province, Argentina. Sci. Total Environ. 358, 97-120.

Bostick, B.C., Fendorf, S., 2003. Arsenite sorption on troilite (FeS) and pyrite ($FeS_2$). Geochim. Cosmochim. Acta 67, 909-921.

Brandvold, L., 2001. Arsenic in ground water in the Socorro Basin, New Mexico. New Mexico Geol. 23, 2-8.

Brummer, J., 1991. Origins of low-angle normal faults along the west side of the Bear River Range in northern Utah [MS thesis]: Logan. Utah State University.

Busbee, M.W., Kocar, B.D., Benner, S.G., 2009. Irrigation produces elevated arsenic in the underlying groundwater of a semi-arid basin in Southwestern Idaho. Appl. Geochem. 24, 843-859.

Costagliola, P., Rimondi, V., Benvenuti, M., Chiarantini, L., Di Benedetto, F., Gasparon, M., Lattanzi, P., Paolieri, M., 2007. Arsenic uptake by natural calcites: preliminary results from sequential extraction of Italian Travertines, IMWA Symposium 2007: Water in mining environments. Universita degli Studi di Cagliari, pp. 415-418.

Dixit, S., Hering, J.G., 2003. Comparison of arsenic(V) and arsenic(III) sorption onto iron oxide minerals: Implications for arsenic mobility. Environ. Sci. Technol. 37, 4182-4189.

Dover, J.H., 2005. Geologic Map of the Logan 30' x 60' Quadrangle, Cache and Rich Counties, Utah and Lincoln and Uinta Counties, Wyoming, Map I-2210, Miscellaneous Investigations Series. Utah Geological Survey, Salt Lake City.

Drahota, P., Filippi, M., 2009. Secondary arsenic minerals in the environment: a review. Environ. Int. 35, 1243-1255.

Evans, J.P., Oaks, R.Q., 1996. Three-dimensional variations in extensional fault shape and basin form: The Cache Valley Basin, eastern Basin and Range province, United States. Geol. Soc. Am. Bull. 108, 1580-1593.

Fendorf, S., Michael, H.A., van Geen, A., 2010. Spatial and temporal variations of groundwater arsenic in South and Southeast Asia. Science 328, 1123-1127.

Fujii, R., Swain, W.C., 1995. Areal distribution of selected trace elements, salinity, and major ions in shallow ground water, Tulare Basin, Southern San Joaquin Valley, California, Water-Resources Investigations Report 95-4048. U.S. Geological Survey, Sacramento, CA.

Georgiadis, M., Cai, Y., Solo-Gabriele, H.M., 2006. Extraction of arsenate and arsenite species from soils and sediments. Environ. Pollut. 141, 22-29.

Grafe, M., Eick, M.J., Grossl, P.R., 2001. Adsorption of arsenate(V) and arsenite(III) on goethite in the presence and absence of dissolved organic carbon. Soil Sci. Soc. Am. J. 65, 1680-1687.

Grafe, M., Eick, M.J., Grossl, P.R., Saunders, A.M., 2002. Adsorption of arsenate and arsenite on ferrihydrite in the presence and absence of dissolved organic carbon. J. Environ. Qual. 31, 1115-1123.

Grossl, P.R., Sparks, D.L., 1995. Evaluation of contaminant ion adsorption/desorption on goethite using pressure jump relaxation kinetics. Geoderma 67, 87-101.

Heron, G., Crouzet, C., Bourg, A.C.M., Christensen, T.H., 1994. Speciation of Fe(II) and Fe(III) in contaminated aquifer sediments using chemical-extraction techniques. Environ. Sci. Technol. 28, 1698-1705.

Hinkle, S.R., Polette, D.J., 1999. Arsenic in ground water of the Willamette Basin, Oregon, Water-Resources Investigations Report 98–4205. U.S. Dept. of the Interior, U.S. Geological Survey, Portland, OR.

Hintze, L.F., 2005. Utah's spectacular geology: how it came to be. Department of Geology, Brigham Young University.

Horneman, A., Van Geen, A., Kent, D.V., Mathe, P.E., Zheng, Y., Dhar, R.K., O'Connell, S., Hoque, M.A., Aziz, Z., Shamsudduha, M., Seddique, A.A., Ahmed, K.M., 2004. Decoupling of As and Fe release to Bangladesh groundwater under reducing conditions. Part 1: Evidence from sediment profiles. Geochim. Cosmochim. Acta 68, 3459-3473.

Huang, J.H., Kretzschmar, R., 2010. Sequential extraction method for speciation of arsenate and arsenite in mineral soils. Anal. Chem. 82, 5534-5540.

Islam, A.B.M.R., Maity, J.P., Bundschuh, J., Chen, C.-Y., Bhowmik, B.K., Tazaki, K., 2013. Arsenic mineral dissolution and possible mobilization in mineral–microbe–groundwater environment. J. Hazard. Mater. 262, 989-996.

Jain, A., Loeppert, R.H., 2000. Effect of competing anions on the adsorption of arsenate and arsenite by ferrihydrite. J. Environ. Qual. 29, 1422-1430.

Kariya, K.A., Roark, D.M., Hanson, K.M., Geological Survey (U.S.), Utah. Division of Water Resources., Utah. Division of Water Rights., 1994. Hydrology of Cache Valley, Cache County, Utah, and adjacent part of Idaho, with emphasis on simulation of ground-water flow. State of Utah Natural Resources [Salt Lake City, Utah].

Keon, N.E., Swartz, C.H., Brabander, D.J., Harvey, C., Hemond, H.F., 2001. Validation of an arsenic sequential extraction method for evaluating mobility in sediments. Environ. Sci. Technol. 35, 3396-3396.

Klute, A., 1986. Methods of Soil Analysis. Part 1. Physical and Mineralogical Methods. American Society of Agronomy, Inc., Madison, WI.

Kocar, B.D., Polizzotto, M.L., Benner, S.G., Ying, S.C., Ung, M., Ouch, K., Samreth, S., Suy, B., Phan, K., Sampson, M., Fendorf, S., 2008. Integrated biogeochemical and hydrologic processes driving arsenic release from shallow sediments to groundwaters of the Mekong delta. Appl. Geochem. 23, 3059-3071.

Kottek, M., Grieser, J., Beck, C., Rudolf, B., Rubel, F., 2006. World map of the Koppen-Geiger climate classification updated. Meteorol Z 15, 259-263.

Lengke, M.F., Sanpawanitchakit, C., Tempel, R.N., 2009. The oxidation and dissolution of Arsenic-Bearing Sulfides. Can. Mineral. 47, 593-613.

Liao, V.H.C., Chu, Y.J., Su, Y.C., Lin, P.C., Hwang, Y.H., Liu, C.W., Liao, C.M., Chang, F.J., Yu, C.W., 2011. Assessing the mechanisms controlling the mobilization of arsenic in the arsenic contaminated shallow alluvial aquifer in the blackfoot disease endemic area. J. Hazard. Mater. 197, 397-403.

Lovley, D.R., Phillips, E.J.P., 1986. Availability of ferric iron for microbial reduction in bottom sediments of the fresh-water tidal Potomac River. Appl. Environ. Microbiol. 52, 751-757.

Lowe, M., Wallace, J., Bishop, C., Hurlow, H., 2003. Ground-water quality classification and recommended septic tank soil-absorption-system density maps, Utah Geological Survey Special Study 101. Utah Geological Survey, Salt Lake City, UT, p. 31.

Manning, B.A., Goldberg, S., 1996. Modeling competitive adsorption of arsenate with phosphate and molybdate on oxide minerals. Soil Sci. Soc. Am. J. 60, 121-131.

Manning, B.A., Goldberg, S., 1997. Arsenic(III) and arsenic(V) absorption on three California soils. Soil Sci. 162, 886-895.

McArthur, J.M., Ravenscroft, P., Safiulla, S., Thirlwall, M.F., 2001. Arsenic in groundwater: Testing pollution mechanisms for sedimentary aquifers in Bangladesh. Water Resour. Res. 37, 109-117.

McCleskey, R.B., Nordstrom, D.K., Maest, A.S., 2004. Preservation of water samples for arsenic(III/V) determinations: an evaluation of the literature and new analytical results. Appl. Geochem. 19, 995-1009.

Mirza, B.S., Muruganadam, S., Meng, X., Sorensen, D.L., Dupont, R.R., McLean, J.E., 2014. Arsenic(V) reduction in relation to iron(III) transformation and molecular characterization of the structural and functional microbial community in sediments of a Northern Utah, basin-fill aquifer. Appl. Environ. Microbiol., AEM. 00240-00214.

Ng, J.C., Wang, J.P., Shraim, A., 2003. A global health problem caused by arsenic from natural sources. Chemosphere 52, 1353-1359.

Nickson, R.T., McArthur, J.M., Ravenscroft, P., Burgess, W.G., Ahmed, K.M., 2000. Mechanism of arsenic release to groundwater, Bangladesh and West Bengal. Appl. Geochem. 15, 403-413.

O'Day, P.A., Vlassopoulos, D., Root, R., Rivera, N., 2004. The influence of sulfur and iron on dissolved arsenic concentrations in the shallow subsurface under changing redox conditions. Proc. Natl. Acad. Sci. USA 101, 13703-13708.

Ohtsuka, T., Yamaguchi, N., Makino, T., Sakurai, K., Kimura, K., Kudo, K., Homma, E., Dong, D.T., Amachi, S., 2013. Arsenic Dissolution from Japanese Paddy Soil by a Dissimilatory Arsenate-Reducing Bacterium *Geobacter* sp. OR-1. Environ. Sci. Technol. 47, 6263-6271.

Oviatt, C.G., Currey, D.R., Sack, D., 1992. Radiocarbon Chronology of Lake Bonneville, Eastern Great-Basin, USA. Palaeogeogr. Palaeocl. 99, 225-241.

Pederick, R.L., Gault, A.G., Charnock, J.M., Polya, D.A., Lloyd, J.R., 2007. Probing the biogeochemistry of arsenic: response of two contrasting aquifer sediments from Cambodia to stimulation by arsenate and ferric iron. J. Environ. Sci. Part A 42, 1763-1774.

Pedersen, H., Postma, D., Jakobsen, R., Larsen, O., 2005. Fast transformation of iron oxyhydroxides by the catalytic action of aqueous Fe(II). Geochim. Cosmochim. Acta 69, 3967-3977.

Pierce, M.L., Moore, C.B., 1982. Adsorption of arsenite and arsenate on amorphous iron hydroxide. Water Res. 16, 1247-1253.

Polizzotto, M.L., Harvey, C.F., Li, G.C., Badruzzman, B., Ali, A., Newville, M., Sutton, S., Fendorf, S., 2006. Solid-phases and desorption processes of arsenic within Bangladesh sediments. Chem. Geol. 228, 97-111.

Polizzotto, M.L., Harvey, C.F., Sutton, S.R., Fendorf, S., 2005. Processes conducive to the release and transport of arsenic into aquifers of Bangladesh. Proc. Natl. Acad. Sci. USA 102, 18819-18823.

Ravenscroft, P., McArthur, J.M., Hoque, B.A., 2001. Geochemical and palaeohydrological controls on pollution of groundwater by arsenic. In: W.R. Chappell, C.O. Abernathy, R.L. Calderon (Eds.), 4th Internat. Conf. on Arsenic Exposure and Health Effects, Elsevier, Oxford.

Robertson, F.N., 1989. Arsenic in groundwater under oxidizing conditions, South-West United-States. Environ. Geochem. Health 11, 171-185.

Rowland, H.A.L., Gault, A.G., Lythgoe, P., Polya, D.A., 2008. Geochemistry of aquifer sediments and arsenic-rich groundwaters from Kandal Province, Cambodia. Appl. Geochem. 23, 3029-3046.

Rowland, H.A.L., Omoregie, E.O., Millot, R., Jimenez, C., Mertens, J., Baciu, C., Hug, S.J., Berg, M., 2011. Geochemistry and arsenic behaviour in groundwater

resources of the Pannonian Basin (Hungary and Romania). Appl. Geochem. 26, 1-17.

Rowland, H.A.L., Pederick, R.L., Polya, D.A., Pancost, R.D., Van Dongen, B.E., Gault, A.G., Vaughan, D.J., Bryant, C., Anderson, B., Lloyd, J.R., 2007. The control of organic matter on microbially mediated iron reduction and arsenic release in shallow alluvial aquifers, Cambodia. Geobiol. 5, 281-292.

Ryu, J.H., Gao, S.D., Tanji, K.K., 2010. Speciation and behavior of arsenic in evaporation basins, California, USA. Environ. Earth Sci. 61, 1599-1612.

Scanlon, B.R., Nicot, J.P., Reedy, R.C., Kurtzman, D., Mukherjee, A., Nordstrom, D.K., 2009. Elevated naturally occurring arsenic in a semiarid oxidizing system, Southern High Plains aquifer, Texas, USA. Appl. Geochem. 24, 2061-2071.

Seddique, A.A., Masuda, H., Mitamura, M., Shinoda, K., Yamanaka, T., Nakaya, S., Ahmed, K.M., 2011. Mineralogy and geochemistry of shallow sediments of Sonargaon, Bangladesh and implications for arsenic dynamics: Focusing on the role of organic matter. Appl. Geochem. 26, 587-599.

Smedley, P.L., Kinniburgh, D.G., 2002. A review of the source, behaviour and distribution of arsenic in natural waters. Appl. Geochem. 17, 517-568.

So, H.U., Postma, D., Jakobsen, R., Larsen, F., 2008. Sorption and desorption of arsenate and arsenite on calcite. Geochim. Cosmochim. Acta 72, 5871-5884.

Sparks, D.L., Soil Science Society of America., American Society of Agronomy, 1996. Methods of soil analysis. Part 3, Chemical methods. Soil Science Society of America: American Society of Agronomy, Madison, WI.

Swartz, C.H., Blute, N.K., Badruzzman, B., Ali, A., Brabander, D., Jay, J., Besancon, J., Islam, S., Hemond, H.F., Harvey, C.F., 2004. Mobility of arsenic in a Bangladesh aquifer: Inferences from geochemical profiles, leaching data, and mineralogical characterization. Geochim. Cosmochim. Acta 68, 4539-4557.

Tessier, A., Campbell, P.G.C., Bisson, M., 1979. Sequential extraction procedure for the speciation of particulate trace-metals. Anal. Chem. 51, 844-851.

Thornburg, K., Sahai, N., 2004. Arsenic occurrence, mobility, and 14 retardation in sandstone and dolomite formations of the Fox River Valley, eastern Wisconsin. Environ. Sci. Technol. 38, 5087-5094.

Tufano, K.J., Reyes, C., Saltikov, C.W., Fendorf, S., 2008. Reductive processes controlling arsenic retention: revealing the relative importance of iron and arsenic reduction. Environ. Sci. Technol. 42, 8283-8289.

USGS, 1962. Lake Bonneville. U.S. Govt. Print. Off., Washington, DC.

van Griethuysen, C., Gillissen, F., Koelmans, A.A., 2002. Measuring acid volatile sulphide in floodplain lake sediments: effect of reaction time, sample size and aeration. Chemosphere 47, 395-400.

Weber, F.A., Hofacker, A.F., Voegelin, A., Kretzschmar, R., 2010. Temperature dependence and coupling of iron and arsenic reduction and release during flooding of a contaminated soil. Environ. Sci. Technol. 44, 116-122.

Wenzel, W.W., Kirchbaumer, N., Prohaska, T., Stingeder, G., Lombi, E., Adriano, D.C., 2001. Arsenic fractionation in soils using an improved sequential extraction procedure. Anal. Chim. Acta 436, 309-323.

Yang, L., Steefel, C.I., Marcus, M.A., Bargar, J.R., 2010. Kinetics of Fe(II)-catalyzed transformation of 6-line ferrihydrite under anaerobic flow conditions. Environ. Sci. Technol. 44, 5469-5475.

Yee, N., Shaw, S., Benning, L.G., Nguyen, T.H., 2006. The rate of ferrihydrite transformation to goethite via the Fe(II) pathway. Am. Mineral. 91, 92-96.

# CHAPTER 4

# REDOX-CONTROLLED VARIATION IN ARSENIC MINERALOGY IN TWO SEDIMENT PROFILES IN THE CACHE VALLEY BASIN, UTAH: AN XAS STUDY


## Abstract

Elevated arsenic concentrations in groundwater have been reported in the semi-arid to arid Western U.S. Information defining arsenic speciation, including oxidation state and mineral association, is necessary to delineate the mechanism(s) of solubilization. In this study, two cores were collected from a shallow, basin-fill aquifer in the Cache Valley Basin, Utah where arsenic-bearing groundwater (up to 100 µg/L) and sediment (3.8 to 52 mg/kg) have been documented. These cores were chosen to investigate the arsenic speciation down the sediment profile using multiscale spectroscopic techniques including Quantitative Evaluation of Minerals by scanning electron microscopy (QEMSCAN), synchrotron-based bulk X-ray absorption near edge structure (XANES), and synchrotron based microfocused X-ray fluorescence spectroscopy (µXRF) and XANES. Results show the presence of arsenic sulfides and As(III) in the vadose zone sediments, which may indicate the deposition of primary arsenic-bearing minerals in the surface soil from volcanic rock exposed on the margins of the valley and in the surrounding mountains. Beneath the vadose zone, the dominant arsenic mineral association switched from a Mn-bearing mineral, probably Mn carbonate, to Fe oxides. The arsenic-bearing sulfides formed in the depletion zone prevent arsenic from solubilizing. This study demonstrated that arsenic speciation varied in these two sediment profiles due to groundwater fluctuation. The mechanism of arsenic solubilization differs

along the sediment profile due to the varying arsenic mineral association as influenced by redox conditions.

## 1. Introduction

The geochemistry of arsenic (As) has been intensively studied due to the need to identify geologic sources and mechanisms of solubilization, and for risk assessment and remediation of this common groundwater contaminant. The solubility of As is governed by the mineral association of As, the geochemistry of the groundwater, and physical/chemical/biological processes occurring within the aquifer (Smedley and Kinniburgh, 2002). Understandably the aquifer sediments in contact with groundwater have been the focus of field and laboratory studies that describe the reductive dissolution of iron (Fe) oxides as controlling As solubility. The presence of As associated with Fe oxides, a bioavailable carbon and energy source, reducing conditions, and an appropriate microbial community are necessary to facilitate As solubilization (McLean et al., 2006; Fendorf et al., 2010; Weber et al., 2010; Mirza et al., 2014). The major mechanism for As solubilization under reducing conditions is microbial reductive dissolution of host Fe oxide minerals (Nickson et al., 2000; Ravenscroft et al., 2001; McArthur et al., 2004). The direct microbial reductive dissolution of As(V)-bearing minerals (Tufano et al., 2008; Ohtsuka et al., 2013) can also occur. This research has included microcosm studies defining the role of synthetic and natural mineral forms of As-sorbed Fe oxides, organic carbon (OC) and microbes (Islam et al., 2004; Liao et al., 2011; Mirza et al., 2014); chemical extraction of aquifer minerals to describe association of As with defined mineral phases (Rowland et al., 2008; Busbee et al., 2009; Ryu et al., 2010); and advanced imaging techniques, including a synchrotron-based X-ray absorption

spectroscope (Foster et al., 1998; Walker et al., 2005; Arai et al., 2006; Voegelin et al., 2007).

The occurrence of As-bearing minerals, however, is not limited to the depth where reducing conditions are encountered. Correspondingly, processes other than reduction reactions can alter As biogeochemistry and mineralogy affecting As solubility. Polizotto et al. (2006) and Fendorf et al. (2010) suggest that As deposited as As-bearing pyritic materials in the river basins draining the Himalayas would be oxidized before leaching into the deeper profile. The rapid weathering of biotite under warm and humid conditions in the shallow sediments of Bangladesh (Seddique et al., 2011) may also be a surficial source of As. Polizzotto et al. (2006) argue that As must be re-supplied to the subsurface from surface sources for the continued high concentrations to be observed in groundwater. A study site in Cache Valley Basin, Northern Utah, supports this argument that As-bearing minerals are present in the top layers of the profile (Chapter 3). Surface sources of As from deposition of volcanic ash have been described in other semi-arid and arid regions (Bhattacharya et al., 2006; Scanlon et al., 2009). For example, arsenic concentration in groundwater located in the Snake River Plain, ID, originate from surface accumulated As(V) (Busbee et al., 2009).

Arsenic liberated after the weathering of surface deposits is sequestered by Fe oxides (Mok and Wai, 1994; Thornton, 1996; Polizzotto et al., 2006). Reductive dissolution of these Fe oxides would occur with seasonal flooding in monsoonal driven climate regions. Deeper in the profile, highly reducing conditions lead to the formation of stable As(III) sulfide minerals, as long as sufficient organic matter and sulfate is supplied to support dissimilatory sulfate reduction to form sulfide to react with the As (O'Day et

al., 2004; Hering et al., 2009). Although these profile processes have been described for conditions in Southern and Southeastern Asia, such studies have not been frequently reported for arid and semi-arid regions where mineral composition and redox cycling may be distinct from more humid regions.

Arsenic concentration has been estimated to exceed 10 μg/L, which is the maximum concentration of As allowed in drinking water (USEPA), in 43% of the groundwater collected from the basin fill aquifers of the Southwestern U.S. (Anning et al., 2012). A conceptual model of the processes occurring down a soil-aquifer profile was developed for the present study site (Chapter 3) using bulk geochemistry, sequential chemical extractions and statistical methods. A combination of spectroscopic techniques was utilized to define As speciation in two sediments profiles. The aim was to determine the change in As oxidation state and mineral association and thereby understand As solubilization mechanisms. Synchrotron-based microfocused X-ray absorption edge structure (XANES) and X-ray fluorescence (XRF) were used to elucidate the spatial distribution of As oxidation state and mineral association to test the conceptual model developed using conventional chemical methods. The specific objectives were to delineate: (1) the source of As occurring in the near surface material of this site, (2) the mineral association of As at the depths affected by fluctuation of the groundwater, and (3) the stability of As in the sediments under permanent reducing conditions.

## 2. Materials and Methods

### 2.1. Site Background

The Cache Valley Basin sits on the Utah/Idaho border and is approximately 80 km long and 24 km wide. The valley is bound on the east by the Bear River Range and on

the west by the Wellsville Mountains. The tertiary aged sediments, known as the Salt Lake Formation, consist of tuffaceous sandstones and siltstones, limestones, and conglomerates. Quateranry lactustrine and fluvial deposits (Alpine, Bonneville, and Provo Formations) overlay the Tertiary Formations in the Cache Valley Basin (Evans and Oaks, 1996). Much of the Quaternary sediment in the valley is associated with lake cycles within the Great Basin. Most recently, Lake Bonneville filled the valley from about 30,000 to 16,400 years ago. The Lake Bonneville shoreline was at an elevation of 1550 m above sea level for about 500 years. A catastrophic failure of the natural spillway at Red Rock Pass, Idaho, and climatic changes caused Lake Bonneville to retreat from Cache Valley about 14,000 years ago (Inkenbrandt, 2010). The Quaternary sediments extend to a depth of 150 m. The source of As may be associated with Tertiary age formations that are exposed at high elevations in the Bear River Range east of the basin and on the eastern side of the Wellsville Range. The Bear River Range was mined for copper, lead and silver and contains copper arsenic sulfosalts, including enargite and tennanite. A groundwater survey by the Utah Geological Survey indicated that 15% of a total of 157 groundwater wells tested had As concentrations exceeding the USEPA drinking water limit of 10 μg/L, with the highest reported concentration at 100 μg/L (Lowe et al., 2003).

## 2.2. Sampling

Two sediments cores, NP9 and NP13, were collected using a Geoprobe with direct push technique to a depth of 150 cm into a permanently saturated zone defined by low chroma minerals. Total core length, from the soil surface was 610 cm for NP9 and 457 cm for NP13. Each profile was divided in the field into zones based on visible

redoximorphic features and redox chemistry: vadose, water table, redox transition, and depletion. The core collection and zonation were described in Chapter 3. Briefly, the vadose zone included surface soil and the unsaturated sediments, whereas the carbonate enrichment zone included the sediments that contained the highest carbonate content. Red-brown Fe oxide and black Mn oxide patches in the sediment matrix were indicators of varying redox conditions defining the redox transition zone. The depletion zones, below 345 cm below ground surface (bgs) in NP9 and 358 cm bgs in NP13, were indicated by the greenish and bluish coloration that indicates prolonged saturation. A second core from each site was returned to the Utah Water Research Laboratory within 1 hour of collection. These second cores were sectioned according to the field observations and laboratory-observed changes in color and texture. The NP9 core generated 16 sections, while the NP13 core generated 14 sections. Each layer was analyzed for pore water quality and sediment geochemistry (Chapter 3). Use of chemical methods allowed for a description of bulk As mineralogy that included oxidation state (Chapter 3). To further support observations by these traditional methods, one layer from each zone was selected for spectroscopic analyses.

The sediments that contained relatively high bulk As content were preferred in order to ensure the identification of As minerals. The physiochemical properties of the selected sediments are shown in Table 4-1.

### 2.3. Powder Samples for Bulk XANES

For bulk XANES, the sediment samples for the select layers were mixed with de-gassed, deionized water to obtain a uniform sample, as described in Chapter 3. The sediment samples were dried in a glove bag filled with nitrogen (Coy Laboratory

Table 4-1
Physiochemical properties of eight sediments selected from two sediment cores.

| Profile | Sample ID | Depth | Redox profile | Clay | Silt | $CaCO_3$ | $As_T$ | $Fe_T$ |
|---|---|---|---|---|---|---|---|---|
| | | cm | | w/w% | w/w% | w/w% | mg/kg | g/kg |
| NP9 | NP9-1 | 0-28 | Vadose | 57 | 43 | 4.3 | 6.4 | 40.5 |
| | NP9-4 | 79-108 | Water table | 59 | 41 | 31.6 | 12.5 | 28.0 |
| | NP9-9 | 208-281 | Redox transition | 53 | 47 | 21.7 | 26.1 | 28.5 |
| | NP9-16 | 569-610 | Depletion | 65 | 35 | 17.3 | 14.6 | 41.4 |
| NP13 | NP13-1 | 0-22 | Vadose | 62 | 38 | 19.8 | 3.8 | 26.4 |
| | NP13-4 | 79-104 | Water table | 64 | 36 | 39.0 | 11.6 | 25.4 |
| | NP13-8 | 229-272 | Redox transition | 32 | 68 | 29.1 | 8.4 | 18.9 |
| | NP13-12 | 358-401 | Depletion | 53 | 47 | 21.7 | 7.4 | 25.8 |

Products, Grass Lake, MI) in a 15°C±2°C constant temperature room. Each of the sediments was ground to pass through a 38μm sieve and then spread onto a piece of 1 mil kapton tape. Larger particles were removed by rubbing the solids on the tape (Personal communication with Dale Brewe, a beamline scientist at the Argonne National Laboratory) to obtain the desired very fine particles. The particles left on the tape were then sealed with another piece of kapton tape. Each of the tape-sealed samples was folded two to four times to obtain a layered homogenous sample.

### 2.4. Reference Minerals

Reference minerals included As-bearing sulfides, sodium arsenate and arsenite salts, and As-adsorbed minerals. Arsenopyrite (FeAsS), enargite ($Cu_3AsS_4$), realgar (AsS), and orpiment ($As_2S_3$) were obtained from the mineral collection of the Department of Mines and Earth Sciences at the University of Utah. Sodium arsenate dibasic heptahydrate ($Na_2HAsO_4 \cdot 7H_2O$) and sodium arsenite ($NaAsO_2$) were used as standards for As(V) as arsenate and As(III) as arsenite. These sodium As salts were also used to prepare reference minerals for As(V)- and As(III)-adsorbed Fe oxides and calcite. Two-line ferrihydrite was synthesized in the lab (Schwertmann and Cornell, 2008), while goethite and calcite were purchased from Alfa Aesar. The adsorption protocol of As onto

Fe oxides was performed in a background electrolyte solution of 0.01 M $NaNO_3$ (Grafe et al., 2001; Grafe et al., 2002). The adsorption of As(V) onto calcite protocol was performed in a calcite-water suspension at approximately pH 8.3 (Alexandratos et al., 2007). As(III)-sorbed calcite was not prepared; it has been reported that very little As(III) sorbs to calcite (Oscarson et al., 1983; So et al., 2008). The sorbate and sorbent concentrations were adjusted to a molar ratio of 1/100. After shaking for 12 h, the slurries were centrifuged and the supernatants were decanted to obtain the solids. The As-sorbed minerals were dried in a glove-bag purged with $N_2$. The As-sorbed to ferrihydrite is referred to as As(III)_FHD and As(V)_FHD, while As(III)_Goe and As(V)_Goe indicate As-sorbed to goethite. Similarly, the As(V)-sorbed to calcite is referred to as As(V)_Ca. The reference minerals were made into tape-sealed powder samples as described for bulk sample preparation.

### 2.5. Thin Sections for µXAS

A Kubiena box (Kubiena, 1938) was inserted into the side of each intact section to extract a sediment block before the selected layers of the core were mixed. The Kubiena Box was a hand-made aluminum box (5 x 3 x 3 cm, L x W x H) with a removable top and bottom. Water was removed from these sediment blocks using the acetone replacement method (Murphy, 1985). The acetone replacement was performed in portable glove-bags purged with $N_2$. The acetone-dried blocks were then impregnated with a Spurr Low-Viscosity Embedding kit (Sigma-Aldrich), following the procedure developed by Swartz and Lindsley-Griffin (1990). The blocks were stored under $N_2$. Two weeks before imaging analysis, the impregnated blocks were sent to the Sample Preparation and Thin Section Laboratory at the College of Mines and Earth Sciences,

University of Utah, for thin section preparation. Grinding and polishing were performed with kerosene rather than water to reduce the influence of atmospheric oxygen. The thin sections were mounted on the Suprasil 3 slides to prevent interference from impurities in standard slide materials. When travelling to the synchrotron facilities, the thin sections were stored in a gas impermeable double zip AnaeroPouch®-Bag with AnaeroPouch®-$CO_2$ gas generators (Mitsubishi Gas Chemical Co. JP.).

### 2.6. QEMSCAN Analysis

Limited time was granted for SXAS analyses, so preliminary exploration of thin sections by Quantitative Evaluation of Minerals using scanning electron microscopy (QEMSCAN) provided information to improve the efficiency when using the advanced synchrotron instrument. Thin sections made from the selected sediments were analyzed for mineral composition using the QEMSCAN® 4300 at the College of Mines and Earth Sciences, University of Utah, as introduced in Chapter 3. Improvements, however, were made compared to the previous QEMSCAN analyses. In the present study, measurements in field scan mode were carried out on thin sections, rather than powder embedded with epoxy plugs. This approach provided not only a complete characterization of mineral composition across the scanned area but also a map reflecting spatial distribution of mineral species. Spectra were collected with 1000 total X-ray counts at a 30 μm spacing, and were compared to a Species Identification Protocol (SIP) that discriminated minerals on the basis of their characteristic X-ray and electron backscatter intensities. Compared to the original Barick 710 SIP, which was used in Chapter 3, a modified version was used in this study to improve measurement of Fe oxides. Each 5 x 3 $cm^2$ thin section was scanned for 480k points for an area of 27 x 9 $mm^2$.

## 2.7. Bulk-XANES

The bulk-XANES spectra were collected for reference minerals and sediments as tape-sealed powder samples at Sector 20-BM at the Advanced Photon Source (Argonne National Laboratory, Argonne, IL). The samples were mounted in a windowed chamber, and the window was sealed with 1 Mil Kapton tape to allow the beam in and out. The chamber was purged with inert gas (80% $N_2$ and 20% Ar). The standard minerals were analyzed under transmission mode, while the sediment samples were analyzed under fluorescence mode due to their low As content. Five to eight XANES spectra were collected up to 300 eV about the As Kα edge, with a beam size of ~200 μm using a 13-element detector. The handling of XANES spectra was performed using Athena in the Demeter Software Package (Version 0.9.20 by Bruce Ravel).

## 2.8. μXRF and μXANES

The μXRF and μXANES analyses were performed with the microprobe-equipped X26 beam at the National Synchrotron Light Source (Brookhaven National Laboratory, Brookhaven, NY). The sample holder was wrapped with a zip-lock bag that was purged with $N_2$ gas. Elemental compositional maps for As, Fe, Mn, Cu, Ca, Sr, and Rb were collected in the areas of interest, according to mineral composition maps from QEMSCAN, using μXRF technique with a pixel size of 10 μm. Sr and Ca were used as markers for carbonate minerals, whereas Rb was used to indicate clay minerals. Once the distribution of As was mapped, μXANES spectra were collected up to 30 eV above the As Kα edge (11867 eV) in florescence mode at several locations within the mapped area. The μXRF and μXANES were conducted with a beam size of ~10 μm using Si drift detectors consisting of two single channel detectors and one four-channel detector (SII

Inc., USA). The μXRF maps were plotted from raw data using XMap Plotter (IDL programs). The processing of XANES spectra was also performed using Athena.

## 3. Results and Discussion

### 3.1. Bulk Mineralogy by QEMSCAN

In all samples, the dominant mineral phase was consistently feldspar, primarily as plagioclase (Table 4-2). Other minerals included quartz, chlorite, calcite, dolomite, $FeO_X/CO_3$, other silicates, and pyrite. Although the mineral composition was similar in these samples, the abundance of each mineral changed by zone. In NP9, calcite and dolomite were concentrated in the carbonate enrichment zone sediments (Table 4-2). Although this observation was consistent with the relative distribution of calcium carbonate equivalent determined by chemical methods (Table 4-1), the concentrations determined by QEMSCAN were significantly lower. Most of the carbonate minerals were present in a very fine-textured amorphous phase rather than as crystalline granular particles.

Table 4-2
Mineral composition in area percent (%Area) measured by QEMSCAN.

| | Vadose Zone | | Carbonate enrichment zone | | Redox Transition Zone | | Depletion Zone | |
|---|---|---|---|---|---|---|---|---|
| | NP9-1 | NP13-1 | NP9-4 | NP13-4 | NP9-10 | NP13-8 | NP9-16 | NP13-12 |
| Plagioclase | 64.3 | 86.9 | 86.0 | 68.8 | 95.3 | 55.4 | 75.4 | 82.2 |
| Feldspar | 16.9 | 1.85 | 1.76 | 15.0 | 0.90 | 4.67 | 4.39 | 2.46 |
| Quartz | 11.9 | 6.99 | 7.41 | 11.5 | 2.30 | 26.7 | 15.2 | 12.6 |
| Chlorite | 5.93 | 1.84 | 0.98 | 3.34 | 0.84 | 2.83 | 3.32 | 0.64 |
| Calcite | 0.15 | 0.96 | 1.16 | 0.23 | 0.27 | 1.12 | 0.31 | 0.71 |
| Dolomite | 0.21 | 0.75 | 1.76 | 0.32 | 0.14 | 1.25 | 0.36 | 0.69 |
| Fe-Ox/$CO_3$ | 0.17 | 0.18 | 0.13 | 0.10 | 0.06 | 6.42 | 0.30 | 0.13 |
| Other_oxides | 0.01 | 0.04 | -- | 0.03 | -- | 0.01 | 0.11 | 0.06 |
| Pyrite | 0.01 | -- | 0.03 | -- | -- | -- | 0.04 | 0.20 |
| Other_Sulfides | -- | 0.01 | 0.05 | 0.01 | -- | 0.01 | -- | 0.01 |

Other researchers have not been able to detect As minerals in sediment samples using X-ray diffraction (XRD) (Akai et al., 2004; Rowland et al., 2008; Seddique et al., 2011) due to low concentrations of As minerals or association of As with amorphous Fe oxides. No primary As-bearing mineral was detected using QEMSCAN either. Since these sediments contain As (Table 4-1), most of the As must exist in the sorbed phase or as very small particles. Unlike XRD that cannot be used to identify amorphous minerals, QEMSCAN identified amorphous Fe oxides ("Fe-$O_x$/$CO_3$") in all thin sections. In NP13-8, where red-brown patches were visible, the Fe bearing minerals "Fe-$O_x$/$CO_3$" were identified at a concentration of 6.42%. The percentage of Fe-$O_x$/$CO_3$ in the other samples ranged from 0.06% to 0.18%. Goethite content was less than 0.01% and hematite was not detected indicating the non-crystalline nature of Fe oxides in the samples. Pyrite content was identified only in the depletion zone sediment of the NP13 profile. In the NP9 profile, pyrite was identified in all samples except in the redox transition zone (NP9-10).

An additional benefit of using QEMSCAN was that laterally-resolved mineral composition maps were generated. The mineral composition maps were utilized to ensure that potential mineral phases that host As were included and other major mineral species were not excluded providing representative sampling for the subsequent micron scale analysis; μXRF and μXANES analyses were performed at the locations where the potential As-bearing minerals were identified by QEMSCAN (Fig. 4-1 and Fig. C1-3 in Appendix C).

### 3.2. Bulk XAS

The determination of As species using this method was based on the white line position (eV) of the XANES spectrum, where the first derivative crossed zero. The white

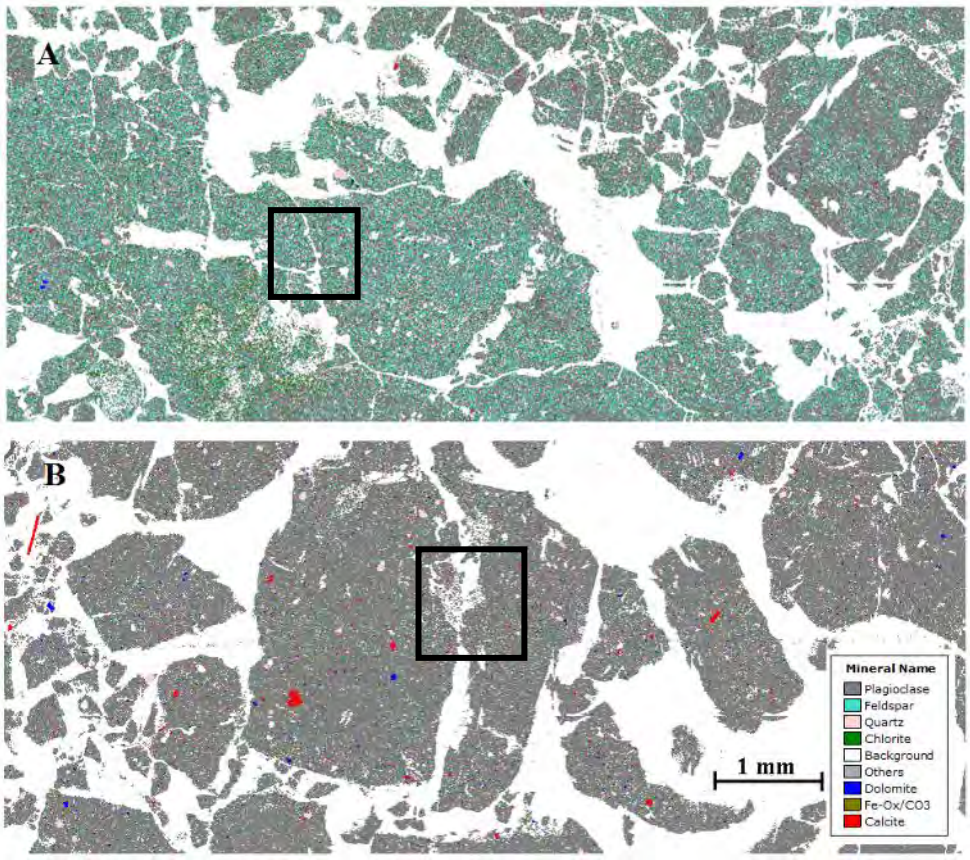


Fig. 4-1. Mineral composition maps of NP9-1(A) and NP13-1(B). Colors indicate the mineral species classified by SIP. The blocked area indicates the area scanned for μXRF and μXANES.

line comparison strategy has been successfully used to identify the phase of As in sediment samples (Foster et al., 1998; Smith et al., 2005). The white line positions of As(V) and As(III) in sodium arsenic salts were located at 11874.5 eV and 11871.0 eV (Fig. 4-2 A). The white lines of As(V)- and As(III)-sorbed minerals were shifted by approximately +0.5 eV compared to the sodium salts used as standards (Fig. 4-2 A). It is difficult to distinguish the mineral phases, i.e., ferrihydrite, goethite, or calcite, with which arsenic is associated by collecting only XANES. The white lines of $Cu_3AsS_4$ and FeAsS were located at 11871.0 eV and 11869.5 eV, respectively. The white lines of AsS

and $As_2S_3$ were located close together at 11869.3 eV and 11869.5 eV. A previous study also suggested that As in AsS and $As_2S_3$ are difficult to distinguish by XANES (Bostick and Fendorf, 2003).

Due to low As concentrations, the XANES spectra of As collected from the sediment samples were noisy in the vadose zone (9-1 and 13-1) and depletion zone sediments (9-16 and 13-12) (Fig. 4-2 B). Most of the spectra have white line positions at approximately 11875 eV, indicating that the As was primarily As(V) sorbed to a mineral phase. Because minor species at concentrations less than 5%–10% cannot be detected (Grafe et al., 2014), the percentage of As(V) was higher than 90% in the sediments that contained a single white line. In NP9-16 and NP13-12, the shoulders before the white line

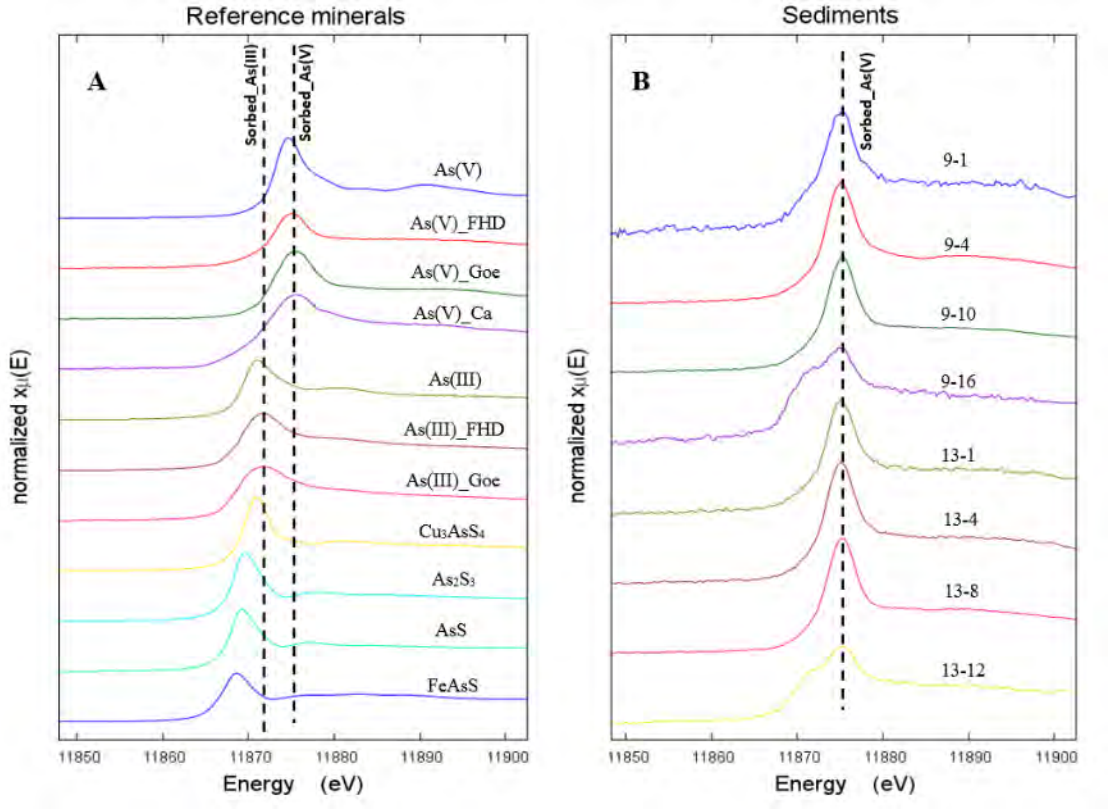


Fig. 4-2. Bulk-XANES spectra collected at As Kα for reference minerals (A) and selected sediment samples (B).

indicated that As in an oxidation state other than As(V) was present at >10%. Linear combination fit (LCF), which determines the percentage of As at each oxidation state was not performed for NP9-16 and NP13-12 due to the low quality spectra.

### 3.3. µXRF and µXANES for Vadose Zone Sediments

In NP9-1 and NP13-1, the As hotspots were small pixels that were discrete phases in the sediment matrix (Fig. 4-3 A & B). The As was scattered and showed no co-distribution with any specific mineral phase that was identified in the QEMSCAN mineral composition maps (Fig. 4-1). Calculation for absolute abundance of an element using XRF was difficult due to the matrix effect in heterogeneous material. Therefore, the fluorescence signals were used qualitatively to reflect the relative abundance of an individual element among locations. The fluorescence counts for each element were proportional to the intensity of each color; e.g., a spot with brighter red coloration indicated that the As content was relatively high compared to a less bright red spot.

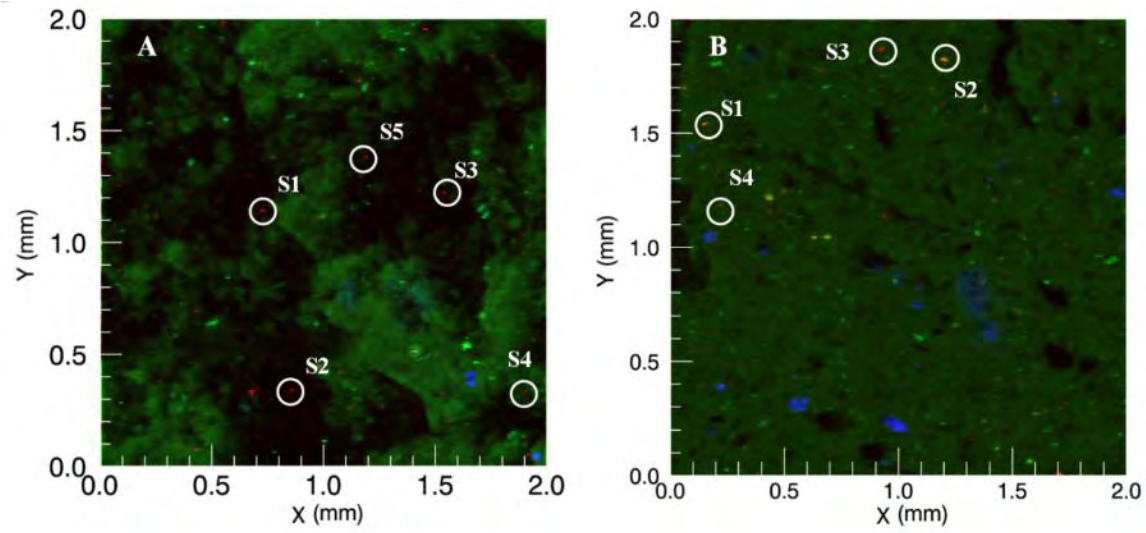


Fig. 4-3. µXRF RGB maps of vadose zone samples for As Kα (red), Fe Kα (green), and Mn Kα (blue) for NP9-1 (A) and NP13 (B). The scale of the maps is in millimeters. Circled regions represent the area where µXANES spectra were collected.

Fluorescence counts for all spots of interest are shown in Table C-1 and Table C-2.

In NP9-1 As was not co-distributed with Fe and Mn (Fig. 4-3 A) nor with the other investigated elements, including Ca, Cu, Rb, and Sr (Fig. C-4), suggesting discrete primary As minerals were present in this core. The As in NP13-1 was as scattered as in NP9-1, but about half of the As pixels were not red, but orange, as exemplified by S1 and S2 (Fig. 4-3 B). The orange coloration is due to co-occurrence of elevated Fe (bright green) and As (red).

Five As spots (S1-S5 in Fig. 4-3 A) were selected on NP9-1 for μXANES collection. At S1 and S3-S5 of NP9-1 the white line positions of μXANES spectra were similar to that of FeAsS (11868.5 eV) (Fig. 4-4 A). The white line position of As at S2 was at a higher energy than FeAsS but lower than arsenite (11871.5 eV) indicating the occurrence of AsS or $As_2S_3$. The presence of primary As minerals, as indicated by chemical extraction (Chapter 3), was confirmed in NP9-1. In comparison to the As sulfides in NP9-1, arsenic in NP13-1 was revealed as arsenite and arsenate: S1 and S2 contained As(V), while S3 and S4 contained As(III) (Fig. 4-4 B). Since As was co-distributed with elevated Fe in S1 and S2, the As(V) was arsenate that was sorbed to Fe oxides. The absence of elevated Fe in S3 and S4 suggested that As(III) was arsenite sorbed by other mineral(s). All examined spots in NP9-1 and two out of four in NP13-1 showed As species other than sorbed-As(V), which contrast with the bulk XANES results. The utilization of micron scale XANES on a thin section revealed spatial heterogeneity in As speciation; relying on bulk XANES may lead to a distorted picture.

Busbee et al. (2009) proposed that irrigation water in a semi-arid basin in Southwestern Idaho transports As(V) deposited on the soil surface to deeper within the

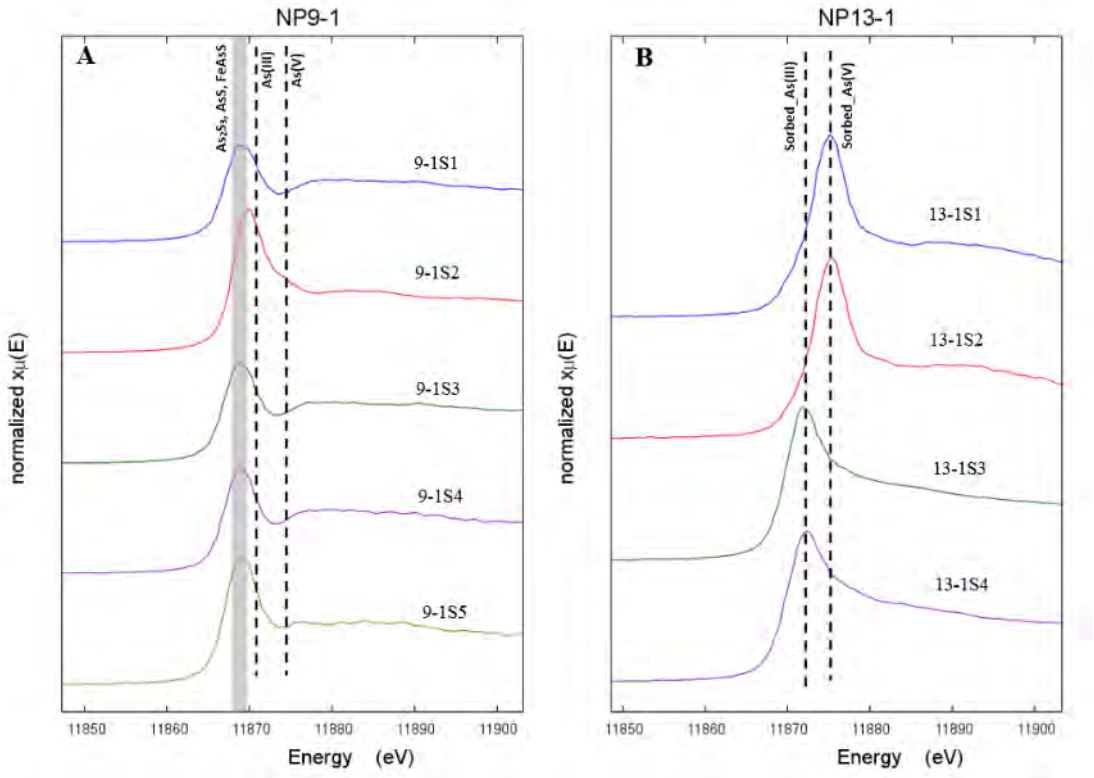


Fig. 4-4. μXANES spectra collected at As Kα for NP9-1 (A) and NP13-1 (B).

profile causing elevated groundwater contamination with As, but the mineral association and origin of As were left unknown. Polizzotto et al. (2006) concluded that As released with the oxidation of As-S minerals was transported deeper into the profile due to redox cycling. The source of the As-S minerals was presumed to be eroded deposits from the Himalayan Mountains. Near surface deposition of As-bearing pyrite has been identified as a source of As in several other locations including the Ganges Delta (Chowdhury et al., 1999) and the Mekong Delta (Kocar et al., 2008). Climatic conditions in the semi-arid Cache Valley Basin are obviously distinct from conditions in Southern Asia, but the geological settings are similar. Basin-fill aquifers underlay both regions, and both are located near mountains that contain volcanic deposits. The mountains surrounding the

Cache Valley, previous mined for copper, contain deposits of copper arsenic sulfosalts, including enargite ($Cu_3AsS_4$) and tennanite ($Cu_{12}AsS_{13}$). Chemical extractions and pore water analysis (Chapter 3) indicated the presence of As-primary minerals in the Cache Valley Basin. The presence of the un-altered As sulfide minerals in the vadose zone sediment of NP9, determined by μXRF in conjunction with μXANES, indicate that the study site received deposition of As-bearing sulfides. As-sulfide minerals were deposited with cycling of Lake Bonneville. These minerals may occur in micro reduced environments and/or this is a continued slow deposition of these minerals from wind and water erosion of exposed Salt Lake Formation in the surrounding mountains and at the margins of the valley.

Given the heterogeneity in soil/sediment samples, the absence of As sulfides in the NP13-1 thin section examined does not exclude the presence of these minerals in the vadose zone at this site. Over 50% of the As in the vadose zone was extractable with reagents targeting crystalline sulfide, crystalline Fe oxides and residual minerals. This bulk chemical analysis confirms the presences of insoluble As minerals, not just surface bound As as identified by XAS. The sorbed As(III) and As(V) occurring in NP13-1 may indicate that As sulfides were oxidized and the As re-partitioned onto surfaces. It is also possible that the As(III) was derived from As reduction in the surface soil under seasonal flooding (Parsons et al., 2013; Weber et al., 2010).

### 3.4. μXRF and μXANES in Carbonate Enrichment Zone Sediments

In both sediments from the carbonate enrichment zone, NP9-4 and NP13-4, more areas across the thin section contained elevated As counts compared to the vadose zone sediments (Fig. 4-5 vs. Fig. 4-3), which was consistent with the results from bulk

chemical extraction (Table 4-1). In NP9-4, the As was associated with dispersed phases (Fig. 4-5 A) rather than the discrete phases observed in the vadose zone sample from this plus blue), arsenic must be adsorbed to Mn-bearing minerals in NP9-4. Although accumulation of Ca was also observed in NP9-4, as indicated by high Ca florescence counts (Table C-1), As was not co-distributed with Ca (Fig. 4-3 C). Three types of As core (Fig. 4-3 A). Since As was co-distributed with Mn, indicated by the purple color (red

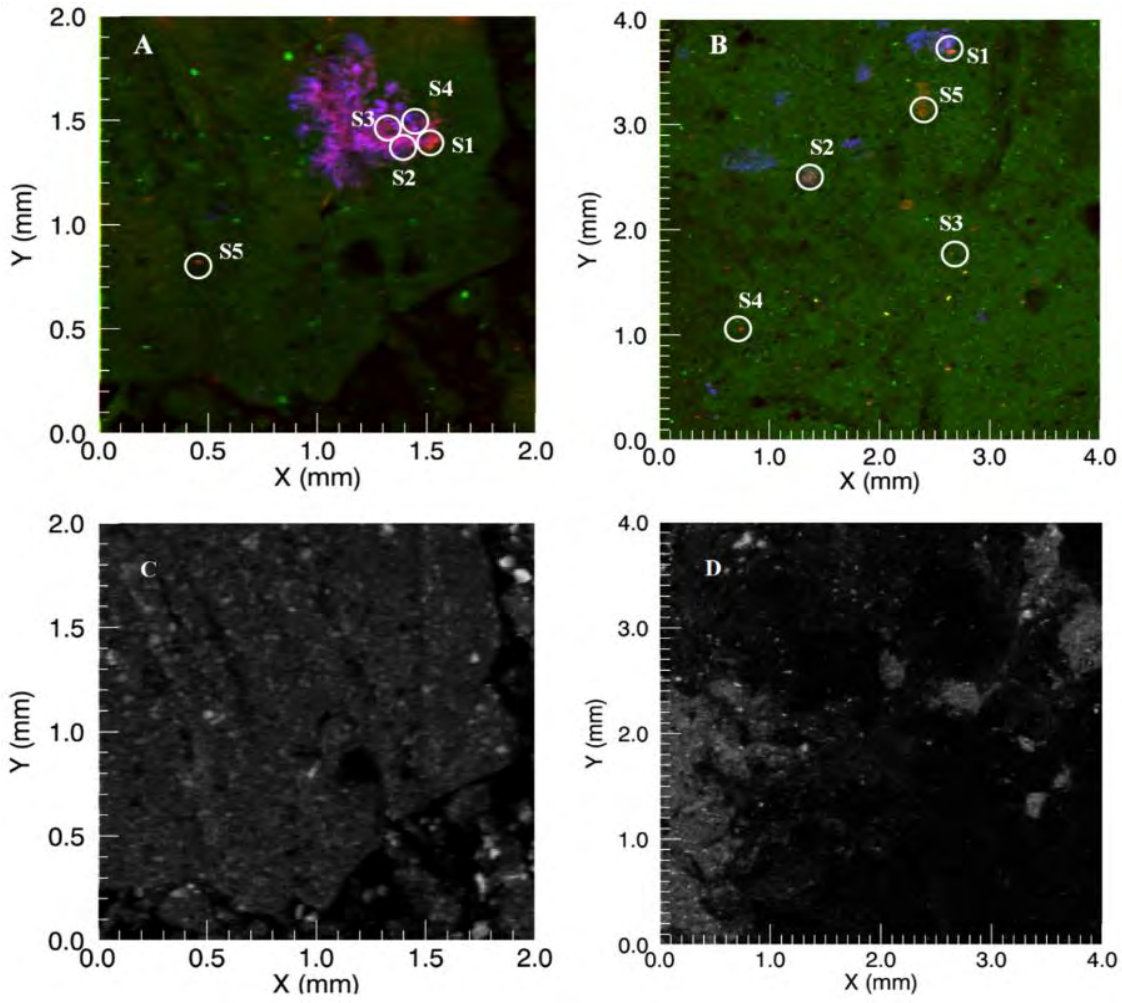


Fig. 4-5**.** µXRF maps of water table samples. RGB maps of As Kα (red), Fe Kα (green), and Mn Kα (blue) for NP9-1 (A) and NP13 (B) and greyscale maps of Ca Kα for NP9-1 (C) and NP13 (D). The scale of the maps is in millimeters. Circled regions represent the areas where µXANES spectra were collected.

plus blue), arsenic must be adsorbed to Mn-bearing minerals in NP9-4. Although accumulation of Ca was also observed in NP9-4, as indicated by high Ca florescence counts (Table C-1), As was not co-distributed with Ca (Fig. 4-3 C). Three types of As were identified in NP13-4 (Fig. 4-5 B): (1) clustered As associated with Mn (S1 and S2), (2) scattered fine As pixels not associated with any element that was considered in this study (S3 and S4), and (3) clustered As not associated with any element that was considered in this study (S5). Specific associations were delineated by μXANES, discussed below. In NP13-4 the As was also not co-distributed with Ca (Fig. 4-5 D).

In NP9-4, XANES were collected at four locations within a region where As was co-distributed with Mn (S1-S4) and one location that was not Mn associated (S5; Fig.4-5 A). All XANES collected from NP9-4 consistently had a white line position similar to sorbed-As(V) (Fig. 4-6 A). The spectra also have similar white line positions and patterns as an As(V)-Mn(II) precipitate (reported by Foster et al.,2003). To determine coordination chemistry, extended X-ray absorption fine structure (EXAFS) was attempted, but As concentration at these locations was too low for EXAFS collection. Co-occurring Mn indicated that the As was primarily associated with Mn-bearing minerals

Although three types of As were identified in NP13-4, the As spots analyzed in NP13-4 contain exclusively As(V). The As clustered as patches are sorbed to Mn-bearing minerals (S1 and S2) and to another unidentified mineral (S5). The scattered As pixels, S3 and S4, were not arsenate salt or As(V) sorbed to ferrihydrite, goethite, or calcite because of the bumps between 11890 and 11900 eV; the As was sequestered by some unknown association.

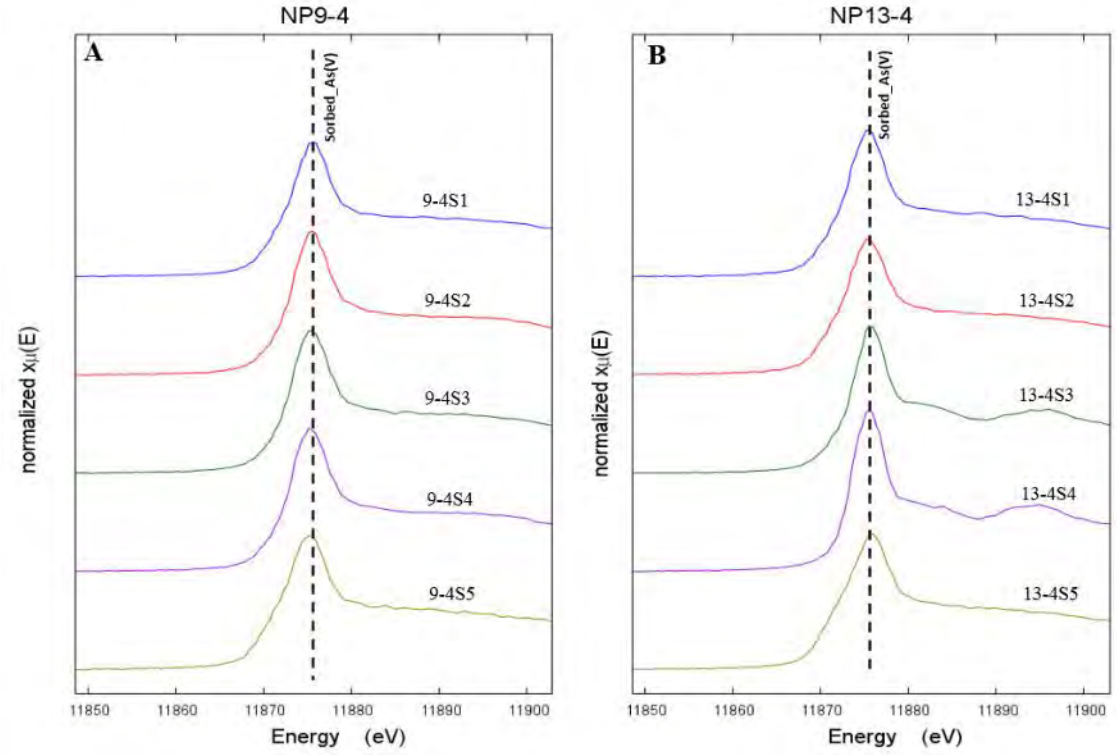


Fig. 4-6. μXANES spectra collected at As Kα for NP9-4 (left) and NP13-4 (right).

Costagliola et al. (2013) reported that a considerable amount of As(V) was sequestered by naturally occurring calcite in a study site where $CaCO_3$ ranged from 64.5 to 87.5 wt%. In the two cores from our study site, up to 18.3% of the As was associated with carbonate minerals, as indicated by chemical extraction analyses (Chapter 3). Association between As and Ca, however, was not identified by μXRF analysis, which indicated that Ca-bearing carbonate minerals, including calcite and dolomite, were not the sink for As. The As was co-distributed with Mn throughout the measured area of NP9-4 and at many locations in NP13-4, represented by S1 and S2 in Fig. 5B, suggesting the importance of Mn-bearing mineral in sequestering As in the carbonate enrichment zone sediments. The Mn-bearing minerals can be either Mn oxides or Mn-bearing carbonate. Similar to Fe oxide, Mn oxide is also an effective sorbent of As in the aquifer

system (Hess and Blanchar, 1976). Breit et al. (2004) reported that the occurrence of Mn oxide above the depth of Fe oxides is an indicator for seasonal fluctuation of the water table. From 55% to 72% of the total solid phase Mn, however, was extracted from the carbonate enrichment zone sediments using an ammonium acetate buffer at pH 5, which was the solution used to define dissolved carbonates, in the sequential extractions performed in Chapter 3. The association between As and Fe was very rarely identified in the carbonate enrichment zone, indicating that the commonly identified As sink in the subsurface, Fe oxides, was not exclusive. A microcosm study with the water table sediments suggested that As released to the solution phase resulted from minerals soluble in an ammonium acetate buffer at pH 5 under both aerobic and anoxic incubation. Thus As(V) associated with this fraction was subject to release into groundwater during groundwater fluctuation. The role of Mn-bearing carbonates in hosting and releasing As deserves further research attention.

### 3.5. μXRF and μXANES for Redox Transition Zone Sediments

Fe oxide patches were visible in the matrix of NP9-10 and NP13-8, which were from the zone that was under varying redox conditions. A fine resolution QEMSCAN map was not collected for NP9-10, but the visible Fe oxide was included in the area of interest for μXRF. The XRF maps of NP9-10 indicated that As was associated with Fe and Mn (Fig. 4-7 A). In NP13-8, a circular patch of Fe oxide with radius of approximately 3mm was mapped by QEMSCAN (Fig. C-2B). An area inside the Fe oxide circle (Area 1; Fig. C-2B) and an area outside (Area 2; Fig. C-2B) were identified for μXRF and μXANES analyses. Arsenic was detectable throughout the Fe-oxide-containing Area 1 (Fig. 4-7 B). In Area 1, both As and Fe fluorescence counts (Table C-2)

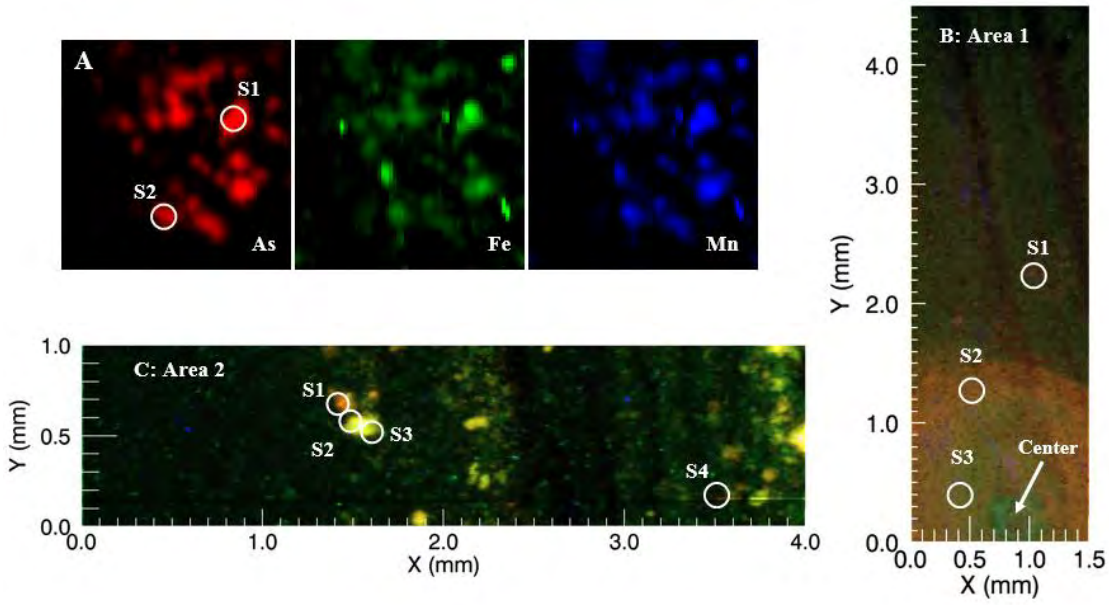


Fig. 4-7. μXRF maps of redox transition zone sediments. (A) Maps of As Kα (red), Fe Kα (green), and Mn Kα (blue) for NP9-10 collected at APS and generated by ImageJ Software; (B) and (C) are RGB maps of As Kα (red), Fe Kα (green), and Mn Kα (blue) for two areas in NP13-8. The scale of the maps is in millimeters. Circled regions represent the area where μ-XANES spectra were collected.

were higher toward the center of the circular Fe oxide patch. The As in Area 2 was co-distributed with Fe (Fig. 4-7 C), although Fe-bearing minerals were not identified using QEMSCAN (Fig. C-2B). The average Fe fluorescence count (Table C-2) in Area 2 of NP13-8 was only one-third of that in Area 1, indicating low Fe concentration in Area 2; this explains why QEMSCAN did not identify any Fe-bearing phase in this area. Mn was identified in both Areas 1 and 2 in NP13-8, but As was not co-distributed with Mn.

All the XANES spectra collected from the redox transition zone sediments have a white line position and pattern identical to the As(V) sorbed to minerals, with the exception of the spectrum collected at S4 in Area 2 of NP13-8. XRF maps indicated that As is co-distributed with Fe (Fig. 4-7). Thus, As was primarily As(V) associated with Fe oxides. Although As(V) was the dominant oxidation state, As(III) was identified at S4 in

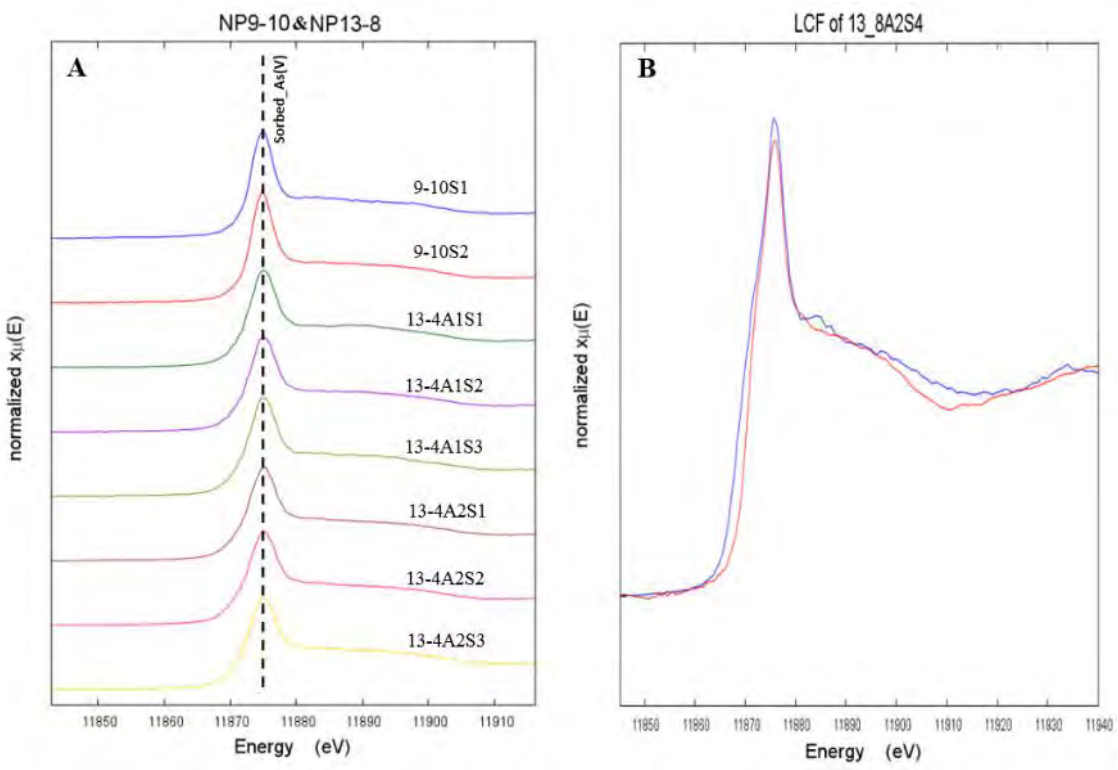


Fig. 4-8. μXANES spectra collected at As Kα for NP9-10 and NP13-8 (A). LCF fitting results for an As spot in NP13-8 (B).

Area 2 of NP13-8; the As consisted of As(V) (~61%) and As(III) (~39%) as adsorbed phases, according to LCF using spectra of As(V) and As(III) adsorbed to ferrihyrite (Fig. 4-8 B).

Chemical extraction indicated that 81% and 70% of total As were associated with Fe oxide related pools (very poorly crystalline, poorly crystalline, and crystalline Fe oxides) in NP9-10 and NP13-8, respectively (Chapter 3). The imaging analysis was in agreement with the sequential extraction result. The association between As and Fe in the redox transition zone agreed with the commonly accepted hypothesis that Fe oxides are the primary sink of As in the subsurface (Smedley and Kinniburgh, 2002). Our study, however, indicated that the association between As and Fe oxides did not dominate As

mineralogy until the redox transition zone was reached. The redox transition zone experienced seasonal redox cycling, being reduced during the high water table period and oxidized during the low water table period. A low water table facilitates the formation of Fe oxides by allowing oxygen to enter pore spaces. Arsenic sorption was enhanced in the redox transition zone attenuating As solubility. A portion of the leached As from the surface was also retained in the solid phase when it reached the redox transition zone (Chapter 3). This was supported by the accumulation of As in the redox transition zone. In the wet season, the shift from oxidizing conditions to reducing conditions could cause dissolution of Fe oxides, thereby releasing previously adsorbed As (McArthur et al., 2004; Nickson et al., 2000). A microcosm study performed with two sediments from the redox transition zone, however, suggested that the major loss of As was from the carbonate minerals during anoxic incubation, although Fe and $SO_4$ reduction was observed (Chapter 2). The reductive dissolution of Fe oxides may not be sufficient to cause elevated As in the groundwater even though As has been confirmed to be associated with Fe oxides. The dissolution of Fe oxides could be limited by the bioavailability of organic carbon in the sediment and the crystallinity of the Fe oxides.

### 3.6. μXRF and μXANES for Depletion Zone Sediments

In both NP9-16 and NP13-12, pyrite was captured by QEMSCAN (Fig. C-3). Accordingly, the pyrite grains were located with XRF analysis (Fig. 4-9). QEMSCAN results showed that Fe-bearing chlorite was the fourth most abundant mineral phase in NP9-16 (Table 4-2). Thus the elevated Fe surrounding the pyrite grain in NP9-16 was probably derived from chlorite. Overall, the area that contains elevated As content dramatically decreased compared to the carbonate enrichment zone and redox transition

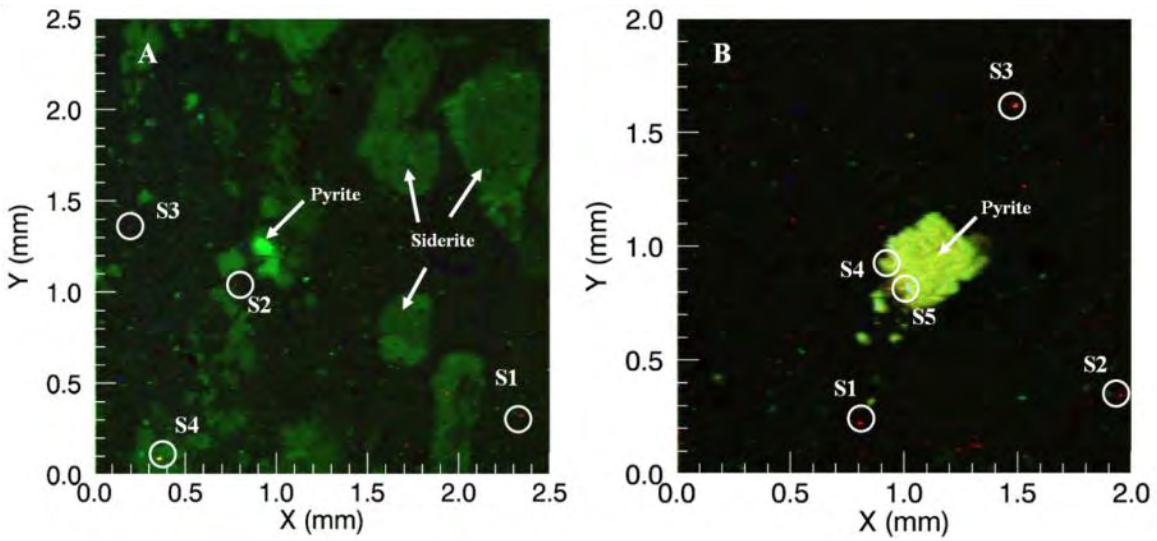


Fig. 4-9. μXRF RGB maps of depletion zone sediments for As Kα (red), Fe Kα (green), and Mn Kα (blue) for NP9-16 (A) and NP13-12 (B). The scale of the maps is in millimeters. Circled regions represent the areas where μXANES spectra were collected.

zone (Fig. 4-9). In NP9-16, there are only sparse As pixels, and none showed association with the pyrite grain (Fig. 4-9 A). The surrounding Fe patches did not host any As. The distribution of As in the measured area of NP9-16 was independent of Fe or Mn (Fig. 4-9 A). In comparison, the As in NP13-12 (S4 and S5) was primarily associated with the pyrite grain, with some discrete fine As pixels (S1–S3) (Fig. 4-9 B). The As count on the pyrite was below 100, while the As count in the fine pixels ranged from 200 to 500 (Table C-2).

S1–S3 of NP9-16 contained As(V) since their white line positions were at ~11875 eV. The spectra however were different from either As(V) as arsenate or As(V)-sorbed ferrihydrite (Fig. 4-10 A), leaving the association unknown. The As in S4 was FeAsS. None of the examined NP13-12 locations contained As(V) (Fig. 4-10 B). For S1–S3, the

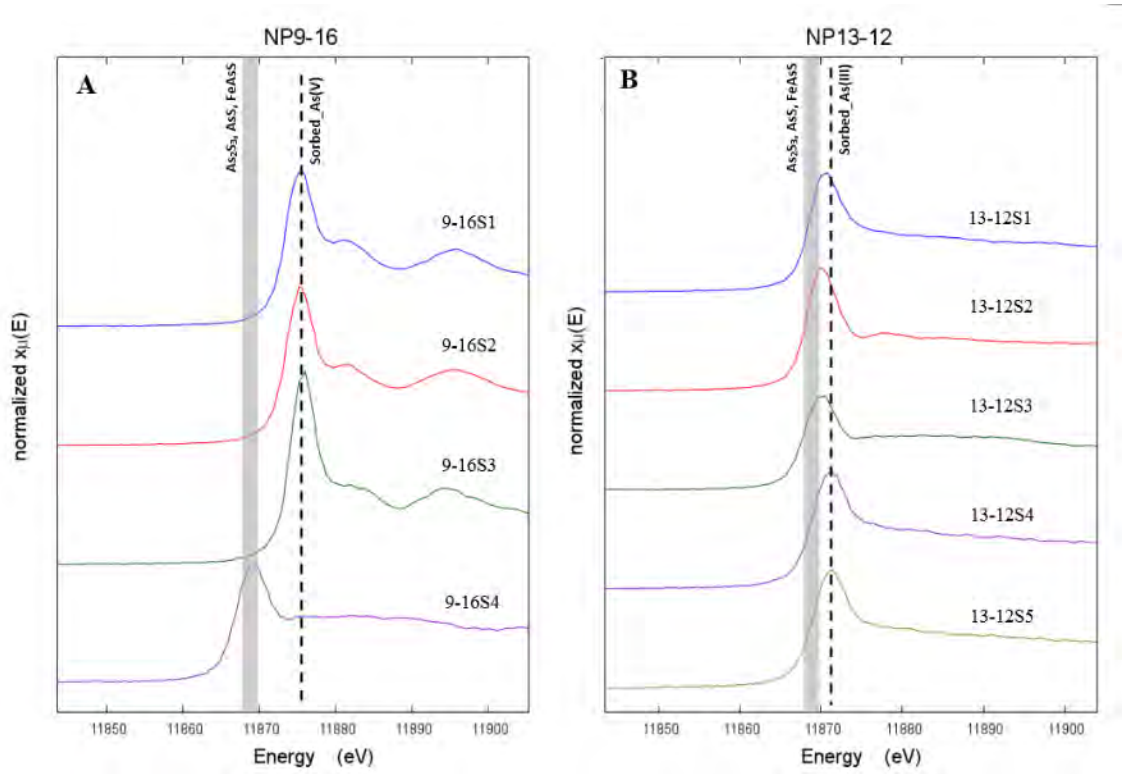


Fig. 4-10**.** μXANES spectra collected at As Kα for NP9-16 (A) and NP13-12 (B).

As pixels outside the pyrite grain, the white line positions of As were similar to AsS and $As_2S_3$. The As was As(III) at S4 and S5.

Chemical sequential extractions performed in Chapter 3 indicated that crystalline sulfides are the largest As pool in the depletion zone sediments and As in this pool was dominated by As(V). At three out of four measured locations in NP9-16, however, As(V) is not associated with sulfide minerals, supporting our argument in Chapter 3 that As(V) is probably due to solubilization of mineral phases that have similar solubilities to crystalline sulfides. In NP13-12, the XANES result confirmed the association between As and sulfides, but refuted the finding that As(V) is the dominant oxidation state of As (Chapter 3). The discrepancy may indicate that the oxidation state of As was not preserved effectively in the chemical extraction.

Pyrite has been reported to adsorb arsenite with a maximal sorption density of 231 μmol As/g pyrite (Bostick and Fendorf, 2003), which is 10 times lower than adsorption on ferrihydrite but higher than on goethite. Bostick and Fendorf (2003) suggested that the white line position of pyrite-sorbed As(III) was shifted to near pyrite, which was probably due to formation of FeAsS-like surface precipitation. Couture et al.(2013), however, indicated that the white line position of arsenite remained stable after sorption onto pyrite. NP9-16 and NP13-12 were from the depletion zone, which experienced prolonged water saturation. The redox-induced change in bulk mineralogy caused a significant decrease in the capacity of the sediment to retain As in the solid phase. The As identified in NP9-16 was mostly As(V), indicating that some As(V) was effectively trapped by solid phases, preventing reduction to As(III). The attenuation of As by As-S association in the subsurface was normally thought to be limited due to the lack of bioavailable sulfate (Fendorf et al., 2010; O'Day et al., 2004). Water-soluble sulfate was, however, relatively high in the depletion zones of both studied profiles: 29.0 mg/L in NP9-16 and 42.6 mg/L in NP13-12. The sulfide derived from microbial sulfate reduction resulted in As retention directly by formation of As sulfides and indirectly by formation iron sulfides that sorb As.

## 4. Conclusions

Arsenic sulfides and As(III) and As(V) as sorbed phases were identified in the vadose zone sediment, suggesting deposition and weathering of primary As minerals in the top sediment profile. Contrary to the vadose zone, arsenic in the carbonate enrichment zone and redox transition zone sediments were primarily sorbed As(V). Despite the same oxidation state of As in these two zones, the mineral association of As was different. The

As was revealed to associate with Mn-bearing mineral in the carbonate enrichment zone, which was presumably Mn carbonate, according to the previous study (Chapter 3). The sink for As then switched to Fe oxides in the redox transition zone. This finding suggests that the influence of Fe oxides in As solubilization is limited to the redox transition zone, but not the rest of the sediment profile. Most studies reported in the literature have focused on the redox transition zone, hence highlighting the importance of Fe oxides as a source/sink for As in groundwater contamination settings. In semi-arid and arid regions of the world, carbonate minerals should also be considered as mineral phases involved in the cycling of As.

When reaching the depletion zone, the As speciation changed to a mixture of sorbed-As(V), pyrite-sorbed As(III), and As sulfides, which is similar to the vadose zone sediments. The pyrite-sorbed As(III) and As sulfides, however, are stable in the depletion zone preventing As from future solubilization, unless dramatic drops in water table occur due to dry climate and poor groundwater management, which introduces oxygen into the depletion zone. The retention of As in the solid phase through formation of As and Fe sulfides is a potential attenuation mechanism of As.

Collectively, our results delineate the changes in As speciation, including oxidation state and mineral association, according to sediment-forming processes involving deposition and weathering of primary minerals, redox-induced evolution of Fe oxides, and precipitation of carbonate mineral at the water table. Although the weathering of As-bearing sulfides was proposed to leach As to the deep profile in the Himalayan flood plains, the presence of As-bearing sulfides has not been directly identified as contributing to As contamination in the basin-fill aquifers in the Western US. The Mn-

bearing carbonate should receive more research attention when As solubilization is studied, especially in the arid to semi-arid regions where carbonates are ubiquitous.

## References

Akai J., Izumi K., Fukuhara H., Masuda H., Nakano S., Yoshimura T., Ohfuji H., Anawar H.M. and Akai K. (2004) Mineralogical and geomicrobiological investigations on groundwater arsenic enrichment in Bangladesh. *Appl. Geochem.* **19**, 215-230.

Alexandratos V.G., Elzinga E.J. and Reeder R.J. (2007) Arsenate uptake by calcite: Macroscopic and spectroscopic characterization of adsorption and incorporation mechanisms. *Geochim. Cosmochim. Acta* **71**, 4172-4187.

Anning D.W., Paul A.P., McKinney T.S., Huntington J.M., Bexfield L.M. and Thiros S.A. (2012) Predicted nitrate and arsenic concentrations in basin-fill aquifers of the Southwestern United States, Scientific Investigations Report 2012-5065 U.S. Geological Survey, Reston, VA.

Arai Y., Lanzirotti A., Sutton S.R., Newville M., Dyer J. and Sparks D.L. (2006) Spatial and temporal variability of arsenic solid-state speciation in historically lead arsenate contaminated soils. *Environ. Sci. Technol.* **40**, 673-679.

Bhattacharya P., Claesson M., Bundschuh J., Sracek O., Fagerberg J., Jacks G., Martin R.A., Storniolo A.D. and Thir J.M. (2006) Distribution and mobility of arsenic in the Rio Dulce alluvial aquifers in Santiago del Estero Province, Argentina. *Sci. Total Environ.* **358**, 97-120.

Bostick B.C. and Fendorf S. (2003) Arsenite sorption on troilite (FeS) and pyrite ($FeS_2$). *Geochim. Cosmochim. Acta* **67**, 909-921.

Breit G., Foster A., Perkins R., Yount J., King T., Welch A., Whitney J., Uddin M., Muneem A. and Alam M. (2004) As-rich ferric oxyhydroxide enrichments in the shallow subsurface of Bangladesh. In *Proc. Int. Symp. Water– Rock Interactions, 11th* (eds. R.B. Wanty and R.R. Seal), Saratoga Springs, NY. pp. 1457-1461.

Busbee M.W., Kocar B.D. and Benner S.G. (2009) Irrigation produces elevated arsenic in the underlying groundwater of a semi-arid basin in Southwestern Idaho. *Appl. Geochem.* **24**, 843-859.

Chowdhury T.R., Basu G.K., Mandal B.K., Biswas B.K., Samanta G., Chowdhury U.K., Chanda C.R., Lodh D., Lal Roy S., Saha K.C., Roy S., Kabir S., Quamruzzaman Q. and Chakraborti D. (1999) Arsenic poisoning in the Ganges delta. *Nature* **401**, 545-546.

Costagliola P., Bardelli F., Benvenuti M., Di Benedetto F., Lattanzi P., Romanelli M., Paolieri M., Rimondi V. and Vaggelli G. (2013) Arsenic-bearing calcite in natural

travertines: Evidence from sequential extraction, μXAS, and μXRF. *Environ. Sci. Technol.* **47**, 6231-6238.

Couture R.M., Rose J., Kumar N., Mitchell K., Wallschlager D. and Van Cappellen P. (2013) Sorption of Arsenite, Arsenate, and Thioarsenates to Iron Oxides and Iron Sulfides: A Kinetic and Spectroscopic Investigation. *Environ. Sci. Technol.* **47**, 5652-5659.

Evans J.P. and Oaks R.Q. (1996) Three-dimensional variations in extensional fault shape and basin form: The Cache Valley Basin, eastern Basin and Range province, United States. *Geol. Soc. Am. Bull.* **108**, 1580-1593.

Fendorf S., Michael H.A. and van Geen A. (2010) Spatial and temporal variations of groundwater arsenic in South and Southeast Asia. *Science* **328**, 1123-1127.

Foster A.L., Brown G.E. and Parks G.A. (2003) X-ray absorption fine structure study of As(V) and Se(IV) sorption complexes on hydrous Mn oxides. *Geochim. Cosmochim. Acta* **67**, 1937-1953.

Foster A.L., Brown G.E., Tingle T.N. and Parks G.A. (1998) Quantitative arsenic speciation in mine tailings using X-ray absorption spectroscopy. *Am. Mineral.* **83**, 553-568.

Grafe M., Donner E., Collins R.N. and Lombi E. (2014) Speciation of metal(loid)s in environmental samples by X-ray absorption spectroscopy: a critical review. *Anal. Chim. Acta* **822**, 1-22.

Grafe M., Eick M.J. and Grossl P.R. (2001) Adsorption of arsenate(V) and arsenite(III) on goethite in the presence and absence of dissolved organic carbon. *Soil Sci. Soc. Am. J.* **65**, 1680-1687.

Grafe M., Eick M.J., Grossl P.R. and Saunders A.M. (2002) Adsorption of arsenate and arsenite on ferrihydrite in the presence and absence of dissolved organic carbon. *J Environ. Qual.* **31**, 1115-1123.

Hering J.G., O'Day P.A., Ford R.G., He Y.T., Bilgin A., Reisinger H.J. and Burris D.R. (2009) MNA as a remedy for arsenic mobilized by anthropogenic inputs of organic carbon. *Ground Water Monit. Remediat.* **29**, 84-92.

Hess R.E. and Blanchar R.W. (1976) Arsenic stability in contaminated soils. *Soil Sci. Soc. Am. J.* **40**, 847-852.

Inkenbrandt P.C. (2010) Estimates of the hydraulic parameters of aquifers in Cache Valley, Utah and Idaho. Utah State University, Logan, UT.

Islam F.S., Gault A.G., Boothman C., Polya D.A., Charnock J.M., Chatterjee D. and Lloyd J.R. (2004) Role of metal-reducing bacteria in arsenic release from Bengal delta sediments. *Nature* **430**, 68-71.

Kocar B.D., Polizzotto M.L., Benner S.G., Ying S.C., Ung M., Ouch K., Samreth S., Suy B., Phan K., Sampson M. and Fendorf S. (2008) Integrated biogeochemical and hydrologic processes driving arsenic release from shallow sediments to groundwaters of the Mekong delta. *Appl. Geochem.* **23**, 3059-3071.

Kubiena W.L. (1938) *Micropedology*. Collegiate Press, Ames, IA.

Liao V.H.C., Chu Y.J., Su Y.C., Lin P.C., Hwang Y.H., Liu C.W., Liao C.M., Chang F.J. and Yu C.W. (2011) Assessing the mechanisms controlling the mobilization of arsenic in the arsenic contaminated shallow alluvial aquifer in the blackfoot disease endemic area. *J. Hazard. Mater.* **197**, 397-403.

Lowe M., Wallace J., Bishop C. and Hurlow H. (2003) Ground-water quality classification and recommended septic tank soil-absorption-system density maps, Utah Geological Survey Special Study 101. Utah Geological Survey, Salt Lake City, UT, p. 31.

McArthur J.M., Banerjee D.M., Hudson-Edwards K.A., Mishra R., Purohit R., Ravenscroft P., Cronin A., Howarth R.J., Chatterjee A., Talukder T., Lowry D., Houghton S. and Chadha D.K. (2004) Natural organic matter in sedimentary basins and its relation to arsenic in anoxic ground water: the example of West Bengal and its worldwide implications. *Appl. Geochem.* **19**, 1255-1293.

McLean J.E., Dupont R.R. and Sorensen D.L. (2006) Iron and arsenic release from aquifer solids in response to biostimulation. *J. Environ. Qual.* **35**, 1193-1203.

Mirza B.S., Muruganadam S., Meng X., Sorensen D.L., Dupont R.R. and McLean J.E. (2014) Arsenic(V) reduction in relation to iron(III) transformation and molecular characterization of the structural and functional microbial community in sediments of a Northern Utah, basin-fill aquifer. *Appl. Environ. Microbiol.*, AEM. 00240-00214.

Mok W. and Wai C. (1994) Mobilization of arsenic in contaminated river waters. In *Arsenic in the Environment, Part I, Cycling and Characterization* (ed. J. Nriagu). J. Wiley and Sons, New York. pp. 99-117.

Murphy C. (1985) Faster methods of liquid-phase acetone replacement of water from soils and sediments prior to resin impregnation. *Geoderma* **35**, 39-45.

Nickson R.T., McArthur J.M., Ravenscroft P., Burgess W.G. and Ahmed K.M. (2000) Mechanism of arsenic release to groundwater, Bangladesh and West Bengal. *Appl. Geochem.* **15**, 403-413.

O'Day P.A., Vlassopoulos D., Root R. and Rivera N. (2004) The influence of sulfur and iron on dissolved arsenic concentrations in the shallow subsurface under changing redox conditions. *Proc. Natl. Acad. Sci. USA* **101**, 13703-13708.

Ohtsuka T., Yamaguchi N., Makino T., Sakurai K., Kimura K., Kudo K., Homma E., Dong D.T. and Amachi S. (2013) Arsenic dissolution from Japanese paddy soil by a dissimilatory arsenate-reducing bacterium *Geobacter* sp. OR-1. *Environ. Sci. Technol.* **47**, 6263-6271.

Oscarson D., Huang P., Hammer U. and Liaw W. (1983) Oxidation and sorption of arsenite by manganese dioxide as influenced by surface coatings of iron and aluminum oxides and calcium carbonate. *Water, Air, Soil Pollut.* **20**, 233-244.

Parsons C.T., Couture R.-M., Omoregie E.O., Bardelli F., Greneche J.-M., Roman-Ross G. and Charlet L. (2013) The impact of oscillating redox conditions: arsenic immobilisation in contaminated calcareous floodplain soils. *Environ. Pollut.* **178**, 254-263.

Polizzotto M.L., Harvey C.F., Li G.C., Badruzzman B., Ali A., Newville M., Sutton S. and Fendorf S. (2006) Solid-phases and desorption processes of arsenic within Bangladesh sediments. *Chem. Geol.* **228**, 97-111.

Rowland H.A.L., Gault A.G., Lythgoe P. and Polya D.A. (2008) Geochemistry of aquifer sediments and arsenic-rich groundwaters from Kandal Province, Cambodia. *Appl. Geochem.* **23**, 3029-3046.

Ryu J.H., Gao S.D. and Tanji K.K. (2010) Speciation and behavior of arsenic in evaporation basins, California, USA. *Environ. Earth Sci.* **61**, 1599-1612.

Scanlon B.R., Nicot J.P., Reedy R.C., Kurtzman D., Mukherjee A. and Nordstrom D.K. (2009) Elevated naturally occurring arsenic in a semiarid oxidizing system, Southern High Plains aquifer, Texas, USA. *Appl. Geochem.* **24**, 2061-2071.

Schwertmann U. and Cornell R.M. (2008) Iron Oxides in the Laboratory. Wiley-VCH, Weinheim, Germany.

Seddique A.A., Masuda H., Mitamura M., Shinoda K., Yamanaka T., Nakaya S. and Ahmed K.M. (2011) Mineralogy and geochemistry of shallow sediments of Sonargaon, Bangladesh and implications for arsenic dynamics: focusing on the role of organic matter. *Appl. Geochem.* **26**, 587-599.

Smedley P.L. and Kinniburgh D.G. (2002) A review of the source, behaviour and distribution of arsenic in natural waters. *Appl. Geochem.* **17**, 517-568.

Smith P.G., Koch I., Gordon R.A., Mandoli D.F., Chapman B.D. and Reimer K.J. (2005) X-ray absorption near-edge structure analysis of arsenic species for application to biological environmental samples. *Environ. Sci. Technol.* **39**, 248-254.

So H.U., Postma D., Jakobsen R. and Larsen F. (2008) Sorption and desorption of arsenate and arsenite on calcite. *Geochim. Cosmochim. Acta* **72**, 5871-5884.

Swartz J.F. and Lindsley-Griffin N. (1990) An improved impregnation technique for studying structure of unlithified cohesive sediments. *Proc. Ocean Drill. Prog. Sci. Results* **112**, 87-91.

Thornton I. (1996) Sources and pathways of arsenic in the geochemical environment: health implications, In *Environmental Geochemistry and Health 113* (eds. J.D. Appleton, R. Fuge, and G.J.H. McCall). Geol. Soc. Spec. Publ., London. pp. 153-161.

Tufano K.J., Reyes C., Saltikov C.W. and Fendorf S. (2008) Reductive processes controlling arsenic retention: Revealing the relative importance of iron and arsenic reduction. *Environ. Sci. Technol.* **42**, 8283-8289.

Voegelin A., Weber F.A. and Kretzschmar R. (2007) Distribution and speciation of arsenic around roots in a contaminated riparian floodplain soil: Micro-XRF element mapping and EXAFS spectroscopy. *Geochim. Cosmochim. Acta* **71**, 5804-5820.

Walker S.R., Jamieson H.E., Lanzirotti A., Andrade C.F. and Hall G.E.M. (2005) The speciation of arsenic in iron oxides in mine wastes from the Giant gold mine, NWT: Application of synchrotron micro-XRD and micro-XANES at the grain scale. *Can. Mineral.* **43**, 1205-1224.

Weber F.A., Hofacker A.F., Voegelin A. and Kretzschmar R. (2010) Temperature dependence and coupling of iron and arsenic reduction and release during flooding of a contaminated soil. *Environ. Sci. Technol.* **44**, 116-122.

# CHAPTER 5

# CONCLUSIONS, CONCEPTUAL MODEL AND ENGINEERING SIGNIFICANCE

## Conclusions and Conceptual Model

A systematic approach was taken to study the mechanisms of solubilization of naturally occurring geologic As. The uniqueness in the approach is that the study expanded from the sediments reported most in the literature, which are those below the water table, to include the entire sediment profile, from the ground surface to depths under highly reducing conditions. This study also focused on very specific information, using macro- and micro-scopic techniques on core samples and laboratory microcosm studies, to provide key evidence to elucidate processes controlling As solubility.

The sediments below the water table released a considerable amount of As during incubation with groundwater under laboratory-induced anoxic conditions. This observation is consistent with the widely accepted knowledge that reducing conditions are necessary for the solubilization of As. The mineral phase that released As, however, was revealed to be carbonate minerals rather than commonly concluded Fe oxides. Although the reduction of Fe was observed in all studied sediments, regardless of original redox conditions of the sediments, the loss of As was not from Fe oxides, as defined by chemical extraction. Carbonate minerals are common in subsurface environments of the semi-arid to arid regions; the role of carbonate minerals as a source/sink for As has not been adequately described in the literature.

The sediment profile study and following SXAS analysis revealed that processes occurring at different depths within the same profile were contributing to the

solubilization and transportation of geologic As. Although there are not distinct boundaries in the profile, the dominance of the controlling processes changed according to redox cycling related to groundwater fluctuation in the subsurface. The primary As-bearing sulfides were deposited on the ground surface in the Cache Valley Basin, Utah. The sulfides are potentially from the Salt Lake Formation in the surrounding mountains. The exposed Salt Lake Formation was eroded by lake movement due to the ancient Lake Bonneville, leading to further lacustrine and alluvial deposition. The Salt Lake Formation can also be eroded and transported to the basin by eolian processes. The surficial oxidizing conditions trigger the oxidative dissolution of As-bearing sulfides, resulting in increased dissolved As and As associated with carbonate minerals (Fig. 5-1 A & B). The soluble As is leached to the deeper profile by infiltration. From ground surface to the water table, as the weathering process carries on, an increasing amount of As is associated with phosphate exchangeable surfaces and carbonate minerals. As the water table rises, the variation in moisture content and solute composition cause desorption of As (Fig. 5-1 B). Although carbonate minerals have received less attention in the literature because most previously studied areas are not carbonate-rich, ignoring this pool in carbonaceous sediments in semi-arid and arid regions of the world leads to underestimating the risk of As solubilization.

The most abundant As was observed in the redox transition zone sediments. Sequential extractions and SXAS indicated that poorly crystalline Fe oxide was the primary pool of As in these sediments. The widely accepted hypothesis that As is

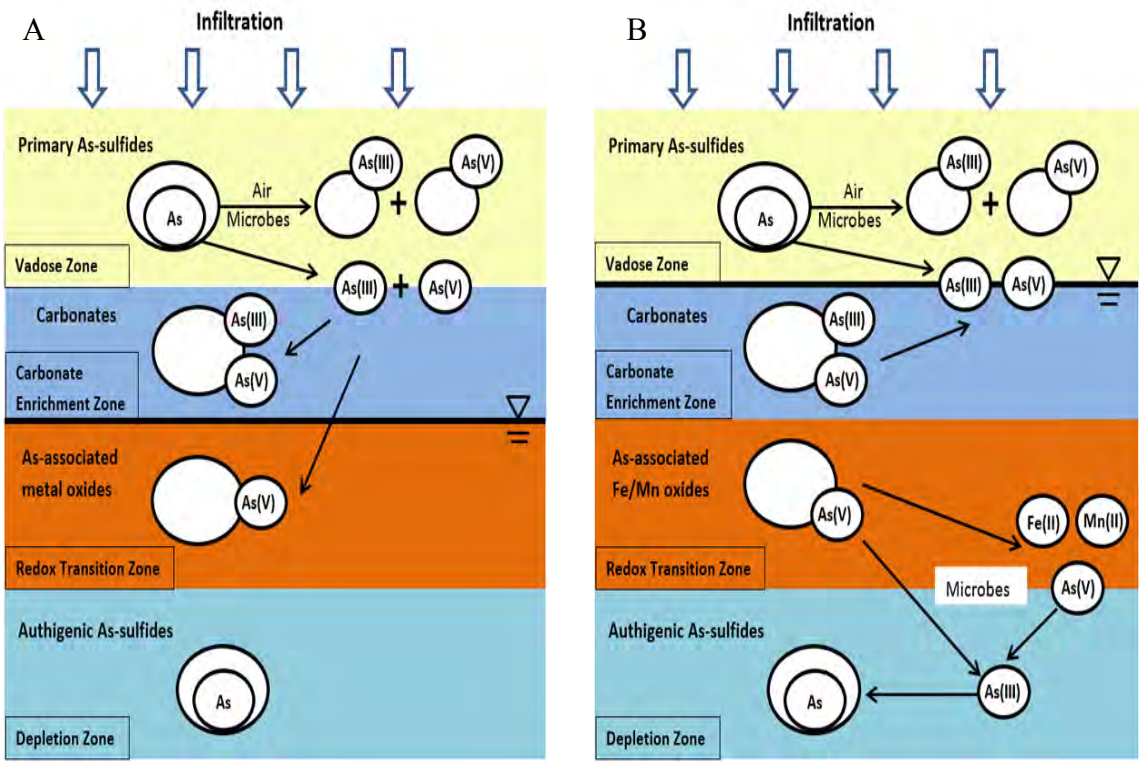


**Fig. 5-1.** Conceptual model of processes controlling As solubilization in the sediment profile: (A) lower water table; (B) rising water table. White open circles represent As host solid phases.

solubilized by reductive dissolution of Fe oxides suggested the As could be released by redox transition zone sediments when Fe reducing conditions occur (Fig. 5-1 B). This process is, however, not supported by observations from the microcosm study, in which solubilized As was found to be associated with carbonate minerals.

In the depletion zone, the profile was under deeply reducing conditions due to permanent saturation. The As was associated with sulfides through adsorption onto pyrite and formation of As-sulfides including realgar and orpiment (Fig. 5-1). The sulfides are table under reducing conditions therefore preventing As from solubilization. In our study site sulfate was sufficient for continued microbial sulfidogenesis processes to occur.

# Engineering Significance

Two sediment profiles of a specific study site located in the Cache Valley Basin, Utah were investigated. The applications of this research are not limited to Cache Valley, Utah; however, include areas of the Western U.S. underlain by basin-fill aquifers. These areas, including parts of California, Nevada, Utah, Arizona, New Mexico, Oregon, Idaho, and Colorado, are predicted by the USGS to contain elevated As contamination in 43% of the groundwater resources (Anning et al., 2012). The methods and conclusions of this study are also applicable to many other redox controlled solubility assessments. For example, selenium and chromium are two other potentially harmful groundwater contaminants that are controlled by similar processes and could be evaluated similarly.

Groundwater with As concentrations higher than 10 μg/L have been found at various locations worldwide, particularly in Southeastern Asia. Chronic exposure to As in drinking water causes serious human diseases, including skin cancers. This has resulted in increasing research attention to As in groundwater all over the globe. At most locations, As contamination in groundwater is from naturally occurring sources and processes (Busbee et al., 2009; Polizzotto et al., 2006; Smedley et al., 2002; Welch and Lico, 1998), although human activity such as irrigation and groundwater withdrawal accelerate these processes. Difficulties in discerning contributing processes lead to uncertainties in risk assessments and modeling works related to As in drinking water. This research provides information for decision-makers or modelers to better understand the biogeochemical parameters important in controlling the solubility and natural attenuation of As. This would directly assist in decision-making and evaluation for selecting safe drinking water sources by estimating their As mobilization potential.

This project also has applications to As remediation of contaminated soils and groundwater. The research provides several approaches to understand the biogeochemistry of As, thereby allowing a better estimate of the applicability and feasibility of specific remediation methods. An innovative biological treatment method that applies DARB and quinone, as an electron shuttle, has been reported to effectively remove As from soils collected from a historic industrial site (Yamamura et al., 2008). Our study indicates that As(V) accumulated in the redox transition zone, and As already exist as reduced forms, As(III) and As in sulfides, in the vadose and depletion zone sediments. The approach of Yamamura et al. (2008) should not be implemented if the sediments are primarily from vadose and depletion zones. Another concern of this approach is the fate of As(III) derived from As(V) reduction. The As(III) could be sequestered by solid phases if sulfides were present; the As is not removed but remains in the solid phase in systems with limited sulfides.

Monitored natural attenuation (MNA) is a potential remedial option for As in groundwater. In this case, our research provides guidelines for the determination of mobility mechanisms and evaluation of As retention capacity which are critical for successful MNA remediation (Hering et al., 2009). Our study also indicates that As solubilization can be derived from a surficial geologic source undergoing naturally occurring processes. Remediation efforts would be in vain if site investigation were limited to the aquifer material at well depth.

The results of this research also help with evaluating As release potential in the presence of inadvertent anthropogenic inputs of organic carbon into the subsurface. It has been demonstrated that leakage of petroleum hydrocarbons from underground storage

tanks and pipelines (Burgess and Pinto, 2005; Reisinger et al., 2005), as well as leachate from sanitary landfills (deLemos et al., 2006; Keimowitz et al., 2005), are capable of inducing mobilization of naturally occurring As. Thus, in consideration of a potential site for a municipal landfill facility, the local potential of As mobilization should be taken into account. The conceptual model presented here would assist in the site investigation process and in the engineering design to prevent As solubilization. If through the conceptual model the biogeochemistry indicates that the profile has a deep redox transition zone and As is associated with amorphous Fe oxides, and if natural sequestration is insufficient, the site should be built to eliminate any seepage potential and should be monitored for those parameters related to As mobilization, or the site should be moved to another location altogether.

On the other hand, intentional organic carbon addition for biostimulation of reductive dechlorination of chlorinated solvents has been shown to induce the mobilization of As in both a field study (He et al., 2010) and in a laboratory microcosm study (McLean et al., 2006). The described potential for As release should also be taken into account for remediation feasibility and applicability evaluation; otherwise site remediation may be successful as far as contamination with chlorinated solvents, but may result in pollution of the groundwater with As.

In summary, the conceptual model developed from this research will aid in evaluating As solubilization potential in the context of a local biogeochemical profile. It would improve the risk assessment process, advance current remediation techniques, and prevent inadvertent contamination. This study makes improvements in drinking water

safety and in preventing careless anthropogenic activities that cause solubilization of geologic As.

## References

Anning, D.W., Paul, A.P., McKinney, T.S., Huntington, J.M., Bexfield, L.M., Thiros, S.A., 2012. Predicted nitrate and arsenic concentrations in basin-fill aquifers of the Southwestern United States, Scientific Investigations Report 2012-5065 U.S. Geological Survey, Reston, Virginia.

Burgess, W.G., Pinto, L., 2005. Preliminary observations on the release of arsenic to groundwater in the presence of hydrocarbon contaminants in UK aquifers. Mineralogical Magazine 69, 887-896.

Busbee, M.W., Kocar, B.D., Benner, S.G., 2009. Irrigation produces elevated arsenic in the underlying groundwater of a semi-arid basin in Southwestern Idaho. Appl. Geochem. 24, 843-859.

deLemos, J.L., Bostick, B.C., Renshaw, C.E., Sturup, S., Feng, X.H., 2006. Landfill-stimulated iron reduction and arsenic release at the Coakley Superfund Site (NH). Environ. Sci. Technol. 40, 67-73.

He, Y.T., Fitzmaurice, A.G., Bilgin, A., Choi, S., O'Day, P., Horst, J., Harrington, J., Reisinger, H.J., Burris, D.R., Hering, J.G., 2010. Geochemical processes controlling arsenic mobility in groundwater: a case study of arsenic mobilization and natural attenuation. Appl. Geochem. 25, 69-80.

Hering, J.G., O'Day, P.A., Ford, R.G., He, Y.T., Bilgin, A., Reisinger, H.J., Burris, D.R., 2009. MNA as a remedy for arsenic mobilized by anthropogenic inputs of organic carbon. Ground Water Monit. Remediat. 29, 84-92.

Keimowitz, A.R., Simpson, H.J., Stute, M., Datta, S., Chillrud, S.N., Ross, J., Tsang, M., 2005. Naturally occurring arsenic: mobilization at a landfill in Maine and implications for remediation. Appl. Geochem. 20, 1985-2002.

McLean, J.E., Dupont, R.R., Sorensen, D.L., 2006. Iron and arsenic release from aquifer solids in response to biostimulation. J. Environ. Qual. 35, 1193-1203.

Polizzotto, M.L., Harvey, C.F., Li, G.C., Badruzzman, B., Ali, A., Newville, M., Sutton, S., Fendorf, S., 2006. Solid-phases and desorption processes of arsenic within Bangladesh sediments. Chem. Geol. 228, 97-111.

Reisinger, H.J., Burris, D.R., Hering, J.G., 2005. Remediating subsurface arsenic contamination with monitored natural attenuation. Environ. Sci. Technol. 39, 458a-464a.

Smedley, P.L., Nicolli, H.B., Macdonald, D.M.J., Barros, A.J., Tullio, J.O., 2002. Hydrogeochemistry of arsenic and other inorganic constituents in groundwaters from La Pampa, Argentina. Appl. Geochem. 17, 259-284.

Welch, A.H., Lico, M.S., 1998. Factors controlling As and U in shallow ground water, southern Carson Desert, Nevada. Appl. Geochem. 13, 521-539.

Yamamura, S., Watanabe, M., Kanzaki, M., Soda, S., Ike, M., 2008. Removal of arsenic from contaminated soils by microbial reduction of arsenate and quinone. Environ. Sci. Technol. 42, 6154-6159.

# APPENDICES

# Appendix A

Supplementary information for Chapter 2: **Arsenic solubilization and redistribution in three sediments, under anoxic conditions, from a basin-fill aquifer in semi-arid Northern Utah**

## AUTHOR INFORMATION

Xianyu Meng — Utah Water Research Laboratory and Department of Civil and Environmental Engineering, 8200 Old Main Hill, Utah State University, Logan UT 84322-8200. Tel.: +1 (435)797-3197. Fax: +1(435)797-3663. Email: xianyu.meng@aggiemail.usu.edu

R. Ryan Dupont — Utah Water Research Laboratory and Department of Civil and Environmental Engineering, 8200 Old Main Hill, Utah State University, Logan UT 84322-8200. Tel.: +1 (435) 797-3227. Fax: +1(435) 797-3663. Email: ryan.dupont@usu.edu

Darwin L. Sorensen — Utah Water Research Laboratory, 8200 Old Main Hill, Utah State University, Logan UT 84322-8200. Tel.: +1 (435) 797-3207. Fax: +1(435) 797-3663. Email: Darwin.sorensen@usu.edu

Astrid R. Jacobson — Department of Plants, Soils and Climate, 4820 Old Main Hill, Utah State University, Logan UT 84322-4820. Tel.: +1 (435) 797-2184. Email: astrid.jacobson@usu.edu

Joan E. McLean* — Utah Water Research Laboratory, 8200 Old Main Hill, Utah State University, Logan UT 84322-8200. Tel.: +1 (435) 797-3199. Fax: +1(435) 797-3663. Email: joan.mclean@usu.edu

**Experimental settings for HCl extraction and sequential extraction**

To perform HCl extraction, 20 mL of 0.5 M trace metal grade HCl (Fisher Scientific) and 1 g (equivalent dry weight) of solids were mixed in a 50 mL polypropylene centrifuge tube. The centrifuge tubes were shaken for 2 hr in the glove bag and then centrifuged at 10,000 x g for 20 min. The supernatants were filtered through 0.2 μm nylon filters into snap-cap vials for analyses of $Fe_T$ (Fe(II)+Fe(III)) and soluble $As_T$ (As(III)+As(V)).

The sequential extraction procedure recovers As and Fe from six chemically defined pools listed as fraction A through F in Table S1. A 1-g (equivalent dry weight) portion of the solids was transferred into a 50 mL polypropylene centrifuge tube. In each step, a certain amount of extractant, as required, was added to the centrifuge tube and mixed with the solids by vortexing. The mixture was treated either by shaking, heating, or both to facilitate extraction. The extract and remaining solids were separated by centrifugation at 10,000 x g for 20 mins. The $As_T$ and $Fe_T$ concentrations in the extracts were measured using ICP-MS. The concentration of $As_T$ and $Fe_T$ in each extraction step was corrected for carry over from the previous extraction step by determining the residual volume by weight.

Table A-1. Distribution of Fe Among Solid Phases in Selected Sediments

| Sample | Loosely Surface bound | | Carbonates | | Mn oxides | | Amorphous Fe oxides | | Crystalline Fe oxides | | Residual | |
|---|---|---|---|---|---|---|---|---|---|---|---|---|
| | Fe(III) mg/kg | Fe(II) mg/kg | Fe(III) mg/kg | Fe(II) mg/kg | $\%Fe_T$ | mg/kg | $\%Fe_T$ | mg/kg | $\%Fe_T$ | mg/kg | $\%Fe_T$ | mg/kg |
| NP1 | 0.1 | 0.8 | 13.6 | 1.4 | 0.51 | 66.6 | 4.7 | 613 | 40 | 5250 | 55 | 7160 |
| NP3 | 0.1 | 0.8 | 18.5 | 3.8 | 0.55 | 66.8 | 5.1 | 620 | 44 | 5300 | 50 | 6070 |
| NP8 | 0.3 | 8.7 | 92.2 | 570 | 0.78 | 116 | 9.8 | 1460 | 35 | 5180 | 50 | 7460 |

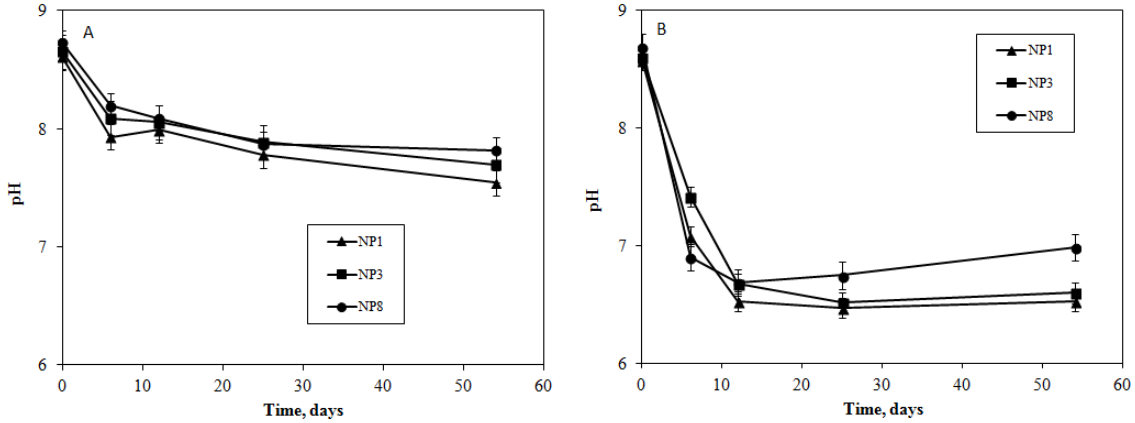


Figure A-1. The changes in pH in the aqueous phase of microcosms containing the three sediments incubated with two treatments: A) groundwater and B) groundwater plus glucose. Error bars represent Tukey HSD (α=0.05).

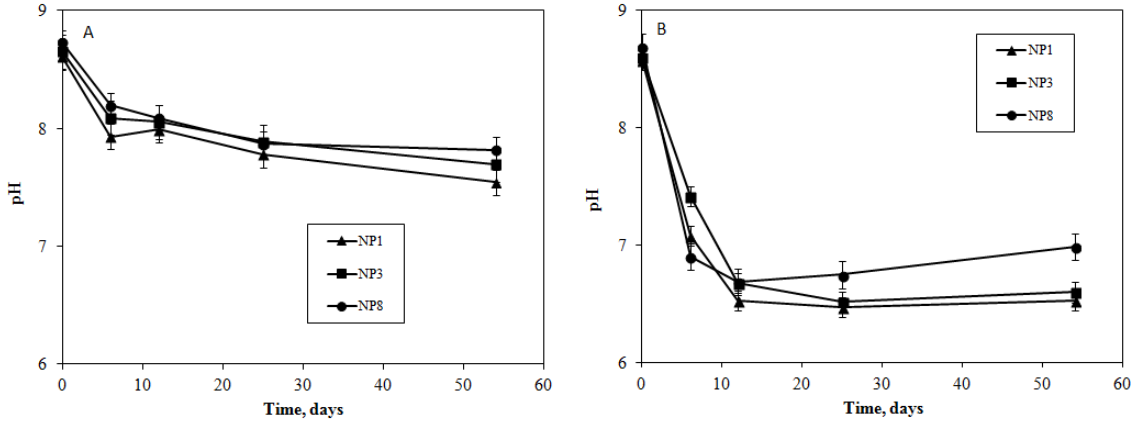


Figure A-2. The changes in sulfate in the aqueous phase of microcosms containing the three sediments incubated with two treatments: A) groundwater and B) groundwater plus glucose. Error bars represent Tukey HSD (α=0.05).

# Appendix B

Supplementary information for Chapter 3: **Arsenic solubilization and redistribution in three sediments, under anoxic conditions, from a basin-fill aquifer in semi-arid Northern Utah**

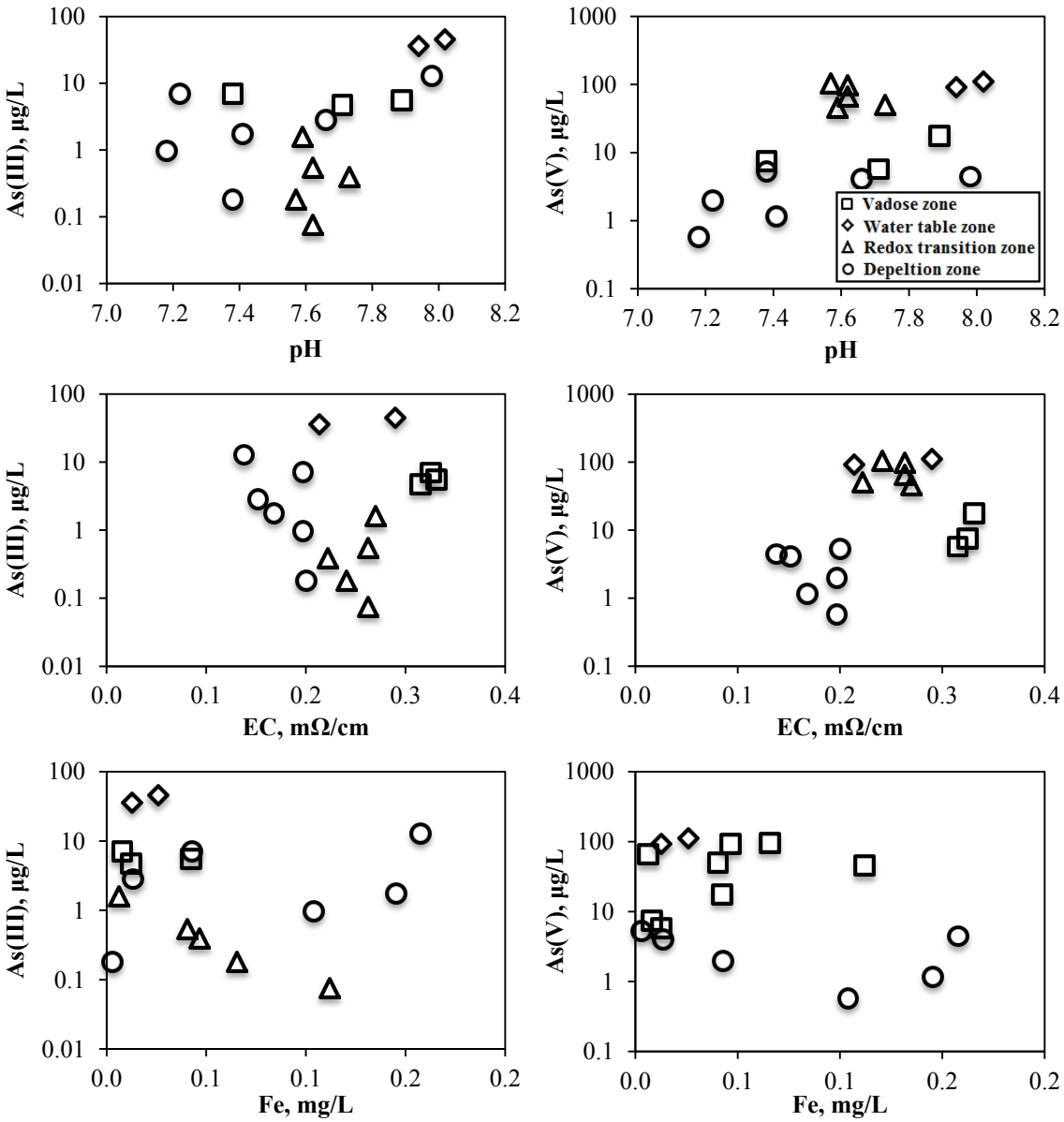

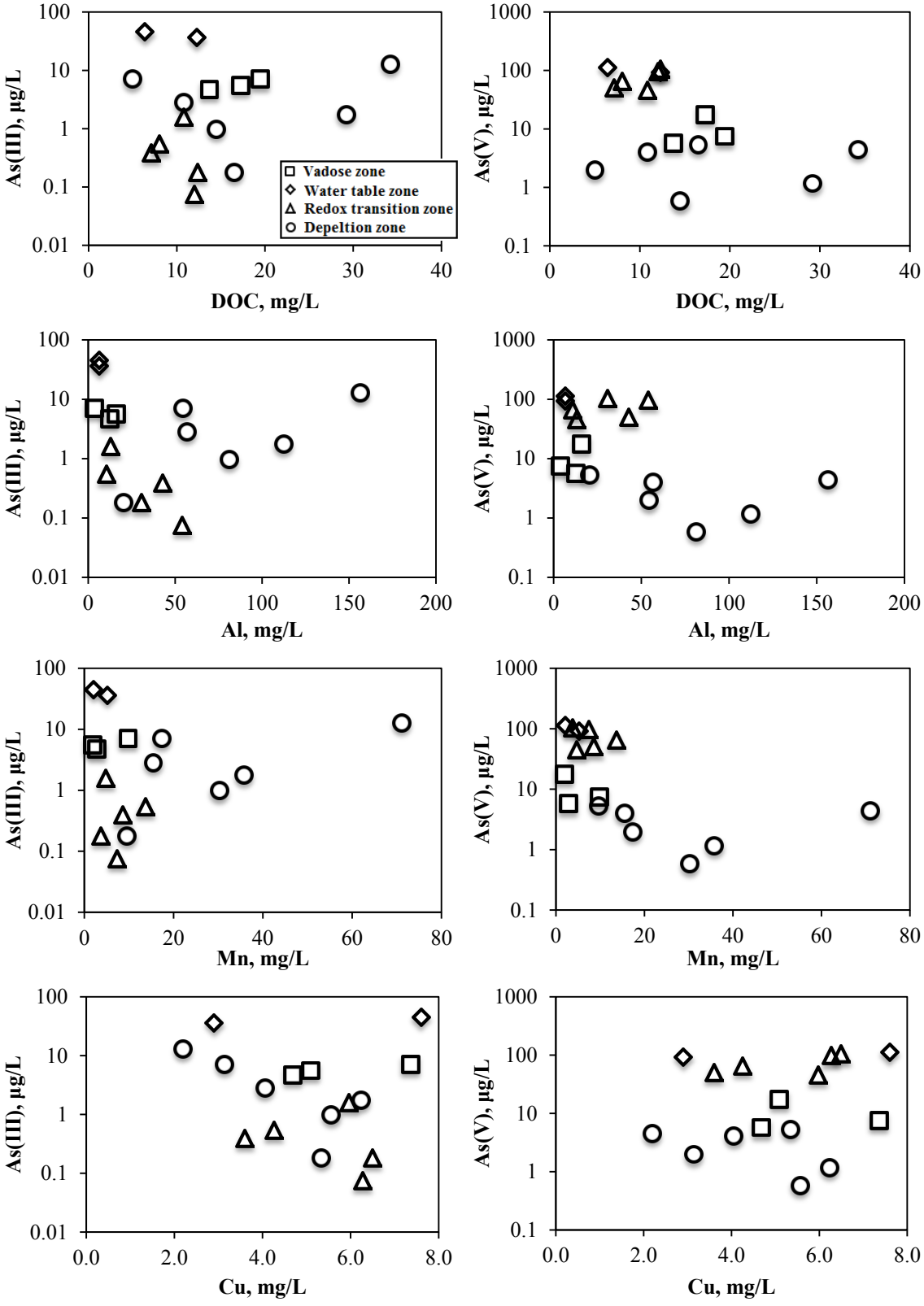
As(III), µg/L
As(V), µg/L
DOC, mg/L
Al, mg/L
Mn, mg/L
Cu, mg/L
Vadose zone
Water table zone
Redox transition zone
Depeltion zone

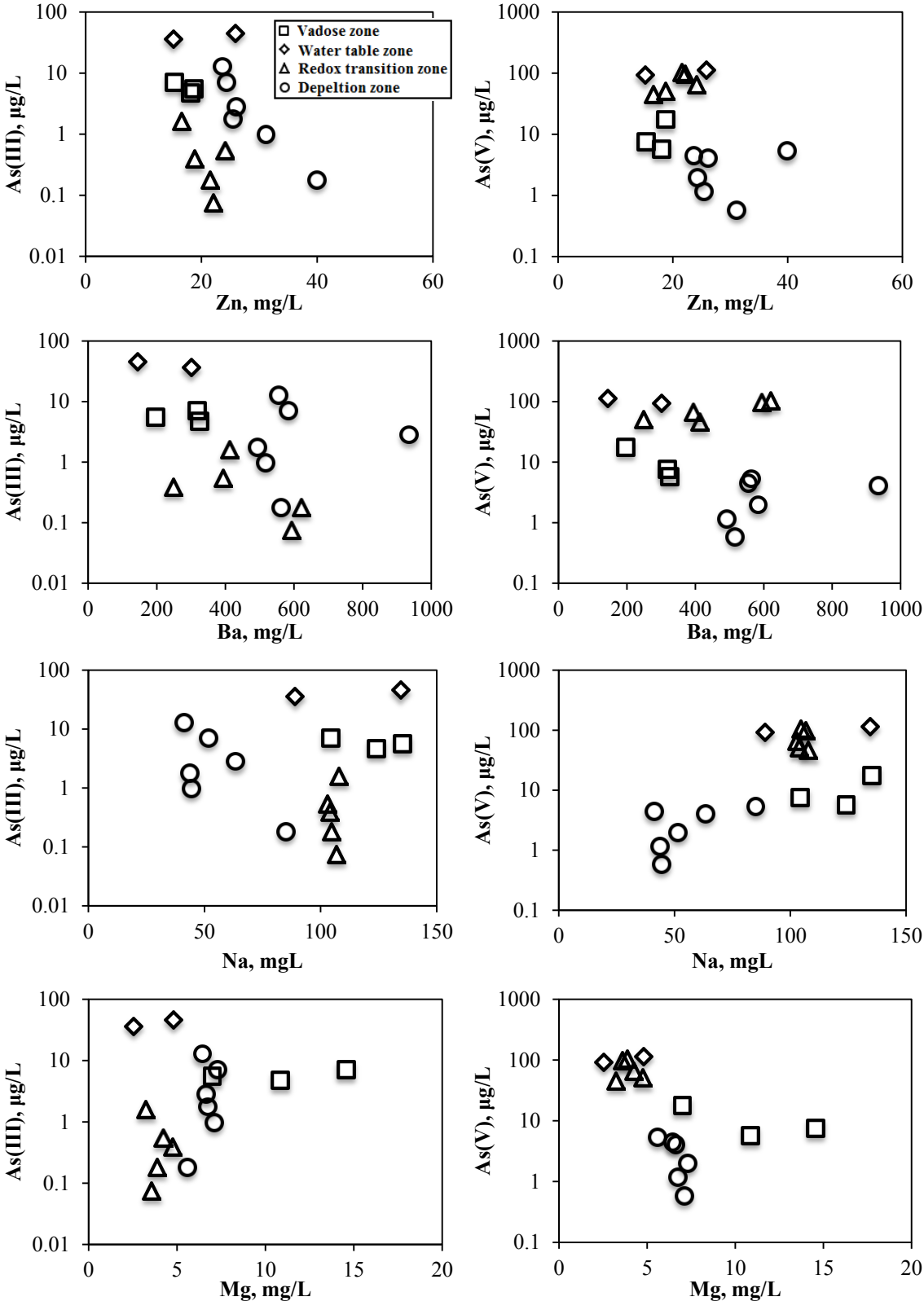
Vadose zone
Water table zone
Redox transition zone
Depeltion zone
As(III), µg/L
As(V), µg/L
Zn, mg/L
Ba, mg/L
Na, mgL
Mg, mg/L

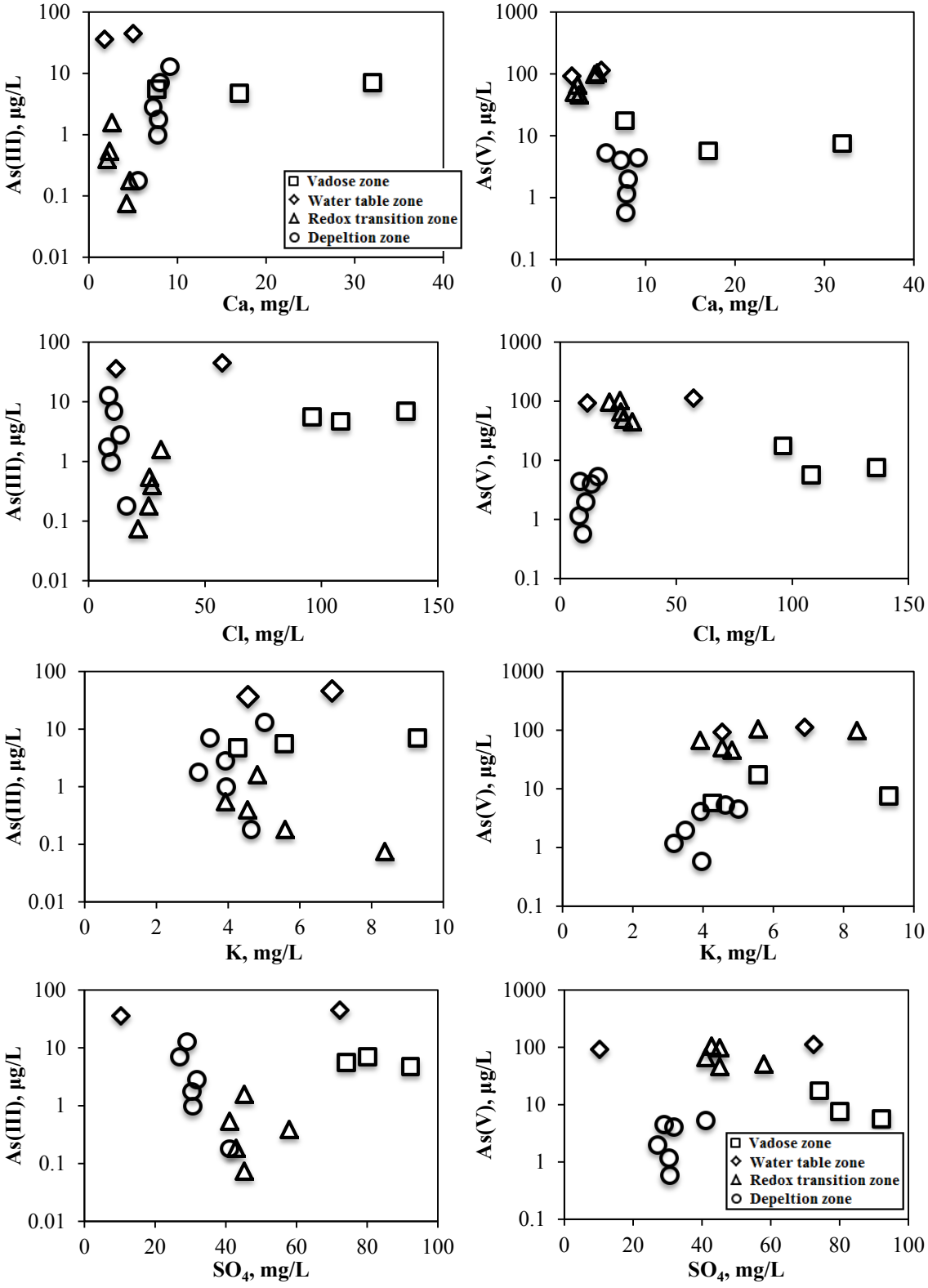


Figure B-1. Scatter plots of As and other chemical parameters in water extractions from NP9.

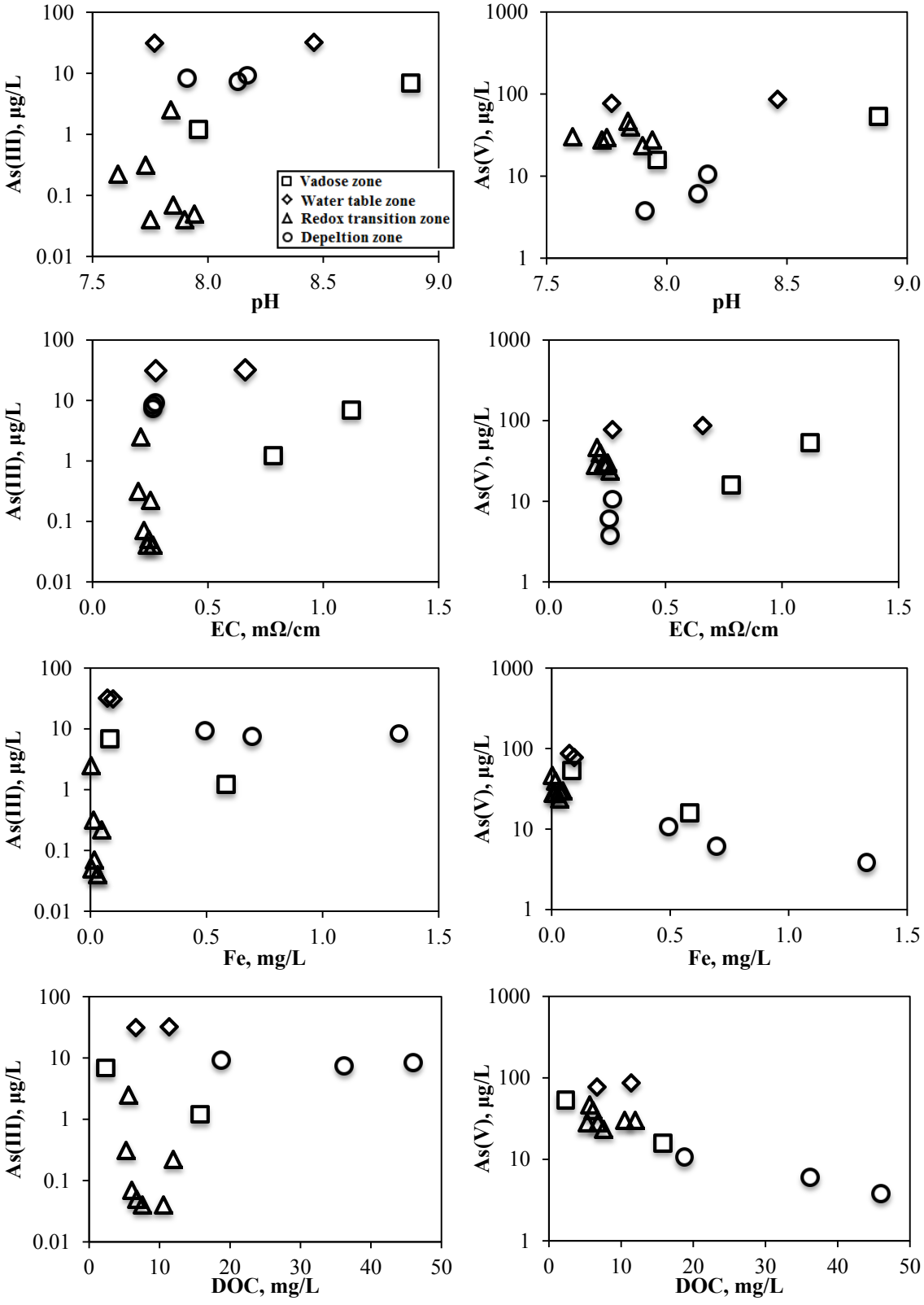
As(III), µg/L
As(V), µg/L
pH
EC, mΩ/cm
Fe, mg/L
DOC, mg/L
Vadose zone
Water table zone
Redox transition zone
Depeltion zone

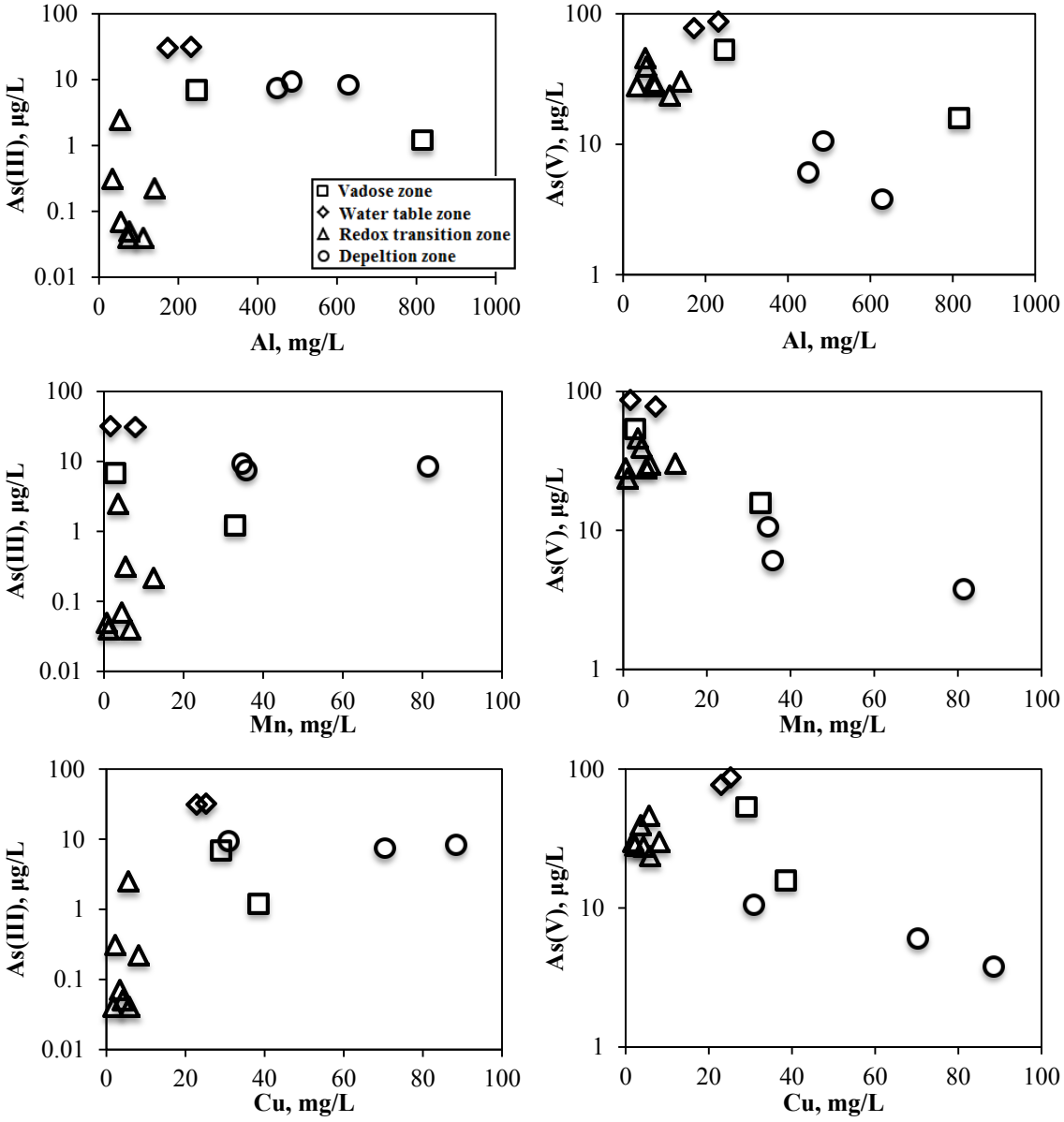
As(III), µg/L
100
10
1
0.1
0.01
0
200
400
600
800
1000
Al, mg/L
Vadose zone
Water table zone
Redox transition zone
Depeltion zone
As(V), µg/L
100
10
1
0
200
400
600
800
1000
Al, mg/L
As(III), µg/L
100
10
1
0.1
0.01
0
20
40
60
80
100
Mn, mg/L
As(V), µg/L
100
10
1
0
20
40
60
80
100
Mn, mg/L
As(III), µg/L
100
10
1
0.1
0.01
0
20
40
60
80
100
Cu, mg/L
As(V), µg/L
100
10
1
0
20
40
60
80
100
Cu, mg/L

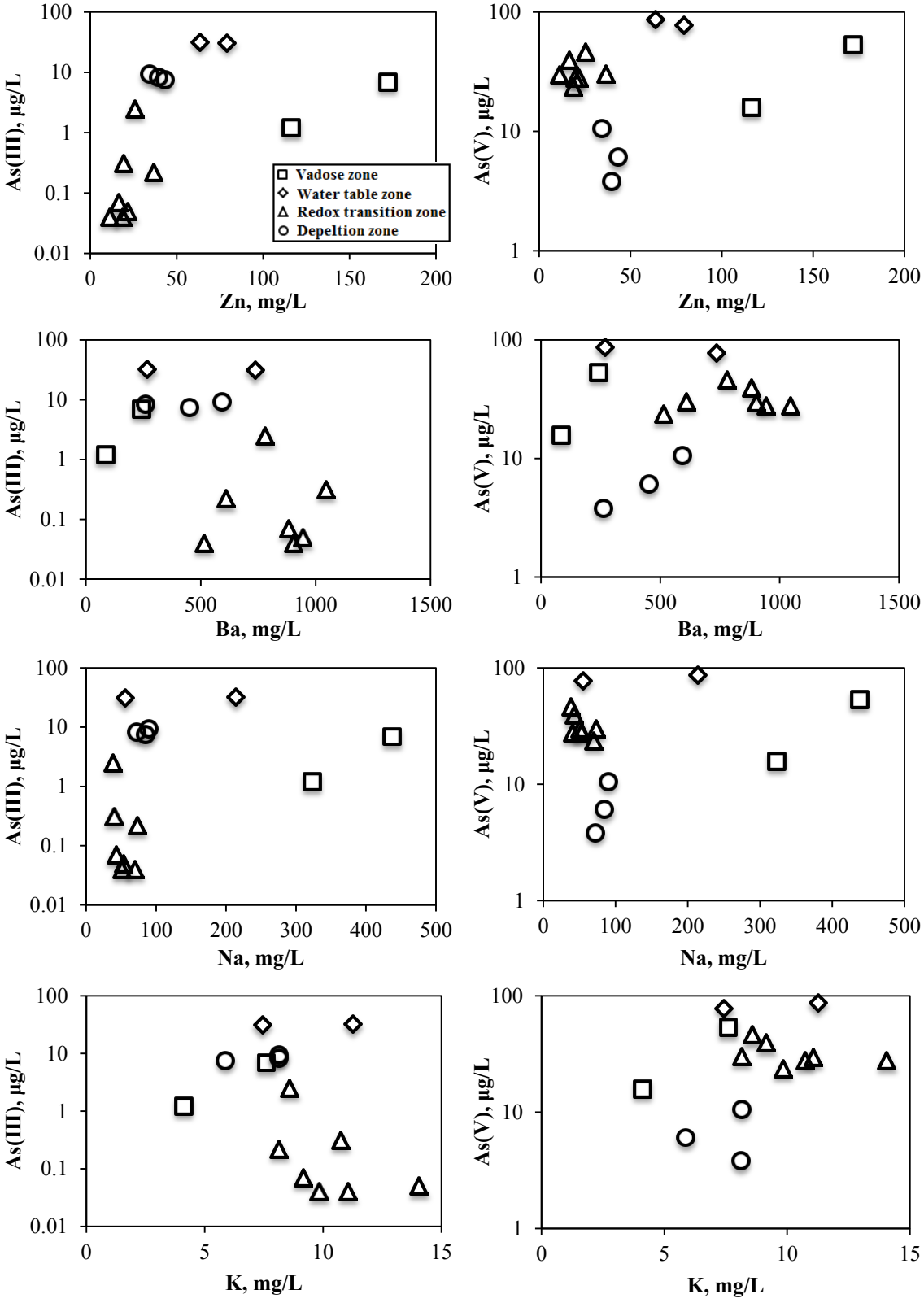
As(III), µg/L
As(V), µg/L
Zn, mg/L
Ba, mg/L
Na, mg/L
K, mg/L
Vadose zone
Water table zone
Redox transition zone
Depeltion zone

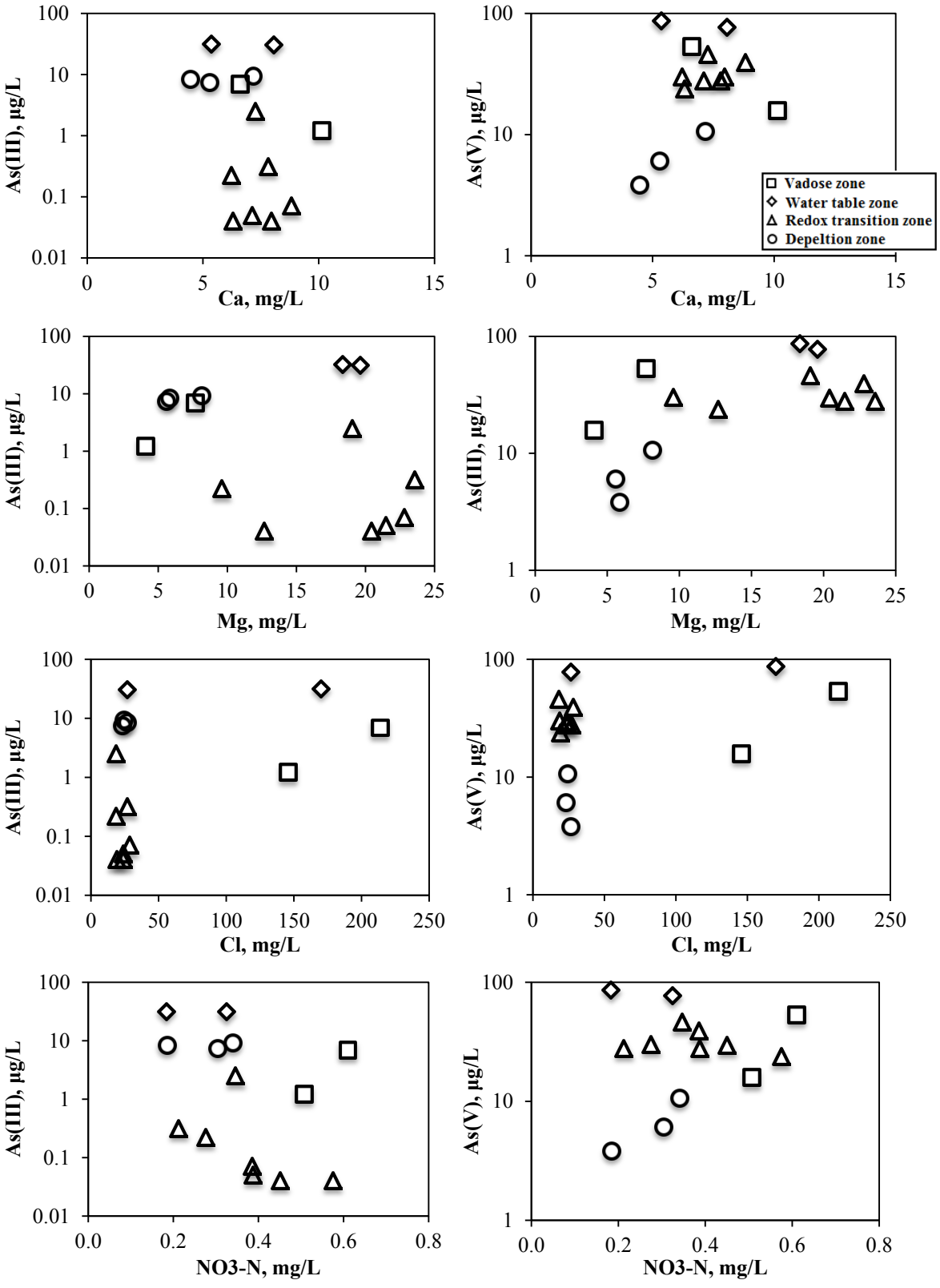
As(III), µg/L
As(V), µg/L
Ca, mg/L
Mg, mg/L
Cl, mg/L
NO3-N, mg/L
Vadose zone
Water table zone
Redox transition zone
Depeltion zone

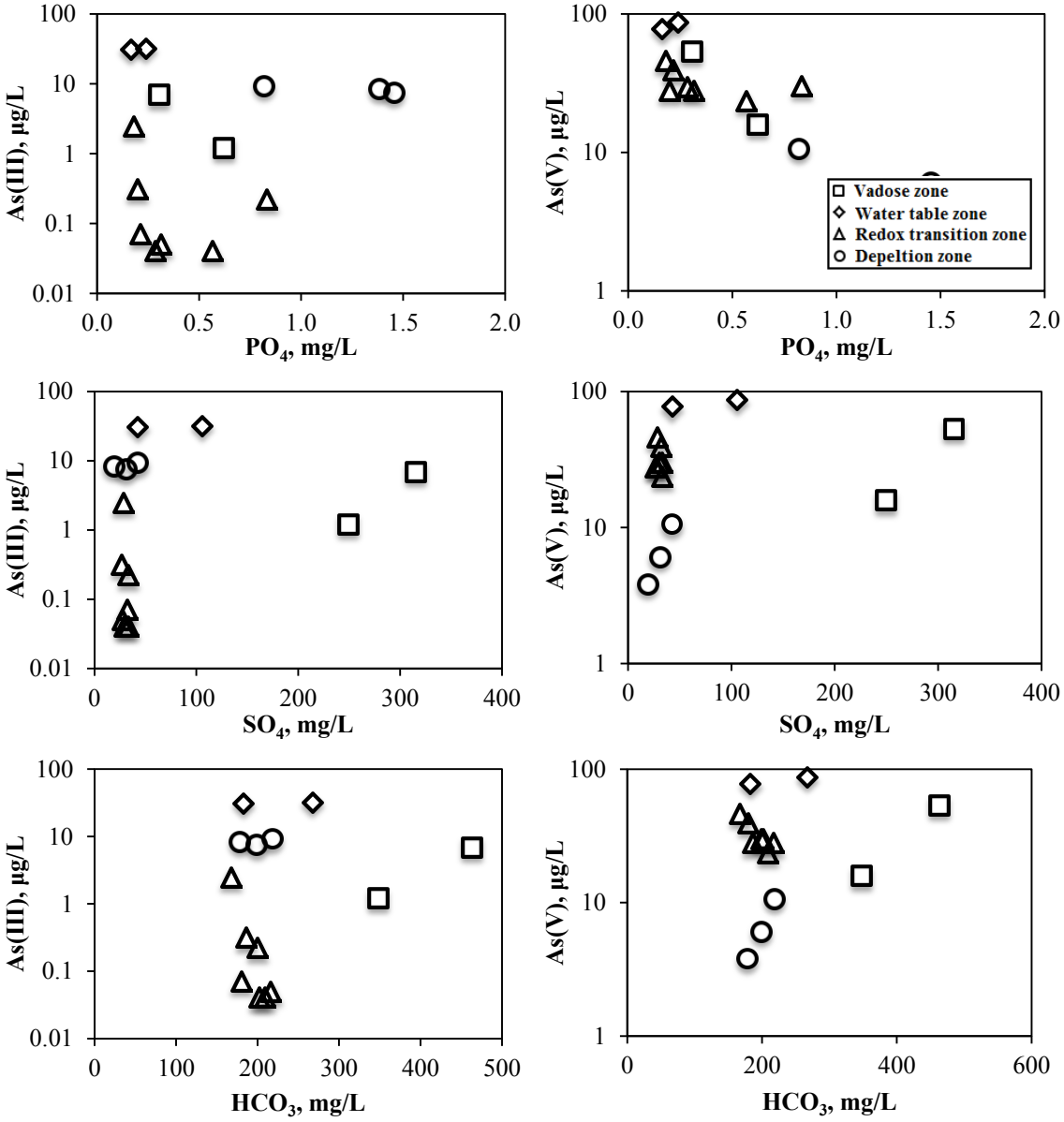


Figure B-2. Scatter plots of As and other chemical parameters in water extractions from NP13.

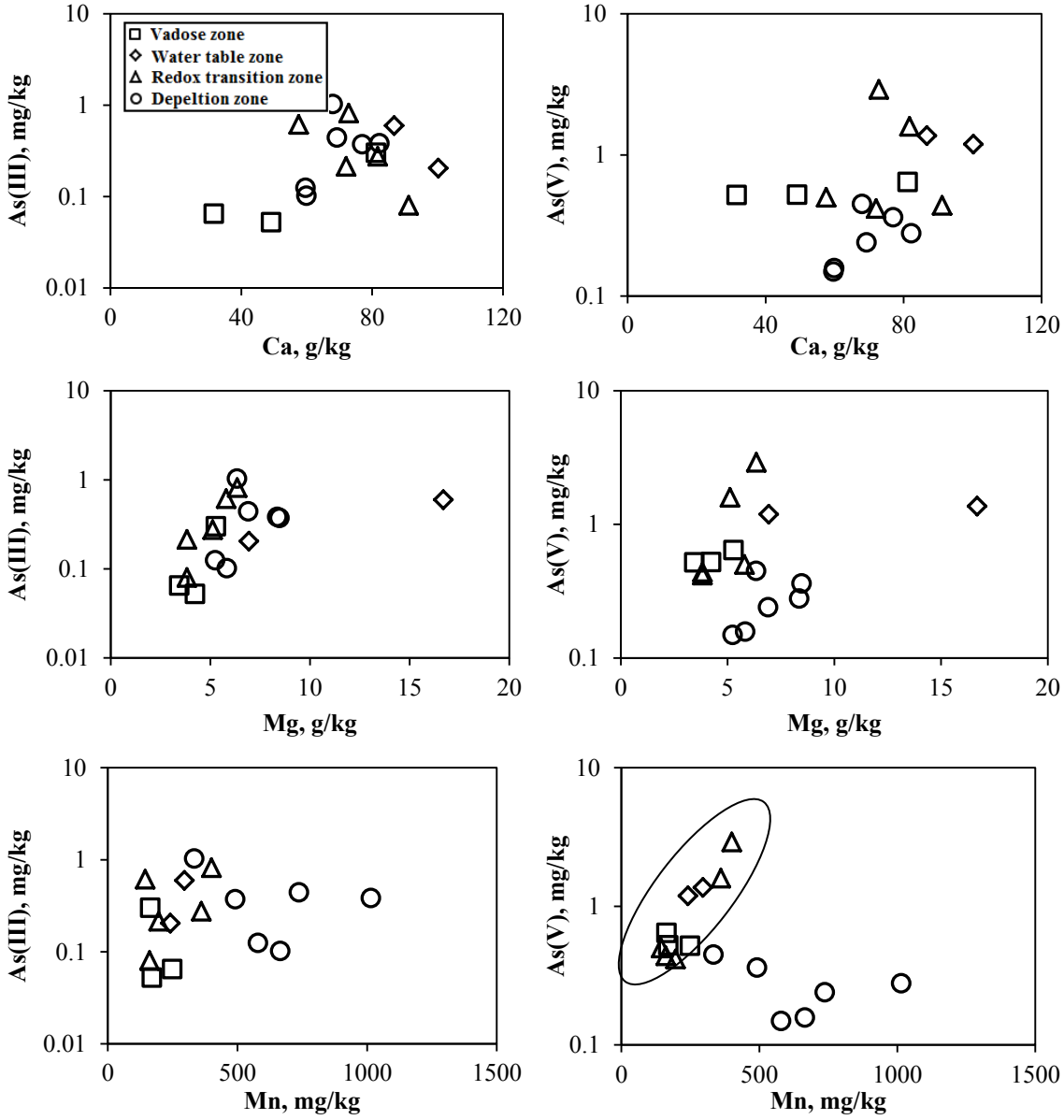


Figure B-3. Scatter plots of As and other elements in carbonate fraction of NP9.

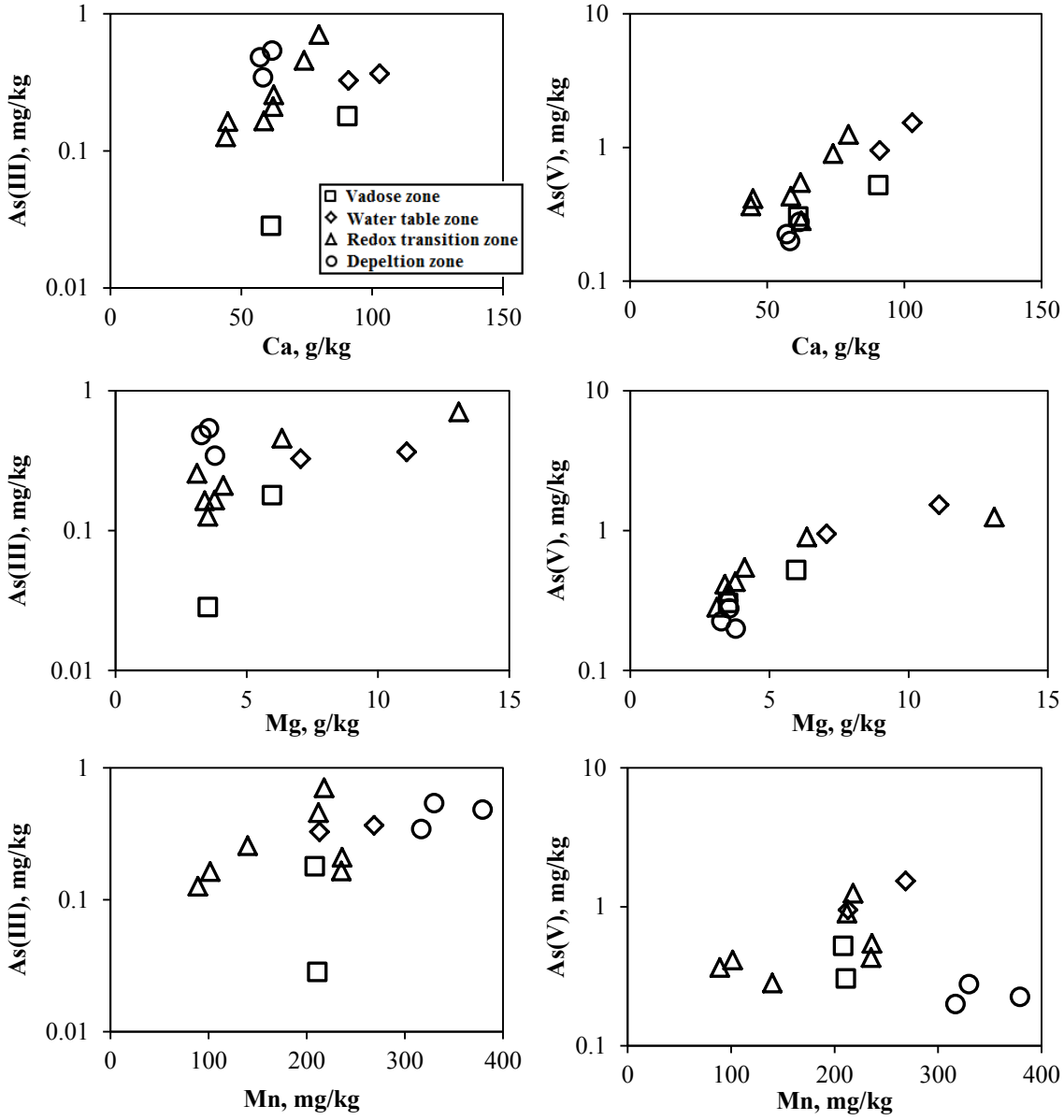


Figure B-4. Scatter plots of As and other elements in carbonate fraction of NP13.

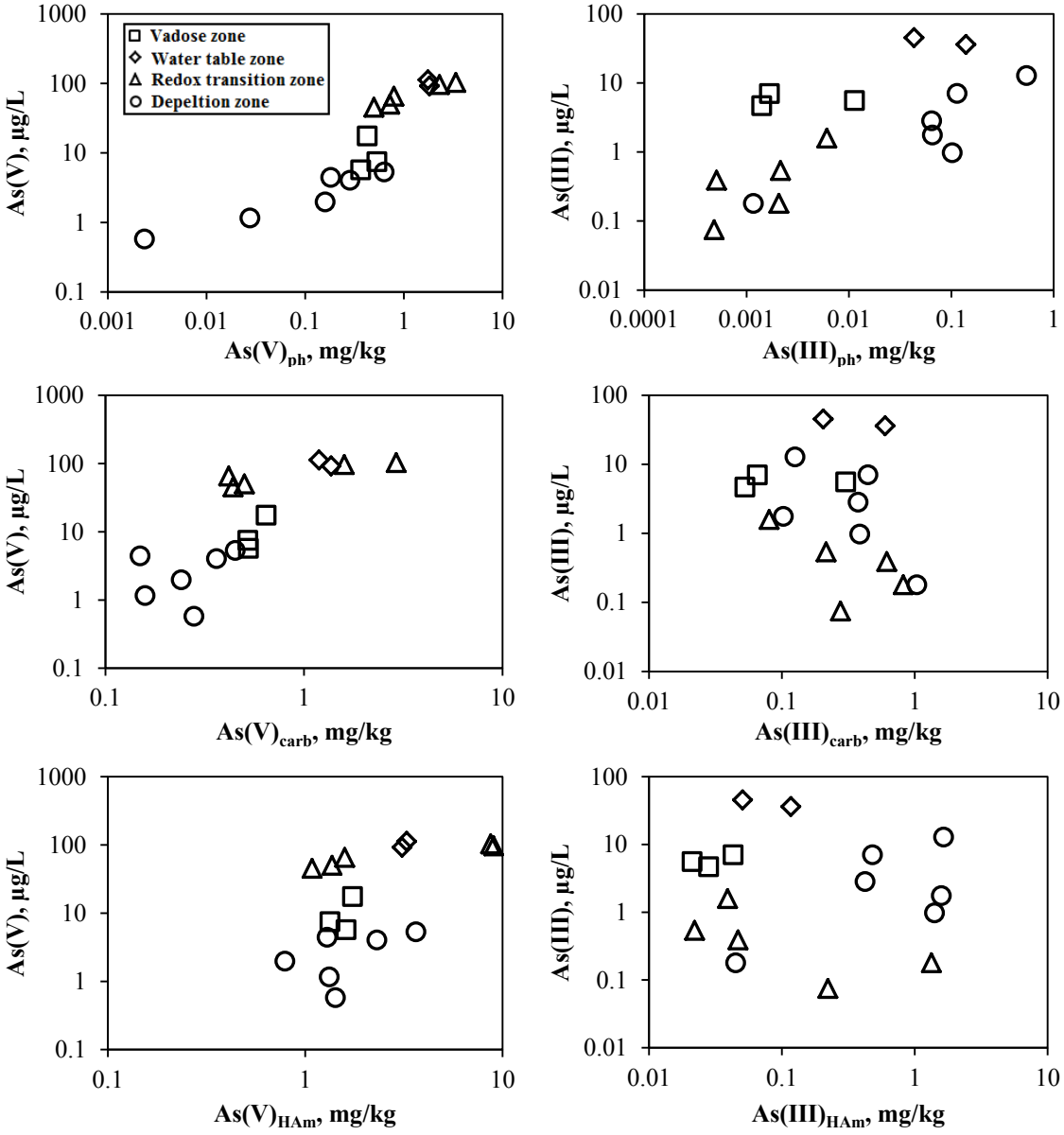
Vadose zone
Water table zone
Redox transition zone
Depeltion zone
As(V), µg/L
As(V)ph, mg/kg
As(III), µg/L
As(III)ph, mg/kg
As(V), µg/L
As(V)carb, mg/kg
As(III), µg/L
As(III)carb, mg/kg
As(V), µg/L
As(V)HAm, mg/kg
As(III), µg/L
As(III)HAm, mg/kg

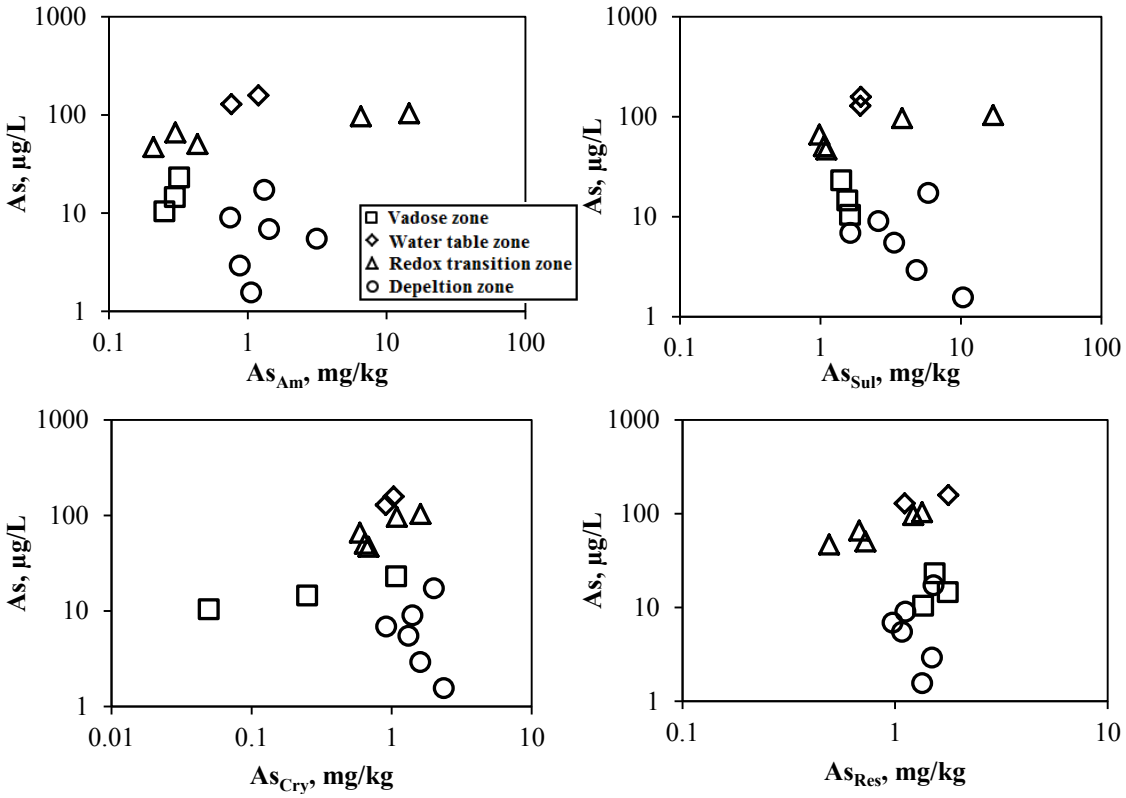


Figure B-5. Scatter plots of water extractable As and As in each sequential extraction fraction of NP9. As(III) and As(V) were distinguished in the first three fractions.

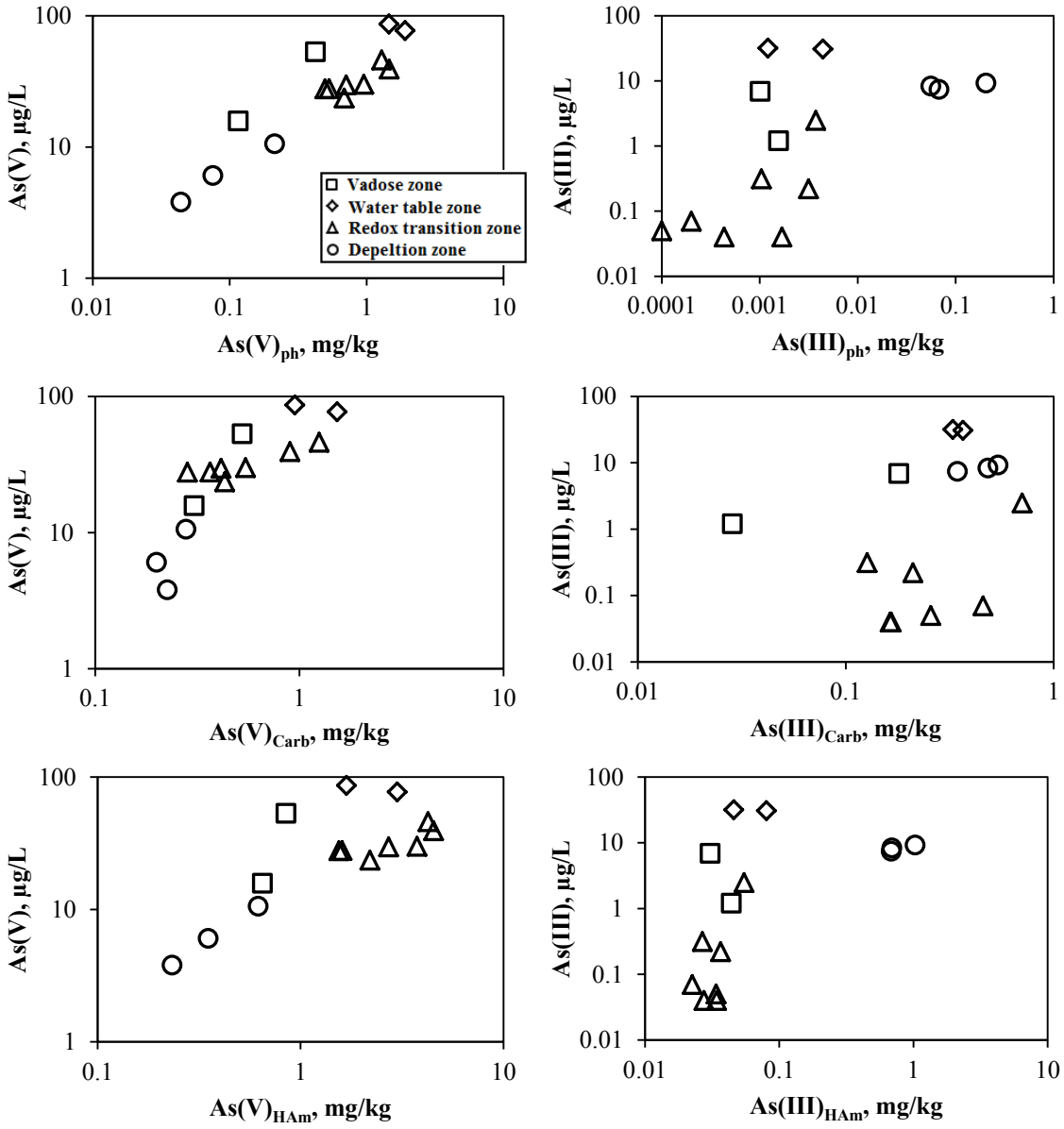
As(V), µg/L
As(V)ph, mg/kg
Vadose zone
Water table zone
Redox transition zone
Depeltion zone
As(III), µg/L
As(III)ph, mg/kg
As(V), µg/L
As(V)Carb, mg/kg
As(III), µg/L
As(III)Carb, mg/kg
As(V), µg/L
As(V)HAm, mg/kg
As(III), µg/L
As(III)HAm, mg/kg

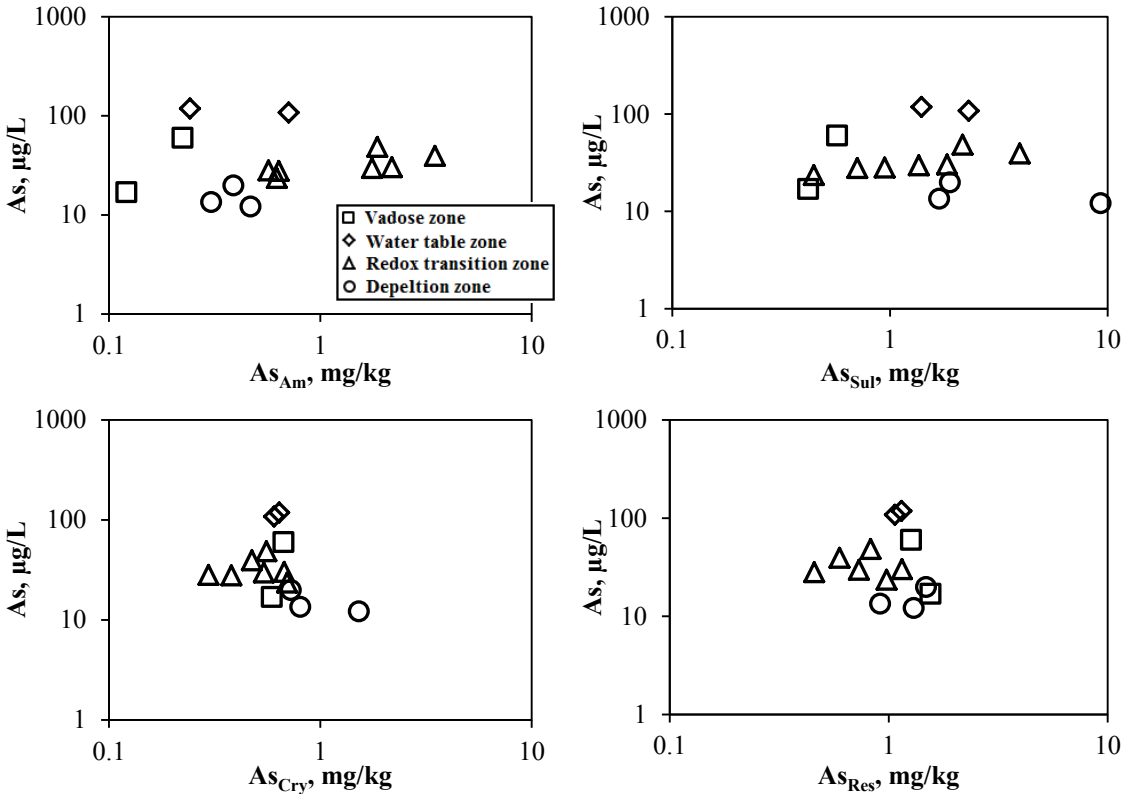


Figure B-6. Scatter plots of water extractable As and As in each sequential extraction fraction of NP13. As(III) and As(V) were distinguished in the first three fractions.

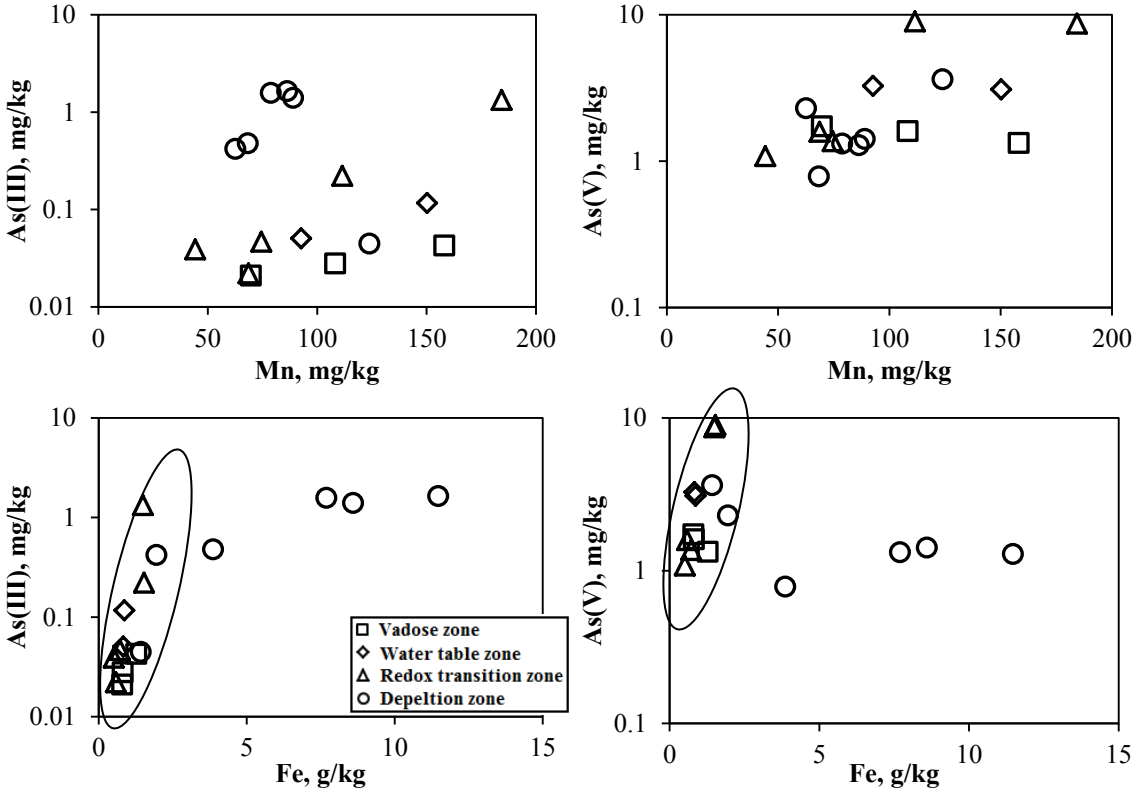


Figure B-7. Scatter plots of As and Mn and Fe in AVS, Mn oxides, and highly amorphous Fe oxides fraction in NP9

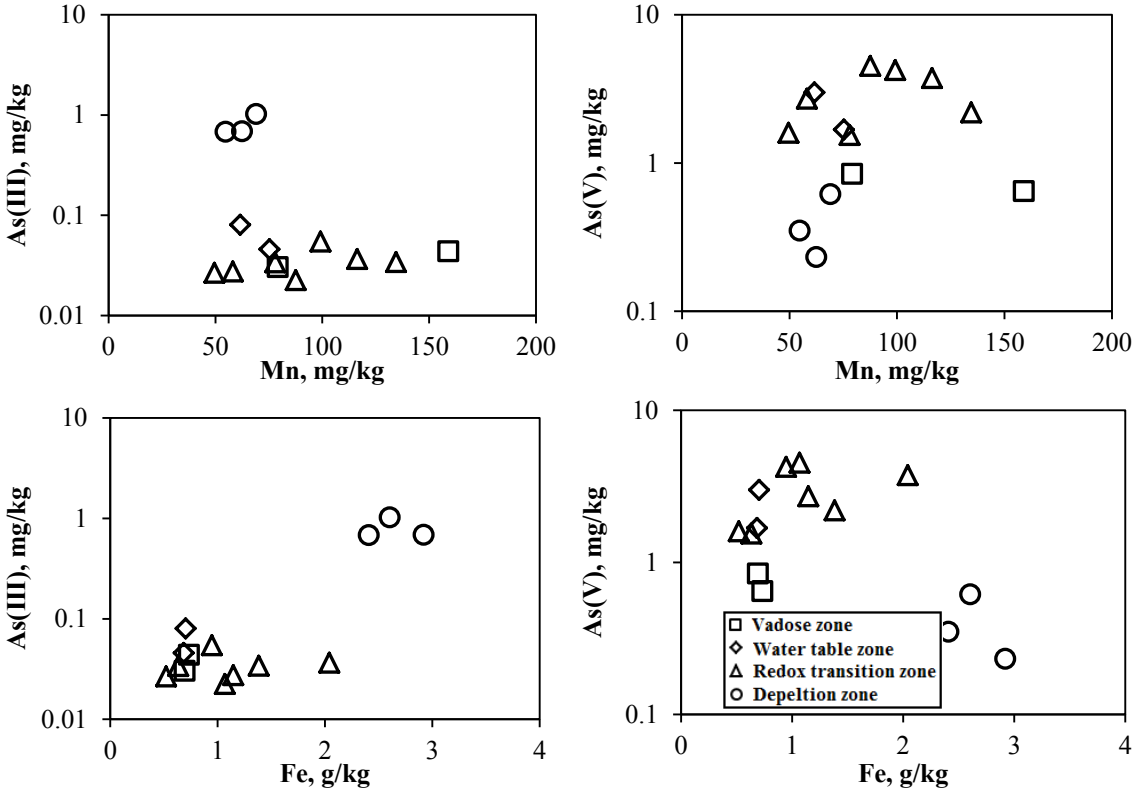


Figure B-8. Scatter plots of As and Mn and Fe in AVS, Mn oxides, and highly amorphous Fe oxides fraction in NP13.

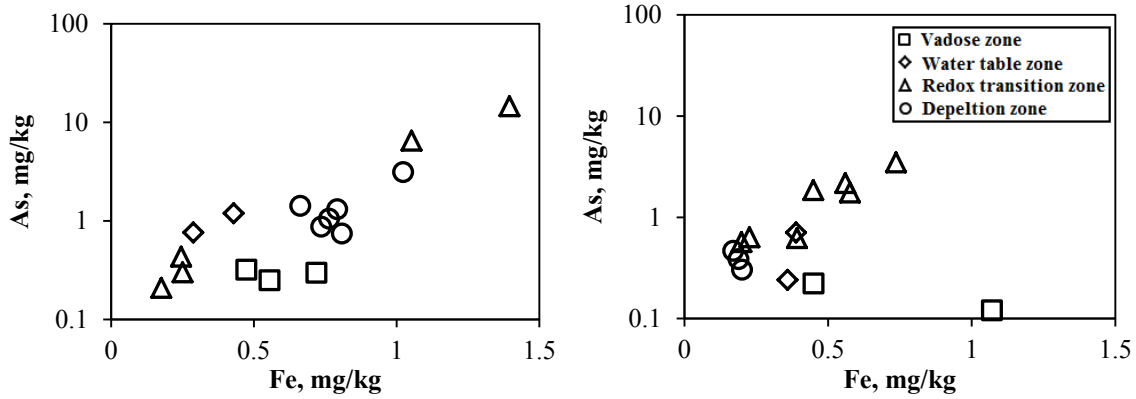


Figure B-9. Scatter plots of As and Fe in amorphous Fe oxides fraction in NP9 (left) and NP13 (right).

# Appendix C

Supplementary information for Chapter 4: **Redox controlled spatial heterogeneity in arsenic mineralogy in two sediment profiles in the semi-arid Cache Valley Basin, Utah: An XAS study**

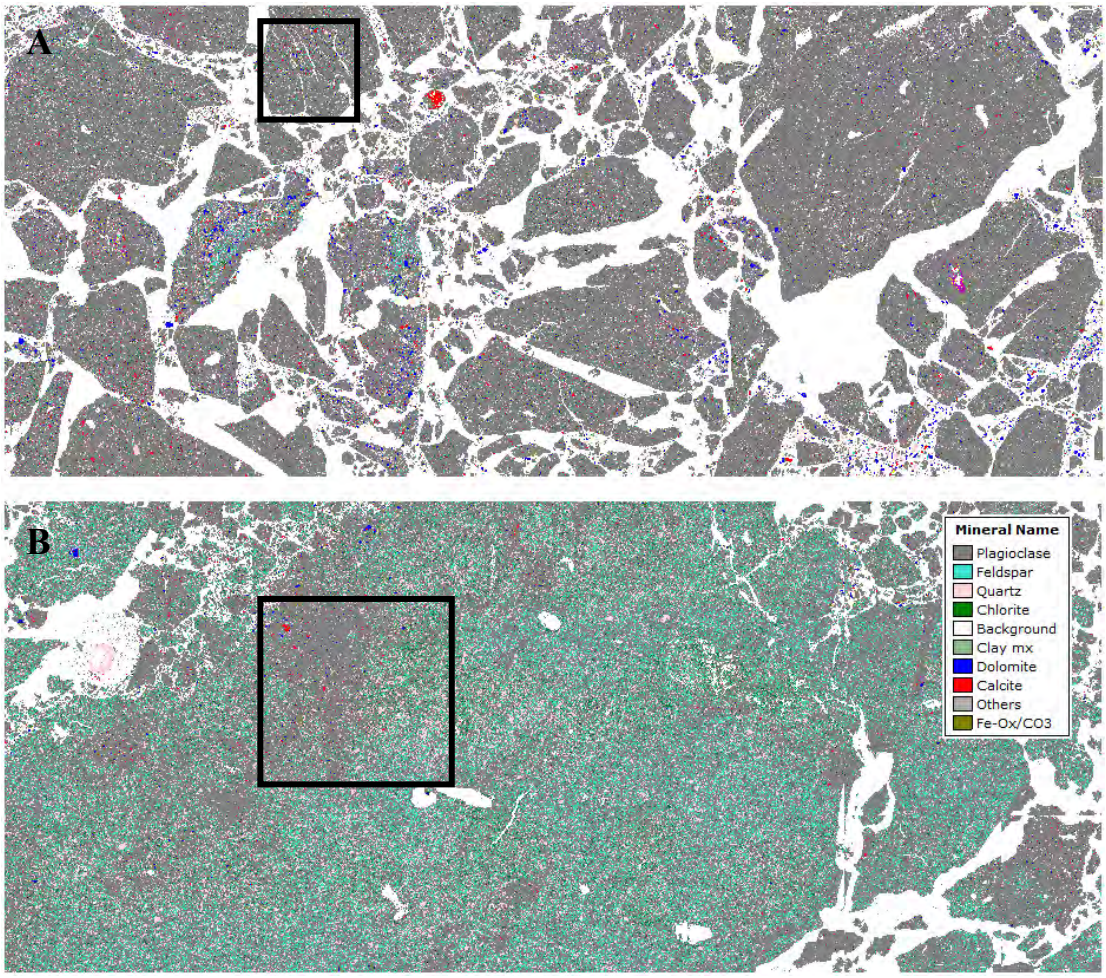


Figure C-1. Composition maps of NP9-4(A) and NP13-4(B). Colors indicate the mineral species classified by SIP. The blocked area indicates the area scanned for μXRF and μXANES.

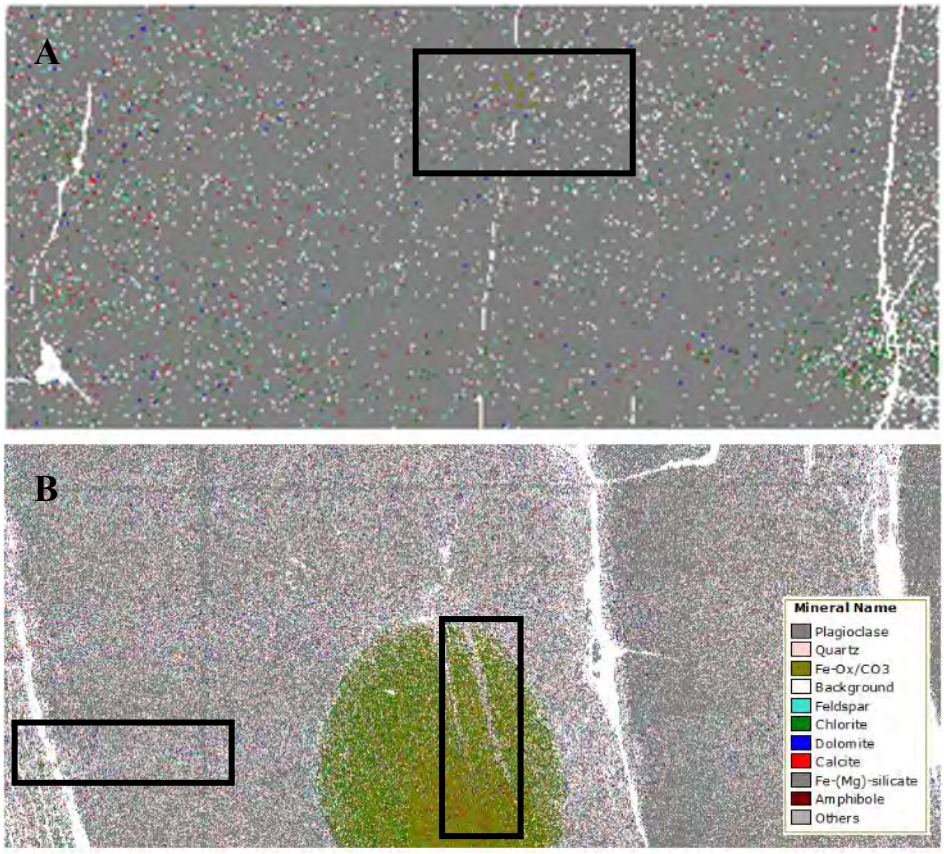


Figure C-2. Composition maps of NP9-10(A) and NP13-8(B). Fine resolution QEMSCAN map was not collected for NP9-10. Colors indicate the mineral species classified by SIP. The blocked area indicates the area scanned for μXRF and μXANES.

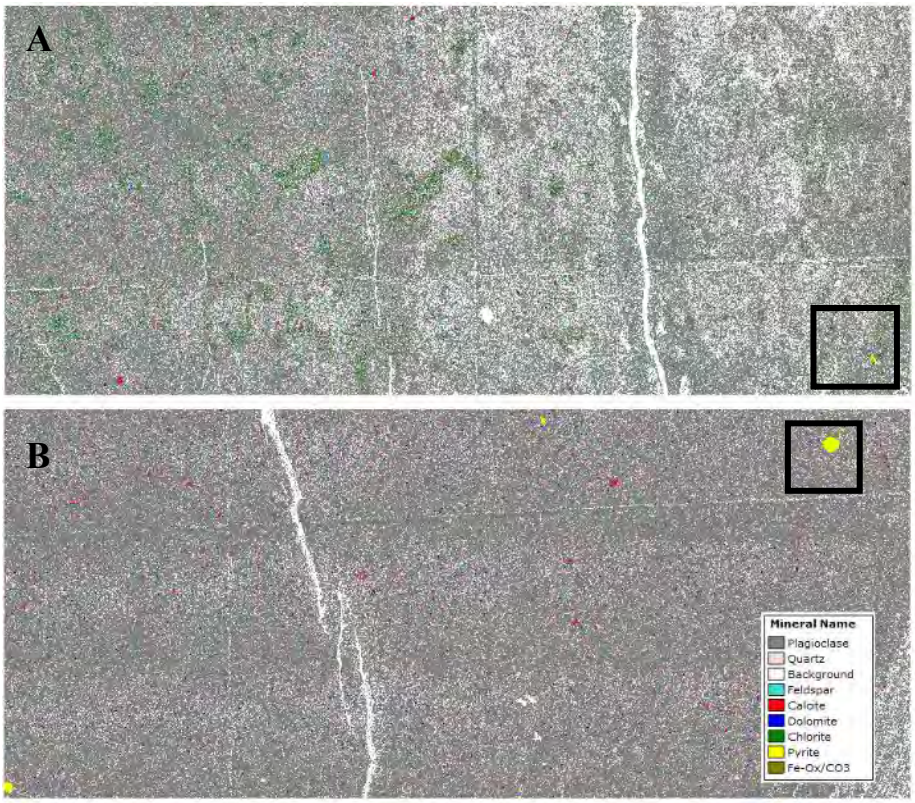


Figure C-3. Composition maps of NP9-16(A) and NP13-12(B). Colors indicate the mineral species classified by SIP. The blocked area indicates the area scanned for μXRF and μXANES.

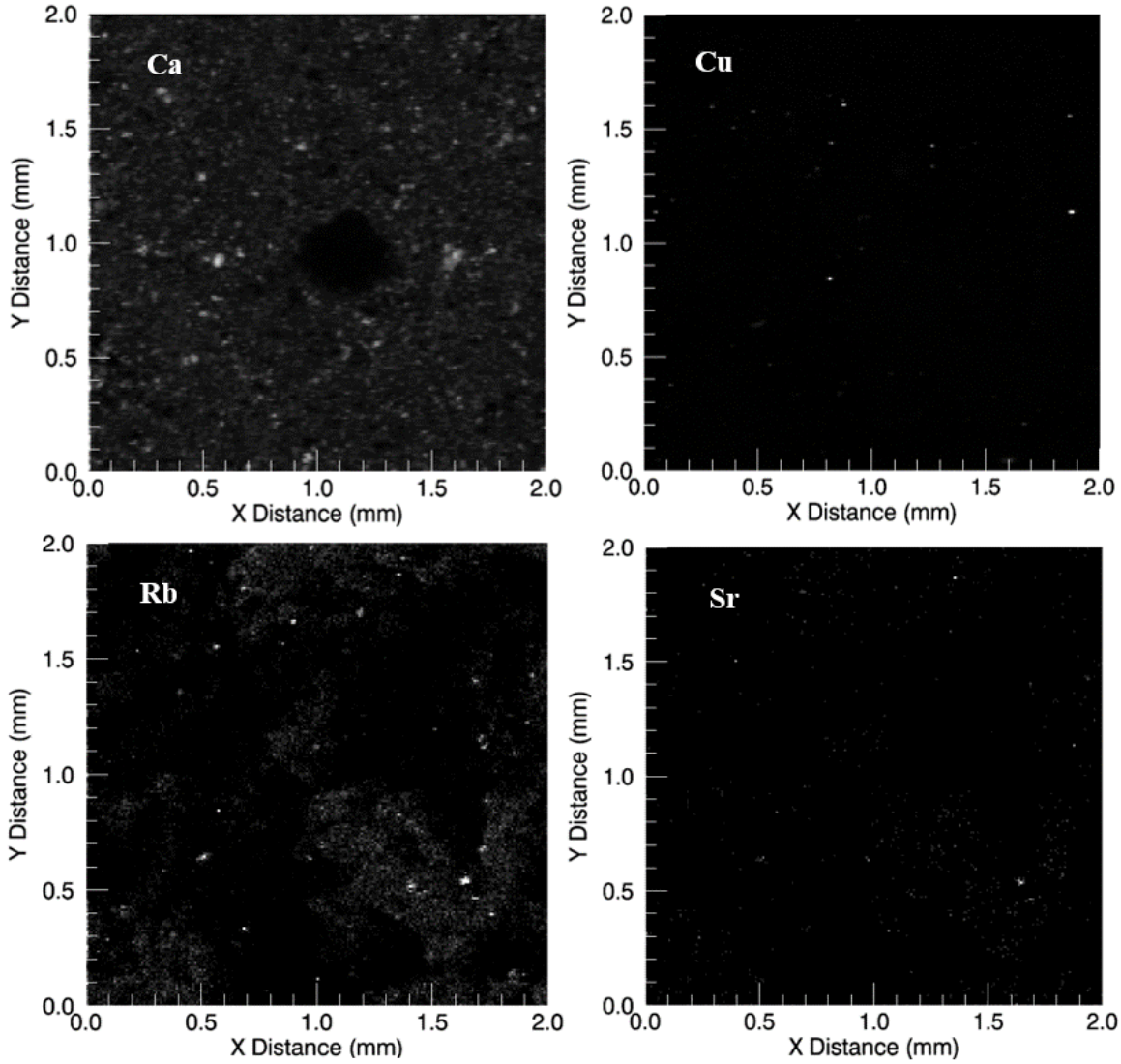


Figure C-4. μXRF maps for Ca Kα, Cu Kα, Rb Kα, and Sr Kα in NP9-1. The scale of maps is in millimeters. Fluorescence counts for each element were proportional to the brightness.

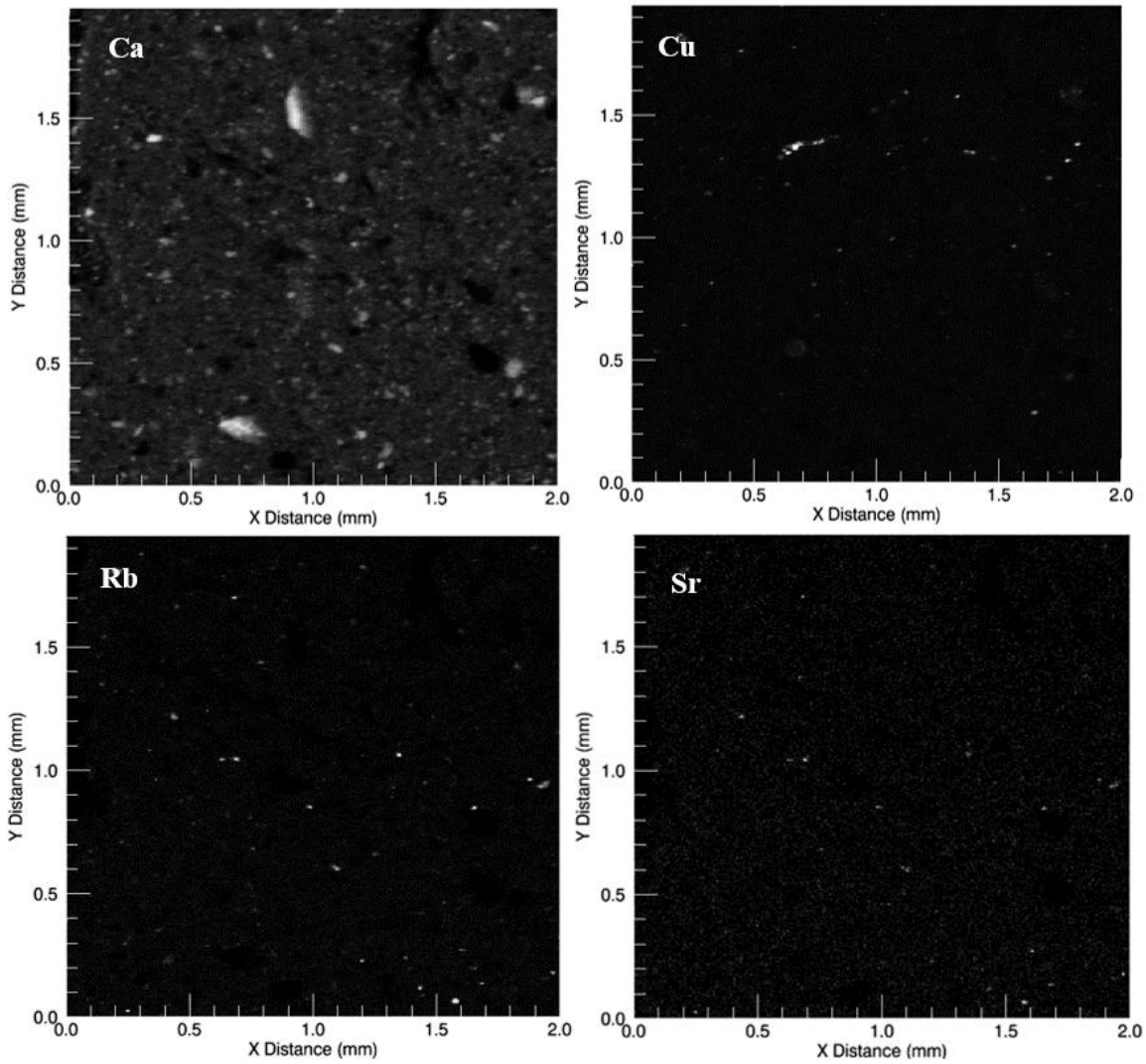


Figure C-5. μXRF maps for Ca Kα, Cu Kα, Rb Kα, and Sr Kα in NP13-1. The scale of maps is in millimeters. Fluorescence counts for each element were proportional to the brightness.

Table C-1. XRF Counts at spots of interest in selected sediments of NP9

| Sample ID | Spot# | Fluorescence counts | | | | | | |
|---|---|---|---|---|---|---|---|---|
| | | As | Fe | Mn | Ca | Cu | Rb | Sr |
| NP9-1 | S1 | 487 | 436 | 7 | 40 | 32 | 0 | 0 |
| | S2 | 126 | 306 | 3 | 24 | 429 | 0 | 0 |
| | S3 | 134 | 597 | 15 | 29 | 17 | 0 | 0 |
| | S4 | 140 | 1566 | 24 | 173 | 52 | 0 | 0 |
| | S5 | 127 | 765 | 10 | 83 | 29 | 0 | 0 |
| NP9-4 | S1 | 203 | 6642 | 2066 | 1069 | 34 | 5 | 1 |
| | S2 | 89 | 4836 | 3053 | 719 | 52 | 3 | 0 |
| | S3 | 94 | 4341 | 2689 | 732 | 67 | 4 | 1 |
| | S4 | 52 | 5622 | 2915 | 768 | 104 | 2 | 1 |
| | S5 | 116 | 6939 | 82 | 1619 | 27 | 5 | 0 |
| NP9-10 | S1 | 842 | 39962 | 311 | 700 | - | 301 | 20 |
| | S2 | 602 | 45699 | 290 | 223 | - | 367 | 30 |
| NP9-16 | S1 | 421 | 3310 | 67 | 371 | 21 | 0 | 0 |
| | S2 | 116 | 2985 | 90 | 649 | 18 | 0 | 0 |
| | S3 | 89 | 2626 | 89 | 587 | 28 | 3 | 0 |
| | S4 | 255 | 20695 | 216 | 356 | 28 | 70 | 3 |

Table C-2. XRF Counts at spots of interest in selected sediments of NP13

| Sample ID | Spot# | Fluorescence counts | | | | | | |
|---|---|---|---|---|---|---|---|---|
| | | As | Fe | Mn | Ca | Cu | Rb | Sr |
| NP13-1 | S1 | 385 | 13739 | 139 | 668 | 32 | 19 | 1 |
| | S2 | 321 | 17813 | 164 | 287 | 35 | 39 | 2 |
| | S3 | 191 | 3124 | 101 | 2322 | 33 | 0 | 0 |
| | S4 | 219 | 4772 | 50 | 643 | 45 | 1 | 1 |
| NP13-4 | S1 | 177 | 11661 | 2817 | 380 | 47 | 12 | 1 |
| | S2 | 94 | 7498 | 3468 | 136 | 37 | 10 | 0 |
| | S3 | 375 | 6722 | 186 | 116 | 34 | 5 | 1 |
| | S4 | 143 | 5297 | 52 | 134 | 459 | 5 | 2 |
| | S5 | 67 | 6434 | 456 | 60 | 41 | 4 | 0 |
| NP13-8 | A1S1 | 220 | 16492 | 123 | 182 | 25 | 47 | 1 |
| | A1S2 | 956 | 41965 | 301 | 639 | 53 | 287 | 10 |
| | A1S3 | 548 | 47565 | 323 | 219 | 45 | 467 | 28 |
| | A2S1 | 478 | 13321 | 107 | 217 | 43 | 81 | 16 |
| | A2S2 | 537 | 33326 | 414 | 189 | 97 | 471 | 29 |
| | A2S3 | 503 | 32679 | 219 | 168 | 55 | 359 | 31 |
| | A2S4 | 200 | 8000 | 84 | 231 | 579 | 11 | 4 |
| NP9-16 | S1 | 512 | 3374 | 98 | 841 | 130 | 2 | 0 |
| | S2 | 554 | 3677 | 91 | 715 | 23 | 6 | 1 |
| | S3 | 347 | 22060 | 233 | 529 | 44 | 84 | 3 |
| | S4 | 245 | 54183 | 375 | 154 | 23 | 671 | 59 |
| | S5 | 283 | 58388 | 354 | 64 | 24 | 765 | 62 |

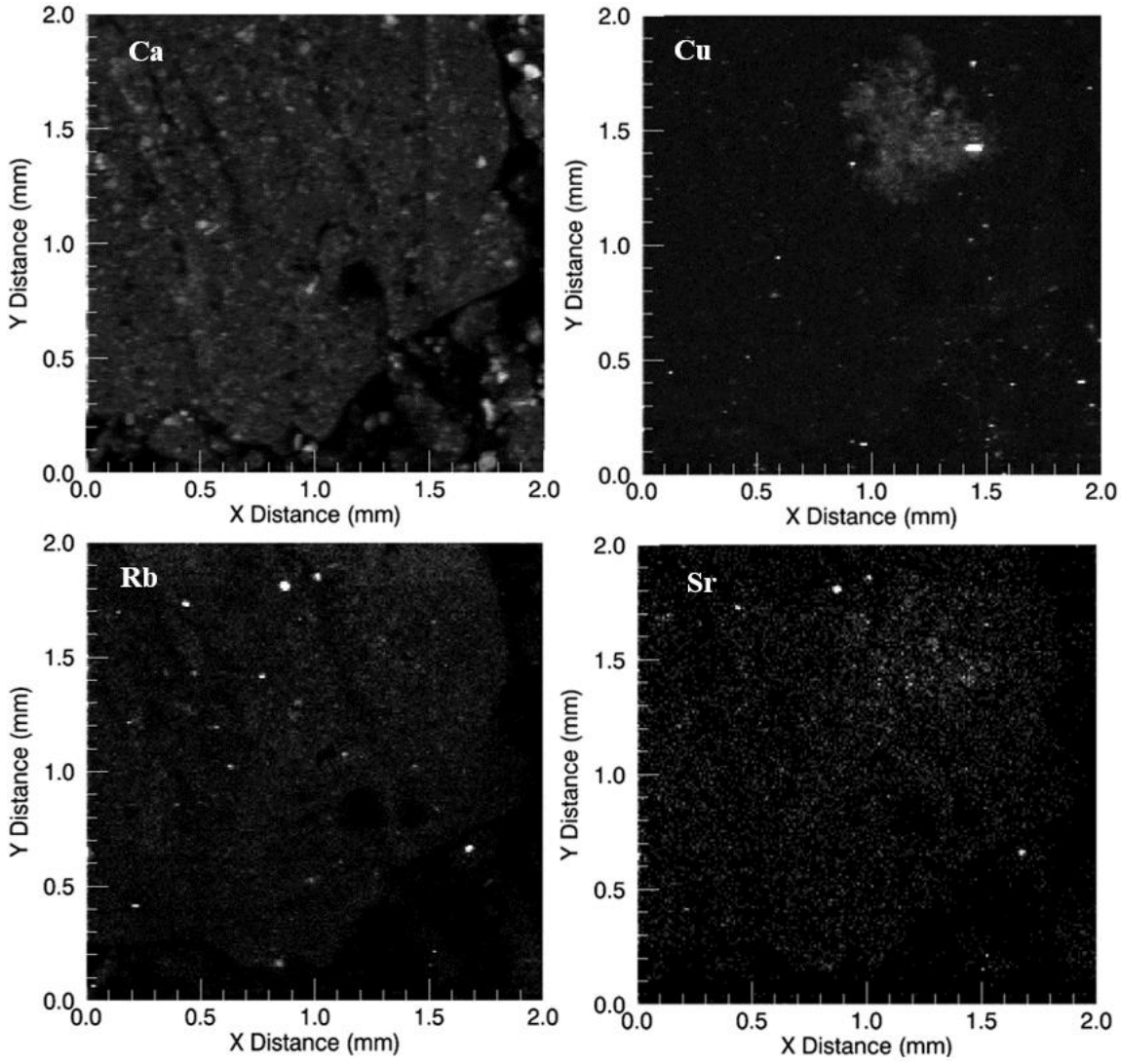


Figure C-6. μXRF maps for Ca Kα, Cu Kα, Rb Kα, and Sr Kα in NP9-4. The scale of maps is in millimeters. Fluorescence counts for each element were proportional to the brightness.

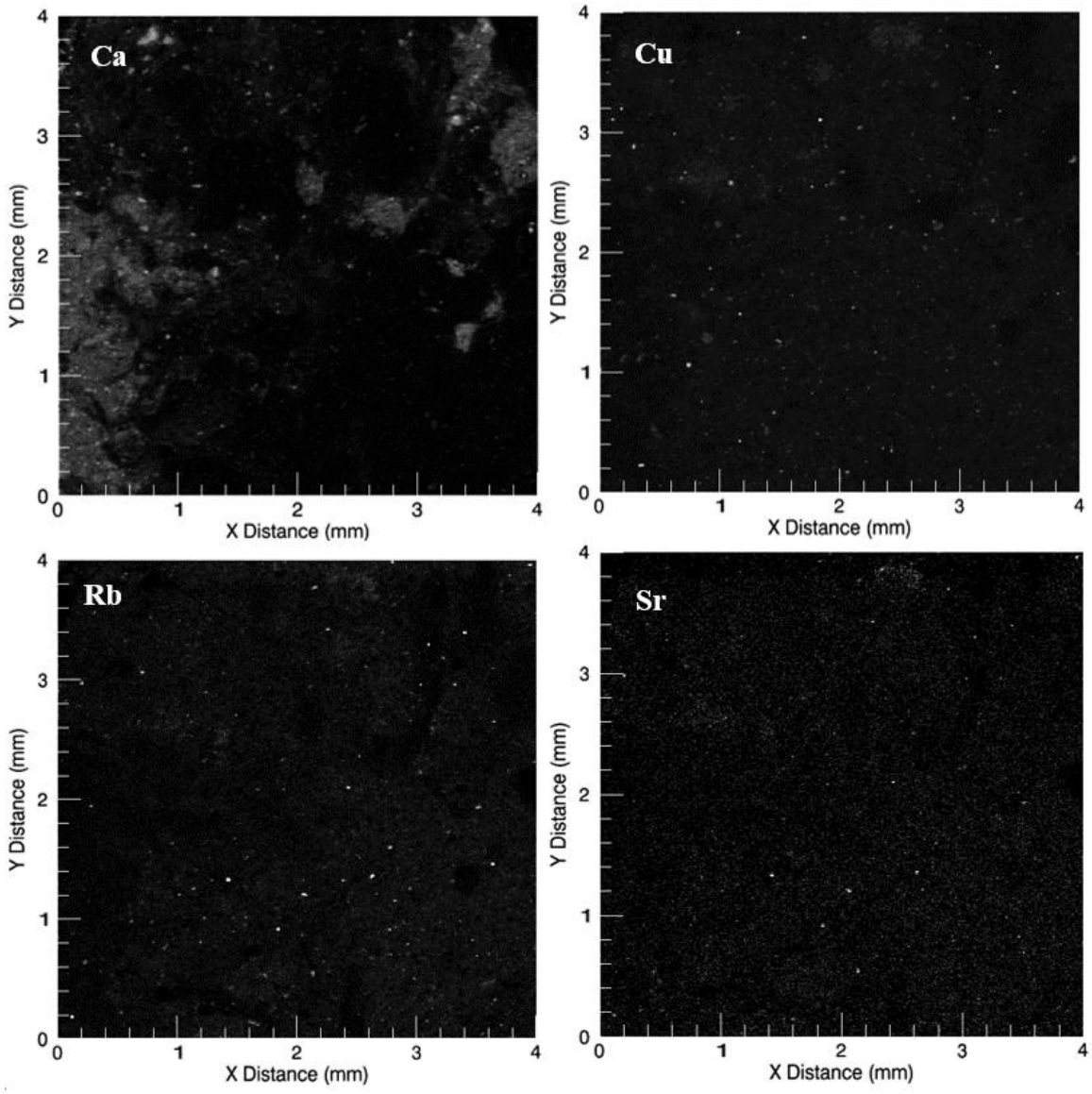


Figure C-7. μXRF maps for Ca Kα, Cu Kα, Rb Kα, and Sr Kα in NP13-4. The scale of maps is in millimeters. Fluorescence counts for each element were proportional to the brightness.

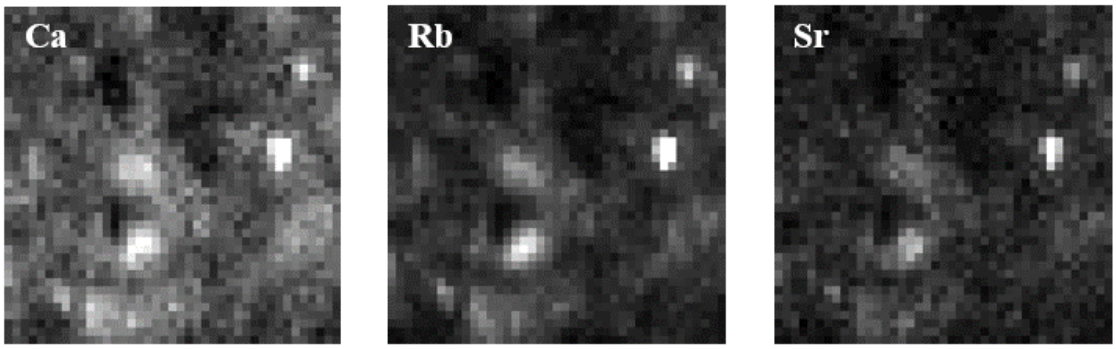


Figure C-8. μXRF maps for Ca Kα, Rb Kα, and Sr Kα in NP9-10. The scale of maps is in millimeters. Fluorescence counts for each element were proportional to the brightness.

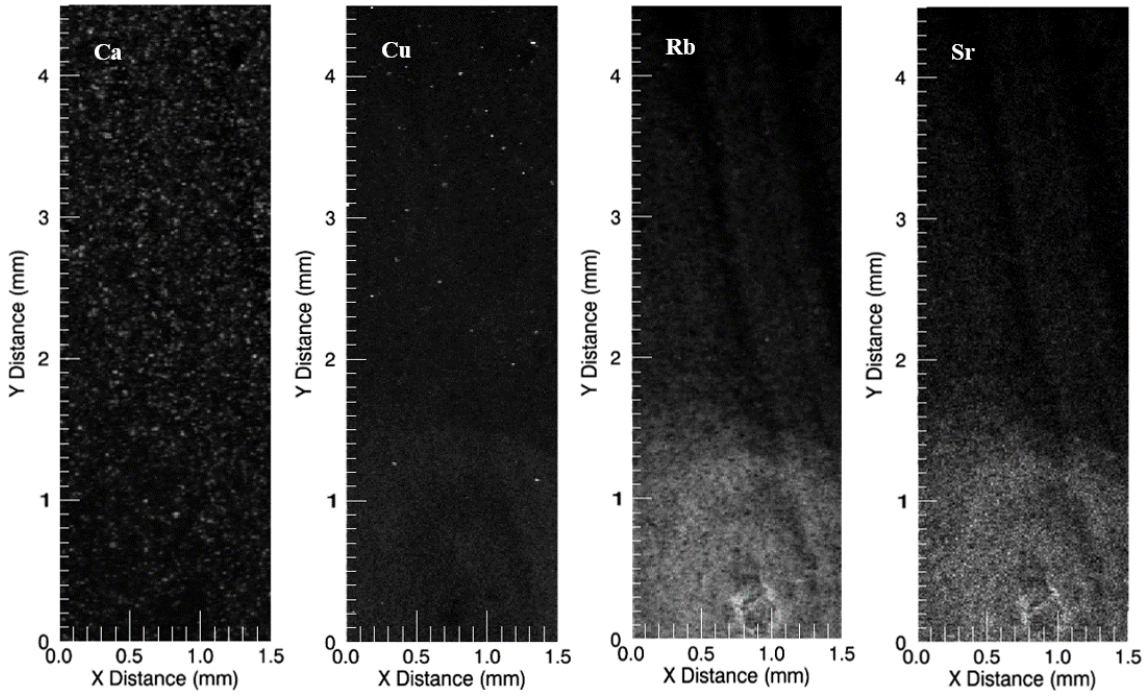


Figure C-9. μXRF maps for Ca Kα, Cu Kα, Rb Kα, and Sr Kα in NP13-8. The scale of maps is in millimeters. Fluorescence counts for each element were proportional to the brightness.

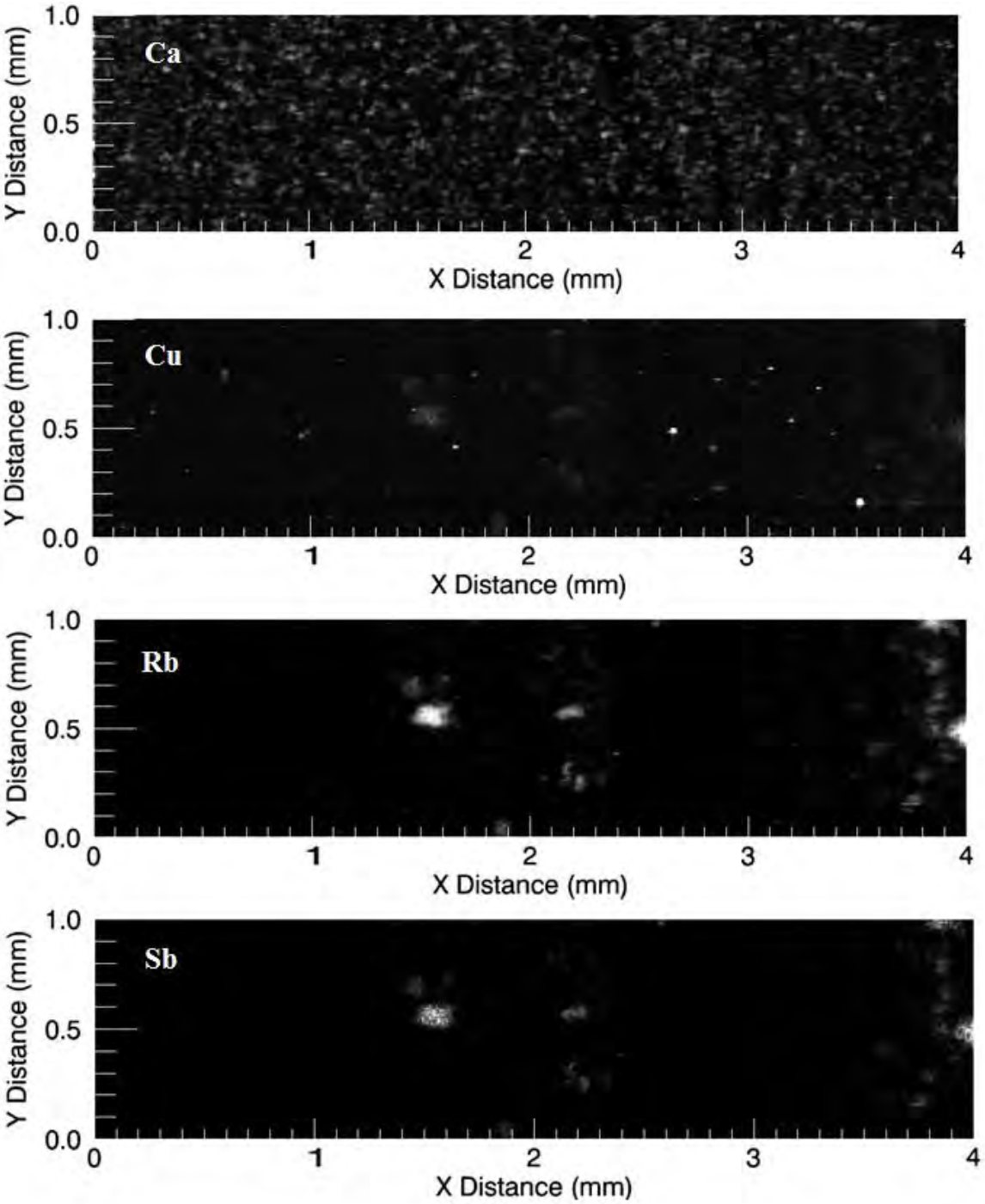


Figure C-10. μXRF maps for Ca Kα, Cu Kα, Rb Kα, and Sr Kα in NP13-8h. The scale of maps is in millimeters. Fluorescence counts for each element were proportional to the brightness.

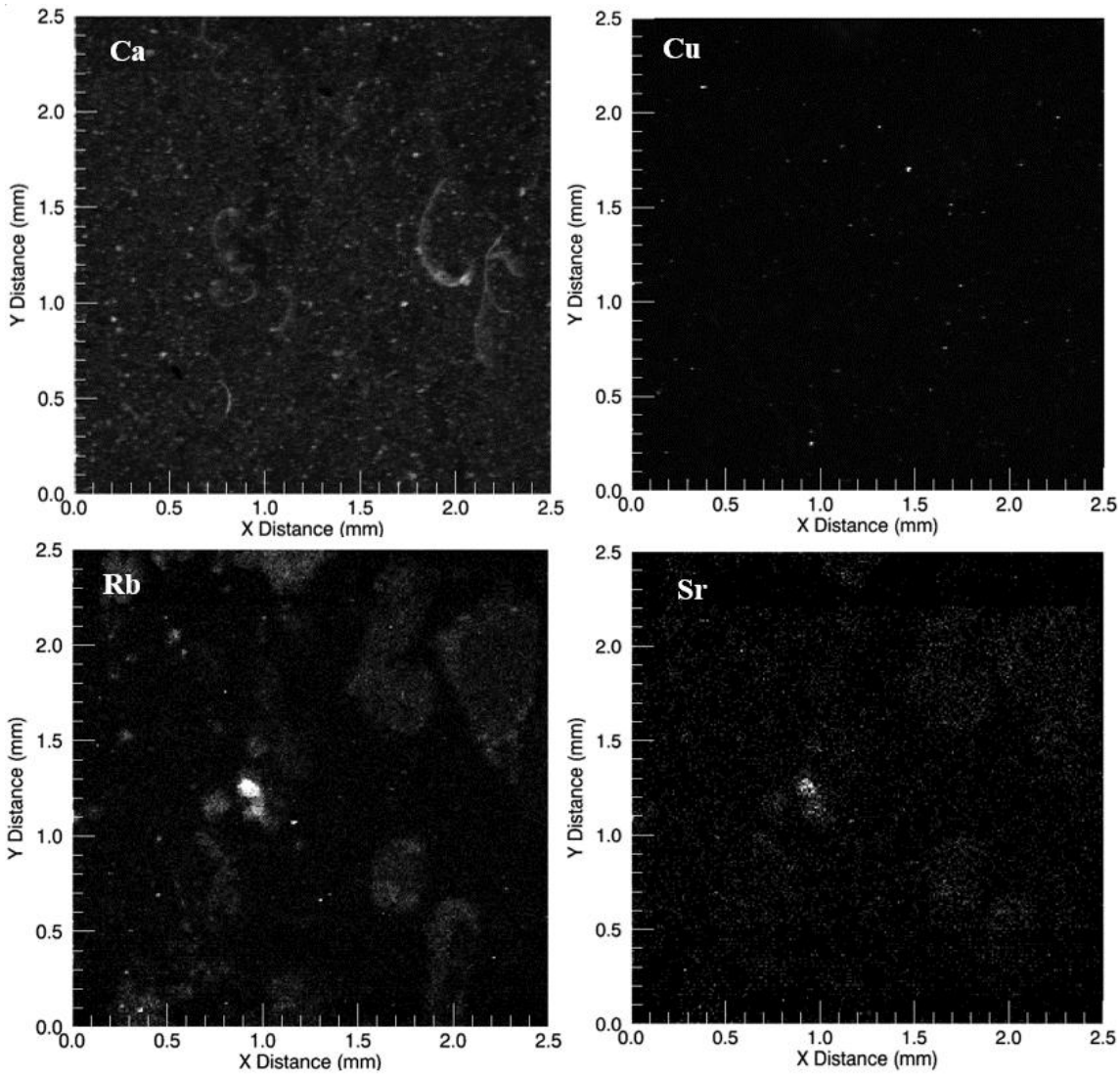


Figure C-11. μXRF maps for Ca Kα, Cu Kα, Rb Kα, and Sr Kα in NP9-16. The scale of maps is in millimeters. Fluorescence counts for each element were proportional to the brightness.

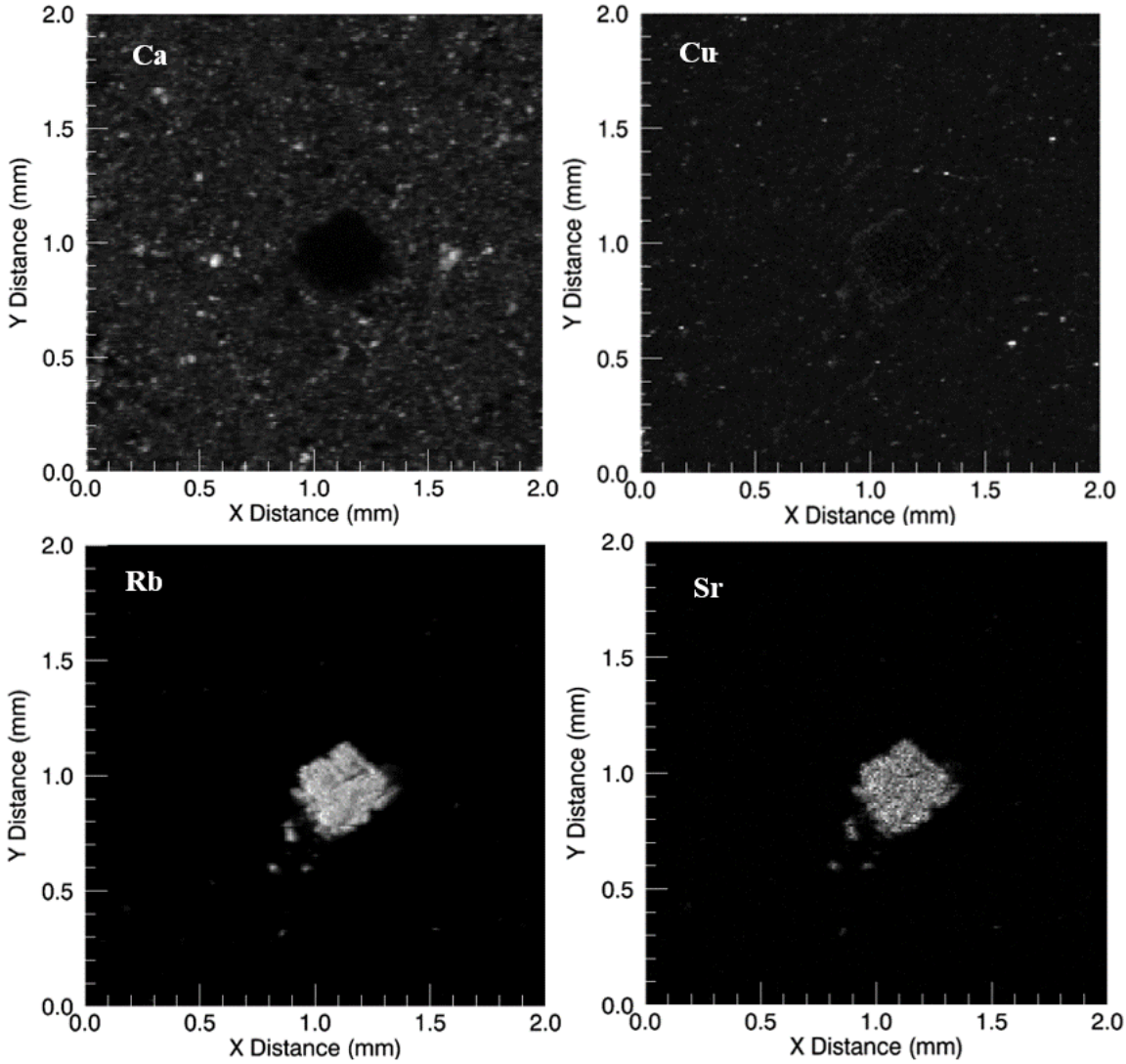


Figure C-12. μXRF maps for Ca Kα, Cu Kα, Rb Kα, and Sr Kα in NP13-12. The scale of maps is in millimeters. Fluorescence counts for each element were proportional to the brightness.

# CURRICULUM VITAE

Name: Xianyu Meng

Mailing Address: 1224 Fern Street SW Apt. A8, Olympia, WA, 98502

Phone: (435)-363-5846

Email: m.xianyu@gmail.com

---

## EDUCATION

Ph.D. in Environmental Engineering, Utah State University
Expected graduation: December 2014
Dissertation title: Redox Controlled Biogeochemical Processes Affecting Arsenic Solubility from Aquifer Solids in Cache Valley, Utah
Overall GPA: 3.8/4.0

M.E. in Municipal Engineering, Tianjin University, 2008
Thesis title: Analysis and Control of Metal Pollutant in Sewage Rivers Pouring into Bo Sea in Tianjin Area
Overall GPA: 3.2/4.0

B.E. in Environmental Engineering, Tianjin University, 2006
Thesis title: Prediction and Control of Eutrophication in City Scenic Waters.

## RESEARCH EXPERIENCE

**Research Assistant,** Utah Water Research Laboratory, Utah State University, 2008-2014

- Performed groundwater and surface water sampling and water quality analyses for evaluating arsenic contamination and determining the movement of arsenic plume
- Conducted microcosm study with three aquifer solids focusing on arsenic solubilization
- Performed polymerase chain reaction and gel electrophoresis to quantify arsenate reducing bacteria in aquifer solids

- Coordinated with geotechnical drilling company to collect sediment cores, using direct push technique, followed by monitoring well installation
- Organized a group of seven people (including myself) to accomplish processing and analyses for sediment cores within a certain time frame to prevent samples from being oxidized after collection
- Composed successful proposals for performing on-site experiments at different synchrotron institutions in the United States
- Determined oxidation state and coordination chemistry of arsenic in sediments using advanced Synchrotron-based X-ray Absorption Spectroscopy at Argonne National Lab and Brookhaven Nation Lab

**Research Assistant,** Tianjin University, China, 2006-2008

- Made sampling plan for water quality monitoring program, which was funded by Chinese National Natural Science Foundation
- Collected water and river sediment samples from two main sewage draining rivers that run through City of Tianjin, China, and finally pour into Po Sea
- Modeled distribution of heavy metal between water body and river sediment
- Directed two undergraduate students' research of monitoring contaminants in rivers

## INSTRUMENTAL SKILLS

- Portable field kits
- Spectrophotometer
- Hydride Generation Atomic Absorption Spectrometry (HG-AAS)
- Inductively Coupled Plasma Mass Spectrometer (ICP-MS)
- Synchrotron X-ray absorption spectroscopic analyses (including X-ray florescence, X-ray absorption near edge structure, and extended X-ray fine structure)

## DATA PROCESSING

- Scientific application: IFEFFIT (Athena and Artemis) and MINEQL.
- Statistical application: JMP (SAS) and R.
- Technical Drawing: Dplot, Surfer 8, AutoCAD, and Photoshop
- General: EXCEL (1998-2013)

## COMPUTER SKILLS

- Operation system: Windows XP, Vista, 7, and 8
- Office application: Microsoft Office 1998-2013 and Endnote

## AWARDS

- Research Assistantship, Utah State University, 2008-present
- Master Student Scholarship, Tianjin University, 2006-2008
- Research Assistantship, Tianjin University, 2006-2008

## AFFILIATIONS

- Member of the American Society of Agronomy (ASA), 2008 to present
- Member of the Soil Science Society of America (SSSA), 2008 to present

## PUBLICATIONS

1. **Meng, X.,** Dupont, R.R., Sorensen, D.L., Jacobson, A. R., McLean, J.E. Arsenic Solubilization and Redistribution Under Anoxic Conditions in Three Aquifer

Sediments From a Basin-fill Aquifer in Semi-arid Northern Utah. Submitted to Environment Science and Technology for publication.

2. Mirza, B.S., Muruganadam, S., **Meng, X.,** Sorensen, D.L., Dupont, R.R., McLean, J.E., 2014. Arsenic (V) Reduction in Relation to Iron (III) Transformation and Molecular Characterization of the Structural and Functional Microbial Community in Sediments of a Northern Utah, Basin-Fill Aquifer. Appl. Environ. Microbiol., AEM. 00240-00214.

3. Li, Y., Li, Y., Zhang T., **Meng, X.,** and Zhao, X. 2008. Water Quality Assessment in Different Water Periods of Beitang Drainage River in Tianjin. China Water and Wastewater, 24(22).

## PRESENTATIONS

### Oral

1) **Meng, X.** and J. E. McLean. 2013. Redox Controlled Transformation of Arsenic Geochemistry in Shallow Basin-Fill Aquifer in Cache Valley, Utah: Implication of Arsenic Solubilization. Annual meetings of the Annual meetings of the Soil Science Society of America. Tampa, FL, November.

2) **Meng, X**. and J. E. McLean. 2012. Redox Controlled Biogeochemical Processes Affecting Arsenic Solubility in a Shallow Aquifer in Semi-arid Cache Valley, Utah. Annual meetings of the Annual meetings of the Soil Science Society of America. Cincinnati, OH, October.

### Poster

1) **Meng, X.,** Muruganandam, S., and J.E. McLean. 2011. Redox Controlled Biogeochemical Processes Affecting Arsenic Solubility Down a Sediment Profile. Annual meetings of the Soil Science Society of America. San Antonio, TX, October.

2) **Meng, X.,** Muruganandam, S., and J.E. McLean. 2010. Mobilization of Geologic Arsenic in Aquifers of Cache Valley, Northern Utah. Annual meetings of the Soil Science Society of America. Long Beach, CA, November.

3) Muruganandam, S., **Meng, X.,** and J.E. McLean. 2010. Arsenic Mobilization and Dissimilatory Arsenate Respiring Bacteria in Landfill Sediments. Annual meetings of the Soil Science Society of America. Long Beach, CA, November.

## HIGHLIGHTS OF QUALIFICATIONS

- Strong background in wet chemistry
- Experienced to study redox sensitive contaminants
- Familiar with collecting, processing, and analysis of water and sediment samples
- Familiar with imaging techniques and related data handling methods
- Sufficient field work experience with investigation and sampling activity
- Capacity for leading a team to achieve goals
- Excellent public speaking and communication skills
- Ability of getting along with co-workers
- Motivation of utilizing advanced technology
- Ability of composing competitive proposals
- Desire to self-improvement

## RELEVENT COURSES

**Ph.D. Courses:**

Environmental Quality Analysis

Process Dynamics

Environmental Data Analysis

Environmental Microbial Ecology

Synthetic Biological Engineering

Aquatic Chemistry

Chemical Inorganic Contamination

Physical/chemical Environmental Processes

Groundwater Engineering

Soil Genesis Morphology

Remediation Engineering

Biological Processes

**Previous Courses:**

Life Sciences and Biotechnology

Experimental Techniques for Water Pollution Control

Applied Functional Analysis

Numerical Analysis in Engineering and Science

Advanced Environmental Chemistry and Modern Environmental Monitoring Technology

Theory and Models of Wastewater Biological Treatment

The Fundamentals of Environmental Engineering

Biofilm Wastewater Treatment Processes

Optimization of Water and Wastewater System

Biological Removal of Nitrogen and Phosphorus from Wastewater

Environmental Geographic Information System